Fermions in an inhomogeneous environment : equilibrium and non-equilibrium properties

Gabriel Gouraud

PSL UNIVERSITÉ PARIS

THÈSE DE DOCTORAT
DE L'UNIVERSITÉ PSL

Préparée à l'Ecole Normale Supérieure

Fermions in an inhomogeneous environment: equilibrium and non-equilibrium properties

Soutenue par
Gabriel Gouraud
Le 21 septembre 2023

Ecole doctorale n° 564
Physique en Île-de-France

Spécialité
Physique Théorique

Composition du jury :

Fabian, Essler Oxford University	*Rapporteur*
Patrizia, Vignolo Université de Nice	*Rapporteur*
Benoît, Douçot Sorbone Université	*Président du jury*
Thierry, Giamarchi Université de Genève	*Examinateur*
Jean-Marie, Stéphan Université Claude Bernard Lyon 1	*Examinateur*
Pierre, Le Doussal Ecole Normale Supérieure	*Directeur de thèse*
Grégory, Schehr Sorbone Université	Invité

ENS | PSL

LPENS
LABORATOIRE DE PHYSIQUE DE L'ÉCOLE NORMALE SUPÉRIEURE

Remerciements

Je commence, ou plutôt je termine ma thèse par quelques remerciements à toutes les personnes que j'ai pu rencontrer durant ces trois dernières années, que ce soit dans le cadre de la recherche ou en dehors de celui-ci.

Je commence par remercier mes directeurs de thèse sans qui ces trois années de recherche n'auraient été possibles : Pierre Le Doussal ainsi que Grégory Schehr, pour leurs bons conseils, leur bienveillance, leurs idées brillantes, mais aussi pour la confiance et la liberté qu'ils m'ont accordées dans mes choix de recherche.

Bien sûr, je remercie les rapporteurs de ma thèse, Fabian Essler et Patrizia Vignolo, d'avoir accepté la lourde responsabilité que je leur ai confiée et le temps qu'ils ont consacré à la relecture de ma thèse. Je remercie également les autres membres du jury, Benoît Douçot, Thierry Giamarchi et Jean-Marie Stéphan, pour leur participation.

Si la thèse est un travail personnel, c'est aussi l'occasion de rencontrer de nombreux chercheurs, post-doctorants et doctorants. Ainsi, je tiens à remercier pour les nombreuses discussions de physique et de mathématiques que j'ai eues : Augustin Lafaye, Silvia Pappalardi, Benjamin de Bruyne, David Dean, Lorenzo Piroli, Tomaz Prosen, Alain Comtet, Camille Aron, Alberto Rosso, Satya Majumdar, Jacopo de Nardis, Guillaume Barraquand, Denis Bernard, Adam Nahum, Jesper Jacobsen et Saverio Bocini.

Ces trois années n'auraient pas été aussi riches en joies, en bonne humeur et en discussions scientifiques sans la chaleureuse présence des doctorants et post-doctorants du LPENS qui m'ont accueilli. Je pense à Ludwig avec qui j'ai donné les cours de physique pour tous, mais aussi à Manuel, Marko, David, Vassilis, Ana, Farah, Tony, Tristan, Alexandre, Dmitri, Gauthier, Elie. Je souhaite également exprimer ma gratitude envers les nouveaux venus, Mikhail, Bastien, Paul, Iason, Olalla, Christiana. Un grand merci à Andonis, Marina, Lucia et à toutes les personnes rencontrées lors de conférences ou d'écoles d'été à Cargèse, Beg Rohu ou encore Les Houches.

Je remercie aussi Amélie pour des discussions plus mathématiques. Mes différents colocataires pour leur bonne humeur quotidienne : Pierre, Cloé; la coloc du haut et celle du bas pour le confinement.

Une thèse, c'est aussi de nombreuses difficultés administratives habilement résolues par une équipe de professionnels. Je pense à Christine, Laura, Médina et Nora. Merci aussi à Yan et son équipe pour leur aide du coté informatique.

Enfin, last but not least, je remercie ma famille et mes amis, mes proches, pour leur présence et leur soutien inconditionnel.

Contents

Introduction

The study of in and out-of-equilibrium quantum many-body physics is known to be a fascinating subject, as it comes with challenging questions. Some of these questions include: How do hydrodynamic theories and degree of freedom reduction emerge from a quantum system at large scales? What is the large-time behavior of a given system, and does it relax? Can the quantum nature of a system be relevant at a large scale; and how can we characterize the dynamics of entanglement entropy? In this thesis, we will utilize the framework of non-interacting spinless fermions as a simple model to explore these questions related to quantum statistical physics. In doing so, we will delve into various domains of physics and mathematics, including random matrices, quantum physics, integrability, statistical physics, large deviations, and differential equations. Each of these domains is interesting in its own right, but what is even more fascinating are the numerous connections between them. Indeed, it has long been a scientific and philosophical quest to define objects through their relationships with their environments, rather than as intrinsically defined entities. Furthermore, when a connection between two systems is identified, a natural question arises: does this connection persist under generalizations of either of the systems?

Returning to the case of non-interacting fermions, we will explore how the well-known mapping to random matrices in one dimension can be employed to predict statistical features of non-interacting fermions in higher dimensions. In the context of out-of-equilibrium physics, we will examine the statistics of noninteracting fermions at the edge of propagating fronts. Additionally, we will investigate how the hydrodynamic theory for integrable systems is modified in the presence of local inhomogeneities or defects.

Random Matrix, History and Applications. The origins of random matrix theory can be traced back to two parallel stories. One of these stories began when Wishart [4] introduced the first random matrix ensemble while working on multivariate statistics. At the time, he was studying the properties of covariance matrices, and in particular, the statistical properties of their eigenvalues.

The other story begins with the discovery by Fermi in the 30s of narrow resonances in the scattering of slow neutrons on nuclei [5]. This was a surprising result, as nuclear physicists at the time were used to studying the physics of electrons, which can be approximated by a weakly coupled regime. In contrast, these results led Bohr [6] to conclude that physicists were dealing with a system of particles in a strongly coupled regime. Wigner showed that the scattering process was a function of the nuclear Hamiltonian spectrum [7], but because of the many-body strong coupling, finding exactly the spectrum was a really hard problem, such that the theory seemed to be in a dead end. However, Wigner

soon realized that he could let go of the exact structure of the spectrum and study only its statistical features. Wigner, who had a particular interest in the spacing distribution of the spectrum [8], "accidentally" read Wishart's article about two decades after its publication, this led to the further development of Random Matrix Theory (RMT). It is worth noting that this was a shift in the paradigm of statistical physics. Previously, statistical physics had focused on ensembles of configurations for a fixed Hamiltonian. With RMT, the focus shifted to ensembles of Hamiltonians for which only the symmetry properties were fixed. For example, in the modeling of a system with time reversal symmetry, the Hamiltonians would be real symmetric matrices.

RMT has a wealth of mathematical objects associated with it, including operators, differential equations, determinants, polynomials, and path integrals. As a result, RMT naturally intersects with various fields, such as statistics, group theory, real and complex analysis, topology, algebraic geometry and number theory. On the physical side, RMT has applications beyond nuclear physics, including subject close to traditional physics as a conjectured role in chaotic quantum systems [9], and links with condensed matter [10], two-dimensional gravity [11]. It has also found diverse applications in less traditional physics areas such as computational neuroscience [12], biology [13], genetics [14], and financial dynamics [15].

Noninteracting fermions and equilibrium properties. Statistical physics is the domain of physics that asks the question: How can macroscopic theories like thermodynamics and hydrodynamics be recovered from microscopic knowledge? Hence, it asks about the behavior of a large assembly of either classical or quantum particles. In this thesis, we will focus on the quantum case, specifically on noninteracting fermions as the main physical system of interest. The interest and limitations of noninteracting fermions arise from their simplicity, which allows for exact computations, while they are subject to the Pauli exclusion principle [16], inducing nontrivial correlations.

In this regard, an interesting application of RMT lies in its relation to noninteracting fermions [17]. For certain specific potentials, the ground state of noninteracting fermions can be mapped to the eigenvalues of specific random matrix ensembles. On one side, noninteracting fermions are subject to the Pauli exclusion principle, which keeps them apart. This manifest itself as the probability density function $P(x_1, ..., x_N)$ of a gas of N fermions cancels when two fermions occupy the same position $x_i = x_j$. On the other side, it is well-known that eigenvalues in RMT tend to repel each other, in certain cases mimicking the statistical properties of noninteracting fermions. These mappings have led to the study of noninteracting fermions with specific potentials using known results from RMT.

For trapped noninteracting fermions which can be mapped to a random matrix ensemble, local correlations exhibit universal local statistics. Universality here means that the statistics have the same limit for large numbers of fermions (or large matrices) regardless of the specific potential. At this stage, it was natural to ask whether these properties would hold for potentials that could not be related to RMT or at non-zero temperature. These questions were addressed using different methods, including the Local Density Approximation (LDA) [18,

19], where the fermionic gas is considered to be locally translation invariant.

Out of equilibrium dynamics. A first method to measure equilibrium statistics was given by Johnson [20] when he measured electric current fluctuations induced by thermal fluctuations in a resting conductor. Later, the interest in current fluctuations was renewed when it was found that an additional type of noise, appears when the system is driven out of equilibrium. This effect was given the name of shot noise. This study of shot noise which is an out-of-equilibrium statistical properties, was driven by Landauer and Büttiker [21, 22], it assumes the system of interest to be in a Non-Equilibrium Steady State (NESS), typically a state with non-zero currents. Therefore, it was naturally that in the following years, the question of the out-of-equilibrium dynamics arose: How is such a NESS reached from some initial state?

An interesting tool regarding this question are quantum quenches [23–25]. A quench starts with the preparation of a system in the equilibrium state of a given Hamiltonian $\hat{H}_0$, then the Hamiltonian is abruptly changed to a new Hamiltonian $\hat{H}$. Depending on the nature of the quench, the large-time dynamics can result in an equilibrium state, a NESS, or a state with persistent oscillations. The nature of the quench can vary, typical examples are a change in the interaction [26], or in a potential [24]. A quench is called a partitioning protocol when two initially independent systems with different states are joined together at the initial time, allowing for the flow of particles from one system to the other [27]. In particular, the Landauer-Büttiker formalism emerges when considering a partitioning protocol with a scattering defect at the junction of the two half systems [28–30].

Integrable systems and quantum quenches. Roughly, integrable systems are systems with more conserved quantities than degrees of freedom. These systems, have proven to be useful in the context of quantum quenches as they have allowed, in some cases, to obtain exact results [31–33]. It seems that at large time, instead of relaxing towards equilibrium state describe by Gibbs Ensemble, integrable systems relax towards steady states described by the so called Generalized Gibbs Ensemble (GGE) [34], thus giving a different thermodynamic. Furthermore, integrable systems recently led to the emergence of a hydrodynamic theory for such systems called Generalised Hydrodynamics (GHD) [35, 36]. Being a hydrodynamic theory, GHD is valid only in the Euler scaling limit, that is when the system varies smoothly in both space and times. GHD has been further generalized to systems with weak integrability breaking induced by additional potentials [37], particle loss [38], or inhomogeneous interactions [39].

The manuscript is organised in the following way.

In the **first chapter** I introduce general notions of RMT. A description of the Gaussian Unitary Ensemble (GUE), first introduced by Wigner, is given as a Hermitian matrix with random complex independent coefficients following a Gaussian distribution. The Wishart Laguerre (WL) ensemble, also known as the Laguerre Unitary Ensemble (LUE), is also introduced. It was originally found by Wishart in the study of statistics as a covariance matrix. Both of these ensembles are related to the unitary group (hence their names) as their probability is invariant under unitary conjugation. The change of variables

from the matrix coefficients to the eigenvalues induces a Jacobian equal to a Vandermonde determinant, given by $\det \lambda_i^{j-1} = \prod_{i<j}(\lambda_i - \lambda_j)$. Consequently, the eigenvalues are not independent variables; instead, they are correlated and tend to repel each other. Furthermore, we discuss the fact that some ensembles of RMT (including GUE and WL) have the nice property of belonging to the class of Determinantal Point Processes (DPP), a type of random point process for which the n-point correlations can be obtained as a determinant of a two-point function called the kernel.

A description of the Coulomb gas method is then provided. This method allows for predictions regarding large matrices by mapping the eigenvalues to a one-dimensional charged gas with two-dimensional Coulomb repulsion. We explain how the presented unitary ensembles can be mapped to trapped non-interacting fermions, whose correlations can therefore be obtained from the aforementioned kernel $K(x, x')$. We discuss how, in the large matrix limit, the kernel exhibits similar local statistics for both random matrix ensembles. The Wigner function is then defined, it provides a phase space description of quantum physics while accounting for the Heisenberg uncertainty principle that prevents it from being a phase space density. The Local Density Approximation is an ansatz for the Wigner function that yields the kernel in the limit of a large number of fermions, even for trapping potentials that have no random matrix counterpart. Finally, we introduce the Full Counting Statistics (FCS), that is the statistics of the number of fermions within a given interval. We discuss how it can be computed using methods such as Painlevé transcendents or the Coulomb gas approach in the large deviation regime (large interval).

In the last section of the first chapter, I present the results of my first article [1]. It involves the computation of the probability of a hole of size R at the center of a noninteracting fermion gas in a d-dimensional harmonic trap. This is achieved using angular decomposition to map the problem onto the one-dimensional Wishart-Laguerre ensemble. The probability is studied across different regimes and the results are matched together. In the microscopic hole regime, our result is found to agree with previous numerical tests. Additionally, we discover a nontrivial relation between a product of Fredholm determinants of the Bessel kernel and a Fredholm determinant of the d-dimensional extension of the sine kernel.

In the **second chapter** we turn ourselves to the out-of-equilibrium dynamics of noninteracting fermions. We introduce the notion of quench. Then the main aspects of GHD are briefly reviewed in the simple case of free fermions and the Lieb-Liniger model, i.e. a Bose gas whose particles interact through a Dirac delta potential. We also provide an introduction to the Landauer-Büttiker formalism, which describes current fluctuations across a defect in a NESS. Then, in the case of a partitioning protocol, we discuss how the behavior of the system in the large system size ℓ and large time t limit can lead to either a state described by a GGE or a NESS with currents, depending on how time is scaled with respect to the system size. Typically, the system relaxes to an GGE if the particles are scattered many times at the boundaries, i.e., when $\frac{t}{\ell} \gg 1$, while a NESS with currents is obtained when the boundaries do not play a role, i.e., if $\frac{t}{\ell} \ll 1$.

In the next sections, we present results mostly coming from my second and third articles [2, 3]. We study a partitioning protocol for noninteracting fermions with a delta Dirac defect $V(x) = g\delta(x)$ in between the two subsystems. Because the fermions are noninteracting, the study of correlations can be reduced to the study of a time-dependent generalization of the kernel. From this quench, depending on the time scales, we show how the system attains either a GGE or a NESS with currents. Additionally, we also discuss the dynamics and give an exact formula for the kernel at all times, studying its large-time decay, which is found to follow a power law. We also consider the low initial temperature limit, which allows us to compare the resulting current in the NESS to previous results obtained in the framework of Conformal Field Theory (CFT). The current we find is different as a consequence of the nature of the delta Dirac defect, which is not a conformal defect.

We then provide a generalization of the partitioning protocol with a Dirac delta defect to a general compactly supported defect $V(x)$ characterized by a scattering matrix and possible bound states. Additionally, we extend our results to the space-time correlations of the NESS that is reached at large time. Interestingly, whether the defect is a delta Dirac or a general defect, we found non-local correlations at large time. These are correlations between symmetric points far away from the impurity, i.e., $\lim_{t\to\infty} K(x,-x) \neq 0$, and they have a physical interpretation in terms of scattering.

Finally, in the last section, we give a brief description of the generalization of GHD that describes the effect of the defect. Surprisingly, this generalization of GHD cannot reproduce the non-local correlations $\lim_{t\to\infty} K(x,-x)$. Hence, we propose an Euler scaling of the Fourier transform of the Wigner function which, together with the aforementioned generalization of GHD, allows us to reproduce the non-local correlations.

In the **third chapter**, we first introduce a partitioning protocol for fermions on a lattice. The system is prepared in a step-like condition, i.e., only the left half-space is filled. As a consequence, a quantum front arises propagating from left to right. Interestingly, in large time, the correlations at the edge of the front are found to be similar to the correlations at the edge of GUE, namely Airy statistics [40]. This result is a direct consequence of the fact that the velocity $v(k)$ at momentum k on the lattice has a global maximum $v(k) \sim \sin(k)$. Hence, in the case of free fermions in the continuum, as the velocity has no extremum $v(k) = k$, we do not expect the large-time emergence of Airy statistics at the edge of the quantum front.

In this chapter, however, we discuss an unpublished result. We propose a different partitioning protocol that leads to the emergence of Airy statistics at the edge of the quantum front. This is achieved by changing the initial condition. Instead of a step-like initial condition, the fermions are prepared in the ground state of the inverse power-law potential $V(x) = \frac{c}{|x|^\gamma}$. Then, we turn off the potential and let the fermions evolve freely. The study of the semiclassical limit (or small Planck constant) of the Wigner function in the initial state yields the emergence of Airy statistics at the edge of the quantum front.

Please note that the boxed equations correspond to new results obtained during this thesis.

Résumé

L'étude de la physique des systèmes à n coprs quantique à l'équilibre et hors équilibre est reconnue comme un sujet fascinant, car elle soulève des questions complexes. Certaines de ces questions incluent : Comment les théories hydrodynamiques et la réduction des degrés de liberté émergent-elles d'un système quantique à grande échelle ? Quel est le comportement à long terme d'un système donné, et relaxe-t-il vers un état stationaire? La nature quantique d'un système peut-elle être pertinente à grande échelle, et comment pouvons-nous caractériser la dynamique de l'entropie d'intrication ? Dans cette thèse, nous étudierons des gaz de fermions sans spin et sans interaction comme modèle simple pour explorer ces questions liées à la physique statistique quantique. Ce faisant, nous plongerons dans divers domaines de la physique et des mathématiques, notamment les matrices aléatoires, la physique quantique, l'intégrabilité, la physique statistique, les grandes déviations et les équations différentielles. Chacun de ces domaines est intéressant en soi, mais ce qui est encore plus fascinant, ce sont les nombreuses connexions entre eux. En effet, il s'agit depuis longtemps d'une quête scientifique et philosophique de définir des objets et des propriétés par l'intermédiaire leurs relations avec leur environnement, c'ést a dire contextuellement plutôt que comme des entités intrinsèquement définies. De plus, lorsqu'une connexion entre deux systèmes est identifiée, une question naturelle se pose : cette connexion se généralise t-elle?

Revenons au cas des fermions sans interaction, nous étudierons comment la correspondance bien connue avec les matrices aléatoires en une dimension peut être utilisée pour prédire les caractéristiques statistiques des fermions sans interaction en dimensions supérieures. Dans le contexte de la physique hors équilibre, nous examinerons la statistique des fermions sans interaction au bord des fronts de propagation. En outre, nous étudierons comment la théorie hydrodynamique pour les systèmes intégrables est modifiée en présence d'inhomogénéités ou de défauts localisé.

Matrice aléatoire, histoire et applications. Les origines de la théorie des matrices aléatoires remontent à deux histoires parallèles. L'une de ces histoires commence lorsque Wishart [4] introduisit le premier ensemble de matrices aléatoires alors qu'il travaillait sur les statistiques multivariées. À l'époque, il étudiait les propriétés des matrices de covariance et, en particulier, les propriétés statistiques de leurs valeurs propres.

L'autre histoire commence avec la découverte par Fermi, dans les années 30, de pics de résonances étroits dans la diffusion de neutrons lents sur des noyaux atomiques. Ce résultat était surprenant, car les physiciens nucléaires de l'époque étaient habitués à étudier la physique des électrons, qui peut être approximée par un régime faiblement couplé. En revanche, ces résultats ont conduit Bohr [6] à conclure que l'on faisait face à un système de particules dans un régime

fortement couplé. Wigner a montré que le processus de diffusion dépendait du spectre de l'hamiltonien nucléaire [7], mais en raison du couplage fort entre de nombreuses paticules, trouver exactement le spectre était un problème très difficile, de sorte que la théorie semblait être dans une impasse. Cependant, Wigner s'est rapidement rendu compte qu'il pouvait se passer de la structure exacte du spectre et n'étudier que ses propriétés statistiques. Wigner, qui s'intéressait particulièrement à la distribution de la distance entre les valeurs propres successives du spectre, lu par hasard l'article de Wishart environ deux décennies après sa publication, ce qui conduisit au développement de la théorie des matrices aléatoires. Remarquons qu'il s'agit d'un changement dans le paradigme de la physique statistique. Auparavant, la physique statistique s'était concentrée sur les ensembles de configurations pour un hamiltonien fixe. Avec les matrices aléatoires, on se tourne vers des ensembles d'hamiltoniens aléatoires pour lesquels seules les propriétés de symétrie sont fixées. Par exemple, dans la modélisation d'un système avec symétrie de renversement temporel, l'hamiltoniens est nécessairement une matrice symétrique réelle.

La theorie des matrices aléatoires est associée à une multitude d'objets mathématiques, en particulier des opérateurs, des équations différentielles, des déterminants, des polynômes et des intégrales de chemin. Par conséquent, cette theorie recoupe naturellement divers domaines, tels que la statistique, la théorie des groupes, l'analyse réelle et complexe, la topologie, la géométrie algébrique et la théorie des nombres. Sur le plan physique, la theorie des matrices aléatoires a des applications au-delà de la physique nucléaire, y compris des sujets proches de la physique traditionnelle comme un rôle conjecturé dans les la theorie du chaos pour les systèmes [9], ainsi que des liens avec la matière condensée [10], la gravité bidimensionnelle [11]. Elle a également trouvé diverses applications dans des domaines moins traditionnels de la physique, tels que les neurosciences computationnelles [12], la biologie [13], la génétique [14], et la dynamique financière [15].

Fermions sans interactions et propriétés à l'équilibre. La physique statistique est le domaine de la physique qui pose la question suivante : "Comment les théories macroscopiques telles que la thermodynamique et l'hydrodynamique peuvent-elles être obtenues à partir de données microscopiques ? Elle s'intéresse donc au comportement d'un grand ensemble de particules classiques ou quantiques. Dans cette thèse, nous nous concentrerons sur le cas quantique, en particulier les gaz de fermions sans interaction seront les principaux systèmes physiques d'intérêt. Les avantanges et les limites des fermions sans interaction proviennent de leur simplicité, celle-ci permet des calculs exacts, alors qu'ils sont soumis au principe d'exclusion de Pauli [16] qui induit des corrélations non triviales entre les particules.

À cet égard, une application intéressante de la théorie des matrices aléatoires réside dans sa relation avec les fermions sans interaction [17]. Pour certains potentiels spécifiques, l'état fondamental des fermions sans interaction est lié aux propriété statistiques des valeurs propres de certains ensembles de matrices aléatoires spécifiques. D'un côté, les fermions sans interaction sont soumis au principe d'exclusion de Pauli, qui tend à les éloigner. Cela se manifeste par le fait que la fonction de densité de probabilité $P(x_1, ..., x_N)$ d'un gaz de N

fermions s'annule lorsque deux fermions occupent la même position $x_i = x_j$. D'autre part, il est bien connu que les valeurs propres des matrices aléatoires ont tendance à se repousser les unes les autres, imitant dans certains cas les propriétés statistiques des fermions sans interaction. Ces liens ont permis d'étudier les fermions piégés sans interaction en utilisant les propriétés des matrices aléatoires.

Pour les fermions piégés sans interaction qui peuvent être mis en correspondance avec un ensemble de matrices aléatoires, les corrélations locales présentent un caractère statistique universel. L'universalité signifie ici que les fonctions de correlation ont la même limite pour si nombre de fermions est grand (ou si les matrices sont grandes) et ce indépendament du potentiel. À ce stade, il est naturel de se demander si ces propriétés subsistent pour des potentiels pour lesquels il n'existe pas de relation entre les fermions et les matrices aléatoires, ou si la température est non nulle. Ces questions ont été abordées à l'aide de différentes méthodes, notamment l'approximation de la densité locale [18, 19], où le gaz fermionique est considéré comme localement invariant par translation.

Dynamique hors équilibre. Une première méthode pour mesurer les statistiques d'équilibre fut donnée par Johnson [20] lorsqu'il mesura les fluctuations du courant électrique induites par les fluctuations thermiques dans un conducteur à l'équilibre thermique. Plus tard, l'intérêt pour les fluctuations de courant a été renouvelé lorsqu'il a été constaté qu'un type de bruit supplémentaire apparaissait lorsque le système était mis dans un état hors équilibre. Cet effet a été baptisé "shot noise". L'étude du shot noise, qui est une propriété statistique hors équilibre, a été menée par Landauer et Büttiker [21, 22], elle suppose que le système étudié se trouve dans un état stationaire hors équilibre, typiquement un état avec des courants non nuls. C'est donc naturellement que, dans les années qui ont suivi, la question de la dynamique hors équilibre s'est posée : Comment un tel état stationaire hors équilibre est-il atteint à partir d'un certain état initial ?

Les quenches quantiques constituent un outil intéressant pour répondre à cette question [23–25]. Un quench commence par la préparation d'un système dans l'état d'équilibre d'un hamiltonien donné $\hat{H}_0$, ensuite l'hamiltonien est brusquement remplacé par un autre hamiltonien $\hat{H}$. Selon la nature du quench, la dynamique à grande échelle peut aboutir à un état d'équilibre, un état stationaire hors équilibre ou un état avec des oscillations persistantes. La nature du quench peut varier, les exemples typiques étant un changement dans l'interaction [26], ou d'un potentiel [24]. Un quench est appelé "partitioning protocol" lorsque deux systèmes initialement indépendants avec des états différents sont réunis au moment initial, ce qui induit un flux de particules d'un système à l'autre [27]. En particulier, le formalisme de Landauer-Büttiker émerge lorsqu'on considère un protocole de partition avec une impureté semi-réfléchissante à la jonction des deux demi-systèmes [28–30].

Systèmes intégrables et Quenches quantiques. De façon grossière, les systèmes intégrables sont des systèmes dont les quantités conservées sont plus nombreuses que les degrés de liberté. Ces systèmes se sont avérés utiles dans le contexte des quenches quantiques car ils ont permis, dans certains cas, d'obtenir des résultats exacts [31–33]. Il semble qu'au lieu de s'équilibrer à grand temps

vers un état respectant l'ensemble de Gibbs, les systèmes intégrables relaxent vers des états stationaire décrits par l'ensemble de Gibbs généralisé [34], ce qui conduit à des propriétés thermodynamiques différentes. En outre, les systèmes intégrables ont récemment conduit à l'émergence d'une théorie hydrodynamique pour de tels systèmes appelée hydrodynamique généralisé (GHD) [35, 36]. Etant une théorie hydrodynamique, l'hydrodynamique généralisé n'est valable que dans la limite d'Euler, c'est-à-dire lorsque les propriétés intensives varient lentement, à la fois dans l'espace et dans le temps. La GHD a été généralisée aux systèmes avec un écart léger à l'intégrabilité, cela peut se faire en ajoutant; un potentiel [37], la perte de particules [38], ou des interactions inhomogènes [39].

Le manuscript est organisé de la façon suivante.

Dans le **premier chapitre**, j'introduis des notions générales de matrices aléatoires. Une description de l'ensemble unitaire gaussien (GUE), introduit pour la première fois par Wigner, est donnée sous la forme d'une matrice hermitienne avec des coefficients aléatoires complexes indépendants suivant une distribution gaussienne. L'ensemble de Wishart Laguerre (WL), également connu sous le nom d'ensemble unitaire de Laguerre (LUE), est également présenté. Il a été découvert à l'origine par Wishart dans le cadre de l'étude des statistiques en tant que matrice de covariance. Ces deux ensembles sont liés au groupe unitaire (d'où leur nom) car leur distribution de probabilité est invariante par conjugaison unitaire. Le changement de variables des coefficients de la matrice aux valeurs propres induit un jacobien égal à un déterminant de Vandermonde, donné par $\det \lambda_i^{j-1} = \prod_{i<j}(\lambda_i - \lambda_j)$. Par conséquent, les valeurs propres ne sont pas des variables indépendantes ; au contraire, elles sont corrélées et ont tendance à se repousser. En outre, nous discutons du fait que certains ensembles de RMT (y compris GUE et WL) ont la propriété intéressante d'appartenir à la classe des processus ponctuels déterminants (DPP), un type de processus ponctuel aléatoire pour lequel les corrélations à n points peuvent s'écrire comme le déterminant d'une fonction à deux points appelée noyau.

Une description de la méthode du gaz de Coulomb est ensuite donnée. Cette méthode permet de faire des prédictions sur les grandes matrices en faisant correspondre les valeurs propres à un gaz chargé unidimensionnel avec une répulsion de Coulomb bidimensionnelle. Nous expliquons comment les ensembles unitaires présentés peuvent être mis en correspondance avec des fermions sans interaction piégés, dont les corrélations peuvent ainsi être obtenues à partir du noyau $K(x, x')$ mentionné ci-dessus. Nous discutons comment, dans la limite des grandes matrices, le noyau présente des statistiques locales similaires pour les deux ensembles de matrices aléatoires. La fonction de Wigner est ensuite définie, elle fournit une description de l'espace de phase en physique quantique tout en tenant compte du principe d'incertitude d'Heisenberg, ce qui empêche d'en faire une densité de probabilité dans l'espace de phase. L'approximation de la densité locale est un ansatz de la fonction de Wigner qui donne le noyau dans la limite d'un grand nombre de fermions, même pour les potentiels de piégeage qui n'ont pas de contrepartie en théorie des matrices aléatoires. Enfin, nous introduisons la "Full Counting Statistic" (FCS), c'est-à-dire le statistique du nombre de fermions dans un intervalle donné. Nous discutons de la manière

dont elle peut être obtenue à l'aide de méthodes telles que les transcendants de Painlevé ou dans le régime de grande déviation par l'approche du gaz de Coulomb.

Dans la dernière section du premier chapitre, je présente les résultats de mon premier article [1]. Il s'agit du calcul de la probabilité d'un trou de taille R au centre d'un gaz de fermions sans interaction dans un piège harmonique de dimension d. Pour ce faire, on utilise la décomposition angulaire pour se ramener a un problème unidimensionel exprimé en terme d'ensemble de Wishart-Laguerre. Cette probabilité est étudiée pour différents régimes et les résultats sont mis en correspondance. Dans le régime des trous microscopiques, notre résultat est en accord avec les tests numériques précédents. En outre, nous découvrons une relation non triviale entre un produit de déterminants de Fredholm du noyau de Bessel et un déterminant de Fredholm de l'extension d-dimensionnelle du noyau sinusoïdal (sine kernel).

Dans le **deuxième chapitre**, nous nous intéressons à la dynamique hors équilibre des fermions sans interaction. Nous introduisons la notion de quench. Ensuite, les principaux aspects de la dynamique hors équilibre sont brièvement passés en revue dans le cas simple des fermions libres et du modèle de Lieb-Liniger, c'est-à-dire un gaz de Bose dont les particules interagissent par l'intermédiaire d'un potentiel delta de Dirac. Nous présentons également le formalisme de Landauer-Büttiker, qui décrit les fluctuations de courant à travers une impureté dans un état stationaire hors équilibre. Ensuite, dans le cas d'un partitioning protocol, nous examinons comment le système se comporte dans la limite de la grande taille ℓ et de grand temps t. En particulier selon la façon dont les deux limites sont considérés, cela peut conduire à un GGE ou à un état non stationaire hors équilibre avec des courants. Typiquement, le système se détend vers un GGE si les particules rebondissent de nombreuses fois aux bords du système, c'est-à-dire lorsque $\frac{t}{\ell} \gg 1$, tandis qu'un état non stationaire hors équilibre avec des courants est obtenu lorsque les frontières ne jouent aucun rôle, c'est-à-dire si $\frac{t}{\ell} \ll 1$.

Dans les sections suivantes, nous présentons des résultats provenant principalement de mes deuxième et troisième articles [2, 3]. Nous étudions un protocole de partitionnement pour des fermions sans interaction avec un défaut delta de Dirac $V(x) = g\delta(x)$ entre les deux sous-systèmes. Comme les fermions n'interagissent pas, l'étude des corrélations peut être réduite à l'étude d'une généralisation temporelle du noyau. A partir de ce quench, en fonction des échelles de temps, nous montrons comment le système atteint soit un GGE, soit un état stationaire hors équilibre. En outre, nous discutons de la dynamique et donnons une formule exacte pour le noyau à tout moment, et étudions sa décroissance à grand temps, qui suit une loi de puissance. Nous considérons également la limite de basse température initiale, ce qui nous permet de comparer le courant résultant dans le NESS aux résultats précédents obtenus dans le cadre de la théorie des champs conformes (CFT). Le courant que nous trouvons est différent en raison de la nature du défaut delta de Dirac, qui n'est pas un défaut conforme.

Nous donnons ensuite une généralisation du protocole de partitionnement

avec un défaut Dirac delta à un défaut général à support compact $V(x)$ caractérisé par une matrice de diffusion et de possibles états liés. De plus, nous étendons nos résultats aux corrélations spatio-temporelles du NESS qui est atteint en temps long. L'un de nos résultat les plus intéressant, est que nous avons trouvé des corrélations non-locales de part et d'autre de l'impureté. Il s'agit de corrélations entre des points symétriques éloignés de l'impureté, c'est-à-dire $\lim_{t\to\infty} K(x,-x) \neq 0$, et elles ont une interprétation physique en termes de transmission et reflection à travers l'impureté.

Enfin, dans la dernière section, nous donnons une brève description d'une généralisation de la GHD qui permet de décrir l'effet du défaut. De manière surprenante, cette généralisation de la GHD ne permet pas de reproduire les corrélations non-locales $\lim_{t\to\infty} K(x,-x)$ que nous avons trouvé. Nous proposons donc une nouvelle limite d'Euler de la transformée de Fourier de la fonction de Wigner qui, associée à la généralisation de la GHD mentioné ci-dessus, permet de reproduire les corrélations non locales manquantes.

Dans le **troisième chapitre**, nous introduisons tout d'abord un partitioning protocol pour les fermions sur un réseau. Le système est préparé de façon à ce que seul le demi-espace gauche soit rempli. En conséquence, un front quantique apparaît, et se propage de gauche à droite. Il est intéressant de noter qu'en temps long, les corrélations au bord du front se révèlent être similaires aux corrélations au bord du GUE, à savoir les statistiques d'Airy [40]. Ce résultat est une conséquence directe du fait que la vélocité $v(k)$ pour la longueur d'onde k sur le réseau a un maximum global $v(k) \sim \sin(k)$. Par conséquent, dans le cas de fermions libres dans le continu, comme la vitesse n'a pas d'extremum $v(k) = k$, nous ne nous attendons pas à l'émergence à grande échelle de statistiques d'Airy au bord du front quantique.

Dans ce chapitre, cependant, nous discutons d'un résultat non publié. Nous proposons un partitioning protocol différent qui conduit à l'émergence de statistiques d'Airy au bord du front quantique. Pour ce faire, nous modifions la condition initiale. Au lieu d'une condition initiale en escalier, les fermions sont préparés dans l'état fondamental du potentiel de loi de puissance inverse $V(x) = \frac{c}{|x|^\gamma}$. Ensuite, nous désactivons le potentiel et laissons les fermions évoluer librement. L'étude de la limite semi-classique de la fonction de Wigner dans l'état initial permet d'observer l'émergence de statistiques d'Airy au bord du front quantique.

Veuillez noter que les équations encadrées correspondent à de nouveaux résultats obtenus au cours de cette thèse.

Publications related to this thesis

[1] Gabriel Gouraud, Pierre Le Doussal, and Grégory Schehr. "Hole probability for noninteracting fermions in a d-dimensional trap". In: *Europhysics Letters* 137.5 (2022), p. 50003. DOI: 10.1209/0295-5075/ac4aca. URL: https://dx.doi.org/10.1209/0295-5075/ac4aca.

[2] Gabriel Gouraud, Pierre Le Doussal, and Grégory Schehr. "Quench dynamics of noninteracting fermions with a delta impurity". In: *Journal of Physics A: Mathematical and Theoretical* 55.39 (2022), p. 395001. DOI: 10.1088/1751-8121/ac83fb. URL: https://dx.doi.org/10.1088/1751-8121/ac83fb.

[3] Gabriel Gouraud, Pierre Le Doussal, and Grégory Schehr. "Stationary time correlations for fermions after a quench in the presence of an impurity". In: *Europhysics Letters* 142.4 (2023), p. 41001. DOI: 10.1209/0295-5075/accec7. URL: https://dx.doi.org/10.1209/0295-5075/accec7.

Chapter 1

Fermions Equilibrium Statistics and Random Matrix Theory

1.1 Point Processes and Random Matrix Theory

1.1.1 Point Processes and Correlations

At first, random matrices look like simple objects, consisting of matrices filled with random coefficients. However, they unveil a plethora of phenomena, the most notable being the strong coupling of their eigenvalues. Specifically, the eigenvalues are not independent random variables and tend to repel each other. This property was what drew Wigner's attention to them, as it reproduces the level spacing of heavy nuclei spectra.

To appreciate the significance of the eigenvalue behavior, we must first grasp the concept of point processes. A point process is a set of points together with a measure or a density function defined on the space of configurations. In the case of a random matrix ensemble of size N, the eigenvalues represent an example of such a point process. More precisely, we say it is an N-point point process because the number of point is fixed to N.

The simplest type of point process is one where the points occur independently from each other. This is known as a Poisson point process [41], where the number of points $N_{\mathcal{D}}$ in a region $\mathcal{D}$ of space follows a Poisson distribution with parameter λ

$$Pr(N_{\mathcal{D}} = n) = \frac{\lambda^n}{n!} e^{-\lambda}. \tag{1.1}$$

Given a one dimensional point process, we are interested in the spacing distribution between two consecutive points. For Poisson process it is well known that this distribution follows

$$P(S) = \frac{1}{D} e^{-\frac{S}{D}}, \tag{1.2}$$

with D the mean spacing between 2 consecutive points. Now, we can compare this with the spacing distribution of nucleus spectrum, such a typical spacing is plotted in Fig. 1.1. The figure clearly shows that the eigenvalues repel each other, as evidenced by the spacing distribution canceling at zero. This means that the eigenvalues cannot be described by a Poisson process with the spacing

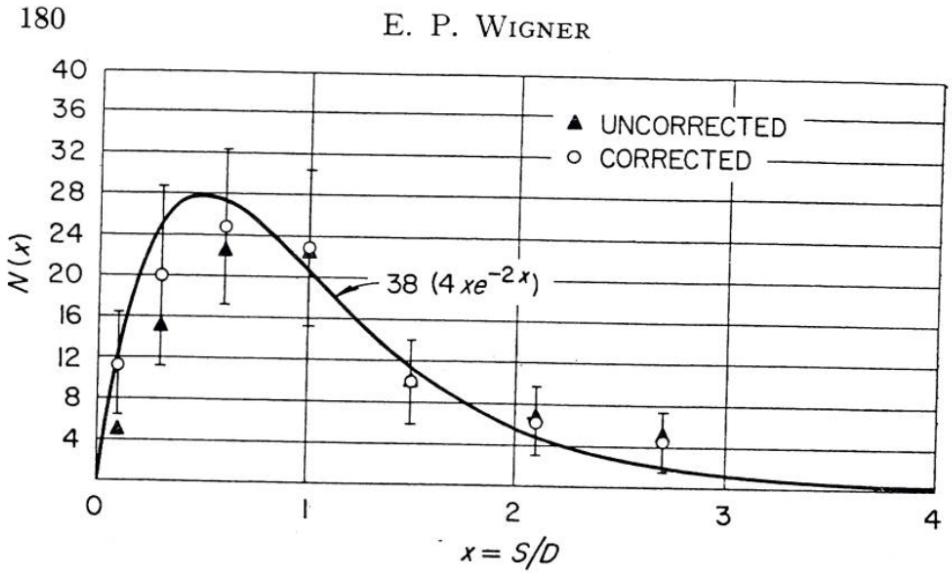

FIGURE 1.1: Typical level spacing distribution of nucleus spectrum eigenvalue [8]. S is the spacing and D its mean value.

distribution given by Eq. (1.2). Instead, the figure suggests that the distribution

$$P(s) = 4\frac{S}{D}e^{-2\frac{S}{D}} \tag{1.3}$$

fits the data well. It is the search of a point process that would exhibit this property that led Wigner to RMT. The distribution Eq. (1.3) is now commonly referred to as the Wigner surmise.

This is the main ingredient that pushed Wigner towards the study of RMT when he was working on the spectrum of heavy nuclei. Let us now present the Gaussian Unitary Ensemble (GUE) that was first introduces by Dyson, [42], we will do this following the RMT book of Mehta [43].

1.1.2 Gaussian Unitary Ensemble

The GUE is defined on the space of $N \times N$ Hermitian matrices by the probability $P(\mathbf{M})d\mathbf{M}$ that the matrix $\mathbf{M}$ belongs to the volume element $d\mathbf{M} = \prod_{i\leq j} Re[d\mathbf{M}_{ij}] \prod_{i<j} Im[d\mathbf{M}_{ij}]$ with the following conditions (in the following, bold characters will indicate vectors or matrices)

- The probability distribution is invariant under unitary conjugation, hence the name of the ensemble

$$P(\mathbf{M}')d\mathbf{M}' = P(\mathbf{M})d\mathbf{M}, \tag{1.4}$$
$$\mathbf{M}' = \mathbf{U}\mathbf{M}\mathbf{U}^\dagger, \quad \mathbf{U} \in \mathcal{U}(N), \tag{1.5}$$

  where $\mathbf{U}$ is unitary.

- Linearly independent components of M are also statistically independent. Which implies that $P(\mathbf{M})$ is a product of functions, each of which depends

on a single variable

$$P(\mathbf{M}) = \prod_{i \leq j} f_{ij}^{(0)}(Re[\mathbf{M}_{ij}]) \prod_{i<j} f_{ij}^{(1)}(Im[\mathbf{M}_{ij}]). \tag{1.6}$$

A more intuitive definition of GUE is given by

$$\mathbf{M} = \frac{1}{2\sqrt{2}\alpha}(\mathbf{X} + \mathbf{X}^T) + \frac{i}{2\sqrt{2}\alpha}(\mathbf{Y} - \mathbf{Y}^T), \tag{1.7}$$

where T is the transpose of a matrix, and $\mathbf{X}, \mathbf{Y}$ being two $N \times N$ matrices for which each entries are Gaussian i.i.d random variables $\mathcal{N}(0,1)$. As each upper diagonal entry of the matrix follows independent Gaussian laws (real or imaginary, and with different variances depending on them being on the diagonal) the probability distribution turns out to simplify to

$$P(\mathbf{M}) \sim e^{-\alpha^2 \mathrm{Tr}\mathbf{M}^2}. \tag{1.8}$$

Since the Lebesgue measure is invariant under unitary conjugation, the density probability is also invariant.

Eigenvalue distribution. Let us focus our attention on point processes. Indeed, the matrices of the GUE are Hermitian hence they can be diagonalised as $\mathbf{M} = \mathbf{U}\mathbf{D}\mathbf{U}^\dagger$ with real valued eigenvalues $\mathbf{D} = diag(\boldsymbol{\lambda})$ and unitary change of basis $\mathbf{U}$. The unitary matrix $\mathbf{U}$ (or eigenvector matrix) and the eigenvalues are random variables. Because of the fundamental properties of the GUE, Eq. (1.4), and (1.6), $\mathbf{U}$ can be shown to be independent from the eigenvalues. Additionally, it is identically distributed on the space of unitary matrix $\mathcal{U}(N)$, that is, it follows the Haar measure. On the other side, the eigenvalues give an example of a point process. If on one side, the entries of the matrix are independent, on the other side, the eigenvalues are strongly correlated random variables. The joint probability distribution function (JPDF) of the eigenvalues $P_{GUE}(\boldsymbol{\lambda})$ can be found by integrating over the uniform Haar distribution of $\mathbf{U}$. The change of variable $\mathbf{M} \to \{\boldsymbol{\lambda}, \mathbf{U}\}$ produces a Jacobian factor which after some rows and column manipulations transforms into a squared Vandermonde determinant. Indeed the infinitesimal matrix can be written

$$d\mathbf{M} = \mathbf{U} d\mathbf{M}' \mathbf{U}^\dagger, \quad d\mathbf{M}' = d\mathbf{H}\mathbf{D} - \mathbf{D}d\mathbf{H} + d\mathbf{D}, \tag{1.9}$$

where $d\mathbf{H} = \mathbf{U}^\dagger d\mathbf{U}$. The Jacobian involved from $d\mathbf{M}$ to $d\mathbf{M}'$ is equal to one. However, writing the coefficients $d\mathbf{M}'_{i,j} = d\mathbf{H}_{i,j}(\lambda_j - \lambda_i) + d\lambda_i \delta_{ij}$, and taking into account the fact that the off diagonal entries are complex, we see that the Jacobian for $\mathbf{M}' \to \{\boldsymbol{\lambda}, \mathbf{U}\}$ is the square of a Vandermonde determinant $|\det J| \sim \prod_{i<j}(\lambda_i - \lambda_j)^2$. Hence one can show that the JPDF is given by

$$P_{GUE}(\boldsymbol{\lambda}) = \frac{1}{\mathcal{Z}_N^{GUE}} \prod_{i<j}(\lambda_i - \lambda_j)^2 e^{-\alpha^2 \sum_i \lambda_i^2}, \tag{1.10}$$

where $\mathcal{Z}_N^{GUE}$ is a normalisation constant. Therefore, we see that the eigenvalues

repel each other as the JPDF decreases to zero when two eigenvalues are brought close to each other. One might ask for a more intuitive understanding of this repulsion. Let us consider the case where two eigenvalues are at the same position. In this case, instead of having N eigenspaces with one eigenvalue, we have $N-2$ eigenspaces with one eigenvalue, and one with two of them. This restricts $\mathbf{U}$ to be sampled in a sub-manifold of the space of the unitary group $\mathcal{U}(N)$ with a lower dimension than the unitary group, that is a null-measure subspace with respect to the Haar measure. Hence the probability of having two eigenvalues at the same position is zero which is consistent with Eq. (1.10).

Generalisation. The GUE is just one example of a family of random matrix ensemble used in nuclear physics to describe systems with different symmetries. In the 60's, Dyson classified these ensembles according to the type of symmetry they describe [42]. The GUE, for instance, corresponds to Hamiltonians with broken time-reversal symmetry, such as those in the presence of magnetic fields. However, if one assumes that the system is time-reversible, two additional ensembles arise depending on the total spin of the system. If the spin of the nucleus is an integer (i.e., if it is a boson), the matrices representing the Hamiltonian are required to be symmetric. On the other hand, if the spin is a half-integer (i.e., if it is a fermion), the matrices become quaternionic. These ensembles have a probability distribution that is invariant under conjugation with elements of the orthogonal group $\mathbf{O}(n)$ (in the case of integer spin) and the symplectic group $\mathbf{Sp}(2n,\mathbb{R})$ (in the case of half-integer spin). This is in contrast to the invariance with respect to the unitary group characteristic of GUE (Eq. (1.4)). These resulting ensembles are known as the Gaussian Orthogonal Ensemble (GOE) and the Gaussian Symplectic Ensemble (GSE), respectively. Similarly to the GUE, these ensembles exhibit eigenvalue repulsion, as the joint probability density function contains a term $\prod_{i<j} |\lambda_i - \lambda_j|^\beta$, where $\beta = 1$ for the GOE, $\beta = 4$ for the GSE, while we already saw that $\beta = 2$ for the GUE (Eq. (1.10)).

Since the beginning, we have focused on the link with nuclear physics. However, the main reason why we are interested in RMT is because some matrix ensembles can be mapped to the statistics of trapped spinless noninteracting fermions. In particular we will see latter that the GUE of size N is equivalent to N non interacting fermions in a harmonic trap at zero temperature.

1.1.3 Wishart-Laguerre Ensemble

The Wishart-Laguerre ensemble (WL) is another random matrix ensemble [43, 44]. They were first introduced as covariance matrix by Wishart and play a role for Principal Component Analysis (PCA) a method used in statistics for data compression. The WL matrix is defined as

$$\mathbf{W} = \mathbf{X}^\dagger \mathbf{X}, \tag{1.11}$$

where $\mathbf{X}$ is an $M \times N$ complex matrix with $M \geq N$ and $\mathbf{X}^\dagger$ is the adjoint matrix of $\mathbf{X}$. Note that if $\mathbf{X}$ represent M sampling of an N dimensional centered random variable $\vec{X}$, then $\mathbf{W}$ is the empirical covariance between the N entries of

$\mathbf{X}$. It is Hermitian, and diagonalisable with real positive eigenvalues. The PCA was introduced by Pearson [45]. It results from the extraction of the largest eigenvalues of $\mathbf{W}$ together with their corresponding eigenvectors. This gives information about how $\vec{X}$ typically spreads.

In order to define the WL ensemble we need the entries of the matrix $\mathbf{X}$ to be independent, identical, centered Gaussian random variables with variance $\frac{1}{\sqrt{b}}$. Without loss of generality, this is equivalent to

$$P(\mathbf{X}) \sim e^{-b\mathrm{Tr}\mathbf{X}^\dagger\mathbf{X}}. \tag{1.12}$$

The measure is also different here as the Hermitianity condition of GUE matrices has been relaxed, it is given by $d\mathbf{X} = \prod_{i,j} d\mathbf{X}_{ij}$

Eigenvalue distribution. The eigenvalues are real positive and they form a point process. Similarly to the case of the GUE, the change of variable from the matrix entries to the eigenvalues introduce a Jacobian which is equal to a Vandermonde determinant. Hence the eigenvalues repel each other and they obey the following JPDF

$$P_{WL}(\boldsymbol{\lambda}) = \frac{1}{\mathcal{Z}^{WL}_{M,N}} \prod_{i<j}(\lambda_i - \lambda_j)^2 \prod_{i,j\leq N} \lambda_i^{M-N} e^{-b\sum_i \lambda_i}, \tag{1.13}$$

where $\mathcal{Z}^{WL}_{M,N}$ is a normalisation constant. Similarly to the case of the GUE, we will see that the WL eigenvalues can be mapped to the ground state of non interacting fermions in a potential $V(x) = Ax^2 + \frac{B}{x^2}$.

Generalisation. Similarly to the generalisation of GUE to GOE and GSE, the WL ensemble can be generalised to include real or quaternionic $\mathbf{X}$ matrices [43]. In that case, the ensemble studied in this section is renamed Laguerre Unitary Ensemble (LUE) and the two others are called respectively Laguerre Orthogonal Ensemble (LOE) and Laguerre Sympleptic Ensemble (LSE).

The case $M < N$ is called inverse Wishart-Laguerre, it has M strictly positive eigenvalues and $N - M$ null eigenvalues. The JPDF is the same as (1.13), but reversing M and N [46, 47].

1.1.4 Density, Correlation Function and the Coulomb Gas

1.1.4.1 Density and Correlations

In this section, we would like to focus on the eigenvalue density. It turns out that in the large N limit the density will converge towards its mean value. We also expect this mean value to have a limit shape when N is taken large. Another reason for looking at this limit is that, because of the Vandermonde repulsion, the mean density exhibits oscillations at finite N which makes it harder to compute. We start by introducing the density function

$$\rho(\lambda, N) = \frac{1}{N}\sum_i \delta(\lambda - \lambda_i). \tag{1.14}$$

This function of λ is a random variable, therefore, by defining the mean as $\langle ... \rangle = \int \prod_i d\lambda_i ... P(\boldsymbol{\lambda})$, where $P(\boldsymbol{\lambda})$ is the eigenvalue JPDF of the studied matrix ensemble (whether it is GUE, as given in Eq. (1.10), or WL, as given in Eq. (1.13)), we obtain the mean density

$$\tilde{\rho}(\lambda, N) = \langle \rho(\lambda, N) \rangle \,. \tag{1.15}$$

Note that this is also the marginal distribution of the JPDF, i.e.

$$\tilde{\rho}(\lambda, N) = \int \prod_{i=2}^{N} d\lambda_i P(\lambda, \lambda_2, ..., \lambda_N), \tag{1.16}$$

such that the mean density is normalised to unity as $\int d\lambda \tilde{\rho}(\lambda, N) = 1$.

A similar object for the study of correlations is the two point density

$$\rho(\lambda, \lambda', N) = \frac{1}{N(N-1)} \sum_{i \neq j} \delta(\lambda - \lambda_i)\delta(\lambda' - \lambda_j), \tag{1.17}$$

and its mean, which is a two variables marginal distribution

$$\tilde{\rho}(\lambda, \lambda', N) = \langle \rho(\lambda, \lambda', N) \rangle = \int \prod_{i=3}^{N} d\lambda_i P(\lambda, \lambda', \lambda_3, ..., \lambda_N). \tag{1.18}$$

The two point density is normalised as $\int d\lambda d\lambda' \tilde{\rho}(\lambda, \lambda', N) = 1$. This is related to the two points correlation function $\mathcal{R}_2(\lambda, \lambda') = N(N-1)\tilde{\rho}(\lambda, \lambda', N)$.

More generally, we introduce the n-point correlation function, which will be a central object to this thesis

$$\mathcal{R}_n(\lambda_1, ..., \lambda_n) = \frac{N!}{(N-n)!} \int \prod_{i=n+1}^{N} d\lambda_i P(\lambda_1, ..., \lambda_n, \lambda_{n+1}, ..., \lambda_N). \tag{1.19}$$

It can also be written as the mean of an n-point random variable as for the one and two points cases.

1.1.4.2 Coulomb Gas Method

The Coulomb gas for GUE. Now we introduce a useful method to understand the behaviour of those point processes in the large N limit. This method is based on an analogy with a gas of particles [44]. Additionally, in this analogy, the large N limit translates into a low temperature limit. Indeed, one can rewrite (1.10)

as

$$P_{GUE}(\boldsymbol{\lambda}) = \frac{1}{\mathcal{Z}_N^{GUE}} e^{-E_N(\boldsymbol{\lambda})}, \tag{1.20}$$

$$E_N(\boldsymbol{\lambda}) = \alpha^2 \sum_i \lambda_i^2 - \sum_{i \neq j} \ln|\lambda_i - \lambda_j|, \tag{1.21}$$

$$\mathcal{Z}_N^{GUE} = \int \prod_i d\lambda_i e^{-E_N(\boldsymbol{\lambda})}. \tag{1.22}$$

This way we interpret GUE as the Boltzmann weight of one dimensional particles in the canonical ensemble at inverse temperature one. The effective energy $E_N(\boldsymbol{\lambda})$ is the sum of two contributions, a harmonic confinement and the two dimensional Coulomb repulsion between two charges of the same sign (i.e. a logarithmic repulsive potential).

Large N limit. We expect the λ_i to converge towards a limit density at large N. The eigenvalues are rescaled as follows $\{x_i\} = \{\frac{\alpha}{\sqrt{N}}\lambda_i\}$ such that all terms of the effective energy $E_N(\boldsymbol{\lambda})$ are of the same magnitude. In order to describe our problem as a functional of this density, we rescale the one and two points density function as

$$\rho(\lambda, N) = \frac{\alpha}{\sqrt{N}} n(\frac{\alpha}{\sqrt{N}}\lambda), \quad n(x) = \frac{1}{N}\sum_i \delta(x - x_i), \tag{1.23}$$

$$\rho(\lambda, \lambda', N) = \frac{\alpha^2}{N} n(\frac{\alpha}{\sqrt{N}}\lambda, \frac{\alpha}{\sqrt{N}}\lambda'), \tag{1.24}$$

$$n(x, x') = \frac{1}{N(N-1)}\sum_{i \neq j} \delta(x - x_i)\delta(x' - x_j). \tag{1.25}$$

Here $n(x)$ and $n(x, x')$ are normalised dimensionless functions and we are looking for their mean values in the large N limit. In term of those functions, the effective energy in Eq. (1.20) can be written

$$E_N(\boldsymbol{\lambda}) = N^2 \int_{\mathbb{R}} dx n(x) x^2 - \frac{N(N-1)}{2}\ln(\frac{N}{\alpha^2}) \tag{1.26}$$

$$- N(N-1) \iint_{\mathbb{R}^2} dx dx' n(x, x') \ln|x - x'|. \tag{1.27}$$

The two-point function can be written in terms of the one-point function as $n(x, x') = \frac{N}{N-1} n(x)n(x') - \frac{1}{N-1} n(x)\delta(x - x')$ such that in the large N limit keeping only the first order contributions, we obtain the effective energy as a functional of the one-point function n

$$P_{GUE}(\boldsymbol{\lambda}) = \frac{1}{\mathcal{Z}_N} e^{-N^2 E[n]}, \tag{1.28}$$

$$E[n] = \int_{\mathbb{R}} dx n(x) x^2 - \iint_{\mathbb{R}^2} dx dx' n(x)n(x') \ln|x - x'| + o(1),$$

where $\mathcal{Z}_N = (\frac{N}{\alpha^2})^{-\frac{N^2}{2}} \mathcal{Z}_N^{GUE}$ and $\mathcal{Z}_N^{GUE}$ is now a path integral over density functions. For finite N the mean density was given by the minimisation of the free energy of our system. However, now that we rescaled the problem we see that the inverse temperature is N^2 such that we only need to understand the zero temperature problem as $N \to \infty$. Therefore, we only need to minimize the energy or identically solve the saddle point equation for the path integral $\mathcal{Z}_N^{GUE}$. The functional minimisation with respect to n gives

$$\frac{\delta[E[n] + \mu(\int n - 1)]}{\delta n}|_{n=n^*} = 0, \tag{1.29}$$

where we enforce normalisation of the density with the Lagrange multiplier μ, while n^* is the solution of the equation. This leads to the following integral equation

$$2 \int_{\mathbb{R}} dx' n^*(x') \ln|x - x'| = \mu + x^2, \quad x \in \mathcal{I}, \tag{1.30}$$

where $\mathcal{I}$ is the support of n^*. It is easier to work with the derivative of this equation with respect to x

$$⨍_{\mathbb{R}} dx' \frac{n^*(x')}{x - x'} = x, \quad x \in \mathcal{I}, \tag{1.31}$$

where $⨍$ is the Cauchy principal value integral. The question is how to invert this equation in order to get the optimal density n^*. Fortunately, a formula introduced by Tricomi [48] allows to solve such singular equations. This formula concerns the slightly more general equation

$$⨍_{\mathbb{R}} dx' \frac{f(x')}{x - x'} = g(x), \quad x \in [a, b], \tag{1.32}$$

with a general source function $g(x)$, and $f(x)$ the unknown of the equation with compact support $[a, b]$. The solution is then given by

$$f(x) = \frac{1}{\pi\sqrt{(b-x)(x-a)}} \left(c - ⨍_a^b \frac{dx'}{\pi} \frac{\sqrt{(b-x')(x'-a)}}{x - x'} g(x') \right), \tag{1.33}$$

where $c = \int_a^b dx f(x)$ is a constant. In our case, the $c = 1$ to ensure normalisation, and the source function is $g(x) = x$. With this particular source function, the principal value can be computed exactly. The system being symmetric we expect that $a = -b$. We also expect the density n^* to be continuous and to cancel at the edges of its support, hence $n^*(a) = n^*(b) = 0$. This constraints allows to completely determine the solution which yields

$$\mathcal{I} = [-\sqrt{2}, \sqrt{2}], \tag{1.34}$$

and, the eigenvalue density converges towards the celebrated Wigner semicircle law plotted in Fig. 1.2,

$$\tilde{\rho}(\lambda, N) \underset{N\to\infty}{\simeq} \frac{\alpha}{\sqrt{N}} n^*(\frac{\alpha}{\sqrt{N}}\lambda), \quad n^*(x) = \frac{1}{\pi}\sqrt{2-x^2}\mathbb{1}_{\mathcal{I}}(x), \tag{1.35}$$

where $\mathbb{1}_{\mathcal{I}}(x)$ is the indicator function on $\mathcal{I}$. As expected, the eigenvalues tend to distribute near the center of the potential. However, the confinement effect is limited by the Coulomb repulsion such that the eigenvalues spread on a region of size $\sim \sqrt{N}$. It should be noted that the density at the edges $x = \pm\sqrt{2}$ vanishes as a square root, which is a universal feature of random matrix models at their edges, known as soft edges. This phenomenon occurs when the potential is continuous at the edge, as is the case in Eq. (1.28) where the potential is simply x^2 and smooth everywhere. However, in later examples, we will encounter different regimes which we will call hard edges.

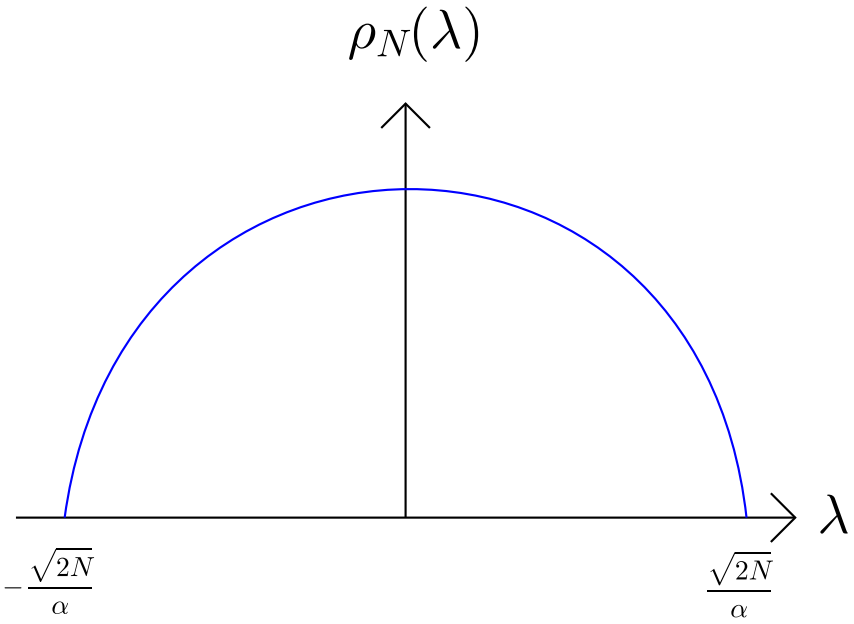

FIGURE 1.2: For the GUE the one particle density distribution takes in the large N limit the form of the Wigner semicircle (1.35), which has a finite support $[-\lambda_{edge}, \lambda_{edge}]$ with $\lambda_{edge} = \frac{\sqrt{2N}}{\alpha}$.

The Coulomb gas for Wishart-Laguerre ensemble. This Coulomb gas method is in fact way more general than what we saw on the GUE and it can be implemented for many matrix ensembles including GOE, GSE, and LUE ensembles. Here we give an outline of the path and result when this approach is applied to the WL ensemble.

For simplicity, we fix the constant defined in (1.1.3) to $b = 1$. The equivalent of equation (1.20) would imply an effective potential energy of the form

$$E_{M,N}(\boldsymbol{\lambda}) = \sum_i (\lambda_i - (M-N)\ln(\lambda_i)) - \sum_{i\neq j} \ln|\lambda_i - \lambda_j|. \tag{1.36}$$

Now we want to take the large N while keeping $M \geq N$. We also want to keep M proportional to N by defining $c = \frac{N}{M}$, otherwise if $M \sim N^{1+\epsilon}, \quad \epsilon > 0$ the logarithmic part of the potential dominates the effective energy Eq. (1.36).The correct rescaling of the eigenvalues that will ensure all terms of the effective energy $E_{M,N}(\boldsymbol{\lambda})$ are of same magnitude is $\{x_i\} = \{\frac{\lambda_i}{N}\}$. This leads to the redefinition of the problem as

$$P_{WL}(\boldsymbol{\lambda}) = \frac{1}{\mathcal{Z}_{N,c}} e^{-N^2 E[n]}, \tag{1.37}$$

$$E[n] = \int_{\mathbb{R}^+} dx n(x) x - (\frac{1-c}{c}) \int_{\mathbb{R}^+} dx n(x) \ln(x) \tag{1.38}$$

$$- \iint_{(\mathbb{R}^+)^2} dx dx' n(x) n(x') \ln|x - x'| + o(1), \} \tag{1.39}$$

with $\mathcal{Z}_{N,c}$ a renormalisation constant. Now we take the large N limit, this is equivalent to the low temperature limit such that we have to minimize the previous energy $E[n]$. This minimisation is encoded in Eq. (1.29), when expanded it yields

$$2 \int_{\mathbb{R}^+} dx' n^*(x') \ln|x - x'| = \mu + x - (\frac{1-c}{c}) \ln x, \quad x \in \mathcal{I}, \tag{1.40}$$

where μ is the Lagrange multiplier associated with the normalisation constraints $\int dx n^*(x)$. Deriving this equation with respect to x gives

$$⨍_{\mathbb{R}} dx' \frac{n^*(x')}{x - x'} = \frac{1}{2} - (\frac{1-c}{2c}) \frac{1}{x}, \quad x \in \mathcal{I}, \tag{1.41}$$

Similarlly to the case of the GUE Coulomb gas, we use Tricomi formula Eq. (1.33)

$$n^*(x) = \frac{1}{\pi \sqrt{(b-x)(x-a)}} \left(1 - ⨍_a^b \frac{dx'}{\pi} \frac{\sqrt{(b-x')(x'-a)}}{x - x'} \left[\frac{1}{2} - \frac{1-c}{2c} \frac{1}{x'} \right] \right) \tag{1.42}$$

Fortunately, this Cauchy principal value can be computed explicitly. Additionally, we expect the density $n^*(x)$ to be a continuous function and to vanish at the edge of its support $[a, b]$. This gives the support

$$\mathcal{I} = [\xi_-, \xi_+], \quad \xi_\pm = (\frac{1}{\sqrt{c}} \pm 1)^2. \tag{1.43}$$

and, the density distribution at large N and fixed c is given by

$$\tilde{\rho}(\lambda, N) \underset{N \to \infty}{\simeq} \frac{1}{N} n^*(\frac{\lambda}{N}), \quad n^*(x) = \frac{1}{2\pi x} \sqrt{(x - \xi_-)(\xi_+ - x)} \mathbb{1}_{\mathcal{I}}(x). \tag{1.44}$$

This is the celebrated Marchenko-Pastur distribution [49]. As in the case of the GUE Coulomb gas the interpretation is simple. The eigenvalues tend to

distribute near the minimum of the potential $\lambda_{min} = N\frac{1-c}{c}$. However, because of the Coulomb repulsion they spread on a region of size $\sim N$. In the case $M = N$ or the limit $c = 1$ we have $\xi_- = 0$, $\xi_+ = 4$, and the optimal density is

$$n^*(x) = \frac{1}{2\pi}\sqrt{\frac{4-x}{x}}. \tag{1.45}$$

The density exhibits a square root vanishing at $x = 4$, indicating a soft edge behavior. However, at $x = 0$, the density diverges as the inverse of a square root, indicating a hard edge. This is due to the fact that the logarithmic term in (1.36) vanishes when $M = N$, leaving only a linear potential with a hard wall potential, encoded in the fact that the eigenvalues have to be strictly positive. We will see later that correlations have universal behaviour at such different edges. Meanwhile for $1 > c > 0$, i.e. $M > N$, the gas has simply two soft edges.

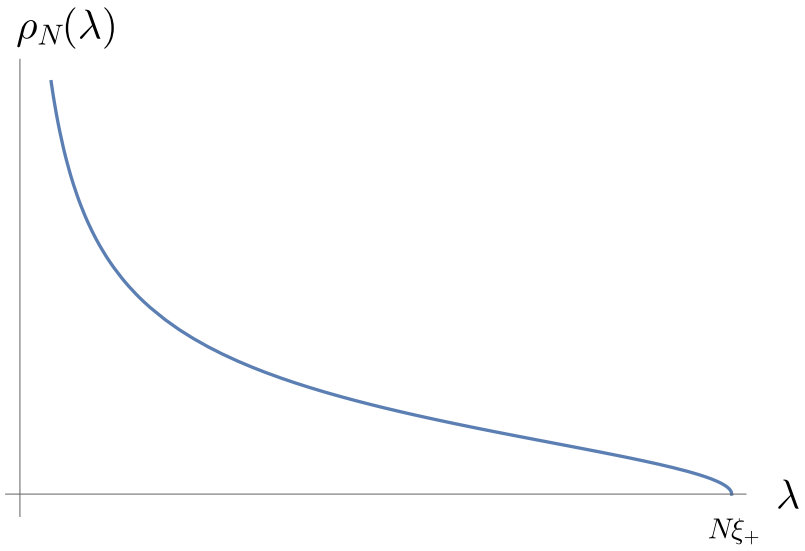

FIGURE 1.3: The Coulomb gas density for the Wishart-Laguerre ensemble with $c = 1$, see Eq. (1.45). Left edge is a hard edge where eigenvalues accumulates as $\sim \frac{1}{\sqrt{x}}$. The right edge is a soft edge with a $\sim \sqrt{x_{edge} - x}$ behaviour.

Generalisation. Here, we have extracted the one particle mean density using the Coulomb gas method, we want to add few things.

- This one particle density can be extracted from various methods some of which will be presented latter. This includes Orthogonal Polynomials, Stieltjes Transform self-equation [50, 51], and semi-classical approximation. Orthogonal polynomials and the Stieltjes transform are commonly used objects in the study of RMT. The semi-classical approximation, is a well-known approximation of quantum mechanics, it can be applied as a consequence of the fact that GUE can be mapped to fermionic systems.

- From the one particle density much information can be extracted. The mean of the maximum (resp minimum) eigenvalue $\langle\lambda_{max}\rangle$ (resp $\langle\lambda_{min}\rangle$) corresponds to the edge of the density. The mean eigenvalue for large

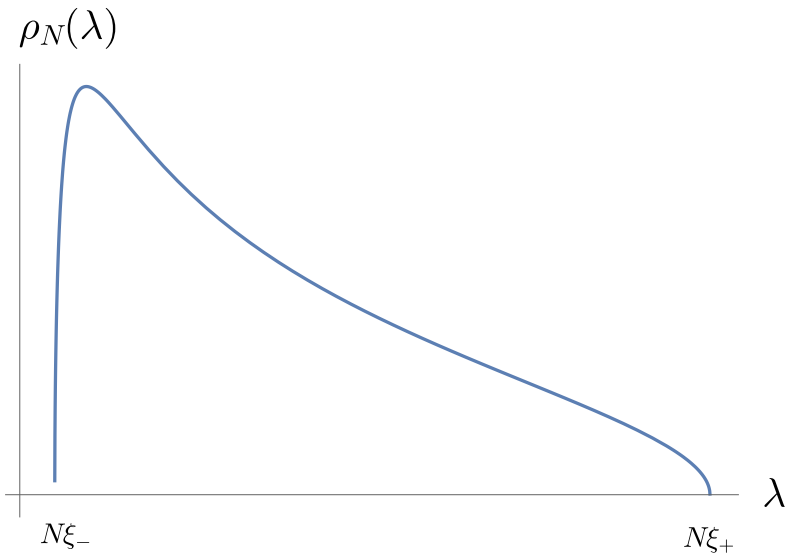

FIGURE 1.4: The Coulomb gas density for the Wishart-Laguerre ensemble with $c \neq 0$, see Eq. (1.44). It has two soft edges where the density behaves as $\sim \sqrt{|x_{edge} - x|}$.

N is given by $\langle\lambda\rangle = \int d\lambda\lambda\tilde{\rho}(\lambda, N)$. More generally the Coulomb gas method gives access to all linear statistics i.e. $\sum_{i=1}^{N} f(\lambda_i)$ where f is a given function (see [52–54]). In the large N limit, this becomes equivalent to $\int d\lambda f(\lambda)n(\lambda)$, for example $f(\lambda) = \lambda^n$ leads to the n^{th} moment.

1.2 Noninteracting Fermions

1.2.1 Determinantal Point Process

The matrix ensembles introduced previously (the GUE and the LUE) have a particular structure that is characteristic of a specific class of point processes, namely Determinantal Point Process (DPP) [55]. Examples of DPP can be constructed from the zeros of random series [56], or spanning trees on a graph. In order for a point process to be a DPP, we need additional conditions.

Definition. For any DPP on $\mathbb{R}$ there exists a kernel $K : \mathbb{R} \times \mathbb{R} \to \mathbb{R}$ verifying

$$\forall n \leq N, \quad \mathcal{R}_n(x_1, ...x_n) = \det_{1\leq i,j\leq n} K(x_i, x_j), \tag{1.46}$$

where $\mathcal{R}_n$ is the correlation function defined as in (1.19). It is worth noting that DPPs have a very restrictive structure that makes them amenable to many computations. Specifically, all statistical information about a DPP can be extracted from its kernel, making it a central object in the study of DPPs.

Additionally, it can be shown that if a kernel verifies the following three conditions

- The kernel is trace-class: $TrK = N$,

- positive: $\forall x_1, ..., x_N \in \mathbb{R} \det_{1\leq i,j\leq N} K(x_i, x_j) \geq 0$,
- self-reproducing: $\int dy K(x,y)K(y,z) = K(x,z)$,

then it generates a point process with probability distribution $P(\lambda_1, ..., \lambda_N) = \frac{1}{N!} \det_{1\leq i,j\leq N} K(x_i, x_j)$. It is important to note that a determinantal point process does not define uniquely a kernel because the correlation functions are invariant under the transformation $K'(x,y) = f(x)K(x,y)f^{-1}(y)$. The kernel is also associated to an integral operator on $\mathcal{L}^2(\mathbb{R})$ defined as $\hat{K}[\phi](x) = \int dy K(x,y)\phi(y)$. This view of the kernel as a trace-class operator will lead us later to introduce Fredholm Determinant. For now, let us just remark that points of DPP naturally repel each other as a consequence of the fundamental property of DPP (1.46).

Link with trapped fermions. Let us consider a simple example of DPP. We consider N noninteracting spinless fermions in a one dimensional trapping potential V. The system is described by the N body Hamiltonian

$$\hat{H} = \sum_{i=1}^{N} \frac{\hat{p}_i^2}{2m} + V(\hat{x}_i), \tag{1.47}$$

where $\hat{p}_i$ and $\hat{x}_i$ are the momentum and position operators of the i-th fermions. The Hamiltonian is just the sum of a single particle Hamiltonian. It is Hermitian and therefore can be diagonalised. Let us write $\{\epsilon_k, \phi_k(x)\}$ the corresponding ordered energies and orthonormal eigenfunctions. Now the ground state wavefunction is given by the Slater determinant

$$\psi_N(x_1, ..., x_N) = \frac{1}{\sqrt{N!}} \det_{1\leq i,j\leq N} \phi_j(x_i), \tag{1.48}$$

which corresponds to filling the N first level with one fermion following the Fermi exclusion principle. In quantum mechanics, the probability distribution is given by the squared modulus of the wave function, hence the JPDF is given by

$$P(x_1, ..., x_N) = |\psi_N(x_1, ..., x_N)|^2 = \frac{1}{N!} |\det_{1\leq i,j\leq N} \phi_j(x_i)|^2. \tag{1.49}$$

Now we rewrite the JPDF using the kernel $K(x,y)$ in the following compact manner

$$P(x_1, ..., x_N) = \frac{1}{N!} \det_{1\leq i,j\leq N} K(x_i, x_j), \tag{1.50}$$

$$K(x,y) = \sum_{k=1}^{N} \phi_k^*(x)\phi_k(y), \tag{1.51}$$

where $*$ is the complex conjugate. In order to show that we have an example of DPP we need to verify the three conditions (1.2.1).

- The trace condition results from the normalisation of the eigenfunctions

$$TrK = \int_{\mathbb{R}} dx \sum_{k=1}^{N} |\phi_k(x)|^2 = N. \tag{1.52}$$

- Positivity is obtained by writing the determinant of the kernel as a squared modulus

$$\det_{1\leq i,j\leq N} K(x_i, x_j) = |\det_{1\leq i,j\leq N} \phi_j(x_i)|^2 \geq 0. \tag{1.53}$$

- The self-reproducing property arises from the orthonormalization of the eigenfunctions, as

$$\int dy K(x,y)K(y,z) = \sum_{k,k'\leq N} \phi_k^*(x)(\int dy \phi_k(y)\phi_{k'}^*(y))\phi_{k'}(z) \tag{1.54}$$

$$= K(x,z). \tag{1.55}$$

This leads to the conclusion that trapped fermions is an example of DPP, hence, the n-point correlations Eq. (1.19) can be computed from the kernel Eq. (1.50) using the DPP definition Eq. (1.46). Note that for noninteracting fermions, the DPP definition Eq. (1.46) can be obtained as a consequence of Wick's theorem [57]. Among those correlations, a particular case is the particle mean density defined by $\rho(x) = \mathcal{R}_1(x)$, which is normalised to N

$$\int dx \rho(x) = N \tag{1.56}$$

and given by the kernel as

$$\rho(x) = K(x,x). \tag{1.57}$$

For most potentials $V(x)$, solving the eigenvalue problem and computing the kernel or the density exactly is a challenging task. However, it can be achieved for certain specific cases. We provide two examples below.

Harmonic trap and GUE. In the case of a harmonic potential

$$V(x) = \frac{1}{2} m\omega^2 x^2, \tag{1.58}$$

it is well known that the wave-functions are related to the Hermite polynomials by

$$\phi_k(x) = \left(\frac{\alpha}{\sqrt{\pi} 2^k k!}\right)^{1/2} e^{-\frac{\alpha^2 x^2}{2}} H_k(\alpha x), \quad k \in \mathbf{N}, \tag{1.59}$$

where $H_k(y)$ are the Hermite polynomials, and $\alpha = \sqrt{m\omega/\hbar}$. Notice the convention, here the integers k start at zero, while it starts at one in Eq. (1.48). The single particle energy levels are given by $\epsilon_k = (k + \frac{1}{2})\hbar\omega$. Now when computing

the JPDF (1.49), the Gaussian factors get out of the determinant

$$P(x_1,...,x_N) = \frac{1}{N!}\prod_{i=0}^{N-1}\frac{\alpha}{\sqrt{\pi}2^i i!}e^{-\alpha^2\sum_i x_i^2}|\det_{1\leq i,j\leq N} H_{j-1}(\alpha x_i)|^2. \tag{1.60}$$

We are left with the computation of a determinant composed of Hermite polynomials. The N-th first Hermite polynomials constitute a basis for polynomials of degree $N-1$. This property allows with rows and columns manipulation to translate the previous determinant to a Vandermonde determinant (up to a constant)

$$\det_{1\leq i,j\leq N} H_{j-1}(\alpha x_i) \sim \det_{1\leq i,j\leq N} x_i^{j-1} = \prod_{i<j}(x_i - x_j). \tag{1.61}$$

In the end, the Gaussian factor from Eq. (1.60) together with the squared Vandermonde determinant reproduce Eq. (1.10), and the JPDF of the N fermions is the same as the JPDF of GUE [19]

$$P(x_1,...,x_N) = P_{GUE}(\lambda_1,...,\lambda_N), \quad \{x_i\} \leftrightarrow \{\lambda_i\}. \tag{1.62}$$

Meanwhile, the finite N kernel of this process is given by

$$K(x,y) = e^{-\alpha^2\frac{x^2+y^2}{2}}\sum_{k=0}^{N-1}\frac{\alpha}{\sqrt{\pi}2^k k!}H_k(\alpha x)H_k(\alpha y) \tag{1.63}$$

which, using the Christoffel-Darboux formula for orthogonal polynomial [43, 44], simplifies to

$$K(x,y) = \frac{e^{-\alpha^2\frac{x^2+y^2}{2}}}{\sqrt{\pi}2^N(N-1)!}\frac{H_N(\alpha x)H_{N-1}(\alpha y) - H_N(\alpha y)H_{N-1}(\alpha x)}{x-y}. \tag{1.64}$$

In that case, the density can be computed exactly in the large N limit,The result matches with the semicricle law (1.35).

Potential $V(x) = Ax^2 + B/x^2$ on $\mathbb{R}^{+,*}$ and LUE. Here we consider the potential on the positive half line

$$V(x) = \frac{b^2}{2}x^2 + \frac{a^2-\frac{1}{4}}{2x^2}. \tag{1.65}$$

For simplicity, we set $m = 1$, and $\hbar = 1$. In that case, the hard wall gives the boundary condition $\phi_k(0) = 0$, and one can find that the wave-functions are related to the generalised Laguerre polynomials $\mathcal{L}_k^a$ of degree k and parameter a by

$$\phi_k(x) = c_k e^{-\frac{b}{2}x^2}x^{a+\frac{1}{2}}\mathcal{L}_k^a(bx^2), \tag{1.66}$$

where k is a positive integer and $c_k = \sqrt{\frac{2b^{a+1}k!}{(k+a)!}}$ a normalisation constant. Their eigenenergies are given by $\epsilon_k = b(2k+a+1)$. Again, using properties of orthogonal polynomials one constructs the JPDF which contains a Vandermonde

determinant

$$P(x_1,...,x_N) = \frac{1}{\mathcal{Z}_{a,N}} e^{-b\sum_i x_i^2} \prod_{i=1}^{N} x_i^{2a+1} \prod_{i<j} (x_i^2 - x_j^2)^2, \tag{1.67}$$

where $\frac{1}{\mathcal{Z}_{a,N}}$ is a normalisation constant. Making the change of variable $\{\lambda_i\} = \{x_i^2\}$ and $a = M - N$ yields

$$P(\lambda_1,...,\lambda_N) = \frac{1}{2^N \mathcal{Z}_{a,N}} \prod_{i<j} (\lambda_i - \lambda_j)^2 \prod_{i,j\leq N} \lambda_i^{M-N} e^{-b\sum_i \lambda_i}. \tag{1.68}$$

This is the eigenvalue distribution of the WL ensemble, given by Eq. (1.13), with the normalization constant $\mathcal{Z}_{M,N}^{WL}$ matched to $2^N \mathcal{Z}_{a,N}$.

Meanwhile, for finite N, the kernel of the process is given by

$$K(x,y) = (xy)^{a+\frac{1}{2}} e^{-\frac{b}{2}(x^2+y^2)} \sum_{k=0}^{N-1} \frac{2b^{a+1}k!}{(k+a)!} \mathcal{L}_k^a(bx^2)\mathcal{L}_k^a(by^2). \tag{1.69}$$

Using the Christoffel-Darboux formula [43, 44], the kernel is reduced to

$$K(x,y) = \frac{N! 2b^a (xy)^{a+\frac{1}{2}} e^{-\frac{b}{2}(x^2+y^2)}}{(N+a-1)!} \tag{1.70}$$

$$\times \frac{\mathcal{L}_{N-1}^a(bx^2)\mathcal{L}_N^a(by^2) - \mathcal{L}_N^a(bx^2)\mathcal{L}_{N-1}^a(bx^2)}{x^2 - y^2}. \tag{1.71}$$

Similarly to the case of GUE and the harmonic oscillator, the density can be computed in the large N limit, which yields back the Marchenko-Pastur distribution Eq. (1.44) if a is of order N or Eq. (1.45) if a is of order one.

We have seen that for some specific potentials, trapped fermions can be mapped to random matrix models. Now it is time to evoke universal statistical properties of RMT.

1.2.2 Statistical Universality

From here, an interesting point concerning RMT is that it locally exhibits universality in its statistics. This means that the local behavior of the system is independent of the specific matrix ensemble being considered.

Bulk behaviour. For noninteracting fermions in the harmonic trap Eq. (1.64), or in the potential $V(x) = \frac{b^2}{2}x^2 + \frac{a^2-\frac{1}{4}}{2x^2}$ Eq. (1.70), in the bulk of the density $\rho_N(x)$, the interparticle distance $\ell_N(x)$ is defined as

$$\int_x^{x+\ell_N(x)} dy \rho_N(y) \simeq \ell_N(x)\rho_N(x) \sim \frac{1}{N}, \tag{1.72}$$

i.e. on average, one particle has to be found in the interval $[x, x+\ell_N(x)]$. Now taking two generics x and y with typical distance of order $\ell_N(x)$. Then in the

large N limit, it can be shown that the exact formulae Eq. (1.64) and (1.70) of the kernels for noninteracting fermions in both traps that it converges towards the sine kernel [17, 19, 43] as

$$K(x,y) \underset{N\to\infty}{\simeq} \frac{1}{\ell(x)} K_{Sine}(\frac{x-y}{\ell(x)}), \tag{1.73}$$

where $\ell(x) = \frac{1}{\pi N \rho_N(x)}$ and the sine kernel is defined as

$$K_{Sine}(z) = \frac{\sin(z)}{\pi z}. \tag{1.74}$$

Eventually, through a more comprehensive study, it has been established that this property can be extended to trapped fermions, even for systems that are not directly equivalent to a random matrix ensemble. Later on, we will explore a method that enables us to prove this universality in the context of trapped fermions. Additionally, on the side of RMT similar eigenvalue correlation where found to be universal [58] even for matrix ensembles that have no mapping to noninterecting fermions.

Soft Edge behaviour. Now let us shift our focus to the statistics at the edges of the GUE spectrum. In these regions, the interparticle distance becomes large, and the equation Eq. (1.73) is no longer valid. Instead, we encounter a different behavior characterized by

$$\int_{x_{edge}-w_N}^{x_{edge}} dy \rho_N(y) \simeq \int_0^{w_N} dy \frac{\alpha}{\sqrt{N}} \sqrt{\frac{2\sqrt{2N}y}{\alpha}} \sim \frac{1}{N}, \tag{1.75}$$

with $x_{edge} = \frac{\sqrt{2N}}{\alpha}$ the positive edge of the spectrum, and let w_N denote the interparticle distance at the edge. In this regime, the interparticle distance is constrained to be of the order of $\frac{1}{N^{1/6}}$. Additionally, if we set

$$w_N = \frac{1}{\sqrt{2}\alpha N^{1/6}}, \tag{1.76}$$

it can be shown the kernel has the scaling limit

$$K(x,y) \underset{N\to\infty}{\simeq} K_{Ai}(\frac{x-x_{edge}}{w_N}, \frac{y-x_{edge}}{w_N}), \tag{1.77}$$

with K_{Ai} the celebrated Airy kernel [59, 60]

$$K_{Ai}(x,y) = \frac{Ai(x)Ai'(y) - Ai(y)Ai'(x)}{x-y}, \tag{1.78}$$

and Ai is the Airy function. This result is also valid at the soft edge of the LUE. Intuitively, near the edge, if one linearizes the potential, the Schrödinger equation leads to a differential equation whose solutions are Airy functions. This result can be utilized to obtain finite N corrections to the one-point density, revealing that the semicircle starts to oscillate and then exponentially decays

after the edge. This behavior allows the matching of the infinite N density which is singular (it has a discontinuity in the derivative) with a regular finite N density.

Hard edges. For the LUE, the universality at the soft edge remains valid if $M = cN$ as $N \to \infty$, where c is a strictly positive constant. However, if $M = N + a$ with a fixed a, then the two edges exhibit different behaviors. The right edge remains a soft edge with the Airy kernel, while the left edge of the spectrum approaches zero where the eigenvalues accumulate (see Fig. 1.3, 1.4), and this edge is referred to as a hard edge. The typical interparticle distance can be evaluated from the one-point density using the standard method

$$\int_0^{\ell_N} dy \rho_N(y) \sim \frac{1}{N}, \quad \ell_N \sim \frac{1}{\sqrt{N}}, \tag{1.79}$$

and the kernel has the scaling form

$$K(x,y) \underset{N\to\infty}{\simeq} 2k_F^2 \sqrt{xy} K_a^{Be}(k_F^2 x^2, k_F^2 y^2), \tag{1.80}$$

where $k_F = \sqrt{2\mu}$ is the Fermi momentum and $\mu \simeq 2bN$ is the chemical potential (i.e. the energy of the last eigenstate fulfilled). The Bessel kernel [61] is defined using the Bessel function J_a as

$$K_a^{Be}(b,b') = \frac{1}{4}\int_0^1 dz J_a(\sqrt{bz}) J_a(\sqrt{b'z}) \tag{1.81}$$

$$= \frac{\sqrt{b'} J_a'(b') J_a(b) - \sqrt{b} J_a'(b) J_a(b')}{2(b-b')}. \tag{1.82}$$

Similarly, hard edges can also be found for noninteracting fermions in a hard box, which corresponds to a system that has a related random matrix ensemble. For each of this local universal kernels, formula (1.46), allows to recover local correlation functions. We saw how, for certain random matrix ensembles, the correlations in the bulk are governed by the sine kernel (1.73). Now, we want to present an approximation that shows the presence of the sine kernel in the bulk of a fermionic gas with a smooth potential, even if there is no mapping to a random matrix ensemble for this potential. Before doing so, we need to introduce the so called Wigner function.

1.2.3 Wigner function

In quantum mechanics, the position probability density function is given by the squared modulus of the wave function, $\rho(x) = |\psi(x)|^2$, where ρ represents the spatial density. Similarly, the momentum density function is related to the squared modulus of the Fourier transform of the wave function, $\hat{\rho}(p) = |\hat{\psi}(p)|^2$, where $\hat{\psi}$ is the Fourier transform of ψ, and $\hat{\rho}$ represents the momentum density. However, due to the uncertainty principle, a well-defined joint probability density function (JPDF) in the position-momentum phase space $(\boldsymbol{x}, \boldsymbol{p})$ cannot be obtained.

To address this issue, Wigner introduced the concept of the Wigner function in 1932 [62]. The Wigner function provides an attempt at describing the phase-space properties of quantum systems. For a wave function of N fermions in one dimension, the Wigner function is defined as follows:

$$W_N(x,p) = \int_{-\infty}^{+\infty} \frac{dy}{2\pi\hbar} \prod_{i=2}^{N} dx_i e^{\frac{ipy}{\hbar}} \psi^*(x+\frac{y}{2}, x_2, ..., x_N)\psi(x-\frac{y}{2}, x_2, ..., x_N). \tag{1.83}$$

From this, integrating over momentum, or position space, yields the spatial and momentum particle densities

$$\int_{-\infty}^{+\infty} dp W_N(x,p) = \rho_N(x), \quad \int_{-\infty}^{+\infty} dx W_N(x,p) = \hat{\rho}_N(p),$$
$$\iint_{-\infty}^{+\infty} dx dp W_N(x,p) = N. \tag{1.84}$$

With the definition

$$\rho_N(x) = \langle \sum_{i=1}^{N} \delta(x-x_i) \rangle , \quad \hat{\rho}_N(p) = \langle \sum_{i=1}^{N} \delta(p-p_i) \rangle , \tag{1.85}$$

where $\langle ... \rangle$ is the average over the quantum state of wave function ψ. Note that the two densities are well normalised $\int dx \rho_N(x) = \int dp \hat{\rho}_N(p) = N$. However, the Wigner function does not represent a probability distribution as it can take negative values, although it remains a real-valued function.

In the case of noninteracting fermions, it can be related to the kernel through the Weyl transform

$$W(x,p) = \int_{-\infty}^{+\infty} \frac{dy}{2\pi\hbar} e^{\frac{ipy}{\hbar}} K(x+\frac{y}{2}, x-\frac{y}{2}). \tag{1.86}$$

Together with its inversion formula

$$K(x,x') = \int_{-\infty}^{+\infty} dp e^{-i\frac{p}{\hbar}(x-x')} W(\frac{x+x'}{2}, p). \tag{1.87}$$

Now we want to delve into the semiclassical behaviour of the Wigner function.

1.2.4 Local Density Approximation (LDA)

In the case of trapped fermions, the Local Density Approximation [18, 19] assumes that in the large $N \to \infty$ limit, the trapping potential varies slowly compared to the inter-particle distance, such that the gas can be locally considered a translation invariant free fermionic gas. This is formalised by writing the Wigner function in a ground state of Fermi momentum p_F at position x as the ground state Wigner function of a free fermionic gas and local Fermi momentum $p_F(x) = \sqrt{2m(p_F^2 - V(x))}$. Hence, the Wigner function is excepted

to behave as

$$W_N(x,p) \underset{N\to\infty}{\simeq} \frac{1}{2\pi\hbar}\Theta(\mu - H(x,p)), \tag{1.88}$$

where $\Theta(x)$ is the Heaviside theta function, $\mu = \frac{p_F^2}{2m}$ is the chemical potential, and $H(x,p) = \frac{p^2}{2m} + V(x)$ is the classical one particle Hamiltonian of a particle in a smooth potential. The space density is straightforwardly given by

$$\rho_N(x) \underset{N\to\infty}{\simeq} \int_{-\infty}^{+\infty} \frac{dp}{2\pi\hbar}\Theta(\mu - H(x,p)) = \frac{1}{\pi\hbar}\sqrt{2m(\mu - V(x))}, \tag{1.89}$$

where the density is implicitly zero if $\mu < V(x)$, and vanishes at the edges $V(x_{edge}) = \mu$ as a square root $\rho_N(x) \simeq \sqrt{|x_{edge} - x|}$. Note that this is false for the hard edge of LUE, which has a non smooth potential. Remark also that in the case of the harmonic potential, this gives back the Wigner semi-circle law (1.35) as well as in the case of the potential $V(x) = \frac{b^2}{2}x^2 + \frac{a^2-\frac{1}{4}}{2x^2}$ it yields back the Marchenko-Pasture distribution (1.44). Furthermore, substituting the classical Wigner function (1.88) into the relation (1.87) one gets

$$K(x,x') \underset{N\to\infty}{\simeq} \int_{-\infty}^{+\infty} \frac{dp}{2\pi\hbar} e^{-i\frac{p}{\hbar}(x-x')}\Theta(\mu - H(\tilde{x},p)) = \frac{1}{\ell_N(\tilde{x})}K_{Sine}(\frac{x-x'}{\ell_N(\tilde{x})}), \tag{1.90}$$

where $\tilde{x} = \frac{x+x'}{2}$, K_{Sine} is the Sine kernel defined in (1.73), with $\ell_N(\tilde{x}) = \frac{1}{\pi\rho_N(\tilde{x})}$ is the local interparticle distance. The LDA is known to accurately describe the density and correlations of fermions in the bulk region, where the system can be approximated as a free gas with translational invariance over the interparticle mean distance $\ell_N(\tilde{x})$. However, the LDA fails near the edges of the system where $\ell_N(\tilde{x})$ diverges. One notable advantage of the LDA compared to the previous RMT method is its ability to provide the kernel for noninteracting fermions in any smooth potential, extending beyond the scope of systems that can be mapped to a Random Matrix ensemble.

We provide a detailed justification for the assumption made for the Wigner function (1.88) in the Section 3.1.1 of the third Chapter. Additionally, in this section, we refine our result beyond the LDA in a way that allows to recover the soft edge Airy kernel at the edges of noninteracting fermionic gases even in the absence of a mapping to RMT. In fact the Airy kernel was proven recently to remain valid at the edges of some interacting systems [63].

Remark. As we work now with fermions rather than eigenvalues of a random matrix, we can also be interested in the statistics of momentum. Indeed, from the Wigner function, we already defined a momentum density $\hat{\rho}_N(p)$ (1.84), similarly, an equivalent of the kernel but for momentum can be defined. We point out that statistics in momentum space has also attracted attention for noninteracting fermions [64, 65], or interacting bose gas [66–68]. This also comes with time of flight experiments [69, 70] measuring the momentum statistics.

We already mentioned that the kernel can be used to compute correlation functions; however, these are not the only relevant objects to study. In the next subsections, we will illustrate how the kernel can be used to extract the Full Counting Statistics (FCS) through Painlevé transcendents.

1.2.5 Full Counting Statistics and Fredholm Determinant

The FCS of a random variable is the data of all the moments of that random variable. In our case, we are particularly interested in the FCS of the number of fermions $\mathcal{N}_{\mathcal{I}}$ within an interval $\mathcal{I}$. Therefore, the FCS provides us with information regarding the physical behavior of the fermionic gas under consideration. The FCS has attracted significant attention and has been obtained in various scenarios, such as for noninteracting trapped fermions [40], or in a rotating trap [71], as well as for interacting trapped fermions [72], in momentum space for interacting bosons [73], and in out-of-equilibrium setups [28, 29, 40, 74, 75]. Now, we aim to highlight a relationship between the FCS and the kernel.

Let us consider the ground state of a fermionic system with its corresponding kernel, denoted as K. If $\mathcal{I}$ is a given interval, then $\mathcal{N}_{\mathcal{I}} = \sum_{i=1}^{N} \mathbb{1}_{\mathcal{I}}(x_i)$, where $\mathbb{1}_{\mathcal{I}}$ is the indicator function on the set $\mathcal{I}$ is a random variable. This random variable counts the number of fermions present in the interval $\mathcal{I}$. In this context, the FCS is given by $\langle z^{\mathcal{N}_{\mathcal{I}}} \rangle$, which is the moment generating function of $\mathcal{N}_{\mathcal{I}}$. The cumulants or connected moments are denoted as $\langle \mathcal{N}_{\mathcal{I}}^n \rangle_c$ and are defined by

$$\ln \langle e^{t\mathcal{N}_{\mathcal{I}}} \rangle = \sum_{n \geq 1} \frac{t^n}{n!} \langle \mathcal{N}_{\mathcal{I}}^n \rangle_c \,. \tag{1.91}$$

Using the fact that $\mathbb{1}_{\mathcal{I}}(x_i)$ is a binary random variable, we can rewrite the generating function as follows

$$\langle z^{\mathcal{N}_{\mathcal{I}}} \rangle = \langle \prod_{i=1}^{N} (1 - (1-z)\mathbb{1}_{\mathcal{I}}(x_i)) \rangle. \tag{1.92}$$

Using Cauchy-Binet formula [76]

$$N! \det[\int dx h(x) f_i(x) g_j(x)] = \int dx_1 ... dx_N \det[f_i(x_j)] \det[g_k(x_l)] \prod_{i=1}^{N} h(x_i), \tag{1.93}$$

one can show that the generating function can be expressed as

$$\langle z^{\mathcal{N}_{\mathcal{I}}} \rangle = \mathrm{Det}(\mathbb{1} - (1-z)K_{\mathcal{I}}), \tag{1.94}$$

where the determinant is a Fredholm determinant defined as $\mathrm{Det}(\mathbb{1} - K) = Exp(-\sum_{i \geq 1} \frac{TrK^i}{i})$, and $K_{\mathcal{I}}$ is the integral operator, whose kernel is the kernel K restricted to the interval $\mathcal{I}$. Fredholm determinant where introduced by Fredholm in [77] while studying integral equations. For example, in order to get the hole probability, that is, the probability that there are no fermions in the interval, we evaluate the equation (1.94) at $z = 0$

$$P(\mathcal{N}_{\mathcal{I}} = 0) = \mathrm{Det}(\mathbb{1} - K_{\mathcal{I}}). \tag{1.95}$$

Hence, we have translated the FCS question into a Fredholm Determinant problem. Before diving into the methods to solve this problem, let us give a little more context to FCS.

1.2.6 Entropy and Full Counting Statistics

One reason why there is so much enthusiasm towards computing the FCS is because of its connection with entanglement entropy [78, 79]. The entanglement entropy is a useful tool in quantum many-body physics for detecting phase transitions or long-range order. One important characteristic of the von Neumann entropy is how it scales with the size of the system. In the ground state of gapped systems, the von Neumann entropy follows an area law [80] , meaning it scales with the area of the system as $\mathcal{S} \sim \ell^{d-1}$ (where ℓ is the system size and d is the dimension). This property has garnered attention as systems obeying the area law can be efficiently represented using tensor networks. However, in critical or gappless systems, the area law is broken and a logarithmic correction is introduced $\mathcal{S} \sim \ell^{d-1} \ln \ell$ [81]. Let us now define the order-q Rényi entanglement entropy as

$$\mathcal{S}_q = \frac{1}{1-q} \ln \mathrm{Tr} \rho_{\mathcal{I}}^q, \tag{1.96}$$

where $\rho_{\mathcal{I}}$ is the reduced density matrix $\rho_{\mathcal{I}} = Tr_{\mathcal{I}^c} \rho$, with $\mathcal{I}^c$ the complementary set of $\mathcal{I}$. This gets reduced to the von Neumann entropy in the $q \to 1$ limit

$$\mathcal{S}_1 = -Tr \rho_{\mathcal{I}} \ln \rho_{\mathcal{I}}. \tag{1.97}$$

Note that from the knowledge of the full Rényi entropies, one can extract the spectrum of $\rho_{\mathcal{I}}$. A quantum state is said to follow area law if the entropy grows proportionally to the boundary between $\mathcal{I}$ and $\mathcal{I}^c$. An interesting property of entanglement entropy is that area law is common for ground states of gapped quantum many-body systems [79].

In the case of free fermions, the entanglement entropies can be computed in any dimension d [82]. Additionally, a generic relation was shown to hold between the FCS and entanglement entropies in the ground state of a noninteracting fermionic system [83, 84]

$$\mathcal{S}_q = \sum_{m \geq 2} \alpha_{q,m} \left\langle \mathcal{N}_{\mathcal{I}}^m \right\rangle_c , \tag{1.98}$$

where the coefficients $\alpha_{q,m}$ are given by integral relations. In the case of $q = 1$, we have $\alpha_{q,m} = \frac{(2\pi)^m |B_m|}{m!}$, where B_m are the Bernoulli numbers.

In the special case of the random matrix ensembles GUE, in the limit of large interval size (taken after the large N limit), the random variable $\mathcal{N}_{\mathcal{I}}$ is Gaussian [85]. Hence, using (1.98), the Rényi entropies depend only on the variance $\langle \mathcal{N}_{\mathcal{I}}^2 \rangle_c$ [86]

$$\mathcal{S}_q = \frac{\pi^2}{6} (1 + \frac{1}{q}) \left\langle \mathcal{N}_{\mathcal{I}}^2 \right\rangle_c . \tag{1.99}$$

1.2.7 Painlevé Transcendents

Now that we understand the significance of studying FCS, let us delve into the computation of Fredholm determinants, which can be challenging. Fortunately, there is a useful connection with Painlevé transcendents that enables the computation of certain Fredholm determinants.

Sine kernel. For the Sine kernel, the probability $E(n,s)$ of having n fermions in an interval of size s in the bulk, is given by

$$E(n,s) = \frac{(-1)^n}{n!}\frac{\partial^n D_{sine}(s,\lambda)}{\partial_\lambda^n}|_{\lambda=1}, \tag{1.100}$$

with $D_{sine}(s,\lambda) = \mathrm{Det}(\mathbb{1}-\lambda K_{sine,[0,s]})$, and $K_{sine,[0,s]}$ is the sine kernel Eq. (1.74) restricted to the interval $[0,s]$. It was shown [87] that

$$D_{sine}(s,\lambda) = \mathrm{Exp}\left(\int_0^{\pi s} dx \frac{\sigma(x,\lambda)}{x}\right), \tag{1.101}$$

where σ is the solution to the Painlevé V equation

$$(x\sigma'')^2 + 4(x\sigma' - \sigma)(x\sigma' - \sigma + (\sigma')^2) = 0, \tag{1.102}$$

along with the boundary condition $\sigma(x,\lambda) \simeq -\frac{\lambda}{\pi}x$ as $x \to 0$ and $' = \frac{d}{dx}$. The point is that this equation can be then used to extract the asymptotic behaviour of $E(n,s)$.

Airy kernel. From the Airy kernel, we can compute the maximal eigenvalue density distribution for GUE. We rescale the maximal eigenvalue as indicated by (1.75) $\lambda_{max} = x_{edge} + w_N\chi_2$. Now, if the cumulative distribution of the random variable χ_2 is $\mathcal{F}_2(s) = P(\chi_2 \leq s)$. It can be written as a Fredholm determinant

$$\mathcal{F}_2(s) = \mathrm{Det}(\mathbb{1} - K_{Ai,[s,\infty[}), \tag{1.103}$$

where $K_{Ai,[s,\infty[}$ is the Airy kernel restricted to the interval $[s,\infty[$. Again, one can recast this as

$$\mathcal{F}_2(s) = \mathrm{Exp}\left(-\int_s^\infty dx(x-s)q^2(x)\right). \tag{1.104}$$

It was shown by Tracy and Widom [60, 88], that $q(x)$ obeys the Painlevé II equation

$$q'' = xq + 2q^3, \tag{1.105}$$

together with the boundary condition $q(x) \simeq Ai(x)$, as $x \to \infty$. This is the celebrated Tracy Widom (TW) distribution (see Fig. 1.5). The tail of the distribution is given by

$$\mathcal{F}_2'(s) \sim \begin{cases} exp(-\frac{|s|^3}{12}), & s \to -\infty \\ exp(-\frac{4s^{3/2}}{3}), & s \to +\infty \end{cases} \tag{1.106}$$

Notice the asymmetry, which can be qualitatively understood as follows: for $s < 0$, all the gas is pushed towards lower eigenvalues, while for $s > 0$, only one

eigenvalue needs to be larger than s (see [89]).

Note that similar expressions can be found from Painlevé II equation for the maximal eigenvalue of GOE and GSE [90].

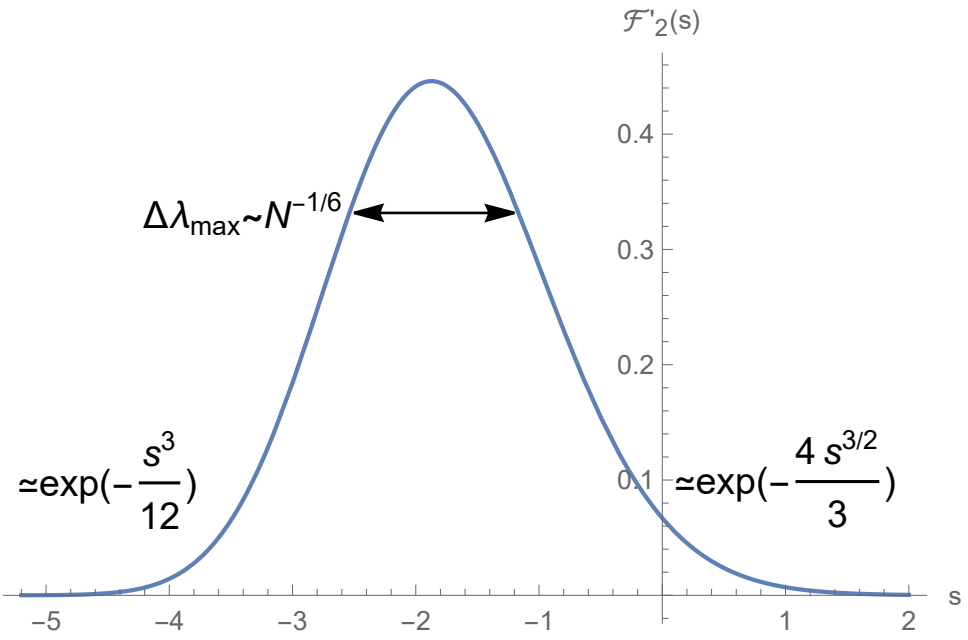

FIGURE 1.5: Plot of the Tracy-Widom distribution $\mathcal{F}_2'(s)$. Notice the asymmetric behaviour.

Bessel kernel. We close this chapter with the relation between the Bessel kernel and Painlevé equation. As shown by Tracy and Widom [61], the hole probability for the Bessel process $D_{Be,a}(s, \lambda = 1) = \mathrm{Det}(\mathbb{1} - K^{Be}_{a,[0,s]})$ can be written

$$D_{Be,a}(s, \lambda = 1) = \mathrm{Exp}\left(-\int_0^s dx \frac{\sigma(x,a)}{x}\right), \tag{1.107}$$

where σ is the solution of the Painlevé III equation

$$(x\sigma'')^2 + \sigma'(\sigma - x\sigma')(4\sigma' - 1) - a^2(\sigma')^2 = 0. \tag{1.108}$$

Note that in the large a limit, if rescaled properly, the Bessel function converges to the Airy function and so does the Bessel kernel to the Airy kernel as

$$\lim_{a\to\infty} 2^{2/3}a^{4/3}K_a^{Be}(a^2 + 2^{2/3}a^{4/3}\tilde{b}, a^2 + 2^{2/3}a^{4/3}\tilde{b}') = K_{Ai}(-\tilde{b}, -\tilde{b}'). \tag{1.109}$$

Particularly, this implies that

$$D_{Be,a}(s, \lambda = 1) \underset{a\to\infty}{\simeq} \mathcal{F}_2\left(\frac{a^2 - s}{2^{2/3}a^{4/3}}\right). \tag{1.110}$$

Hence, in this limit, the smallest eigenvalue follows the TW distribution.

1.2.8 Large Deviation, the Coulomb Gas Approach

The Painlevé equation method presented in the previous section allows for the computation of the typical density distribution of the smallest and largest eigenvalues. However, in the large deviation regime, when x is taken far away from the edge of the gas, the limiting kernels we used (Sine, Airy, Bessel) are no longer valid, and the Painlevé method breaks down. In this regime, one could attempt to compute the spacing distribution or the probability density of the largest eigenvalue directly from the JPDF of a given matrix ensemble by integrating out the remaining degrees of freedom. However, this direct approach proves to be too difficult. Therefore, we need an alternative method. Here, we illustrate how the Coulomb Gas method [91, 92] can be extended to recover the large deviation regime by retaining only the information relevant to this question. We will focus on the case of the smallest eigenvalue $\lambda_{\min}$ of the WL (1.13), as it will be the case of interest for us later on.

We recall that for the WL, in the limit of large M and N with a fixed ratio $c = \frac{N}{M}$, the edge of the gas is determined by $N\xi_-$, where $\xi_- = \left(\frac{1}{\sqrt{c}} - 1\right)^2$ (see Eq. (1.44)). We have previously mentioned that for $c < 1$, the edge is soft, and

$$\lambda_{min} = N\xi_- + \xi_-^{2/3} c^{1/6} N^{1/3} \chi, \tag{1.111}$$

where χ follows the TW distribution.

Large deviation to the right, the pushed gas. In term of JPDF of the eigenvalues, the cumulative probability of the minimal eigenvalue $P_{min}(t) = P(\lambda_{min} \geq t)$ can be written

$$P_{min}(t) = \frac{\mathcal{Z}(t)}{\mathcal{Z}(0)}, \tag{1.112}$$

$$\mathcal{Z}(t) = \int_t^\infty ... \int_t^\infty d\lambda_1 ... d\lambda_N \prod_{i<j} (\lambda_i - \lambda_j)^2 \prod_{i,j \leq N} \lambda_i^{M-N} e^{-\sum_i \lambda_i}. \tag{1.113}$$

Note that $\mathcal{Z}(0) = \mathcal{Z}_{M,N}^{WL}$. The interpretation is a Coulomb gas with an additional hard wall at position t that constrains the eigenvalues to be larger than t. Now we just need to recast this as a Coulomb Gas problem, following the idea of Eq. (1.37) in Sec. (1.1.4.2). $\mathcal{Z}(t)$ which can be understood as a partition function is written as the following path integral

$$\begin{aligned} \mathcal{Z}(t = Ns) &= \int Dn e^{-N^2 E_s[n]}, \\ E_s[n] &= \int_s^\infty dx n(x) x - \left(\frac{1-c}{c}\right) \int_s^\infty dx n(x) \ln(x) \\ &\quad - \iint_s^\infty dx dx' n(x) n(x') \ln|x - x'| + o(1), \end{aligned} \tag{1.114}$$

where the path integral $\int Dn$ runs over all density function normalised to unity i.e. such that $\int dx n(x) = 1$. The interpretation is that $\mathcal{Z}(t)$ is the partition function of a pushed Coulomb Gas, that is to say a Coulomb Gas but with the

additional constraint of a hard wall at position t pushing the particles to its right. Again, we solve this in the large N limit with a saddle point approximation over the path with the correct Lagrange multiplier

$$\frac{\delta[E_s[n] + \mu(\int_s^\infty dx n(x) - 1)]}{\delta n}|_{n=n_s^*} = 0. \tag{1.115}$$

The end is a bit technical. It is useful to differentiate the previous equation, then the minimal density is found using Tricomi formula Eq. (1.33). Finally, the probability is given by

$$P_{min}(t = Ns) = e^{-N^2\Phi_+^{min}(s)}, \quad t > N\xi_-, \tag{1.116}$$
$$\Phi_+^{min}(s) = E_s[n_s^*] - E_0[n_0^*]. \tag{1.117}$$

The minimizing density is illustrated in Fig. 1.6. One can refer to [92] for the exact expressions of n_t^* and $E_t[n_t^*]$ which are a bit cumbersome. Note that $E_{\xi_-}[n_{\xi_-}^*] = E_0[n_0^*]$, as putting a hard wall at the left of the edge of the gas has no influence. This allows to verify that the previous equation is well normalised.

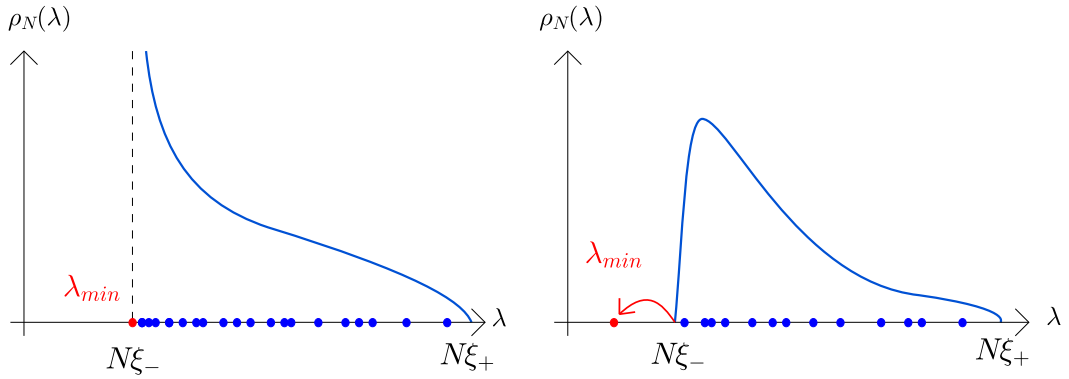

FIGURE 1.6: Left: The gas is pushed to the right; hence the density is deformed towards a higher energy configuration. Particles accumulate at the edge with a $\frac{1}{\sqrt{\lambda-\lambda_{min}}}$ divergence. Right: one particle is pulled to the left away from the gas.

Large deviation to the left, the pulled gas. Here we keep the Coulomb Gas in the usual configuration without a wall hence it is still described by the density n^* from (1.44). However, we will constrain one eigenvalue to be pulled away from the gas support at position t. This will have an energy cost equal to the sum of the potential energy of the pulled particle plus the interaction energy between the pulled particle and the rest of the gas

$$\Delta E(t) = t - N(\frac{1-c}{c}) \ln t - \sum_i \ln|t - \lambda_i|. \tag{1.118}$$

This cost can be evaluated using the Coulomb Gas density and the scaling $t = Ns$ (this is illustrated on the right panel of Fig. 1.6)

$$\Delta E(Ns) = N(\Delta e(s) - \frac{1}{c}\ln N), \quad \Delta e(s) = s - (\frac{1-c}{c})\ln s - \int dx n^*(x)\ln|s-x|, \tag{1.119}$$

in the end

$$P_{min}(t = Ns) = e^{-N\Phi_-^{min}(s)}, \quad t < N\xi_-, \tag{1.120}$$
$$\Phi_-^{min}(s) = \Delta e(s) - \Delta e(\xi_-). \tag{1.121}$$

Note that the expansion of $\Phi_+^{min}(s)$ and $\Phi_-^{min}(s)$ in the limit $s \to \xi_-$ gives

$$\Phi_+^{min}(s) \underset{s\to\xi_-^+}{\simeq} \frac{1}{12\xi_-^2 c^{1/2}}(s-\xi_-)^3, \tag{1.122}$$

$$\Phi_-^{min}(s) \underset{s\to\xi_-^-}{\simeq} \frac{4}{3\xi_- c^{1/4}}(\xi_- - s)^{3/2}, \tag{1.123}$$

which matches with the left and right asymptotics of the TW distribution, as given by Eq. (1.106). In addition, the large argument asymptotes are given by

$$\Phi_+^{min}(s) \underset{s\to+\infty}{\simeq} s - \frac{1-c}{c}\ln s + (\frac{3}{2} - E_{\xi_-}[n^*_{\xi_-}]), \tag{1.124}$$
$$\Phi_-^{min}(s) \underset{s\to 0}{\simeq} -\frac{1-c}{c}\ln s + (2\frac{1-c}{c}\ln\frac{1-c}{c} + \frac{\ln c}{c} - \xi_- - 2\sqrt{\xi_-}).$$

Linear Statistics. The method of pushed and pulled Coulomb gas can be generalized to compute the large deviations of the aforementioned linear statistics. For example in [52, 53] the large deviation of the number N_+ of positive eigenvalues was computed. More precisely, if $N_+ = cN$ with $c > 1/2$, the computation involve the minimisation of the Coulomb gas for the GUE Eq. (1.29) with the additional constraint that $\int_0^\infty dx n(x) = c$. The resulting minimal density has a support with two components (for $1/2 < c < 1$) with both soft and hard edges. This method was also used to compute the large deviations of linear statistics at the edge of GUE [54].

1.3 Statistics of noninteracting fermions in higher dimensions $d > 1$

In higher dimensions, even if the DPP structures is kept for noninteracting fermions, few results are known. This is due to the fact that we loose generically the simple exact mapping to RMT. However, some results for the hole probability in two specific examples in d = 2

- in mathematics, for the zeroes of random series in the complex plane
- in the Ginibre ensemble of random matrices, whose eigenvalues are complex and hence, spreads in a two dimensional space. It transposes to noninteracting fermions in a harmonic trap rotating at a critical frequency

such that the problem can be mapped to the lowest Landau levels of a quantum Hall system. In that case, there are exact formulae for the probability that there is no eigenvalue inside a disk [71, 93].

Apart from these examples, very few results are known when it comes to the hole probability of noninteracting fermions in dimension $d > 1$. In order to explore the higher dimensional properties of noninteracting fermionic gases, we proceed in this section to the computation of the hole probability for noninteracting fermions trapped in a d-dimensional harmonic potential.

1.3.1 Angular decomposition: from d dimensions to one dimension

The system considered here is noninteracting fermions in dimension d with unit $m = \hbar = 1$, and the single particle Hamiltonian

$$\hat{H} = \frac{p^2}{2} + V(\hat{r}) \tag{1.125}$$

where V is a central potential, and $\hat{r} = |\hat{x}|$ with a small abuse of notation. The ground state is obtained as a Slater determinant where all the eigenstates of the single particle Hamiltonian $\hat{H}$ in (1.125) are occupied up to the Fermi energy μ.

The main trick to compute the hole probability in this rotationnaly invariant system is to use the spherical coordinates $\mathbf{x} = (r, \boldsymbol{\theta})$ where $\boldsymbol{\theta}$ is a $d-1$ dimensional angular vector [64]. The Hamiltonian $\hat{H}$ can be written as $\hat{H} = -\frac{1}{2} r^{1-d} \partial_r \left(r^{d-1} \partial_r \right) + \frac{1}{2r^2} \hat{\boldsymbol{L}}^2 + V(r)$, and commutes with the angular momentum operator $\hat{\boldsymbol{L}}$. The eigenfunctions of $\hat{H}$ thus take the form $\psi_{n,\mathbf{L}}(r, \boldsymbol{\theta}) = r^{\frac{1-d}{2}} \chi_{n,l}(r) Y_{\mathbf{L}}(\boldsymbol{\theta})$ where the d-dimensional spherical harmonics $Y_{\mathbf{L}}(\boldsymbol{\theta})$, labeled by the set of angular quantum numbers $\mathbf{L}$, are eigenfunctions of $\hat{\boldsymbol{L}}^2$ with eigenvalues $\ell(\ell + d - 2)$, $\ell = 0, 1, \ldots$, which defines the angular sector. The radial parts $\chi_{n,\ell}(r)$ are the eigenfunctions of a collection of 1D radial Hamiltonians $\hat{H}_\ell = -\frac{1}{2}\partial_r^2 + V_\ell(r)$, $r \geq 0$, with potentials

$$V_\ell(r) = V(r) + \frac{a^2 - \frac{1}{4}}{2r^2} \quad , \quad a = \ell + \frac{d}{2} - 1 \tag{1.126}$$

with eigenenergies $\epsilon_{n,\ell}$, $n = 0, 1, \ldots$, each with degeneracy

$$g_d(\ell) = \frac{(2\ell + d - 2)\Gamma(\ell + d - 2)}{\Gamma(\ell + 1)\Gamma(d - 1)}, \text{ if } \ell \geq 1, \quad \text{and} \quad g_d(0) = 1. \tag{1.127}$$

In the ground state of the N fermions, each angular sector the lowest m_ℓ energy levels are occupied, i.e $n = 0, \ldots, m_\ell - 1$, such that $\epsilon_{n,\ell} \leq \mu$ and $N = \sum_\ell g_d(\ell) m_\ell$. The ground state wavefunction is given by $\Psi_0(\mathbf{x}_1, \cdots, \mathbf{x}_N) = \frac{1}{\sqrt{N!}} \det_{1 \leq i,j \leq N} \left[\psi_{\mathbf{k}_i}(\mathbf{x}_j) \right]$, where $\mathbf{k}_i = (n_i, \mathbf{L}_i)$ labels the single particle eigenfunction of the occupied eigenstates. We assume here that the ground state is non-degenerate (i.e., the last level is fully occupied, see discussion in [64]).

We now compute the hole probability $P(R)$ as the probability that there is no fermion in the sphere of radius R centred on the origin.

$$P(R) = \prod_{i=1}^{N} \int_{|\mathbf{x}_i|>R} d^d\mathbf{x}_i \, |\Psi_0(\mathbf{x}_1, \cdots, \mathbf{x}_N)|^2 \, . \tag{1.128}$$

Using the Cauchy-Binet formula (see e.g. [64, 82]) it can be written as a determinant

$$P(R) = \det_{1\le i,j\le N} [\delta_{ij} - \mathbb{A}_{ij}] \tag{1.129}$$

in terms of the overlap matrix $\mathbb{A}_{ij} = \int_{|x|\le R} d^d\mathbf{x}\, \psi^*_{n_i,\mathbf{L}_i}(\mathbf{x})\psi_{n_j,\mathbf{L}_j}(\mathbf{x})$. Using the orthogonality of the spherical harmonics, the angular integration gives $\mathbb{A}_{ij} = \delta_{\mathbf{L}_i,\mathbf{L}_j}\mathbb{A}^{(\ell)}_{ij}$ with $\mathbb{A}^{(\ell)}_{ij} = \int_0^R dr\, \chi_{n_i,\ell_i}(r)\chi_{n_j,\ell_i}(r)$. Hence the matrix $\mathbb{A}$ is diagonal in the variables $\mathbf{L}_i$, and the determinant factorises over the angular sectors [64]

$$\begin{aligned} P(R) &= \prod_{\ell=0}^{\ell_{\max}(\mu)} P_\ell(R)^{g_d(\ell)} \, , \\ P_\ell(R) &= \det_{1\le i,j\le m_\ell} \left[\delta_{ij} - \mathbb{A}^{(\ell)}_{ij}\right] \, , \end{aligned} \tag{1.130}$$

where $P_\ell(R)$ is the probability that the interval $[0, R]$ is empty in the ground state of m_ℓ noninteracting fermions described by the single particle Hamiltonian $\hat{H}_\ell$. Note that formulae (1.129) and (1.130) are valid for any central potential $V(r)$.

We start by studying the 1D radial problem to obtain $P_\ell(R)$ within each ℓ sector, and then we evaluate the product (1.130). For a general potential $V(r)$ this is a difficult problem, however in the case of the harmonic oscillator we can make further progress by using a connection to the random matrix theory [44, 94, 95]. Indeed in the case $V(r) = \frac{1}{2}r^2$, the potential (1.126) turns into (1.65) with $b = 1$, and the eigenfunctions are given by equation (1.66) with $\chi_{n,\ell}(r) = \phi_n(r)$, the eigenenergies are $\epsilon_{n,\ell} = 2n + a + 1$, where $a = \ell + \frac{d}{2} - 1$. The number of occupied states in the ground state within the ℓ sector is thus $m_\ell = \mathrm{Int}(\frac{\mu-\ell-d/2}{2} + 1)$, where $\mathrm{Int}(z)$ denotes the integer part of z (i.e., the floor function). Note that $m_\ell = 0$ for $\ell > \ell_{\max}(\mu) = \mu - \frac{d}{2}$ (where μ is integer for even d and half-integer for odd d).

We already saw that up to the change of variable $\{x_i^2\} = \{\lambda_i\}$, together with $m_\ell = N$ and $a = M - N = \ell + \frac{d}{2} - 1$, this is equivalent to the JPDF (1.13)

$$P_{WL}(\boldsymbol{\lambda}) = \frac{1}{\mathcal{Z}^{WL}_{M,N}} \prod_{i<j}(\lambda_i - \lambda_j)^2 \prod_{i,j\le N} \lambda_i^{M-N} e^{-b\sum_i \lambda_i} \tag{1.131}$$

which is in case of a positive integer $a = M - N$ (hence even dimension d) (see [96] for the case $M < N$) corresponds to LUE or WL ensemble.

The calculation of $P_\ell(R)$ is then equivalent to computing the cumulative distribution function (CDF) of the smallest eigenvalue $\lambda_{\min}$ in the WL ensemble,

i.e.

$$P_\ell(R) = \text{Prob}(\lambda_{\min} > R^2) \tag{1.132}$$

This CDF was studied in several works [61, 97–101] in RMT. In particular in [97] a useful determinantal formula was found in the case where $a = M - N$ is a positive integer. Translated into the fermion problem in the case of d an even integer, $P_\ell(R)$ is given by a $a \times a$ determinant (with $a = \ell + \frac{d}{2} - 1$). Together with (1.130) it gives an exact formula for the hole probability for N fermions in the d-dimensional harmonic potential, displayed in Eqs. (74) and (75) in [102]. It allows to plot the exact hole probability for a small number of fermions.

1.3.2 Large N limit: Microscopic and Macroscopic Regime

We now consider the limit of a large number of fermions, $N \gg 1$, equivalently large Fermi energy. In this limit there are two distinct regimes, a microscopic and a macroscopic one. The mean density of fermions is given by the LDA (1.89) (or its generalisation in dimension d)

$$\rho(r) = c_d k_F(r)^d, \quad c_d = \frac{1}{2^d \pi^{d/2} \Gamma(1 + d/2)}, \quad k_F(r) = \sqrt{2\mu - r^2} \tag{1.133}$$

for the harmonic oscillator [17]. Near the center of the trap, the typical distance between particles is thus $1/k_F(0) = 1/\sqrt{2\mu}$, which defines the microscopic scale, $R = O(1/k_F(0))$. On the other hand, the edge of the Fermi gas is a sphere of macroscopic radius $R_e = \sqrt{2\mu} \gg 1/k_F(0)$ which defines the macroscopic scale, $R = O(R_e)$.

Free Fermions and Microscopic Regime. We first obtain, in the case of free fermions (i.e., $V = 0$), an exact formula for the probability $P(R) = \mathsf{P}_d(k_F R)$ (in the ground state). Here $k_F = \sqrt{2\mu}$ is the Fermi wave vector and μ is the Fermi energy. Before giving details of the derivation, we write the main result. The scaling function $\mathsf{P}_d(z)$ can be expressed as a product of Fredholm determinants associated to the so-called hard edge Bessel kernel, well known in random matrix theory (RMT), see Eqs. (1.136), (1.137), (1.138) below. Its asymptotic behaviour at small distance is given as $z \to 0$ by

$$\boxed{\mathsf{P}_d(z) = 1 - B_d z^d + \frac{d}{(d+2)^2} B_d^2 z^{2d+2} + O(z^{3d+2}, z^{2d+4})} \tag{1.134}$$

with $B_d = \frac{1}{2^d \Gamma(1+\frac{d}{2})^2}$ (see [102] for higher orders), which generalizes the result for $d = 1$ in which case the level spacing distribution is given by $p(s) \propto \mathsf{P}_1''(s)$.

At large distance one finds that the hole probability decays super-exponentially

$$\boxed{\mathsf{P}_d(z) \underset{z\to\infty}{\sim} \exp(-\kappa_d z^{d+1}) \ , \ \kappa_d = \frac{2}{(d+1)^2 \Gamma(d+1)} \ .} \tag{1.135}$$

This result agrees for $d \to 1$ with $\kappa_1 = \frac{1}{2}$ obtained in [87]. The plot of $-\frac{d}{dz}\mathsf{P}_d(z)$ is shown in Fig. 1.7 and represents the scaled probability density of

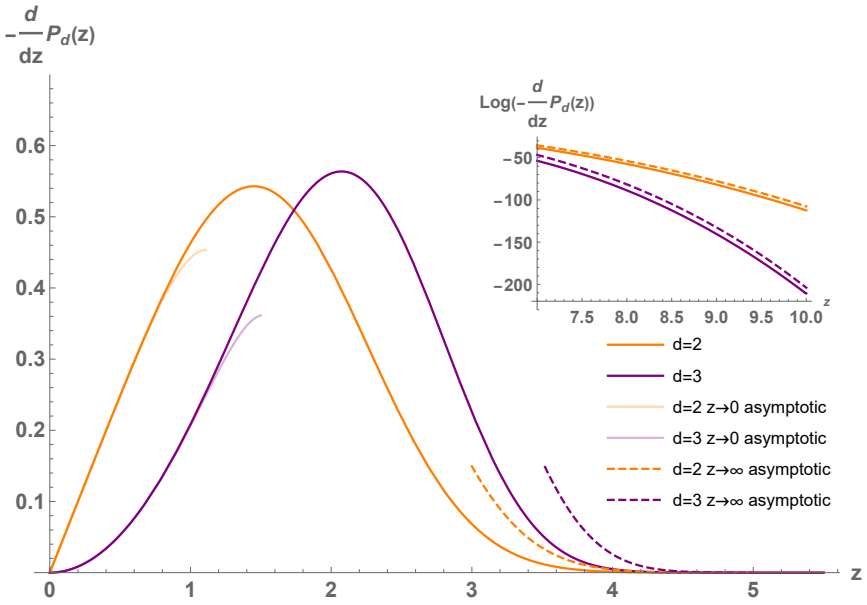

FIGURE 1.7: Plot of $-\frac{d}{dz}\mathsf{P}_d(z)$ vs. z in dimension $d = 2, 3$ from a numerical evaluation (thick line) of (1.138) using (1.136). At small z it is well described by the asymptotics (lighter line) from (1.134). **Inset**: same plot in semi-logarithmic scale, which fits well with the large z super-exponential behavior in (1.135).

dimension d	numerics [104]	exact result
$d = 1$	0.5	$\frac{1}{2}$
$d = 2$	0.1175 ± 0.0007	$\frac{1}{9} = 0.1111$
$d = 3$	0.02287 ± 0.0003	$\frac{1}{48} = 0.02083$
$d = 4$	0.00392 ± 0.00015	$\frac{1}{300} = 0.00333$

TABLE 1.1: Comparison between our exact result (1.135) for κ_d (last column) and the numerical estimates of Ref. [104].

the position of the fermion closest to the origin. We can also compare these results with the numerical data analysis of [103, 104] for free fermions. In that work the power law z^{d+1} in the exponential was conjectured to hold in all dimensions, and the coefficient κ_d was measured numerically. The comparison with our analytic prediction is presented in Table 1.1. Although the agreement is quite good the exact values lie somewhat outside of the error bars, which suggests that obtaining numerically the true asymptotic requires larger values of z.

In the microscopic regime (Harmonic potential) we find that the hole probability takes the scaling form $P(R) \simeq \mathsf{P}_d(k_F(0)R)$, where $\mathsf{P}_d(z)$ is the same universal scaling function as obtained above for free fermions, with a non universal scale $1/k_F(0)$. This universality extends to any microscopic sphere located anywhere inside the bulk in the presence of a general smooth potential. For a sphere centered around $\mathbf{x}$, $k_F(0)$ is replaced by $k_F(r = |\mathbf{x}|)$ defined in (1.133).

In order to show how we get this result we must come back to the decomposition in angular sectors (1.130) and (1.132). Since μ is large in each sector the number of fermions $m_\ell \simeq (\mu - \ell)/2$ is also large. It is easy to see that only sectors with $\ell = O(1)$ contribute to the product in (1.130). Indeed, the centrifugal energy $(a^2 - 1/4)/(2r^2)$ in $V_\ell(r)$ in (1.126) must remain at most of $O(\mu)$, and therefore for $r \sim 1/\sqrt{\mu}$ only values of $a = O(1)$ are allowed. Hence one can approximate $m_\ell \simeq \mu/2$ for all ℓ in that regime. Note that the potential term $V(r) = \frac{1}{2}r^2$ is negligible, hence it is identical to free fermions.

This regime corresponds in the RMT context to the so-called hard edge scaling regime, see (1.80). In that regime the m_ℓ eigenvalues of the WL ensemble of parameter a, with m_ℓ large, are of order $\lambda_i = O(1/m_\ell)$. More precisely, the scaled eigenvalues $b_i = 4m_\ell\lambda_i$ follow the Bessel process of order $a = \ell + d/2 - 1$, described by the kernel (1.81). where $J_a(z)$ is the Bessel function of index a. The hole probability in the ℓ sector is given as a Fredholm determinant [55, 105]

$$F_a(b) := \mathrm{Prob}(b_{\min} > b) = \mathrm{Det}(I - K^{Be}_{a,[0,b]}) \ , \tag{1.136}$$

where $b_{\min} = \min_i b_i$ and $P_{[0,b]}$ is the projector on the interval $[0, b]$. We recall that this FD can be expressed as $\log F_a(b) = -\int_0^b \frac{ds\,\sigma(s)}{s}$ from the solution $\sigma(s)$ of the Painlevé III equation (1.108) with the asymptotic $\sigma(s) \simeq \frac{s^{1+a}}{2^{2a+2}\Gamma(1+a)\Gamma(2+a)}$ at small s. For even space dimension d, i.e., integer a, as discussed above, there are other representations for the hole probability, which in this microscopic regime lead to the remarkably simple formula [97]

$$F_a(b) = e^{-b/4} \det_{1\le j,k\le a} I_{j-k}(\sqrt{b}) \ , \tag{1.137}$$

where $I_n(x)$ is the modified Bessel function. Using formula (1.130), we obtain that in this scaling regime, the hole probability $P(R)$ for the fermions in any dimension d, takes the scaling form $P(R) \simeq \mathsf{P}_d(k_F(0)R)$, where the scaling function is given as an infinite product

$$\mathsf{P}_d(z) = \prod_{\ell=0}^{+\infty} F_{\ell+\frac{d}{2}-1}(z^2)^{g_d(\ell)} \ . \tag{1.138}$$

This result, which we derived for the harmonic oscillator (with $k_F(0) = \sqrt{2\mu}$) holds asymptotically for large N for any smooth trapping potential. In addition, it is *exact* for free fermions in d dimensions, with $k_F = \sqrt{2\mu}$. Note that for free fermions, an alternative formula exists using the d-dimensional extension of the sine-kernel [17, 103]

$$K_d(\mathbf{r}, \mathbf{r}') = \frac{J_{d/2}(|\mathbf{r} - \mathbf{r}'|)}{(2\pi|\mathbf{r} - \mathbf{r}'|)^{d/2}}. \tag{1.139}$$

The hole probability is given as a Fredholm determinant

$$\mathsf{P}_d(z) = \boxed{\mathrm{Det}(I - K_{d,|\mathbf{r}|<z}) = \prod_{\ell=0}^{+\infty} \mathrm{Det}(I - K^{Be}_{\ell+d/2-1,[0,z^2]})^{g_d(\ell)}} \tag{1.140}$$

where $K_{d,|\mathbf{r}|<z}$ is the previous kernel restricted to $|\mathbf{r}| < z$. We found that the formulae (1.138) and (1.140) are in fact equivalent which is not a trivial property. Both formulae can be expanded in small z, leading to Eq. (1.134) and pushed to higher orders in [102]. While the expansion of (1.140) is straightforward, expanding (1.138) requires to solve the Painlevé III equation at small arguments. The formula (1.138) however allows to study the asymptotic behavior of P(z) at large z, as we now show.

In the large z limit one needs the asymptotics of $F_a(b)$ at large b. One can check [102] that the asymptotics of the infinite product in (1.138) is dominated by large values of ℓ, for which the decay of $F_a(b)$ occurs on scale $b \sim \ell^2$. This double limit for (1.137) was studied, using Coulomb gas techniques, in the context of lattice QCD in [106, 107] and later in the study of the longest increasing subsequence of random permutations [108] (see also [92]) and it was shown to take the scaling form (with $a \sim \ell$)

$$\boxed{\begin{aligned} &F_a(b) \sim \exp\left[-\ell^2 \phi_+\left(\gamma = \frac{\sqrt{b}}{\ell}\right)\right] , \\ &\phi_+(\gamma) = \theta(\gamma-1)\left(\frac{\gamma^2}{4} - \gamma + \frac{1}{2}\log\gamma + \frac{3}{4}\right) , \end{aligned}} \tag{1.141}$$

where $\theta(x)$ is the Heaviside function. Inserting this expression into (1.138), approximating the sum over ℓ by an integral, using $g_d(\ell) \simeq \frac{2\ell^{d-2}}{\Gamma(d-1)}$ at large ℓ, one obtains

$$\mathsf{P}_d(z) \sim \exp\left[-\frac{2}{\Gamma(d-1)}\int_0^{+\infty} d\ell \ell^d \phi_+\left(\frac{z}{\ell}\right)\right] \tag{1.142}$$

leading to our main result (1.135), with $\kappa_d = \frac{2}{\Gamma(d-1)}\int_1^{+\infty}\frac{d\gamma}{\gamma^{d+2}}\phi_+(\gamma) = \frac{2}{(d+1)^2\Gamma(d+1)}$. Note that the calculations of [106, 108] use the formula (1.137) valid only for even d, however we obtained (1.141) in any d using the Painlevé equation [102].

Macroscopic Regime. The microscopic regime previously presented describes typical fluctuations of the hole. Now we want to study the macroscopic fluctuations of the hole, that is the regime of large deviation. In one dimension, this was done using the Coulomb gas method, here we will see that the decomposition in angular sectors, allows to recast the problem in term of Coulomb gas. In the case of a hole of macroscopic size, $R = O(R_e)$ the probability $P(R)$ is very small and is characterized by a large deviation form

$$\boxed{P(R) \sim \exp\left(-(k_F(0)R_e)^{d+1}\Psi(\tilde{R} = R/R_e)\right)} \tag{1.143}$$

where the rate function $\Psi(\tilde{R})$ is not universal and depends on some details of the potential $V(r)$. Here we calculate it explicitly in the case of the harmonic potential $V(r) = \frac{1}{2}r^2$, in which case $R_e = \sqrt{2\mu} = k_F(0)$. The function $\Psi(\tilde{R})$ is given in (1.148) and plotted in Fig. 1.8. It is related to the large deviations in the WL ensemble of random matrices (see Section 1.2.8 [92]). Its behavior at

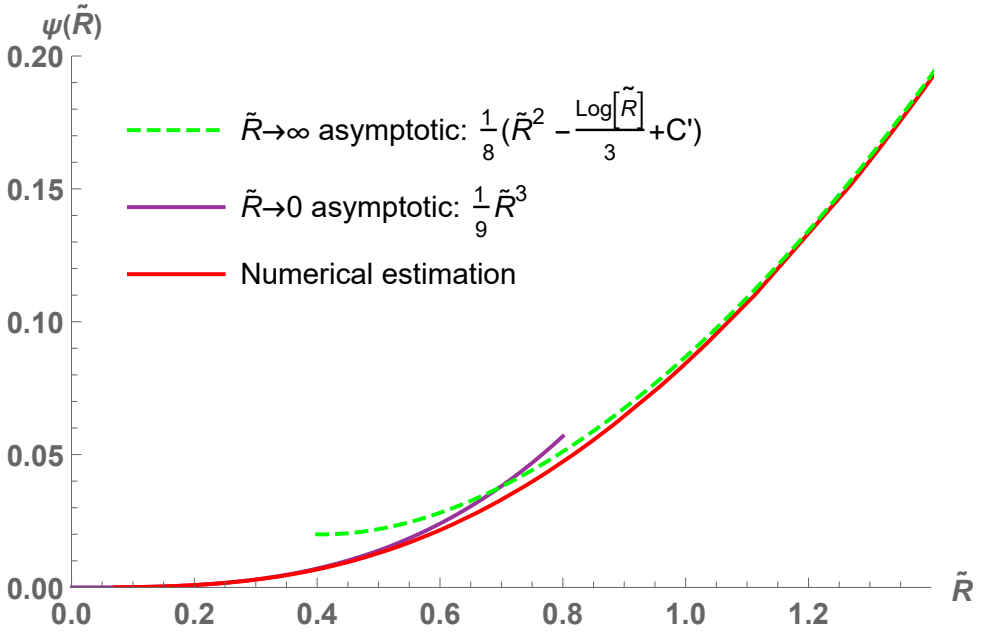

FIGURE 1.8: Large deviation function $\Psi(\tilde{R})$ vs. $\tilde{R} = \frac{R}{\sqrt{2\mu}}$ in dimension 2. The numerical evaluation (Red line) compares well with the small $\tilde{R}$ asymptotic (Purple line) itself matching with Eq. (1.135), and(1.144). It also fits well to the large $\tilde{R}$ behavior (Green line) from Eq. (1.145).

small argument is found to be

$$\boxed{\Psi(\tilde{R}) \underset{\tilde{R}\to 0}{\simeq} \kappa_d \tilde{R}^{d+1}} \tag{1.144}$$

which matches smoothly with the large distance behavior from microscopic scales, see Eq. (1.135). For large $\tilde{R}$ it behaves as

$$\boxed{\Psi(\tilde{R}) \underset{\tilde{R}\to\infty}{\simeq} \frac{1}{2^d \Gamma(d+1)} \tilde{R}^2 - \frac{d-1}{2^d \Gamma(d+2)} \ln \tilde{R}} \tag{1.145}$$

and in $d = 1$ it is exactly $\Psi(\tilde{R}) = \frac{1}{2}\tilde{R}^2$, as found for GUE matrices [53, 102].

Let us give more details on the derivation. Since μ is large, in each angular sector the number of fermions is again $m_\ell \simeq (\mu - \ell)/2$, however in this regime the product in (1.130) is controlled by the values of $\ell = O(\mu)$. We saw already (see Fig. 1.4) that in this regime the spectrum of the WL matrices has support on the interval $[N\zeta_-, N\zeta_+]$ with $\zeta_\pm = (1 \pm \frac{1}{\sqrt{c}})^2$. The correspondence with fermions shows that within each ℓ sector, the mean fermion density $\rho_\ell(r)$ has support $[r_-(\ell), r_+(\ell)]$ with

$$r_\pm(\ell)^2 = \lambda_\pm = m_\ell \zeta_\pm \simeq \mu \pm \sqrt{\mu^2 - \ell^2}. \tag{1.146}$$

For each sector ℓ, there are a priori three different scaling regimes for $P_\ell(R) = \text{Prob}(\lambda_{\min} > R^2)$ when $R = O(\sqrt{\mu})$ and $\ell = O(\mu)$. Indeed, we mentioned

previously that the smallest eigenvalue λ_{min} of a WL random matrix (1.131) exhibits three regimes [89]. We came to the conclusion that the product (1.130) is dominated by the angular sectors that are described by the pushed Coulomb gas regime. In that case, following Section 1.2.8, we see that $P_\ell(R)$ reads

$$P_\ell(R) \sim e^{-2m_\ell^2 \Phi_+\left(\frac{R^2-m_\ell \zeta_-}{m_\ell}, \frac{\ell}{m_\ell}\right)} \tag{1.147}$$

In computing the logarithm of (1.130), the sum is truncated up to ℓ_{max} such every angular sectors in the pushed Coulomb gas regime are taken into account. Then we approximate the sum over ℓ by an integral and $g_d(\ell) \simeq \frac{2\ell^{d-2}}{\Gamma(d-1)}$. Performing the change of variable $v = \ell/\mu$ we obtain the large deviation formula for the hole probability in the form (1.143) with $k_F(0)R_e = 2\mu$ and $\tilde{R} = R/\sqrt{2\mu}$ with the rate function

$$\boxed{\Psi(\tilde{R}) = \int_0^{v_{\max}(\tilde{R})} dv\, \frac{v^{d-2}(1-v)^2}{2^{d+1}\Gamma(d-1)} \Phi_+\left(\frac{4\tilde{R}^2}{1-v} - (1-\sqrt{1+\alpha_v})^2, \alpha_v\right)} \tag{1.148}$$

where $\alpha_v = \frac{2v}{1-v}$ and $v_{\max}(\tilde{R}) = 2\tilde{R}\sqrt{1-\tilde{R}^2}$ for $\tilde{R}^2 < 1/2$ and $v_{\max}(\tilde{R}) = 1$ for $\tilde{R}^2 > 1/2$. The function $\Phi_+(z, \alpha)$ being quite complicated, the integral in (1.148) has been evaluated numerically in Fig. 1.8. It exhibits a transition of high order at $\tilde{R} = 1/\sqrt{2}$ [1] and the asymptotics of $\Psi(\tilde{R})$ can be extracted (see [102]) resulting in (1.144), and (1.145).

1.3.3 Numerical evaluation of the free fermion hole probability

To evaluate numerically the free fermion hole probability $\mathsf{P}_d(z)$ we need to evaluate the product of Fredholm determinants in Eq. (1.138) associated to the Bessel process where $F_a(b = z^2)$ is given in (1.136). This was performed using the Bornemann's method, an algorithm that allows to compute such determinant in an efficient manner [109]. At this point one has to tune parameters on which the precision of the result depends. We made sure that those parameters ensure high enough precision by running multiple numerical tests. Because we cannot compute an infinite number of determinants, we use the fact that for a given z, high enough ℓ does not influence the total product. In practice, we cut the product at $\ell = \ell_{\max}(z) = \mathrm{Int}(1.1\sqrt{z})$ and checked that the product converges when $\ell_{\max}(z)$ goes from 0 to $\mathrm{Int}(1.1\sqrt{z})$. For $z < 16$ we just set $\ell_{\max}(z) = 4$.

[1] A detailed calculation shows that the transition is of sixth order, i.e., the sixth derivative is discontinuous.

Article 1

Hole Probability for Noninteracting Fermions in a d-dimensional Trap [1]

Abstract. The hole probability, i.e., the probability that a region is void of particles, is a benchmark of correlations in many body systems. We compute analytically this probability $P(R)$ for a sphere of radius R in the case of N noninteracting fermions in their ground state in a d-dimensional trapping potential. Using a connection to the Laguerre-Wishart ensembles of random matrices, we show that, for large N and in the bulk of the Fermi gas, $P(R)$ is described by a universal scaling function of $k_F R$, for which we obtain an exact formula (k_F being the local Fermi wave-vector). It exhibits a super exponential tail $P(R) \propto e^{-\kappa_d (k_F R)^{d+1}}$ where κ_d is a universal amplitude, in good agreement with existing numerical simulations. When R is of the order of the radius of the Fermi gas, the hole probability is described by a large deviation form which is not universal and which we compute exactly for the harmonic potential. Similar results also hold in momentum space.

Chapter 2

Non-equilibrium Dynamics of Noninteracting Fermions in Presence of a Defect.

In Chapter 1, we discussed the equilibrium properties of noninteracting fermions in one dimension. In the simplest cases, this was done by solving the time-independent Schrödinger equation,

$$\hat{H}\phi = \epsilon\phi, \tag{2.1}$$

where,

$$\hat{H} = -\frac{\partial_x^2}{2m} + \hat{V}, \tag{2.2}$$

is the one-particle Hamiltonian, leading to a set of eigenfunctions and eigenenergies $\{\epsilon_k, \phi_k\}$ with $k = 1, 2, 3...$ such that the ground state is ϕ_1. From this knowledge we demonstrated how the kernel can be built. For example we gave the kernel in the ground state of the system with N fermions

$$K(x, x') = \sum_{k=1}^{N} \phi_k^*(x)\phi_k(x'). \tag{2.3}$$

Then we demonstrated how the kernel allows us to compute many interesting quantities, such as the particle density, the n-point correlations Eq. (1.46), the FCS Eq. (1.94) and the entanglement entropies Eq. (1.96).

Now we turn our attention to the non-equilibrium problem that arises from the time-dependent Schrödinger equation

$$i\hbar\partial_t\phi = \hat{H}\phi. \tag{2.4}$$

Because the Hamiltonian in Eq. (2.2) is quadratic in the creation/annihilation operators and does not involve any interactions, the determinantal structure of the system remains unaffected. This means that the n-point correlation functions at time t can be computed using equation (1.46) together with the

following time-dependent kernel

$$K(x,x';t)=\sum_{k=1}^{N}\phi_k^*(x,t)\phi_k(x',t), \tag{2.5}$$

where $\phi_k(x,t)$ is the solution of Eq. (2.4) with initial condition $\phi_k(x,t=0)=\phi_k(x)$. Hence, in the non-equilibrium context, the kernel still allows for the computation of various interesting quantities such as n-point correlation functions, density, FCS, and entanglement entropies. Hence, the time-dependent kernel will be a central object to this chapter.

Additionally to those quantities, non-equilibrium problems are characterised by non zero currents. For example, the particle current is defined as

$$J(x,t)=\frac{1}{2i}\sum_{k=1}^{N}\left[\phi_k^*(x,t)\partial_x\phi_k(x,t)-\partial_x\phi_k^*(x,t)\phi_k(x,t)\right] \tag{2.6}$$

It turns out to have a simple expression in term of time dependent kernel

$$J(x,t)=\frac{1}{2i}\left[(\partial_y-\partial_x)K(x,y;t)\right]_{y=x}. \tag{2.7}$$

From the Schrödinger equation, the current $J(x,t)$ satisfies the conservation equation for the fermion number

$$\partial_t\rho(x,t)+\partial_x J(x,t)=0\,, \tag{2.8}$$

where $\rho(x,t)=K(x,x;t)$ is the time dependent density. Similarly, the continuity equation for the energy density can be obtained from the kernel (2.172).

Quenches. The study of out of equilibrium quantum dynamics is very vast. Here we will focus on one simpler set-up that has attracted a lot of attention in the community both from the theoretical and the experimental perspective [23, 110–112], namely quantum quenches. Typically, we start the system in the ground state, or thermal state $|\psi_{t=0}\rangle$ of some Hamiltonian $\hat{H}_0$. Then, we allow the system to evolve with the time-dependent Hamiltonian $\hat{H}(t)=\lambda(t)\hat{H}_0+(1-\lambda(t))\hat{H}$, where $\lambda(t)$ is a function that goes from one to zero in a very short time and then remains to zero. This means that we quickly transit from $\hat{H}_0$ to $\hat{H}$

$$\hat{H}_0\underset{\delta t}{\to}\hat{H} \tag{2.9}$$

We say that the Hamiltonian is quenched. Of course the nature of the quench can be varied. Sometimes an interaction is changed [26, 113]. Different kind of systems can be studied, for example Luttinger liquids [114, 115] led to interesting results [33, 116–121], critical system have been investigated using CFT tools [121–125]. The quench can be performed either on an integrable system [126–128] which can yields exact computations, or on a non integrable system [129, 130].

One simple case is the homogeneous quench in which both $\hat{H}_0$, and $\hat{H}$ are space translation invariant. In the absence of translational invariance things

get more complicated and quenches can be split in two main categories.

- One with initial inhomogeneous Hamiltonian. For example, the initial state can be the equilibrium state of a Hamiltonian with some trapping potential. Then, if the trapping potential is suppressed at initial time, we will speak of a trap release [131–133]. Among those one dimensional inhomogeneous initial Hamiltonian quench protocol, one will be of particular interest for us, the partitioning protocol [24, 31, 36, 134–139]. In that case, the initial Hamiltonian $\hat{H}_0$ is built such that the initial state is a tensor product of left half and right half state

$$|\psi_{t=0}\rangle = |\psi_R\rangle \otimes |\psi_L\rangle \,. \tag{2.10}$$

  In the case of spin chains or lattice, this can be achieved when the Hamiltonian $\hat{H}_0$ is the sum of two Hamiltonians, one for the right half of the system and one for the left half

$$\hat{H}_0 = \hat{H}_R + \hat{H}_L \tag{2.11}$$

  while in the continuum, the initial Hamiltonian would contain a non-penetrable potential barrier $\hat{V}$.

$$\hat{H}_0 = \hat{H}'_0 + \hat{V} \tag{2.12}$$

  Each state $|\psi_{R/L}\rangle$ would typically be a thermal state, hence characterised by left and right inverse temperatures $\beta_{R/L}$, and chemical potentials $\mu_{R/L}$. Then the Hamiltonian is quenched in such a manner that the left and right part are not independent anymore, which might lead to non zero flows breaking equilibrium. In this context one can study the statistics at the edge of the propagating front [40, 74]

- The second category is when the post quench Hamiltonian $\hat{H}$ is inhomogeneous. This can typically be done by switching on a local defect [123, 140–143].

Remark. Here we will study a quench that belongs to both categories, and we will show that a new effect arises that was not present in each case taken alone.

From here many questions arise. For example does the system relax to some non-equilibrium Steady State (NESS), that is a state with stationary mean values for observable $\langle \hat{O} \rangle$. If so is it described by a GGE, does it have non zero currents, how to characterise the correlations in such state? One of the additional element of the quench set-up is of course the dynamic, i.e. how does the system approach the NESS? If one prepares the system with an empty left initial state, arises the question of the FCS of the number of particles $N_{[x,+\infty[}$ that has crossed the position x [40, 74]. This eventually also brings up the question of the entanglement entropy dynamics.

Integrable Systems. Before diving into the details of our system of interest, we want to give a little context. A very particular property of free fermions is that each particle conserves its energy and momentum, which places them

in the wider category of systems known as integrable systems. Classically, integrable systems are characterized by having enough conserved quantities that the dynamics are restricted to a submanifold of the phase space, leading to periodic or quasi-periodic behavior. For integrable quantum systems with many degrees of freedom, an exciting theory in construction postulates the emergence of a new kind of hydrodynamic theory [35, 36]. Here, following [144–146] we will give a brief introduction to this theory called Generalised Hydrodynamics (GHD).

2.1 Generalised Hydrodynamics

2.1.1 Thermalisation and the Gibbs Ensemble

Thermalization of Classical Systems. A question that emerged as a consequence of equilibrium statistical mechanics is whether a many-body system, initialized far from equilibrium, will or will not relax towards equilibrium. Whether we speak of classical or quantum systems, the consensus is that integrable systems are very peculiar as they do not thermalize, whereas non-integrable systems are expected to thermalize. Following [147], we start by giving a brief description of the mechanism of relaxation for non-integrable systems. Let us focus first on the thermalization of classical systems. A system is said to be Liouville non-integrable if the Hamiltonian system has strictly more degrees of freedom than global first integrals of motion. This is a necessary and, in most cases, sufficient condition for the system to be chaotic, which means that phase space trajectories with close initial conditions exponentially spread with time, making long-term predictions impossible. This is illustrated on Fig. 2.1 where we represent the motion of a particle in two two-dimensional cavities. The system on the right has two degrees of freedom and only one conserved quantity (the energy), making it non-integrable. The system on the left, however, has an additional conserved quantity (angular momentum) and is therefore integrable. We can observe that in the integrable case, the motion exhibits regular patterns. On the other hand, in the non-integrable case, the motion is completely erratic, and trajectories with close initial conditions quickly become uncorrelated in terms of position and direction after a few bounces. In this framework, the mechanism typically used to explain thermalization is ergodicity. A classical ergodic system is one in which trajectories $X(t)$ in phase space (or equivalently, the microstate space) with initial condition $X(0)$ uniformly and randomly explore the entire phase space. For an isolated system, this means that for a trajectory of fixed energy E the time average $\overline{O(X(t))} = \lim_{\tau\to\infty} \frac{1}{\tau}\int_0^\tau dt O(X(t))$ is equivalent to the microcanonical average of the observable $\langle O\rangle_{ME} = \frac{1}{\mathcal{V}}\int_{H(X)\in[E,E+dE]} dX O(X)$ where $H(X)$ is the energy of the phase space point, and $\mathcal{V}$ is the volume of the space over which the integral is performed

$$\overline{O(X)} = \langle O\rangle_{ME}\,. \tag{2.13}$$

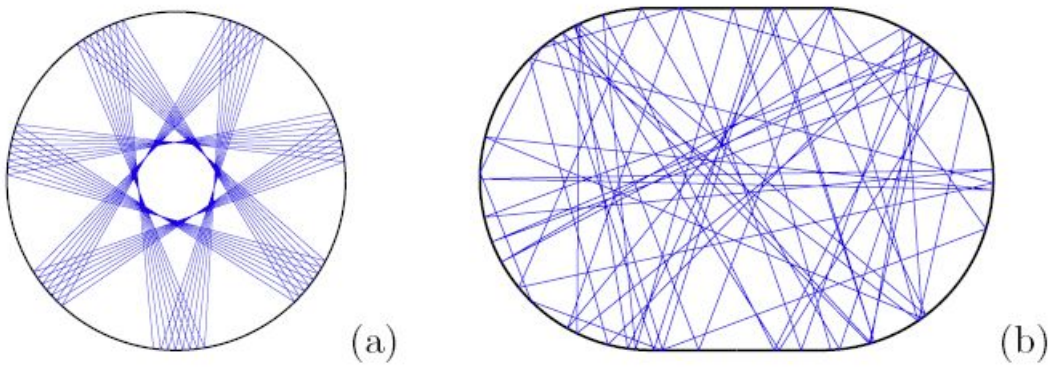

FIGURE 2.1: (a) Trajectory in a circular billiard, the system is integrable. (b) Trajectory in the Bunimovich stadium. Angular momentum is no more conserved, hence the motion is chaotic. The figure originates from [148]

Crucially, this implies that the time average is independent of the initial microstate $X(0)$, and we recover the expected properties of thermodynamic. However, proving ergodicity for a given system can be a challenging task, and it has been achieved for only a few systems. Examples of systems which where proven to be ergodic are two hard balls in a d-dimensional ($d \geq 2$) rectangular box [149], and a particle on the two dimensional torus with a central potential [150]. More recently, the ergodicity hypothesis has been questioned as some non-ergodic systems seem to exhibit statistical mechanics properties [151].

While the thermalization of classical systems remains an open question, it can also be asked in the framework of quantum mechanics.

Observable needs to be local. For now, we assume the system to be homogeneous in the initial state $|\psi(0)\rangle$ and with homogeneous Hamiltonian. At the initial time, we quench (or turn on) the Hamiltonian $\hat{H}$ governing the system's evolution. The evolution of the state is given by $|\psi(t)\rangle = \sum_k c_k e^{-i\epsilon_k t} |\psi_k\rangle$, where $\{\epsilon_k, |\psi_k\rangle\}$ are the eigenenergies and eigenstates of $\hat{H}$, and $c_k = \langle\psi_k|\psi(0)\rangle$ are the overlap between the initial state and the eigenstates. Often, we start by defining the system at finite size L, then, in order to recover statistical properties, we take the thermodynamic limit, that is the large system size limit. Now, given a local observable $\hat{O}$, we want to know if it is going to relax in the thermodynamic and large-time limit, i.e. if its mean value has a well-defined limit $\lim_{t\to\infty}\lim_{L\to\infty} \langle\hat{O}\rangle_t$. Then if we have relaxation, the second question is to know if this large time limit reproduces statitical mechanics ensembles. The mean value of the observable $\hat{O}$ at time t is given by

$$\langle\hat{O}\rangle_t = \sum_{k,k'} c_k^* c_{k'} e^{i(\epsilon_k - \epsilon_{k'})t} O_{k,k'} \tag{2.14}$$

with $O_{k,k'} = \langle\psi_k|\hat{O}|\psi_{k'}\rangle$. Because the dynamic of the quantum system under consideration is unitary, it is a bit optimistic to believe that every observable will relax. Indeed, if we take $\hat{O} = |\psi_1\rangle\langle\psi_2| + |\psi_2\rangle\langle\psi_1|$ which is a well defined

observable. Then it is immediate to see that its mean value will have remanent oscillations at large time with pulsation $\omega = \epsilon_2 - \epsilon_1$. The particular property of such observable is that it is highly non-local. In order to observe relaxation, we restrict our study to observable $\hat{O}_A$, local in the sense that it acts as identity outside some finite support A. The physical intuition behind the relaxation of local observables is that the complement A^c of the support acts as a bath i.e. as an infinite system on the subsystem A. This justification also emphasizes the necessity of considering the thermodynamic limit.

ETH. The relaxation of local observables still remains an open question. However, the beginning of an answer emerged in the 90s with two papers by Deutsch and Srednicki [152, 153], introducing the concept of the Eigenstate Thermalization Hypothesis (ETH).
ETH is an ansatz for the matrix elements of an observable $\hat{O}$ in the eigenbasis of a Hamiltonian that reads

$$O_{k,k'} = O(E_{k,k'})\delta_{k,k'} + e^{-\mathcal{S}(E_{k,k'})/2} f_O(E_{k,k'}, \omega_{k,k'}) R_{k,k'}, \tag{2.15}$$

where $\mathcal{S}(E)$ is the thermodynamic entropy at energy E, $E_{k,k'} = \frac{E_k + E_{k'}}{2}$, $\omega_{k,k'} = E_{k'} - E_k$. Additionally, $O(E)$ and $f_O(E, \omega)$ are smooth functions. $O(E)$ is identical to the expectation value in the Microcanonical Ensemble (ME) at energy E and $R_{k,k'}$ is a real or complex normal random variable with mean zero and unit variance. The random elements $R_{k,k'}$ depends on the symmetry of the Hamiltonian. If the Hamiltonian has time reversal symmetry they are real, otherwise they are complex. The typical behaviour of an observable following ETH is illustrated in Fig. 2.2. Following [147] we can start understanding

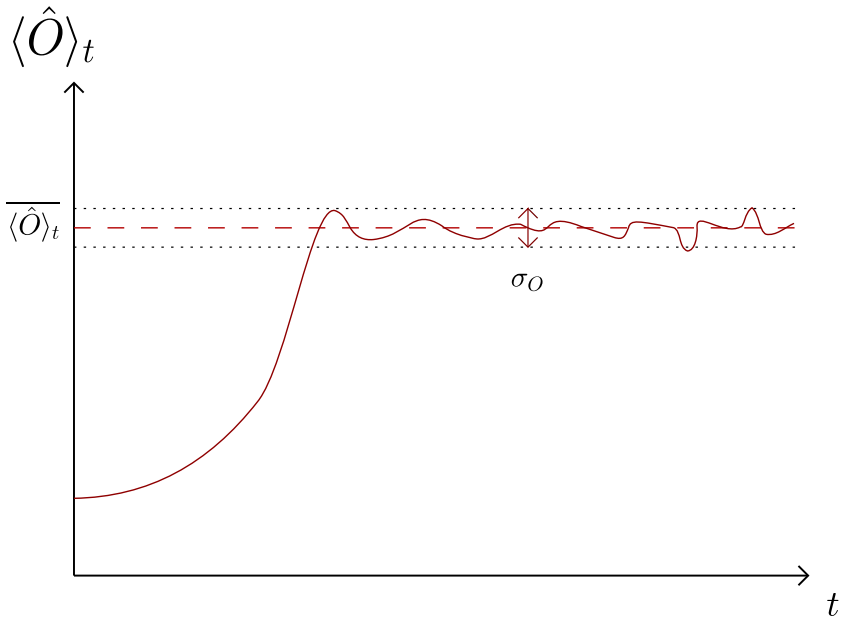

FIGURE 2.2: Typical behaviour of the mean value $\langle \hat{O} \rangle_t$ of an observable following ETH. The mean value approaches its time average and the oscillations around this time average are exponentially small in the system size.

relaxation by looking at the time average defined in Eq. (2.13) which kills the off-diagonal part of Eq. (2.14)

$$\overline{\langle \hat{O} \rangle_t} = \sum_k O_{k,k} |c_k|^2. \tag{2.16}$$

This is called the Diagonal Ensemble (DE) and it is defined by the density matrix

$$\hat{\rho}_{DE} = \sum_k |c_k|^2 \, |\psi_k\rangle \, \langle \psi_k| \, . \tag{2.17}$$

Then if the energy fluctuations in the diagonal ensemble are sufficiently small, the time average of $\langle \hat{O} \rangle_t$ will coincide with the Microcanonical Ensemble whose density matrix is given by $\hat{\rho}_{ME} = \sum_{E_k \in [E, E+dE]} |\psi_k\rangle \, \langle \psi_k|$

$$\overline{\langle \hat{O} \rangle_t} \simeq O(\langle E \rangle) \simeq O_{ME}. \tag{2.18}$$

Furthermore, the long time average of the temporal fluctuations can be computed, and proven to be smaller that the exponential of the entropy

$$\sigma_O^2 = \lim_{\tau \to \infty} \frac{1}{\tau} \int_0^\tau dt \, \langle \hat{O} \rangle_t^2 - \left(\frac{1}{\tau} \int_0^\tau dt \, \langle \hat{O} \rangle_t^2 \right)^2 \tag{2.19}$$

$$= \sum_{k \neq k'} |O_{k,k'}|^2 |c_k|^2 |c_{k'}|^2 \tag{2.20}$$

$$\leq max_{k,k'} |O_{k,k'}|^2 \simeq e^{-\mathcal{S}(E_{k,k'})}. \tag{2.21}$$

Because the entropy is an extensive quantity, we conclude that the long time average of the temporal fluctuations are exponentially small in the system size. In that sense, ETH gives a better understanding of thermalisation.

Connection to Random Matrix Theory. This being said we would like to have an intuition on which systems verify ETH. The answer lies in RMT. Indeed, it has been argued [9, 152] that fro quantum chaotic systems, the spectrum of the Hamiltonian locally mimics the local statistical properties of GOE (or GUE if time reversal symmetry is broken) spectrum, such that the spacing distribution follows the Wigner surmise. Knowing this, let us compute the average $\langle O_{k,k'} \rangle_{GOE}$ of $O_{k,k'}$ over a GOE (resp GUE) of size N. The observable can be diagonalised as $\hat{O} = \sum_i O_i \, |i\rangle \, \langle i|$ such that $O_{k,k'} = \sum_i O_i \, \langle \psi_k | i \rangle \, \langle i | \psi_{k'} \rangle$. Then computing the mean and variance of the diagonal and off-diagonal $O_{k,k'}$ results from the properties of GOE (resp GUE) eigenvectors. This leads to the conclusion that

$$\langle O_{k,k'} \rangle_{GOE} = \begin{cases} \langle O \rangle_{GOE} \text{ if } k = k' \\ 0 \text{ if } k \neq k' \end{cases} \tag{2.22}$$

$$\langle |O_{k,k'}|^2 \rangle_{GOE} - |\, \langle O_{k,k'} \rangle_{GOE} \, |^2 = \begin{cases} O(N^{-1}) \text{ if } k = k' \\ \frac{1}{N} \langle O^2 \rangle_{GOE} \end{cases} \tag{2.23}$$

where $\langle O\rangle_{GOE} = \frac{1}{N}\sum_i O_i$, and $\langle O^2\rangle_{GOE} = \frac{1}{N}\sum_i O_i^2$, if we assume the eigenvalue O_i do not scale with N, we conclude that both $\langle O\rangle_{GOE}$ and $\langle O^2\rangle_{GOE}$ are of order one in N. One can check that this properties are reproduced by the following ansatz

$$O_{k,k'} \simeq \langle O\rangle_{GOE}\,\delta_{k,k'} + \sqrt{\frac{\langle O^2\rangle_{GOE}}{N}}\,R_{k,k'} \tag{2.24}$$

where $R_{k,k'}$ are random variables with zero mean and unit variance real for GOE and complex for GUE. The conclusion is that if the Hamiltonian is a true random matrix, $O_{k,k}$ is independent of k, and the off-diagonal terms $O_{k,k'}$ are exponentially small in the system size. One can clearly see the similarity with ETH (2.15). If the Hamiltonian was a true random matrix the system would relax, however, this RMT approach is not sufficient to describe real systems. The next step was done by Srednicki [153] who gave ETH, i.e. the generalization of the RMT prediction that is needed to describe observables in physical systems.

2.1.2 Integrable Systems and the Generalised Gibbs Ensemble (GGE)

Integrable systems do not thermalise. We saw that quantum many-body chaotic systems are expected to thermalize at large time. Now we will focus on integrable systems which on the contrary do not thermalize in large time. We give a short introduction to integrable systems and the so called GHD, i.e. the hydrodynamical theory of integrable systems following the review [144]. Those ideas started arising in the 2000s after the experimental realization of a quench for an integrable system [126]. In this experiment, the authors reproduce the equivalent of a quantum Newton's cradle where a rubidium gas contained in a one-dimensional harmonic trap is kicked into an initial non-equilibrium state. After many collisions, one would expect the gas to thermalize due to diffusive effect. However, the gas shows persistent oscillations, remaining as long as the system stays isolated. This can be explained by noticing that in the studied regime, the gas is well modeled by the Lieb-Liniger model (LL), which is an integrable model. In integrable models, thermalization cannot happen due to the presence of an infinite number of conserved charges.

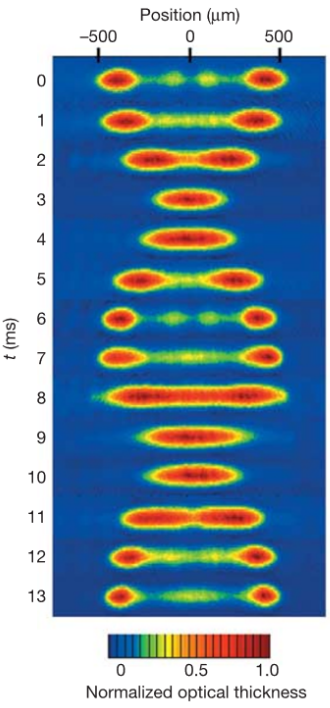

FIGURE 2.3: Absorption images in the first oscilation cycle of a quenched $1d$ Bose gas [126].

Generalized Gibbs Ensemble. Around the same time, theoretical considerations carried out in [34] gave intuitions on the long time behaviour of integrable systems. To be more precise, it was shown that these systems would

relax not to a thermal state, but that local observables would obey the statistics of the Generalized Gibbs Ensemble (GGE). This can be formulated as follows

$$\langle \hat{O}_A \rangle_{GGE} = \mathrm{Tr}[\hat{\rho}_{GGE} \hat{O}_A], \tag{2.25}$$

where $\hat{O}_A$ is the local observable of reference, and $\hat{\rho}_{GGE}$ is the density matrix defined as

$$\hat{\rho}_{GGE} = \frac{1}{Z_{GGE}} e^{-\sum_i \beta_i \hat{Q}_i}. \tag{2.26}$$

Here, Z_{GGE} is a normalization factor, and $\hat{Q}_i$ are the local conserved charges, i.e., charges that commute with the Hamiltonian and with each other

$$\begin{aligned} [\hat{H}, \hat{Q}_i] &= 0, \\ [\hat{Q}_i, \hat{Q}_j] &= 0. \end{aligned} \tag{2.27}$$

The charges are said to be local in the sense that $\hat{Q}_i = \int dx \hat{Q}_{i,x}$, where the integral (or the sum for discrete systems) is performed over all space and $\hat{Q}_{i,x}$ is a local observable as previously defined. The system is descibed by the generalized inverse temperatures β_i which are fixed by the initial condition, such that $\langle \hat{Q}_i \rangle_{GGE} = \langle \hat{Q}_i \rangle_{t=0}$ in order to satisfy conservation of charges.

Note also that relaxation to either the Gibbs Ensemble or the GGE can be expressed as an ergodic principle. This is achieved by assuming that in the final state, minimal information is retained about the initial state such that, one just needs to maximize the entropy of the systems. Then, for each conserved quantity, different Lagrange multipliers are introduced depending on which mean quantities are conserved. For example, in the canonical ensemble, where the mean energy is fixed, the Lagrange multiplier is the inverse temperature β. In the case of the GGE, the Lagrange multipliers are the generalized inverse temperatures β_i.

2.1.3 An example of Integrable Systems: Free Fermions

A simple example of an integrable system are free fermions with periodic boundary conditions. The Hamiltonian can be written in second quantization (for convenience, we work with $\hbar = 1$ and $m = 1$)

$$\hat{\mathcal{H}} = \int_{-L/2}^{L/2} dx \frac{1}{2} \partial_x \hat{c}_x^\dagger \partial_x \hat{c}_x, \tag{2.28}$$

where $\hat{c}_x$, and $\hat{c}_x^\dagger$ are the fermionic creation and annihilation field operators with the corresponding anti-commutation relation $\{\hat{c}_x, \hat{c}_y^\dagger\} = \delta(x-y)$, and the periodicity condition $\hat{c}_x = \hat{c}_{x+L}$. In first quantization it reads

$$\hat{H} = -\sum_{j=1}^{N} \frac{1}{2} \partial_{x_j}^2. \tag{2.29}$$

The Hamiltonian can be diagonalised in terms of the fermionic mode occupation operators

$$\hat{\mathcal{H}} = \sum_{k=-\infty}^{\infty} \frac{k^2}{2} \hat{n}_k, \quad \hat{n}_k = \hat{c}_k^\dagger \hat{c}_k, \tag{2.30}$$

where $\hat{c}_k$ is the free fermionic operator defined as

$$\hat{c}_k = \int_{L/2}^{L/2} dx \phi_{p_n}^*(x) \hat{c}_x, \quad \phi_k(x) = \frac{e^{-ikx}}{\sqrt{L}}, \quad k = \frac{2\pi n}{L}. \tag{2.31}$$

Conserved charges. The system exhibits local conserved charges [154]

$$\hat{Q}_j = \sum_k k^j \hat{n}_k. \tag{2.32}$$

The $\hat{n}_k$ are also conserved charges but they are not local. The $\hat{Q}_j$ are local in the sense that they can be written as one-point differential operators

$$\begin{aligned} \hat{Q}_j &= \frac{1}{L} \sum_k \int dx dy k^j e^{-ik(x-y)} \hat{c}_x^\dagger \hat{c}_y, \\ &= \int dx dy \left[\frac{1}{L} \sum_k k^j e^{-ik(x-y)} \right] \hat{c}_x^\dagger \hat{c}_y, \\ &= \int dx \hat{Q}_j(x), \end{aligned} \tag{2.33}$$

with $\hat{Q}_j(x) = \hat{c}_x^\dagger (-i)^j \partial_x^j \hat{c}_x$. They commute with the Hamiltonian, and also between each other $[\hat{\mathcal{H}}, \hat{Q}_j] = 0$, $[\hat{Q}_j, \hat{Q}_i] = 0$ such that they are conserved by the dynamics generated by the Hamiltonian. Note that they include the total number of fermions operator $\hat{N} = \hat{Q}_0$, the total momentum operator $\hat{P} = \hat{Q}_1$, and the Hamiltonian $\hat{\mathcal{H}} = \frac{\hat{Q}_2}{2}$. Now, the conserved charge operator density obeys the continuity equation

$$\partial_t \hat{Q}_j(x) = i[\hat{\mathcal{H}}, \hat{Q}_j(x)] = -\partial_x \hat{J}_j(x), \tag{2.34}$$

where the currents are defined as

$$\hat{J}_j(x) = \frac{i(-i)^j}{2} (\partial_x \hat{c}_x^\dagger \partial_x^j \hat{c}_x - \hat{c}_x^\dagger \partial_x^{j+1} \hat{c}_x). \tag{2.35}$$

Microstate and Macrostate. A microstate is typically expressed as an eigenstate in the momentum respresentation

$$|k_1, ..., k_N\rangle = \frac{1}{L^{N/2}} \prod_{i=1}^{N} \hat{\eta}_{k_i}^\dagger |0\rangle , \tag{2.36}$$

where $|0\rangle$ is the vacuum state, and N the total number of fermions. The eigenstates are, in fact, simultaneous eigenvectors of all charges

$$\hat{Q}_j \left|k_1, ..., k_N\right\rangle = \sum_{i=1}^{N} k_i^j \left|k_1, ..., k_N\right\rangle, \quad q_j(k) = k^j. \tag{2.37}$$

Now we consider the Thermodynamic Limit (TD), i.e., we take $L \to \infty$, and $N \to \infty$ with fixed ratio $\rho = \frac{N}{L}$ (in the following we just denote it by $L \to \infty$). This allows to define a macrostate for each function $\rho(k) : \mathbb{R} \to [0, 1]$. The macrostate is defined as the set of microstates $\{|k_1, ..., k_N\rangle\}$ such that

$$\frac{2\pi}{L}\text{number of } k_i \text{ in } [k, k + dk[= \rho(k)dk. \tag{2.38}$$

The function $\rho(k)$ is often called the root density. We see that many microstates corresponds to one macrostate and from the root density one can extract the mean value of different observables. For example, the relation Eq. (2.37) simplifies in the TD limit to

$$\frac{1}{L}\sum_{i=1}^{N} k_i^j \underset{L\to\infty}{\simeq} \int_{-\infty}^{+\infty} \frac{dk}{2\pi} q_j(k)\rho(k). \tag{2.39}$$

This allows to write

$$\langle k_1, ..., k_N|\hat{Q}_j(x)|k_1, ..., k_N\rangle \underset{L\to\infty}{\simeq} \int_{-\infty}^{+\infty} \frac{dk}{2\pi} q_j(k)\rho(k). \tag{2.40}$$

We see that in the TD limit, the expectation value of the conserved charges is the same for all microstates, i.e., it depends only on the macrostate. Reciprocally, the relation Eq. (2.32) can be inverted such that imposing the expectation values $\lim_{L\to\infty} \frac{1}{L}\mathrm{Tr}[\hat{\rho}\hat{Q}_j] = q_j$ fixes uniquely the macrostate $\rho(k)$. It is worth asking what the current mean value is; a simple intuitive guess could be that it depends on the density $\rho(k)$ as

$$\langle k_1, ..., k_N|\hat{J}_j(x)|k_1, ..., k_N\rangle \underset{L\to\infty}{\simeq} \int_{-\infty}^{+\infty} \frac{dk}{2\pi} q_j(k)v(k)\rho(k), \tag{2.41}$$

where $v(k)$ is the group velocity of the stable excitations. This is easy to prove in the context of free fermions in the continuum, it turns out to be also valid in the context of spin chains [155].

Similarly, in the TD limit, the two-point correlation depends only on the root density as

$$\begin{aligned}\langle k_1, ..., k_N|\hat{c}_x^\dagger \hat{c}_y|k_1, ..., k_N\rangle &= \frac{1}{L}\sum_{j=1}^{N} e^{-ik_j(x-y)}, \\ &\underset{L\to\infty}{\simeq} \int_{-\infty}^{+\infty} \frac{dk}{2\pi} e^{-ik(x-y)}\rho(k),\end{aligned} \tag{2.42}$$

such that again it depends only on the macrostate. Additionally, using Wick's theorems, this fact remains valid for all multi-point correlation functions with a finite number of points.

Excitations. Finally, we would like to characterise excitations. For a given macrostate, excitations are defined on a specific microstate $|k_1, ..., k_N\rangle$ by the free fermionic operator. It can be a particle excitation

$$\hat{c}_k^\dagger \left|k_1, ..., k_N\right\rangle, \quad k \notin \{k_i\}, \tag{2.43}$$

in which case the conserved charges difference will be positive and given by $\Delta Q_j(k) = k^j$. Otherwise, it can be a hole excitation

$$\hat{c}_k \left|k_1, ..., k_N\right\rangle, \quad k \in \{k_i\}, \tag{2.44}$$

in which case the conserved charges difference will be negative and given by $\Delta Q_j(k) = -k^j$. The group velocity of the stable excitations is given by the dispersion relation $\epsilon(k)$ as

$$v(k) = \epsilon'(k), \tag{2.45}$$

which in our special case is just $v(k) = k$.

Free Fermions on a Lattice. Now, we introduce a slightly more complicated model, free fermions on a lattice (again with periodic boundary conditions). We introduce it because it will have a different relationship to GHD. Indeed, for free fermions in the continuum, GHD is exact, whereas for free fermions on the lattice it is valid only in the latter defined Euler scaling limit (2.67). The Hamiltonian is given by

$$\hat{\mathcal{H}} = \sum_{j=1}^{L} -J(\hat{c}_j^\dagger \hat{c}_{j+1} + \hat{c}_{j+1}^\dagger \hat{c}_j) - \mu \hat{c}_j^\dagger \hat{c}_j, \tag{2.46}$$

where $\hat{c}_j^\dagger$, and $\hat{c}_j$ are fermionic creation and annihilation operators. It can be diagonalised as

$$\hat{\mathcal{H}} = \sum_{i=1}^{L} \epsilon(k_i)\hat{n}_{k_i}, \quad k_i = \frac{2\pi i}{L}, \tag{2.47}$$

where the mode operator are defined as $\hat{n}_k = \hat{c}_k^\dagger \hat{c}_k$, $\hat{c}_k = \sum_{j=1}^{L} \hat{c}_j e^{-ikj}$, and the dispersion relation is given by $\epsilon(k) = -2J\cos(k) - \mu$. From here all the discussion on microstates and macrostates and the properties Eqs. (2.42-2.41-2.45) translate well, from free fermions in the continuum to free fermions on the lattice.

Interacting Integrable Systems. The case of interacting systems is more complicated. Let us briefly review how the previous properties are modified in

that case. A typical example of an integrable interacting system is the Lieb-Liniger model [156]. It represents a one-dimensional Bose gas with delta interactions, where the first and second quantized Hamiltonians are written as

$$\hat{H} = -\sum_{m=1}^{N} \partial_{x_m}^2 + \sum_{m\neq j} g\delta(x_m - x_j), \tag{2.48}$$
$$\hat{\mathcal{H}} = \int_{L/2}^{L/2} dx \partial_x \hat{c}_x^\dagger \partial_x \hat{c}_x + g\hat{c}_x^\dagger \hat{c}_x^\dagger \hat{c}_x \hat{c}_x.$$

This model correctly describes quantum gases in an appropriate regime. For example, the Newton's cradle experiment [126] is described by the LL model. Note that the LL model can be seen as an interpolation between free bosons at $g = 0$ and the Tonks-Girardeau model (the infinite g limit) [157] which has some relation to free fermions. From here, the conserved charges $\hat{Q}_j$ and their associated currents $\hat{J}_j$ can be constructed. The microstates $|k_1, ..., k_N\rangle$, i.e., the eigenstates, can be expressed in terms of the Bethe ansatz [158], where the wave function is written as

$$\psi_{k_1,...,k_N}(x_1, ..., x_N) = \frac{1}{\mathcal{N}} \sum_{\mathcal{P}\in\mathcal{S}_N} \mathrm{sgn}(\mathcal{P}) e^{i\sum_j k_{\mathcal{P}_j} x_j} \prod_{j>k} (k_{\mathcal{P}_j} - k_{\mathcal{P}_k} - ig), \tag{2.49}$$

where $\mathcal{N}$ is a normalisation, $\mathcal{S}_N$ is the set of permutations of N elements and $\mathrm{sgn}(\mathcal{P})$ the signature of such a given permutation. The interpretation of the Bethe ansatz is simple: the first part is just a superposition of plane waves with permuted momenta. The momenta are only permuted because of the conserved charges. For non-integrable model, the set of momenta would change to take into account the redistribution of momenta each time there is a collision. The second part ensures boundary conditions at the edges, $x_m = x_j$, and it encodes the interaction. This part is model-dependent. Now, the significant difference from noninteracting systems is that the momenta k_m are not independent; instead, they obey a non-trivial set of quantization conditions called the Bethe equations, which are written in their logarithmic form as

$$1 \leq m \leq N, \quad 2\pi n_m = k_m L + \sum_{j\neq m} \theta(k_m - k_j), \quad \theta(k) = i \ln\left(\frac{ig + k}{ig - k}\right). \tag{2.50}$$

Hence, we see that there is two way to describe the state, either with the data of the set of N half-integers n_m, or with the data of a set of N momenta k_m.

Following [144], it is possible to define a macrostate in a similar fashion to the case of free theories, i.e. through a density $\rho(k)$ of the roots k_m of the Bethe equations. This density is defined as

$$\text{number of } k_m \text{ in } [k, k + dk[= L\rho(k)dk. \tag{2.51}$$

Interestingly, as a microstate can be defined in term of half-integers n_p, it is also possible to define a macrostate through the density function $\chi(z)$ for the

half-integers n_m defined as

$$\text{number of } n_m/L \text{ in } [z, z+dz[= L\chi(z)dz. \tag{2.52}$$

Both of those densities (2.51) and (2.52) are related by the counting function $z(k)$ defined as

$$\rho(k)dk = \chi(z(k))\frac{dz}{dk}dk, \tag{2.53}$$

The counting function $z(k)$ can be obtained from the thermodynamic limit of the Bethe equations (2.50). This leads to the definition of the occupation function $\vartheta(k) = \chi(z(k))$ which is also constrained by the Bethe equations (2.50) in the thermodynamic limit resulting in the form of the integral equation

$$\frac{1}{2\pi} + \int \frac{dq}{2\pi} K(k-q)\rho(q) = \frac{\rho(k)}{\vartheta(k)}, \quad K(k) = \frac{2g}{g^2+k^2}. \tag{2.54}$$

Most of the properties of the density functions, such as equations Eq. (2.40), remain valid. However, the formula Eq. (2.41) for the mean current is slightly modified. Indeed, here comes the main difference between interacting and non-interacting systems, as the excitation group velocity $v(k)$ in formula (2.41) is now dependent on the state through the density function ρ. The usefulness of the occupation function $\vartheta(k)$ becomes apparent when one tries to compute the group velocity of an excitation which is given by

$$v_\rho(k) = \frac{q_2'(k)}{q_1'(k)}. \tag{2.55}$$

Here, $q_2(k)$ and $q_1(k)$ appear naturally when one considers an excitation over a microstate and then translate the result in term of macrostate. At a microscopic scale, a typical excitation is a particle-hole excitation, i.e. a particle occupying a half-integer n_h is exited to a previously empty half-integer n_p. Let us denote by $\{n_m\}$ the set of half-integers describing the microstate before the excitation and $\{\tilde{n}_m\}$ the one describing the state after the excitation. Both sets have their related Bethe equations and momenta

$$\begin{aligned} 1 \le m \le N, \quad 2\pi n_m &= k_m L + \sum_{j\neq m} \theta(k_m - k_j), \\ 1 \le m \le N, \quad 2\pi \tilde{n}_m &= k_m L + \sum_{j\neq m} \theta(\tilde{k}_m - \tilde{k}_j). \end{aligned} \tag{2.56}$$

From here, manipulations of those two sets of equations and of their thermodynamic limit yields the definition of $q_2(k)$ and $q_1(k)$ (see [144] for more details)

$$\begin{aligned} q_n(k) &= k^n - \int \frac{dq}{2\pi} n q^{n-1} f(q|k), \\ f(k|k') &- \int \frac{dq}{2\pi} \vartheta(k) K(k-q) f(q|k') = \frac{\vartheta(k)\theta(k-k')}{2\pi}. \end{aligned} \tag{2.57}$$

Henceforth, we know how to compute the excitation group velocity, in order to

emphasis its dependence on the macrostate, we will denote it as $v_\rho(k)$ such that the current in a macrostate (2.41) is modified as

$$\langle k_1, ..., k_N | \hat{J}_j(x) | k_1, ..., k_N \rangle \underset{L\to\infty}{\simeq} \int_{-\infty}^{+\infty} \frac{dk}{2\pi} q_j(k) v_\rho(k) \rho(k), \tag{2.58}$$

which will be essential when we attempt to construct a hydrodynamic theory in the next section.

2.1.4 Hydrodynamics for Integrable Systems

Now, we want to move away from the hypothesis of homogeneity. The tool for that is hydrodynamics, which allows a spatial description at a mesoscopic scale. It can emerge from both classical and quantum systems and provides a dynamical evolution towards possible relaxation. The strength of hydrodynamics lies in the massive reduction of the number of degrees of freedom from a microscopic to a mesoscopic description. By mesoscopic, we mean a scale larger than the microscopic scale but smaller than the macroscopic scale. Hydrodynamics assumes that properties of the fluid do not vary on the mesoscopic scale. In other words, hydrodynamics is an emergent universal theory for the low-energy dynamics of many-body systems.

GHD equation. Here we want to sketch how the ideas of hydrodynamics can be applied to quantum integrable systems. The first attempts to do so date back to 2016 by two independent groups [35, 36]. Let us we consider a quantum system evolving via the Schrödinger equation. The density matrix will evolve according to $\hat{\rho}(t) = \hat{U}^\dagger(t)\hat{\rho}(0)\hat{U}(t)$, where $\hat{\rho}(0)$ is the initial density matrix, and $\hat{U}(t) = e^{-i\hat{H}t}$ is the evolution operator. Then, the mean values of local operators are simply given by $\langle \hat{O}(x) \rangle_t = \mathrm{Tr}[\hat{\rho}(t)\hat{O}(x)]$. From the Heisenberg viewpoint, a local observable $\hat{O}(x,t)$ follows the unitary evolution $\hat{O}(x,t) = \hat{U}^\dagger(t)\hat{O}\hat{U}(t)$ such that $\langle \hat{O}(x) \rangle_t = \mathrm{Tr}[\hat{\rho}(0)\hat{O}(x,t)]$. If additionally, the system is integrable, there is a set of conserved charges density operator $\hat{Q}_j(x)$ together with their associated current $\hat{J}_j(x)$. Considering the evolution of the charge density gives the continuity equations

$$\forall n \in \mathbb{N}, \quad \partial_t \hat{Q}_n(x,t) = i[\hat{H}, \hat{Q}_n(x,t)] = -\partial_x \hat{J}_n(x,t). \tag{2.59}$$

Now these equations lead for the mean charge $q_n(x,t) = \mathrm{Tr}[\hat{\rho}(0)\hat{Q}_n(x,t)]$, and mean charge current $j_n(x,t) = \mathrm{Tr}[\hat{\rho}(0)\hat{J}_n(x,t)]$ to the following set of equations

$$\forall n \in \mathbb{N}, \quad \partial_t q_n(x,t) = -\partial_x j_n(x,t). \tag{2.60}$$

On the other hand, we assume that the system is initially prepared in a state with very smooth variation, such that it locally resembles a macrostate $\rho_{x,t=0}(k)$,

hence the mean charge and charge current Eqs. (2.40-2.58) generalise to

$$\begin{aligned}\mathrm{Tr}[\hat{\rho}(0)\hat{Q}_n(x)] &\underset{L\to\infty}{\simeq} \int_{-\infty}^{+\infty} \frac{dk}{2\pi} q_n(k)\rho_{x,t=0}(k), \\ \mathrm{Tr}[\hat{\rho}(0)\hat{J}_n(x)] &\underset{L\to\infty}{\simeq} \int_{-\infty}^{+\infty} \frac{dk}{2\pi} q_n(k)v_{\rho_{x,t=0}}(k)\rho_{x,t=0}(k).\end{aligned} \tag{2.61}$$

Now, following the idea of hydrodynamics, we let the system evolve after the quench for a long enough time such that local relaxation happens. This allows us to describe the system as a macrostate at each position such that

$$\begin{aligned}\mathrm{Tr}[\hat{\rho}(0)\hat{Q}_n(x,t)] &\underset{L\to\infty}{\simeq} \int_{-\infty}^{+\infty} \frac{dk}{2\pi} q_n(k)\rho_{x,t}(k), \\ \mathrm{Tr}[\hat{\rho}(0)\hat{J}_n(x,t)] &\underset{L\to\infty}{\simeq} \int_{-\infty}^{+\infty} \frac{dk}{2\pi} q_n(k)v_{\rho_{x,t}}(k)\rho_{x,t}(k).\end{aligned} \tag{2.62}$$

Combining this with Eq. (2.60) we obtain the set of equations

$$\forall n \in \mathbb{N}, \quad \int_{-\infty}^{+\infty} \frac{dk}{2\pi} q_n(k) \left[\partial_t \rho_{x,t}(k) + \partial_x(v_{\rho_{x,t}}(k)\rho_{x,t}(k))\right] = 0. \tag{2.63}$$

The set of functions $\{q_n(k)\}$ form a basis of functions (for the case of free fermions and LL model this is just the monomial basis $q_n(k) = k^n$), such that we obtain the GHD equation

$$\partial_t \rho_{x,t}(k) + \partial_x(v_{\rho_{x,t}}(k)\rho_{x,t}(k)) = 0, \tag{2.64}$$

where $v_{\rho_{x,t}}$ is model dependent. In the particular case of free fermions studied previously, GHD equation simplifies to

$$\partial_t \rho_{x,t}(k) + \epsilon'(k)\partial_x \rho_{x,t}(k) = 0, \tag{2.65}$$

where $\epsilon'(k) = k$ is the dispersion relation.

GHD and free fermions. Now we want to come back to two simple cases where GHD can be proven rigorously, namely free fermions on the lattice or in the continuum. For free fermions in the continuum (2.28), the Wigner function (1.83) follows the time evolution

$$\partial_t W(x,k,t) + k\partial_x W(x,k,t) = 0. \tag{2.66}$$

This can be obtained from (2.241) in the absence of potential $V(x)$, or directly from the Schrödinger equation. The equation (2.66) implies that GHD is exact in that case which is true only for free fermions in the continuum. Generally, it is believed that GHD is valid in the Euler scaling limit, i.e. when $|x|$ and t are growing to infinity but with fixed ratio $\frac{x}{t}$

$$\rho_{\mathbf{x},\mathbf{t}}(k) = \lim_{\Lambda\to\infty} W(x = \mathbf{x}\Lambda, k, t = \mathbf{t}\Lambda). \tag{2.67}$$

For example, for free fermions on a lattice (2.46), the Wigner function can

still be defined; its evolution is slightly different from (2.66), as the gradient is turned into a discrete gradient. This means that the free version of GHD (2.65) is recovered only in the Euler limit when the discrete gradient converges to the continuous gradient ∂_x.

Now let us make a few remarks:

- In the case of free fermions, the velocity $v(k)$ being independent from the macrostate $\rho_{x,t}(k)$, the GHD equation (2.64) can be solved analytically using the method of characteristics. However in the interacting case, the GHD equation (2.64) is much harder to solve, in most cases, this is done using numerical methods.

- Interestingly, GHD can be generalised for system with weak integrability breaking. This weak integrability breaking can take the form of a particle loss [38], an inhomogeneous potential [37], inhomogeneous interactions [39] or a non-integrable defect [130]. In all these cases collision integrals were used [159].

2.2 Landauer-Büttiker Formalism

Noninteracting fermions with a defect. Starting now, we will investigate the effect of defect on the dynamics of noninteracting fermions. By a defect or an impurity, we mean a potential that varies on a microscopic length scale. The physics of defects has attracted attention in the context of equilibrium systems in particular with the so called "Friedel oscillations" [160–162]. Friedel oscillations are a quantum mechanical analogue of electric charge screening, representing the local perturbation of a Fermi gas (such as in a metallic system) around a defect. In [163], the exact density around a delta function impurity was obtained, including the density at distances shorter than the inter-particle distance, which had not been given before. Later on, this was generalized to an attractive delta function impurity (which can support a bound state) in an inhomogeneous Fermi gas [164]. Moreover, in the case of multiple impurities, the Casimir effect was also studied [165, 166]. Finally, the dynamic of an impurity in a fermionic gas was also considered [167] in which case Friedel oscillations are also observed.

The physics of defects has also attracted attention for systems driven out of equilibrium. It has been proven to be relevant in the context of both electronic systems and cold atoms [168–171]. In this section, we will focus on the effect of local defects or impurities on the out-of-equilibrium dynamics. We start by an overview of the Landauer-Büttiker formalism [21, 172], which treats the current fluctuations in conductors. In the simplest cases, this is modeled as two terminals connected through an impurity represented by a scattering matrix. The system is in a NESS and the current, and current fluctuations are affected by the impurity. Later, we will move on to the study of a quench with an impurity in the post-quench Hamiltonian. The quench in question will be a partitioning protocol with an impurity at the junction of the two systems. This will allow us to observe the dynamical relaxation to a NESS and to recover the Landauer-Büttiker formalism.

Historically, the Landauer-Bütikker formalism arises from the investigation of electric noise sources in mesoscopic conductors. As a first approximation, this noise can be decomposed into two components: thermal noise (or Johnson-Nyquist noise) and noise arising from the discrete nature of the charge carriers (or shot noise). Latter on, Landauer, Bütikker and Martin proposed a quantum treatment of the problem [21, 22, 172, 173].

Thermal Noise. Here, we will review the Landauer-Bütikker formalism following [174, 175]. The investigation of thermal noise began when Johnson [20] measured a temperature-dependent electromotive force in conductors. Johnson's intuition was that this electromotive force, or its related electric current, was caused by the thermal agitation of electric charge carriers. This was soon theoretically explained by Nyquist [176] for a conductor at thermal equilibrium. Assuming equipartition for a mode of frequency ν with resistance R_ν, he found the square of the voltage at frequency ν to be

$$E_\nu^2 = 4R_\nu k_B T, \tag{2.68}$$

with k_B the Boltzmann constant, and T the temperature. This result establishes a connection between electric current fluctuations and conductance, which is related to the fluctuation-dissipation theorem. This relation allows for the measurement of noise through conductivity measurements. However, this expression fails at low temperatures. Specifically, the periodic current I_ν can be related with the number of charge carriers passing through the conductor. This implies that thermal fluctuations are related to the occupation numbers n of a given mode. As the charge carriers are fermions, they obey the Fermi-Dirac statistics such that for an energy ϵ, $\langle n\rangle = f$ with $f = \frac{1}{e^{\beta(\epsilon-\mu)}+1}$, where μ is the chemical potential and β the inverse temperature. Because there can be only zero or one fermion in a mode, $n^2 = n$ and the fluctuations are given by

$$\langle (n - \langle n\rangle)^2\rangle = f(1-f), \tag{2.69}$$

such that this product has to play a role in the thermal noise.

Shot Noise. Shot noise is much different as it only exists in the presence of a current, i.e. in a non-equilibrium set-up. To briefly explain what shot noise is, let us imagine one single particle scattering on a defect and being reflected with probability R or transmitted with probability T. The incident state has an occupation number n_{in}, similarly the reflected and transmitted states are characterised by n_R and n_T. Additionally we assume that there is an incoming particle on the defect with a probability following the Fermi-Dirac statistics $\langle n_{in}\rangle = f$. The reflected and transmitted states obviously follow $\langle n_R\rangle = Rf$, and $\langle n_T\rangle = Tf$. Because there is at most one particle in the incident state, we know that at most one of the left and right channel is occupied such that $\langle n_R n_T\rangle = 0$. This helps to compute the second moments which are given by

$$\begin{aligned}
&\langle (n_R - \langle n_R\rangle)^2\rangle = Rf(1-Rf),\\
&\langle (n_T - \langle n_T\rangle)^2\rangle = Tf(1-Tf),\\
&\langle (n_R - \langle n_R\rangle)(n_T - \langle n_T\rangle)\rangle = -TRf^2.
\end{aligned} \tag{2.70}$$

The first thing to notice is that in the absence of a mean current trough the defect, that is when $\langle n_T \rangle = 0$, there is no fluctuation $\langle (n_T - \langle n_T \rangle)^2 \rangle = 0$, and therefore no current fluctuations either. This is the reason why we call the shot noise a non-equilibrium noise.

In the limit where the transmission factor T or the Fermi factor f is small, the fluctuations of the transmitted number are equal to its mean value:

$$\langle (n_T - \langle n_T \rangle)^2 \rangle \simeq Tf = \langle n_T \rangle \,. \tag{2.71}$$

This implies that the current fluctuations are proportional to the current:

$$\langle (I - \langle I \rangle)^2 \rangle \sim \langle I \rangle \,. \tag{2.72}$$

This property is characteristic of Poissonian statistics. It is easy to see that, because of the $(1 - Tf)$ factor, the fluctuations $\langle (n_T - \langle n_T \rangle)^2 \rangle$ from Eq. (2.70) are suppressed compared to Poissonian fluctuations.

Finally, if the situation is such that charge carriers arrive individually on the defect, the previous computation allows to compute the transmitted current fluctuations. However if one adds multiple incoming leads on the scattering defect, or if the particles are not well separated in time, the situation turns to be more complicated and one has to handle new effects arising from Pauli exclusion principle. For example if two particles arrives at the same time on the defect, they cannot end up in the same lead. This problem was treated in the general case by Landauer and Büttiker [21, 22].

This method typically applies to noninteracting systems in the steady state. We consider a two-terminal (Right/Left) system with one transverse channel (see Fig. 2.4) for which we impose thermal equilibrium for each channel through the Fermi factors

$$f_{R/L}(E) = \frac{1}{e^{\beta_{R/L}(E-\mu_{R/L})} + 1}, \tag{2.73}$$

with $\beta_{R/L}$, right and left inverse temperature, and $\mu_{R/L}$, right and left chemical potential. In the general case treated by Büttiker [21, 173], there are multiple transverse channels which correspond to transverse mode quantification of wires of dimensions strictly larger than one. The method can be generalized to more terminals and channels, but it is only useful to consider this simplified case for later one-dimensional quenches and partitioning protocols. Now, for a given terminal, we distinguish between the mode of particle coming in the defect, from the mode of particle coming out of the defect together with their respective annihilation and creation operators at energy E, $\hat{a}_{R/L}(E)$, $\hat{a}^\dagger_{R/L}(E)$, and $\hat{b}_{R/L}(E)$, $\hat{b}^\dagger_{R/L}(E)$ (a for in-coming mode and b for out-coming mode). They verify the canonical fermionic anti-commutation relations $\{\hat{a}_i(E), \hat{a}^\dagger_j(E')\} = \delta_{i,j}\delta(E-E')$, $\{\hat{b}_i(E), \hat{b}^\dagger_j(E')\} = \delta_{i,j}\delta(E-E')$ where the indices i and j take values R and L. The occupation numbers are given by the operators $\hat{n}_{in,R/L}(E) = \hat{a}^\dagger_{R/L}(E)\hat{a}_{R/L}(E)$, and $\hat{n}_{out,R/L}(E) = \hat{b}^\dagger_{R/L}(E)\hat{b}_{R/L}(E)$. The in-coming and out-coming modes are related through the scattering matrix $\mathbf{S}$

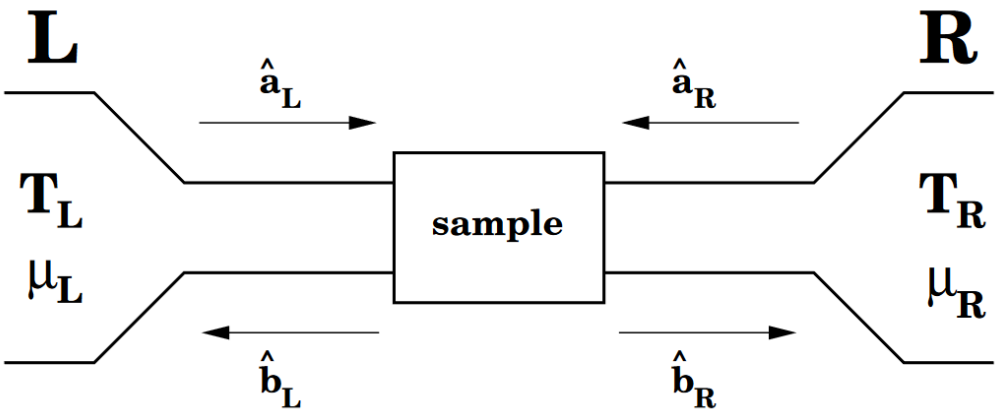

FIGURE 2.4: Two-terminal scattering problem for the case of a single transverse channel (figure taken from [174]).

introduced by John Wheeler [177]:

$$\begin{pmatrix} \hat{b}_L(E) \\ \hat{b}_R(E) \end{pmatrix} = \mathbf{S} \begin{pmatrix} \hat{a}_L(E) \\ \hat{a}_R(E) \end{pmatrix}, \quad \mathbf{S} = \begin{pmatrix} \mathsf{t}_L & \mathsf{r}_R \\ \mathsf{r}_L & \mathsf{t}_R \end{pmatrix}, \tag{2.74}$$

where the scattering matrix is a unitary matrix $\mathbf{S}^\dagger\mathbf{S} = \mathbb{1}$, and the transmission and reflection coefficients are implicitly dependent on the energy E. Additionally the scattering matrix verify $\mathbf{S}\mathbf{S}^\dagger = \mathbb{1}$ which implies that $|\mathsf{t}_R| = |\mathsf{t}_L|$ and $|\mathsf{r}_R| = |\mathsf{r}_L|$. The advantage of this method from Landauer [22] is that the fermionic properties are encoded into the anti-commutation relations such that the rest of the computation is just a matter of algebraic manipulation. In contrast, in [173] the Pauli principle has to be checked for each possible configuration of in-coming and out-coming particles. An other advantage is that the results can be easily generalised to bosonic statistics.

The left and right particle current operators are defined in the usual way,

$$\hat{J}_{R/L}(x,t) = \frac{\hbar}{2mi}\left[\hat{\psi}^\dagger_{R/L}(x,t)\partial_x\hat{\psi}_{R/L}(x,t) - (\partial_x\hat{\psi}^\dagger_{R/L}(x,t))\hat{\psi}_{R/L}(x,t)\right], \tag{2.75}$$

where the field operators are given by

$$\begin{aligned} \hat{\psi}_{R/L}(x,t) &= \int dE \frac{e^{-iEt/\hbar}}{\sqrt{2\pi\hbar v(E)}}\left[\hat{a}_{R/L}(E)e^{ikx} + \hat{b}_{R/L}(E)e^{-ikx}\right], \\ \hat{\psi}^\dagger_{R/L}(x,t) &= \int dE \frac{e^{iEt/\hbar}}{\sqrt{2\pi\hbar v(E)}}\left[\hat{a}^\dagger_{R/L}(E)e^{-ikx} + \hat{b}^\dagger_{R/L}(E)e^{ikx}\right], \end{aligned} \tag{2.76}$$

with $v(E) = \sqrt{\frac{2E}{m}}$ the velocity of the carriers. From Eqs. (2.79) and (2.76), differentiating with respect to x we obtain the simpler expression for the current

$$\hat{J}_{R/L}(x,t) = \frac{1}{\hbar}\iint dE dE' e^{i\frac{E-E'}{\hbar}t}\left[\hat{b}^\dagger_{R/L}(E)\hat{b}_{R/L}(E') - \hat{a}^\dagger_{R/L}(E)\hat{a}_{R/L}(E')\right]. \tag{2.77}$$

Now, let us say that we want to obtain the mean current. In order to do that we assume that the thermal equilibrium of the two reservoirs is not affected by the defect such that the incoming left and right particle follows Fermi-Dirac statistics

$$\langle \hat{a}_i^\dagger(E)\hat{a}_j(E')\rangle = \delta_{i,j}\delta(E-E')f_i(E), \tag{2.78}$$

where i and j indicate left or right terminal, and $\delta_{i,j}$ is the Kroenecker delta symbol encoding the absence of correlations between the two reservoirs incoming particles. From here, using the scattering matrix (2.74) it is possible to compute the mean current. The mean current is found to be stationary, hence independent of both x and of the subscript R/L (because of particle conservation)

$$\langle \hat{J}\rangle = \int \frac{dE}{2\pi\hbar} T(E)\left(f_L(E) - f_R(E)\right), \tag{2.79}$$

where $T(E) = |\mathtt{t}_R(E)|^2 = |\mathtt{t}_L(E)|^2$ is the transmission probability. This result is interesting but in order to match with the result of Johnsson and Nyquist [20, 176] we would like to compute the noise, i.e. the second cumulant of the current. Similarly to the mean current, the current noise can be obtain using (2.77), which yields one of the main result of the Landauer-Bütikker formalism

$$\langle (\hat{J} - \langle \hat{J}\rangle)^2\rangle = \int \frac{dE}{2\pi\hbar}\left[T\left(f_L(1-f_L) + f_R(1-f_R)\right) + T(1-T)\left(f_L - f_R\right)^2\right], \tag{2.80}$$

where the energy dependencies of $T(E)$, $f_L(E)$, and $f_R(E)$ are implicit. Here, the first term is the contribution of thermal equilibrium noise, while the second term is the contribution of non-equilibrium or shot noise. It can be verified that only the first term remains if the current is zero, $\langle \hat{J}\rangle = 0$, while only the second term remains at zero temperature. Note that the second term is of second order in the Fermi factors. At high energies, the Fermi distribution function is equivalent to the Maxwell-Boltzmann distribution, and the shot noise term is negligible compared to the thermal noise.

Latter on, Levitov and Lesovik [178, 179] completed the investigations on current fluctuations by computing the full counting statistics (1.91)

$$\begin{aligned} \ln(\chi(\lambda)) &= \int \frac{dE}{2\pi\hbar}\ln(\chi_E(\lambda)), \\ \chi_E(\lambda) &= 1 + T(e^{i\lambda}-1)f_L(1-f_R) + T(e^{-i\lambda}-1)f_R(1-f_L), \end{aligned} \tag{2.81}$$

where, $\chi(\lambda) = \langle e^{i\lambda\hat{J}}\rangle$ is the imaginary argument moment generating function. This can be used for example to compute the skewness or third cumulant of the current. More recently, Klich provided a more simple and elegant proof of the formula [180].

In the Landauer-Büttiker formalism, the current and its cumulants are stationary at all times. It is also interesting to study a quench scenario, more precisely, a partitioning protocol with a scattering defect or impurity in the middle, where the observables will relax in time towards a non-equilibrium stationary state. This was done in [28], where it was shown numerically that the

stationary state after a quench exhibits the Landauer-Büttiker FCS. This result was later extended by [29, 30] to theoretical studies.

2.3 Relaxing to a GGE or a NESS with currents

As a warm-up, we first consider quenches in the absence of a defect. On this simple example, we will see how a quench can lead to either a NESS with currents or a GGE without currents at different time scales (from now on we will just refer to NESS and GGE). To illustrate this, we consider a partitioning protocol for one-dimensional free fermions as done in [134]. We prepare a system of size ℓ into two independent halves, $[-\frac{\ell}{2}, 0]$ (left L) and $[0, \frac{\ell}{2}]$ (right R). Each half is in a thermal state characterised by its own left and right chemical potentials $\mu_{R/L}$ and inverse temperatures $\beta_{R/L}$. The results presented in the article [134] are given at zero chemical potential, but they can be easily generalized to non-zero left and right chemical potentials $\mu_{R/L}$. Then depending on how the time limit is taken two scenarios can occur:

- The thermodynamic limit $\ell \to \infty$ is taken before the infinite time limit $t \to \infty$. In this case, the boundaries play no role, and the system relaxes to a NESS with non-zero currents.
- For a large system size, the time is taken to be larger compared to the system size $\frac{t}{\ell} \to \infty$, allowing the particles to be reflected on the boundaries multiple times. However, the time should not be too large $\frac{t}{\ell^2} \to 0$ to avoid revivals (see [181] for more details on revivals). In this case, around the defect, the gas relaxes towards a GGE. The effect of boundaries is illustrated in Fig. 2.5.

Initial State. Here, we illustrate the result of [134] but with a slightly more general set up as we allow left and right chemical potential $\mu_{R/L}$ to be non zero. The system is prepared in a thermal tensor state, i.e. the kernel can be written as the sum of two thermal kernels

$$K_0(x, x') = K_L(x, x') + K_R(x, x'), \tag{2.82}$$

where,

$$K_L(x, x') = \theta(-x)\theta(-x') \sum_{n=1}^{\infty} \frac{4}{\ell} f_L(k_n) \sin(k_n x) \sin(k_n x'), \tag{2.83}$$

$$K_R(x, x') = \theta(x)\theta(x') \sum_{n=1}^{\infty} \frac{4}{\ell} f_R(k_n) \sin(k_n x) \sin(k_n x'), \quad k_n = \frac{2\pi n}{\ell},$$

and $\theta(x)$ is the Heaviside theta function. We recall that $f_{R/L}$ are the Fermi factors for free fermions given by

$$f_{R/L}(k) = \frac{1}{e^{\beta_{R/L}(\frac{k^2}{2} - \mu_{R/L})} + 1}. \tag{2.84}$$

It is clear from this expression that within each half of the system, the eigenstates of an infinite quantum well with a size of $\frac{\ell}{2}$ are occupied according to the Fermi-Dirac statistics.

Dynamical Evolution. From here the evolution follows the usual rule Eq. (2.5), which yields

$$K(x,x';t) = K_L(x,x';t) + K_R(x,x';t), \tag{2.85}$$

$$K_{R/L}(x,x';t) = \sum_{k_a,k_b} \phi^*_{k_a}(x)\phi_{k_b}(x')e^{-i(E(k_a)-E(k_b))t} \tag{2.86}$$

$$\times \int_{\ell/2}^{\ell/2} dydy'\phi_{k_a}(y)K_{R/L}(y,y')\phi^*_{k_b}(y'), \tag{2.87}$$

where the $k_{a/b}$ takes value $k_{a/b} = \frac{\pi n}{\ell}, \quad n \in \mathbb{N}^*$, and $\phi_{k_{a/b}}$ are the eigenfunctions of of the infinite quantum of size ℓ (free particle within a box) well namely

$$\phi_k(x) = \sqrt{\frac{2}{\ell}} \begin{cases} \sin(kx), & \text{if } k = \frac{2\pi n}{\ell} \\ \cos(kx), & \text{if } k = \frac{(2n+1)\pi}{\ell} \end{cases} . \tag{2.88}$$

Relaxation to the GGE. Here, we consider the large time limit such that

$$\frac{t}{\ell} \to \infty, \text{ and } \frac{t}{\ell^2} \to 0. \tag{2.89}$$

If we also require that the density is fixed (which is achieved by fixing $\beta_{R/L}$ and $\mu_{R/L}$), then, the authors of [134] argued, based on numerical tests (we provide a theoretical argument for this in Section 2.5) that the kernel has a limit,

$$\lim_{\substack{\ell\to\infty \\ \ell\ll t\ll \ell^2}} K(x,x';t) = K_\infty(x,x'), \tag{2.90}$$

$$K_\infty(x,x') = \int_0^\infty \frac{dk}{2\pi} \left(f_L(k) + f_R(k)\right) \left(\sin(kx)\sin(kx') + \cos(kx)\cos(kx')\right).$$

Because the kernel is real, there is no current (2.7). This way of writing the kernel is advantageous because it highlights that only the diagonal part, where $k_a = k_b$, of Eq. (2.87) contributes. This can also be proven to obey the GGE (2.26) associated with the initial condition (2.82). Another way of writing the kernel, using plane waves, provides a better physical interpretation of the result

$$K_\infty(x,x') = \int_{-\infty}^{+\infty} \frac{dk}{2\pi} \left(\frac{f_L(k) + f_R(k)}{2}\right) e^{-ik(x-x')}. \tag{2.91}$$

We see that plane waves are filled with the mean of left and right Fermi factors, as if they had been diluted in the box of size two times larger.

Similar conclusions where obtained in the case of a trap release [133]. The authors studied the classical limit of a trap release of a noninteracting fermionic gas on a circle (see Fig. 2.5). They conclude that the gas relaxes to GGE and found universal power law relaxation together with oscillations of the density. Additionally they concluded that the power law exponent depends only on the

shape of the potential at its local extrema. Similarly, the authors of [132] investigated the release of noninteracting fermions from a harmonic trap on a circle, taking into account the full quantum dynamics. Their findings were in line with those of the classical treatment [133] discussed above. They observed that the kernel exhibited power-law relaxation with an exponent of $\frac{3}{2}$, which agrees with the universal behavior identified in the classical analysis.

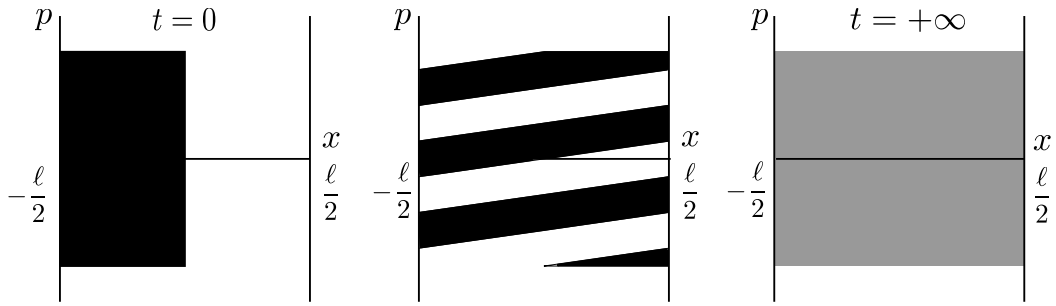

FIGURE 2.5: Illustration of the dynamical evolution of a gas of free fermions in a box of size ℓ. Here, we represent the Wigner function, defined by Eq. (1.83), in the classical limit given by Eq. (1.88), which follows the Liouville evolution Eq. (2.66). At initial time, both half systems are in grounds state such that only the left half space is filed up to Fermi momentum p_F. The middle panel illustrates evolution at time $t = \frac{3\ell}{p_F}$. This illustration demonstrates that as the gas passes through the boundaries multiple times, the observables such as density and kernel will eventually relax to a stationary value. However, the large time Wigner function does not describe a thermal equilibrium state.

Relaxation to a NESS with currents. On the other side, we can first take the thermodynamic limit (defined as $\ell \to \infty$ with fixed densities, i.e., fixed $\beta_{R/L}$ and $\mu_{R/L}$), and then the infinite time limit $t \to \infty$. In that case, using stationary phase approximation, the kernel can be shown to exhibit the following stationary behavior

$$\lim_{t\to\infty}\lim_{\ell\to\infty} K(x,x';t) = K_\infty(x,x';t), \tag{2.92}$$

$$\begin{aligned} K_\infty(x,x') = \int_0^\infty \frac{dk}{2\pi} \left(f_L(k)+f_R(k)\right)\left(\sin(kx)\sin(kx')+\cos(kx)\cos(kx')\right), \\ + i\left(f_L(k)-f_R(k)\right)\left(\cos(kx)\sin(kx')-\sin(kx)\cos(kx')\right). \end{aligned}$$

We observe that compared to Eq. (2.91), there are additional non-diagonal terms that persist in the large time limit. These non-diagonal terms are complex and hence responsible for a non-zero particle (2.7) and energy (2.174) currents. Once again, the kernel is more readable if written in terms of plane waves

$$K_\infty(x,x') = \int_{-\infty}^{+\infty} \frac{dk}{2\pi} \left(\theta(k) f_L(k) + \theta(-k) f_R(k)\right) e^{-ik(x-x')}. \tag{2.93}$$

This integral can be interpreted as plane waves originating from the left (or right) with positive (or negative) velocities, corresponding to the left (or right) initial thermal condition. The particle current (2.7) is a consequence of the asymmetry between positive and negative values of k. It is independent of x and given by

$$J = \int_0^{+\infty} \frac{dk}{2\pi} k \left(f_L(k) - f_R(k) \right), \tag{2.94}$$

Which is consistent with the stationary current given in the Landauer-Büttiker formalism (2.79) with $T(E) = 1$. Additionally, one can verify that this state cannot be described as a GGE

Euler scaling limit or ray regime. Furthermore, instead of computing the kernel at fixed positions x, and x', it is possible to compute the large time limit along positions that scale with times $x = \xi t + y$, and $x' = \xi' t + y'$. This is called ray regime or Euler scaling limit. Here, along the rays, the system relaxes to a stationary state called a Local Quasi Stationary State (LQSS)

$$\lim_{t\to\infty} \lim_{\ell\to\infty} K(\xi t + y, \xi' t + y'; t) = \begin{cases} 0 \text{ if } \xi \neq \xi' \\ K_\xi(y, y') \end{cases}, \tag{2.95}$$

$$K_\xi(y, y') = \int_{-\infty}^{+\infty} \frac{dk}{2\pi} \left(\theta(k > \xi) f_L(k) + \theta(\xi > k) f_R(k) \right) e^{-ik(y-y')},$$

where we used the notation $\theta(x > y) = \theta(x - y)$.

Now, we aim to study both of these regimes within the context of the partitioning protocol, considering the presence of an additional scattering defect at the junction between the two systems. This was done for lattice noninteracting fermions in [143] where is was shown that the NESS is reached.

In the next sections, we show how the NESS can be obtained for fermions in the continuum. First, in Section 2.4, we present the results for the case of a delta Dirac impurity $V(x) = g\delta(x)$, at zero temperature or with general left and right thermal states in Section 2.4.4. For the same quench, we discuss in Section 2.4.5 the large time decay to the NESS, and in Section 2.4.6 a comparison with Conformal Field Theory in the low temperature limit. These results are discussed in my second paper [2]. Then, in Section 2.6, we generalize this approach to multi-time correlations for a partitioning protocol with a general defect, i.e., a scattering matrix (2.74), and possible bound states. This work is presented in my third paper [3]. In between these two parts, in Section 2.5 we will also provide a theoretical argument for the relaxation to the GGE in the presence of a delta defect. Finally, in Section 2.7 we will consider the relationship between the semiclassical limit or GHD and the partitioning protocol with a defect. We observe that a part of the correlations in the Euler scaling limit is not predicted by the semiclassical method, and we propose an extension of this method that allows us to recover these missing correlations.

2.4 Partitioning protocol with a delta Dirac defect: NESS with currents

Here, we will consider a partitioning protocol with different ground states for the left and right initial systems. Subsequently, we will join the two systems together with a delta Dirac impurity in between. We first take the thermodynamic limit with fixed left and right densities and then the large time limit. In this double limit, the system relaxes to a NESS, which we will characterize.

Model. We consider N noninteracting fermions in one dimension and in the presence of a delta impurity at the origin described by the single particle Hamiltonian $\hat{H}_g$

$$\hat{H}_g = -\frac{1}{2}\partial_x^2 + g\delta(x) \; . \tag{2.96}$$

We work here in units where the fermion mass is unity and $\hbar = 1$. In these units, g denotes the strength of the impurity, first we consider only the repulsive defect ($g > 0$), but latter we will also consider the attractive case ($g < 0$). To fully specify the model we define it on the interval $[-\ell/2, \ell/2]$ with a hard wall boundary condition (i.e., vanishing wave-function at $x = \pm\ell/2$). We will be eventually be interested in the problem on the full line obtained by taking the limit $\ell \to +\infty$, with fixed fermion densities.

Initial state. The system is prepared at $t = 0$ in the ground state of the many body Hamiltonian with $g = +\infty$, associated to the single particle Hamiltonian $\hat{H}_\infty$. This corresponds to imposing a hard-wall at $x = 0$, so that the system is cut into two independent halves $x > 0$ and $x < 0$ at $t = 0$. We will denote by N_L and N_R respectively the number of fermions in the left ($x < 0$) and right ($x > 0$) halves. Let us introduce $\phi_n^L(x)$ and $\phi_n^R(x)$, with $n = 1, 2, \cdots$, the normalized eigenfunctions of the single particle Hamiltonian $\hat{H}_\infty$

$$\phi_n^L(x) = \theta(-x)\sqrt{\frac{4}{\ell}}\sin(k_n\, x) \quad , \quad \phi_n^R(x) = \theta(x)\sqrt{\frac{4}{\ell}}\sin(k_n\, x) \; , \tag{2.97}$$

where

$$k_n = \frac{2\pi n}{\ell} \; . \tag{2.98}$$

The corresponding energy levels are $\epsilon_n = \frac{1}{2}k_n^2 = \frac{2\pi^2 n^2}{\ell^2}$ which are doubly degenerate (L, R).

The kernel of this ground state can be shown to be the sum of a left and right part

$$K_0(x, x') = K_L(x, x') + K_R(x, x') \; , \tag{2.99}$$

where

$$K_L(x, x') = \theta(-x)\theta(-x')\sum_{n=1}^{N_L}\frac{4}{\ell}\sin\left(\frac{2\pi n x}{\ell}\right)\sin\left(\frac{2\pi n x'}{\ell}\right) \; , \tag{2.100}$$

$$K_R(x, x') = \theta(x)\theta(x')\sum_{n'=1}^{N_R}\frac{4}{\ell}\sin\left(\frac{2\pi n' x}{\ell}\right)\sin\left(\frac{2\pi n' x'}{\ell}\right) \; . \tag{2.101}$$

In particular, the mean fermion density is given by $\rho(x, t = 0) = K_0(x, x) = \rho_L(x) + \rho_R(x)$ with $\rho_{R/L}(x) = K_{R/L}(x, x)$, where $\rho_L(x)$ and $\rho_R(x)$ denote respectively the average fermion density to the left and to the right of the origin. We also define the Fermi momenta of the left and right half-spaces associated to the initial condition

$$k_L = k_{N_L} = \frac{2\pi N_L}{\ell} \quad , \quad k_R = k_{N_R} = \frac{2\pi N_R}{\ell}, \tag{2.102}$$

and the corresponding Fermi energies

$$\mu_L = \frac{k_L^2}{2} \quad , \quad \mu_R = \frac{k_R^2}{2} \, , \tag{2.103}$$

which will be useful in the following.

Dynamical Evolution. We now consider the time evolution for $t > 0$ described by the single particle Hamiltonian $\hat{H}_g$ (2.96) with a finite strength g of the impurity at $x = 0$. We denote $\psi_n^L(x, t)$ the solution of the Schrödinger equation $i\partial_t \psi_n^L(x, t) = \hat{H}_g \psi_n^L(x, t)$ with initial condition $\psi_n^L(x, t = 0) = \phi_n^L(x)$, and similarly $\psi_n^R(x, t)$ with $\psi_n^R(x, t = 0) = \phi_n^R(x)$ where $\phi_n^{R/L}(x)$ are given in Eq. (2.97). Under this evolution, the n-point correlations keep its determinantal structure Eq. (2.5), and the time dependent correlation kernel $K(x_i, x_j; t)$ reads

$$K(x, x', t) = K_L(x, x', t) + K_R(x, x', t), \tag{2.104}$$

where

$$K_L(x, x', t) = \sum_{n=1}^{N_L} \psi_n^{L*}(x, t)\psi_n^L(x', t) \quad , \quad K_R(x, x', t) = \sum_{n=1}^{N_R} \psi_n^{R*}(x, t)\psi_n^R(x', t) \, . \tag{2.105}$$

Here we compute the time evolution of the density $\rho(x, t)$, of the kernel $K(x, x', t)$ and of the current $J(x, t)$. Since we are interested in the large time behavior of the bulk of the system, we will take the limit $\ell \to +\infty$ before taking $t \to +\infty$. More precisely we will take the limit $\ell \to +\infty$, $N_{R/L} \to +\infty$ with fixed k_L and k_R, i.e. with fixed mean densities

$$\rho_L = \frac{2N_L}{\ell} = \frac{k_L}{\pi} \quad , \quad \rho_R = \frac{2N_R}{\ell} = \frac{k_R}{\pi}, \tag{2.106}$$

or equivalently with fixed Fermi energies μ_L, μ_R (see Eq. (2.103)).

Main results. In this section we present our main results. The first one is the expression for the kernel $K(x, x', t)$ in the thermodynamic limit $\ell \to +\infty$ at any fixed time t. It is a lengthy although fully explicit expression which is given in (2.144) as a sum of terms which are given respectively in (2.145), (B.3), (B.8), (B.9) and (B.12). From this expression one can read the time dependent density from (1.57) and the current from (2.7).

The subsequent results concern the large time behavior obtained from the kernel, once the thermodynamic limit is taken. We have found that there are actually two different scaling regimes. The first one is the NESS where $x, x' = O(1)$ and the second one is the regime of rays where both $x, x' = O(t)$. Since

the analytical computations of the asymptotic behaviors are quite tricky, we have carefully checked numerically our main predictions, which are shown in Figs. 2.6, 2.7 and 2.8 below.

As we will see below some of these results (but not all) can also be obtained from a heuristic semi-classical method which relies on the momentum dependent transmission and reflection coefficients $T(k)$ and $R(k)$, which for a delta function impurity are given by

$$T(k) = \frac{k^2}{k^2+g^2} \quad , \quad R(k) = 1 - T(k) = \frac{g^2}{k^2+g^2} \; . \tag{2.107}$$

The results presented here are derived from first principles, starting from from an exact expansion over the eigenfunctions of the many-body system.

2.4.1 NESS regime: fixed x and x'

The first regime corresponds to fixed spatial positions x, x' with $t \to +\infty$. In this case, the kernel, the density and the particle current reach a stationary limit which we compute explicitly, namely

$$\rho(x,t) \to \rho_\infty(x) \quad , \quad J(x,t) \to J_\infty \quad , \quad K(x,x';t) \to K_\infty(x,x') \; . \tag{2.108}$$

Note that from the fermion number conservation in Eq. (2.8) the current is constant in space in the large time limit. From the symmetry of the problem under the change $x \to -x$, these observables satisfy the following relations

$$\begin{gathered} \rho_\infty(x)|_{k_L,k_R} = \rho_\infty(-x)|_{k_R,k_L} \; , \quad J_\infty|_{k_R,k_L} = -J_\infty|_{k_L,k_R} \; , \\ K_\infty(x,x')|_{k_L,k_R} = K_\infty(-x,-x')|_{k_R,k_L} \; . \end{gathered} \tag{2.109}$$

Density. For the density we find, for $x > 0$

$$\boxed{\rho_\infty(x>0) = \frac{k_R}{\pi} - \int_{k_L}^{k_R} \frac{dk}{2\pi} \frac{k^2}{g^2+k^2} + \frac{g}{\pi} \int_0^{k_R} dk \frac{k \sin(2k|x|) - g\cos(2kx)}{g^2+k^2}.} \tag{2.110}$$

Note that $\rho_\infty(x<0)$ is obtained from this expression Eq. (2.110) together with the symmetry relation (2.109). This result for $\rho_\infty(x)$ is shown in Fig. (2.6) and compared with a numerical evaluation of the exact formula for $\rho(x,t)$ (from (2.143) with $x = x'$) at a relatively large time.

Let us now discuss a few salient features of this result. Far from the impurity, which is located at $x = 0$, the stationary density profile approaches a constant which is different on both sides and given by

$$\lim_{x\to\pm\infty} \rho_\infty(x) = \frac{\rho_L + \rho_R}{2} \pm \int_{k_L}^{k_R} \frac{dk}{2\pi} \frac{g^2}{g^2+k^2}. \tag{2.111}$$

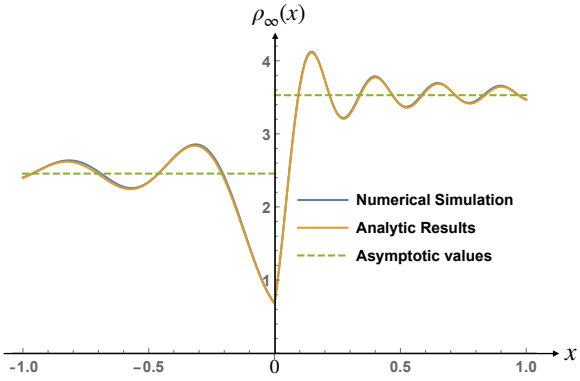

FIGURE 2.6: Plot of the mean fermion density $\rho_\infty(x)$ (in orange) as a function of x in the presence of a repulsive impurity ($g > 0$) in the NESS given by Eq. (2.110) for $\rho_R = 4$, $\rho_L = 2$ and $g = 10$. The oscillating behavior of $\rho_\infty(x)$ is the non-equilibrium analog of the Friedel oscillations [160]. The asymptotic values for $\rho_\infty(\pm\infty)$ given by (2.112) are indicated as horizontal dashed lines. These analytical results are compared with a numerical evaluation (blue) of $\rho(x,t)$ evaluated from the exact formula in (2.143) with $x = x'$ for large time $t = \frac{\ell}{4\pi\rho_R}$ and system size $\ell = 50$. The agreement is excellent. Although large, this time has to be small enough so that the fastest fermions traveling at speed k_R have not been reflected by the boundaries at $x = \pm\frac{\ell}{2}$. This is achieved if $k_R t < \frac{\ell}{2}$, i.e., if $t < t_\ell = \frac{\ell}{2\pi\rho_R}$.

These asymptotic values can also be predicted by the semi classical method (see Section 2.7) and written in the equivalent form

$$\rho_\infty(+\infty) = \frac{k_R}{\pi} - \int_{k_L}^{k_R} \frac{dk}{2\pi} T(k) \quad , \quad \rho_\infty(-\infty) = \frac{k_L}{\pi} + \int_{k_L}^{k_R} \frac{dk}{2\pi} T(k) \, , \quad (2.112)$$

in terms of the transmission coefficient $T(k)$ given in Eq. (2.107). The mean density is continuous at $x = 0$ but exhibits a cusp, with different left and right derivatives given by

$$\rho'_\infty(0^+) = \int_0^{k_R} \frac{dk}{\pi} \frac{2k^2 g}{k^2 + g^2} \quad , \quad \rho'_\infty(0^-) = -\int_0^{k_L} \frac{dk}{\pi} \frac{2k^2 g}{k^2 + g^2} \, . \quad (2.113)$$

At variance with the equilibrium case (see below), this cusp is asymmetric.

Finally, the result for $\rho_\infty(x)$ can be compared to the result obtained in [164] for the mean density $\rho_{\rm eq}(x)$ of the equilibrium problem, i.e. in the ground state with Fermi energy $\mu = \frac{k_F^2}{2}$ in the presence of a repulsive delta impurity of strength $g > 0$ (see formula (60) and (138) there with $\lambda = g$)

$$\rho_{\rm eq}(x) \quad = \frac{k_F}{\pi} + \frac{g}{\pi} \int_0^{k_F} dk \frac{k \sin(2k|x|) - g\cos(2kx)}{k^2 + g^2}. \quad (2.114)$$

We see that for $k_L = k_R = k_F$ the NESS density coincides with the equilibrium (ground state) density (as discussed latter, this holds only in the absence of bound state, that is for $g \geq 0$). This is quite interesting since the initial state

in the present work is far from the ground state of the system in the presence of the impurity. An explanation for this property is that the components of the initial state on the excited states correspond to fermionic waves (quasi particles) propagating towards the edges of the system. If the observation time is smaller than $t_\ell = \frac{\ell}{2\pi\rho_R}$, such that the fastest fermions traveling at speed k_R have not been reflected yet, i.e. $k_R t < \frac{\ell}{2}$, we expect relaxation to the equilibrium state for $k_L = k_R$ (and to the NESS for $k_L \neq k_R$). This will always occur if the limit $\ell \to +\infty$ is taken first.

Current. In addition, in the NESS, we show that there is a non zero particle current given by

$$\boxed{J_\infty = -\int_{k_L}^{k_R} \frac{dk}{2\pi} \frac{k^3}{k^2+g^2} = \frac{1}{2\pi}\left(\mu_L - \mu_R + \frac{g^2}{2}\ln\left(\frac{g^2+2\mu_R}{g^2+2\mu_L}\right)\right)} \ , \tag{2.115}$$

which can alternatively be expressed, using the transmission coefficient $T(k)$ given in Eq. (2.107), as

$$J_\infty = -\int_{k_L}^{k_R} \frac{dk}{2\pi} k\, T(k) \ . \tag{2.116}$$

This result can also be obtained by a semi-classical method, see Section 2.7. The current is shown in Fig. 2.7 for $\rho_R = 4$, $\rho_L = 2$ (note that it is negative in that case). Its maximal (absolute) value is reached for $g = 0$ when there is no defect. In that case one finds $J_\infty = \frac{1}{2\pi}(\mu_L - \mu_R)$ which corresponds to a unit conductance e^2/h. In the limit $g \to +\infty$ it vanishes as

$$J_\infty = \frac{1}{2\pi g^2}(\mu_L^2 - \mu_R^2) + O\left(\frac{1}{g^4}\right) \ , \tag{2.117}$$

which shows, as expected, that for a very strong defect the system is effectively cut into two almost independent halves.

Kernel. Finally we also obtain the kernel in the NESS which reads explicitly for $x, x' > 0$

$$\begin{aligned} K_\infty(x>0, x'>0) = &\int_0^{k_R} \frac{dk}{\pi} \cos\left(k(x-x')\right) - \int_{k_L}^{k_R} \frac{dk}{2\pi} \frac{k^2}{k^2+g^2} e^{-ik(x-x')} \\ &+ \int_0^{k_R} \frac{dk}{\pi} \frac{gk\sin\left(k(x+x')\right) - g^2\cos\left(k(x+x')\right)}{k^2+g^2} \ , \end{aligned} \tag{2.118}$$

while for $x > 0, x' < 0$ it reads

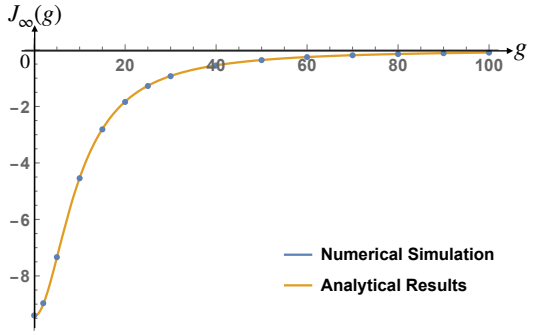

FIGURE 2.7: Plot of the current J_∞ (orange solid line) in the NESS as a function of g, the strength of the delta impurity, as given by formula Eq. (2.115), with $\rho_R = 4$, $\rho_L = 2$. It is compared with a numerical evaluation (blue dots) of the exact expression of $J(x = 0, t)$, obtained from Eq. (2.143) together with (2.7), for large time $t = \frac{\ell^2}{8\pi N_R} = t_\ell/2$ and system size $\ell = 50$ for several values of g.

$$K_\infty(x>0,x'<0) = \left(\int_0^{k_R} + \int_0^{k_L}\right)\frac{dk}{2\pi}\frac{k}{k^2+g^2}(k\cos(k(x-x')) + g\sin(k(x-x')) \tag{2.119}$$
$$+i\int_{k_L}^{k_R}\frac{dk}{2\pi}\frac{k}{k^2+g^2}\left(k\sin k(x-x') - g\cos k(x-x') + ge^{-ik(x+x')}\right),$$

the other cases being obtained by symmetry (see (2.109)). This result can be expressed in a more compact form as

$$\boxed{\begin{aligned} K_\infty(x,x') &= \left(\int_0^{k_L} + \int_0^{k_R}\right)\frac{dk}{2\pi}\left[\phi^\infty_{-,k}(x)\phi^\infty_{-,k}(x') + \phi^\infty_{+,k}(x)\phi^\infty_{+,k}(x')\right] \\ &+ \int_{k_L}^{k_R}\frac{dk}{2\pi}\left[\frac{(g+ik)}{\sqrt{g^2+k^2}}\phi^\infty_{-,k}(x)\phi^\infty_{+,k}(x') + \frac{(g-ik)}{\sqrt{g^2+k^2}}\phi^\infty_{-,k}(x')\phi^\infty_{+,k}(x)\right], \end{aligned}} \tag{2.120}$$

where the $\phi^\infty_{\pm,k}$ are defined as the large ℓ limit of the Hamiltonian's eigenfunctions (2.132), and (2.133)

$$\begin{aligned} \phi^\infty_{\pm,k}(x) &= \lim_{\ell\to\infty}\sqrt{\frac{\ell}{2}}\phi_{\pm,k}(x), \\ \phi^\infty_{-,k}(x) &= \sin(kx), \\ \phi^\infty_{+,k}(x) &= \frac{k\cos(kx) + g\sin(k|x|)}{\sqrt{g^2+k^2}}. \end{aligned} \tag{2.121}$$

The advantage of this form Eq. (2.120), resides in the fact that we see on the first line real diagonal terms in the Hamiltonian basis which produce no current (2.7), and on the second line complex off-diagonal (but degenerate) terms which contain all information on the current (2.115). The kernel simplifies in the limit

where the points $x, x' \to \infty$. In this limit, keeping $x - x' = O(1)$ one finds the asymptotic behavior

$$K_\infty(x,x') \simeq \int_0^{k_R} \frac{dk}{\pi} \cos(k(x-x')) - \int_{k_L}^{k_R} \frac{dk}{2\pi} \frac{k^2}{k^2+g^2} e^{-ik(x-x')}, \quad (2.122)$$

On the other hand, if $x \to +\infty$ and $x' \to -\infty$ with $x + x' = O(1)$ one finds

$$K_\infty(x,x') \simeq i \int_{k_L}^{k_R} \frac{dk}{2\pi} \frac{kg}{k^2+g^2} e^{-ik(x+x')} \ , \quad (2.123)$$

while the asymptotic kernel, for $x, x' \to \infty$, vanishes for generic value of x'/x different from ± 1.

In Section 2.7 we discuss the semi-classical method or GHD results in presence of a defect. It cannot reproduce the full expressions in Eq. (2.120), which is not surprising because microscopic details are erased when we take the Euler scaling limit (2.67). As expected, it does predict the asymptotic form in (2.122). More surprisingly, we will see that the result (2.123) cannot be predicted by this semi-classical method.

2.4.2 Ray regime or LQSS (Large time regime with $\xi = x/t$ fixed)

The second regime corresponds to both $x, t \to \infty$ with a fixed ratio $\xi = x/t$, i.e. along rays. In this case the density and the current reach finite limits, which are only functions of the scaling variable ξ

$$\rho(x,t) \to \tilde{\rho}(\xi) \quad , \quad J(x,t) \to \tilde{J}(\xi) \ . \quad (2.124)$$

Note that the fermion number conservation Eq. (2.8) implies that these two functions must be related via

$$\partial_\xi \tilde{J}(\xi) = \xi \partial_\xi \, \tilde{\rho}(\xi) \ . \quad (2.125)$$

All the results below in that regime hold for any g (positive or negative) since the bound state (that exists for $g < 0$) does not contribute in that limit.

Density. We find through explicit calculation of the large time limit, that the scaling function for the density reads

$$\boxed{\tilde{\rho}(\xi) = \frac{k_L + k_R}{2\pi} + \mathrm{sgn}(\xi) \left(\int_{k_L}^{k_R} \frac{dk}{2\pi} R(k) + \int_{k_L}^{k_R} \frac{dk}{2\pi} T(k) \Theta(|\xi| - k) \right) \ .} \quad (2.126)$$

A plot of $\tilde{\rho}(\xi)$ is shown in the right panel of Fig. 2.8, together with an exact evaluation at finite time illustrating the convergence. Note that $\tilde{\rho}(\xi)$ is a continuous function of ξ except at $\xi = 0$ where it has a jump discontinuity. The values on each side of the jumps at $\xi = 0^\pm$ are found to agree with the large

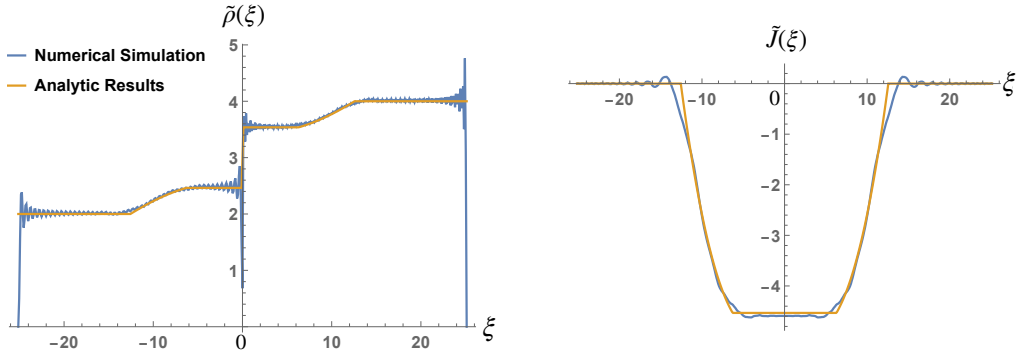

FIGURE 2.8: Asymptotic density (left panel) and current (right panel) at large time in the regime of rays $\xi = x/t$ fixed. (Orange) Plots of $\tilde{\rho}(\xi)$ and $\tilde{J}(\xi)$ as a function of $\xi = x/t$ as given in Eqs. 2.129 and 2.128 for $\rho_R = 4$, $\rho_L = 2$ and $g = 10$. (Blue) For comparison, $\rho(x,t)$ and $J(x,t)$ are plotted versus $\xi = x/t$ for $t = \frac{\ell}{4\pi\rho_R} = t_\ell/2$ and $\ell = 50$. In this problem there are 2 pairs of light cones at $|\xi| = k_R = 4\pi$ and $|\xi| = k_L = 2\pi$. On this scale the density exhibits a jump at $\xi = 0$, which is rounded on a scale $x = O(1)$ in the NESS (see Fig. 2.6) with a perfect matching as $\xi \to 0^{\pm}$, see Eq. (2.128) (the oscillations visible here for $\xi \approx 0$ are actually part of the NESS regime).

distance limit of the density obtained the NESS regime, i.e.

$$\tilde{\rho}(0^{\pm}) = \lim_{x \to \pm\infty} \rho_\infty(x) \ . \tag{2.127}$$

This matching shows that there is no additional intermediate regime between the NESS $x = O(1)$, and the regime of rays $x = O(t)$.

Current. For the scaling function of the current we obtain, again through explicit calculation of the large time limit

$$\boxed{\tilde{J}(\xi) = -\int_{k_L}^{k_R} \frac{dk}{2\pi}\, k\, T(k)\Theta(k - |\xi|) \ ,} \tag{2.128}$$

where $T(k)$ is given in (2.107). A plot of $\tilde{J}(\xi)$ is shown in the right panel of Fig. 2.8, together with an exact evaluation at finite time illustrating the convergence. The function $\tilde{J}(\xi)$ is a continuous function of ξ everywhere. One can check that the conservation equation Eq. (2.125) is obeyed, including at the point $\xi = 0$ (the delta function in $\partial_\xi \tilde{\rho}(\xi)$ is cancelled by the factor ξ in Eq. (2.125)). Note that in this model there are two pairs of light cones at $\xi = \pm k_L$ and $\xi = \pm k_R$ respectively. Outside these two light cones ($|\xi| > \max(k_R, k_L)$) the current vanishes at large time. Inside these two light cones ($|\xi| < \min(k_R, k_L)$) the current is constant and equal to its value in the NESS (and so is the density).

Kernel. We have found by explicit calculation that in this ray regime the kernel $K(x = \xi t, x' = \xi' t, t)$ vanishes unless $\xi = \xi'$ or $\xi = -\xi'$. More precisely

one obtains the limiting scaling forms for $y, y' = O(1)$

$$\boxed{\lim_{t\to+\infty} K(\xi t + y, \pm\xi t + y') = K^{\pm}_{\xi}(y, y') \ .} \tag{2.129}$$

The expression for $K^{+}_{\xi}(y, y')$ is obtained as

$$\boxed{\begin{aligned} K^{+}_{\xi}(y, y') &= -\mathrm{sign}(\xi) \int_{k_L}^{k_R} \frac{dk}{2\pi} T(k) e^{-i\mathrm{sign}(\xi)k(y-y')} \Theta(k - |\xi|) \\ &+ \int_0^{k_R} \frac{dk}{\pi} \cos(k(y-y'))\Theta(\xi) + \int_0^{k_L} \frac{dk}{\pi} \cos(k(y-y'))\Theta(-\xi). \end{aligned}} \tag{2.130}$$

where we recall that $T(k) = k^2/(k^2+g^2)$. Note that $K^{+}_{\xi}(y, y')$ is a function of $y - y'$ only. From this expression (2.130) in the limit of coinciding points one recovers the density $\tilde{\rho}(\xi)$ in Eq. (2.126) (using $R(k) = 1 - T(k)$) and the current $J(\xi)$ in Eq. (2.128) using (2.7). It is important to note that the kernel (2.130) matches exactly in the limit $\xi \to 0^+$ with the result (2.122) for the kernel $K_\infty(x, x')$ of the NESS in the large distance limit $x, x' > 0$.

The expression for $K^{-}_{\xi}(y, y')$ is given by

$$\boxed{K^{-}_{\xi}(y, y') = i\,\mathrm{sign}(\xi) \int_{k_L}^{k_R} \frac{dk}{2\pi} \frac{gk}{g^2+k^2} e^{-i\mathrm{sign}(\xi)k(y+y')} \Theta(k - |\xi|) \ .} \tag{2.131}$$

This measures the quantum correlation between opposite rays. Once again the kernel (2.131) matches exactly in the limit $\xi \to 0^+$ with the result (2.123) for the kernel $K_\infty(x, x')$ of the NESS in the limit of very separated points $x > 0, x' < 0$.

Notice the following important points:

- If there is either no inhomogeneity in the initial state (like in [140]) or an inhomogeneous initial state without defect (like in [134] or (2.95)) then there is no opposite rays correlation $K^{-}_{\xi}(y, y') = 0$, hence this is a new phenomenon due to the inhomogeneity of the Hamiltonian (2.96) and the asymmetry in the left and right initial chemical potential $\mu_{R/L}$.

- It is important to remark that the results for the density (2.126), the current (2.128) and the kernel at coinciding rays (2.130) can be also obtained using the semi-classical method as we will see in Section 2.7. However the result for $K^{-}_{\xi}(y, y')$ for opposite rays in Eq. (2.131) cannot be obtained from this semi-classical method. Indeed, it contains additional information about correlations between two opposite rays i.e. between two points far away from the defect and almost symmetric with respect to the defect. Physically, it corresponds to a particle that is either reflected or transmitted at the defect.

2.4.3 Derivation of the NESS

2.4.3.1 Exact kernel at Finite Time and Finite Size.

The Hamiltonian eigenbasis. First we derive an exact formula for the kernel at any time t in a system with of size ℓ. This will be the starting point for the asymptotic analysis for $\ell \to +\infty$ and subsequently for the computation of the large time limit performed latter on.

In order to proceed, we need the eigenbasis of $\hat{H}_g$. We first consider here $g > 0$, and a finite interval $x \in [-\ell/2, \ell/2]$ and specify further $\hat{H}_g$ by imposing the vanishing of the wavefunctions at $x = \pm\ell/2$. The eigenfunctions of $\hat{H}_g$ are either even or odd in x, respectively labelled by a subscript '+' or '−'. The odd eigenfunctions do not feel the delta impurity (since they vanish at the location of the impurity) hence they read

$$\phi_{-,q}(x) = \sqrt{\frac{2}{\ell}} \sin(qx) \quad , \quad q \in \Lambda_- = \left\{ \frac{2\pi n}{\ell}, n \in \mathbb{N}^* \right\} , \tag{2.132}$$

where we denote Λ_- the lattice of possible values for the wavevector q.

The even eigenfunctions are also plane waves, and denoted by $\phi_{+,q}(x)$, but with a different quantization condition on q. They read

$$\phi_{+,q}(x) = \frac{1}{\sqrt{(g^2+q^2)\frac{\ell}{2}+g}} (q\cos(qx) + g\sin(q|x|)) , \tag{2.133}$$

with the quantification condition (see Fig. (2.9))

$$q\cos\left(\frac{q\ell}{2}\right) + g\sin\left(\frac{q\ell}{2}\right) = 0 \quad \Leftrightarrow e^{-iq\ell} = -\frac{q-ig}{q+ig} , \tag{2.134}$$

i.e., $q\ell = -2\text{atan}(q/g) + m\pi$, which defines the lattice of possible wavevectors $q \in \Lambda_+$

$$\Lambda_+ = \left\{ q, q\cos(\frac{q\ell}{2}) + g\sin(\frac{q\ell}{2}) = 0 \cap q > 0 \right\} . \tag{2.135}$$

Note that q and $-q$ correspond to the same state, hence the condition $q > 0$. Equivalently the states can be labeled by the strictly positive integers $m \in \mathbb{N}^*$ (see Fig. (2.9)).

Finally, both the odd and even eigenstates $\phi_{\pm,q}(x)$ are associated to the eigenenergy

$$E(q) = \frac{q^2}{2} . \tag{2.136}$$

Time Dependent Kernel. As discussed above, see Eq. (2.104), the time dependent kernel splits into two parts

$$K(x, x'; t) = K_L(x, x'; t) + K_R(x, x'; t), \tag{2.137}$$

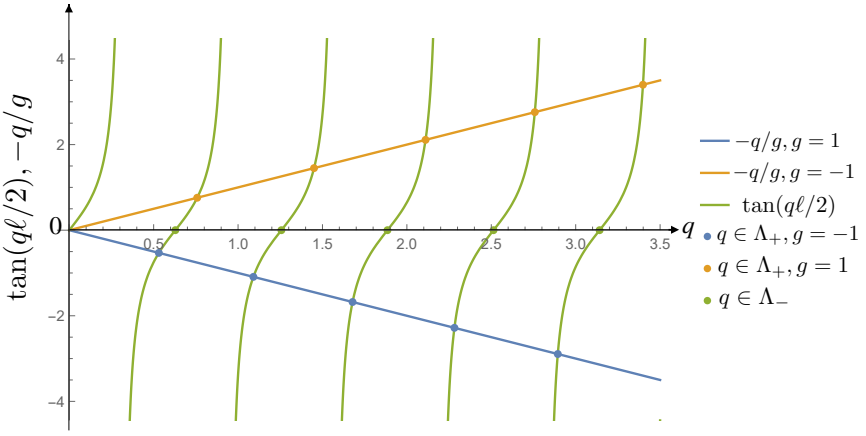

FIGURE 2.9: Graphical representation of the quantization condition in Eq. (2.134). It is plotted here for $g = \pm 1$ and $\ell = 10$. The intersection points $-\frac{q}{g} = \tan(\frac{q\ell}{2})$ generate the lattice $q \in \Lambda_+$ (2.135). The lattice Λ_- corresponds to the roots of the equation $0 = \tan(\frac{q\ell}{2}) = \sin(\frac{q\ell}{2})$ (see Eq. (2.132)). Therefore the two lattices Λ_+ and Λ_- are intertwined. For $g < 0$ the situation is almost the same but now $-\frac{q}{g}$ has a positive slope. Note that for $g < 0$, there is an additional bound state which cannot be shown on this figure.

where each component evolves independently

$$K_{R/L}(x, x'; t) = \sum_{n=1}^{N_L} \psi_n^{R/L*}(x, t)\psi_n^{R/L}(x', t) \, . \tag{2.138}$$

Since the $\psi_n^{R/L}$'s evolve according to the Schrödinger equation with Hamiltonian $\hat{H}_g$ in Eq. (2.96) these components can be rewritten using the real time Green's function

$$G(x, y, t) = \langle x|e^{-i\hat{H}_g t}|y\rangle = \sum_{\sigma=\pm, q\in\Lambda_\sigma} \phi_{\sigma,q}(x)\phi^*_{\sigma,q}(y)e^{-iE(q)t} \, , \tag{2.139}$$

where the eigenfunctions $\phi_{\sigma,q}(x)$ of $\hat{H}_g$ are given in (2.132) and (2.133). This leads to

$$K_{R/L}(x, x'; t) = \int_{-\ell/2}^{\ell/2} dy dy' G^*(x, y, t)G(x', y', t)K_{R/L}(y, y') \, . \tag{2.140}$$

The time evolution of the total kernel is thus obtained as the sum as in (2.137).

Let us first study $K_R(x, x'; t)$ in Eq. (2.140). Inserting the decomposition (2.139) of the Green's function together with the explicit expression of $K_R(y, y')$

in Eq. (2.101) we obtain

$$K_R(x,x',t) = \sum_{\sigma_a=\pm,k_a\in\Lambda_{\sigma_a}} \sum_{\sigma_b=\pm,k_b\in\Lambda_{\sigma_b}} \sum_{k\in\Lambda_-,k\le k_R} \phi^*_{\sigma_a,k_a}(x)\phi_{\sigma_b,k_b}(x')e^{i(E(k_a)-E(k_b))t} \int_0^{\ell/2} dy\sqrt{\frac{4}{\ell}}\phi_{\sigma_a,k_a}(y)\sin(ky)\int_0^{\ell/2} dy'\sqrt{\frac{4}{\ell}}\phi^*_{\sigma_b,k_b}(y')\sin(ky')\ , \quad (2.141)$$

where, we have just reorganized the discrete sums and the integrals over y and y'. The same manipulations can be performed for $K_L(x,x',t)$. The overlap integrals over y and y' can be performed explicitly, which gives

$$\begin{aligned} K_{R/L}(x,x',t) = &\sum_{\sigma_a=\pm,k_a\in\Lambda_{\sigma_a}} \sum_{\sigma_b=\pm,k_b\in\Lambda_{\sigma_b}} \sum_{k\in\Lambda_-,k\le k_{R/L}} \phi^*_{\sigma_a,k_a}(x)\phi_{\sigma_b,k_b}(x')e^{i(E(k_a)-E(k_b))t} \\ &\times\left(\frac{1}{\sqrt{2}}\delta_{\sigma_a,-}\delta_{k,k_a} \pm \frac{2^{3/2}}{\ell}\frac{kk_a}{(k^2-k_a^2)\sqrt{g^2+k_a^2+\frac{2g}{\ell}}}\delta_{\sigma_a,+}\right) \\ &\times\left(\frac{1}{\sqrt{2}}\delta_{\sigma_b,-}\delta_{k,k_b} \pm \frac{2^{3/2}}{\ell}\frac{kk_b}{(k^2-k_b^2)\sqrt{g^2+k_b^2+\frac{2g}{\ell}}}\delta_{\sigma_b,+}\right)\ , \quad (2.142) \end{aligned}$$

where, in the last two factors in brackets, the $+$ sign refers to K_R and the $-$ to K_L. To compute the full kernel we add the two halves and develop the product to get

$$\begin{aligned} K(x,x',t) = &\underbrace{\left(\sum_{n=1}^{N_R}+\sum_{n=1}^{N_L}\right)\frac{1}{2}\frac{2}{\ell}\phi^\infty_{-,\frac{2\pi n}{\ell}}(x)\phi^\infty_{-,\frac{2\pi n}{\ell}}(x')}_{A=A_R+A_L} \quad (2.143) \\ &+\left(\sum_{k\in\Lambda_-,k\le k_R}+\sum_{k\in\Lambda_-,k\le k_L}\right)\sum_{k_a\in\Lambda_+,k_b\in\Lambda_+} 2\left(\frac{2}{\ell}\right)^3\frac{\phi^\infty_{+,k_a}(x)\phi^\infty_{+,k_b}(x')}{\sqrt{g^2+k_a^2}\sqrt{g^2+k_b^2}} \\ &\qquad\times\underbrace{\frac{k^2k_ak_b}{(k_a^2-k^2)(k_b^2-k^2)}e^{i(E(k_a)-E(k_b))t}}_{B=B_R+B_L} \\ &\underbrace{+\sum_{k\in\Lambda_-,k_L<k\le k_R}\sum_{k_b\in\Lambda_+}(\frac{2}{\ell})^2\phi^\infty_{-,k}(x)\frac{\phi^\infty_{+,k_b}(x')}{\sqrt{g^2+k_b^2}}\frac{kk_b}{k^2-k_b^2}e^{i(E(k)-E(k_b))t}}_{C} \\ &+\underbrace{\sum_{k\in\Lambda_-,k_L<k\le k_R}\sum_{k_a\in\Lambda_+}(\frac{2}{\ell})^2\phi^\infty_{-,k}(x')\frac{\phi^\infty_{+,k_a}(x)}{\sqrt{g^2+k_a^2}}\frac{kk_a}{k^2-k_a^2}e^{i(E(k_a)-E(k))t}}_{D}\ , \end{aligned}$$

which is the sum of four terms denoted $A = A_R + A_L, B = B_R + B_L, C, D$ as indicated in the equation. These terms satisfy the symmetries: $A(x,x')$ is real and symmetric, $B(x,x') = B^*(x',x)$ and $D(x,x') = C^*(x',x)$. Here $\phi^\infty_{\pm,k}(x)$ is defined in (2.121). Additionally, for simplicity, we have replaced the

normalisation constant of the wave functions by their large system size limits, see [2] for the exact formula.

Let us make a few remarks:

- *Symmetries:* Since the initial kernel is unchanged under the simultaneous transformation $(k_L, k_R, x) \to (k_R, k_L, -x)$ and because of the invariance of $\hat{H}_g$ under parity transformation $x \to -x$, it follows that $K(x, x', t)$ is also unchanged under $(k_L, k_R, x) \to (k_R, k_L, -x)$. The density $\rho(x, t)$ has thus the same invariance and the current satisfies $J_{k_L,k_R}(x, t) = -J_{k_R,k_L}(-x, t)$. This property is the finite time analog of the relations valid for the NESS stated in Eq. (2.109).

- *Contribution to the current:* Since the term A is real, it does not contribute to $J(x, t)$, i.e., $J_A(x, t) = 0$ (see Eq. (2.7)). It is easy to see that the term B gives only an odd contribution to the current, i.e. $J_B(x, t) = -J_B(-x, t)$. Hence the term B cannot contribute to J_∞, the current in the NESS, which is uniform. It does however contribute to $\rho_\infty(x)$. The current in the NESS is thus only determined by $C + D$ which gives an even contribution at all time t, i.e., $J_{C+D}(x, t) = J_{C+D}(-x, t)$.

2.4.3.2 Double limit of the kernel $\ell \to +\infty$, and $t \to +\infty$.

Let us recall that we take the limit $\ell \to \infty$ while fixing the left and right initial densities $\frac{2N_{R/L}}{\ell} = \rho_{R/L} = \frac{k_{R/L}}{\pi}$. Then we take the large time limit. Here we consider the case of a repulsive impurity $g > 0$ – the analysis of an attractive impurity $g < 0$ is performed in Section 2.6.4. This computation is possible thanks to a contour integration trick that we explain in a general version in Appendix A. From the exact expression for the kernel in (2.143), one can write

$$K(x, x', t) = A_L(x, x') + A_R(x, x') + D^*(x', x, t) + D(x, x', t) + B_L(x, x', t) + B_R(x, x', t) \,, \tag{2.144}$$

where we have used the relation $D(x, x', t) = C^*(x', x, t)$. We now consider the terms $A_{R/L}, B_{R/L}$ and D separately.

The term $A(x, x')$: From (2.143) we see that it is time independent and, in the large ℓ limit, it is given by the reflected sine-kernel (see e.g. [182, 183])

$$\begin{aligned} A_{R/L}(x, x') &= \lim_{\ell\to\infty} \frac{1}{\ell} \sum_{n=1}^{N_{R/L}} \sin\left(\frac{2\pi n x}{\ell}\right) \sin\left(\frac{2\pi n x'}{\ell}\right) \\ &= \int_0^{k_{R/L}} \frac{dk}{2\pi} \phi^\infty_{-,k}(x) \phi^\infty_{-,k}(x') \,, \end{aligned} \tag{2.145}$$

where, $\phi^{\infty}_{-,k}(x) = \sin(kx)$ defined in (2.121). We see that the limit of $A(x,x')$ is the first term of (2.120).

The term $D(x,x',t)$: From (2.143) the term D is given by a double sum

$$D = D(x,x',t) = \frac{4}{\ell^2} \sum_{k_b \in \Lambda_+} \sum_{k \in \Lambda_-, k = k_L^+}^{k_R} \frac{h_{x,x',t}(k,k_b)}{k-k_b} \tag{2.146}$$

with $k_L = 2\pi N_L/\ell$, $k_L^+ = 2\pi(N_L+1)/\ell$ and $k_R = 2\pi N_R/\ell$ and we recall that the lattices Λ_- and Λ_+ are defined in Eqs. (2.132) and (2.135) respectively. We have also defined the function [1]

$$h_{x,x',t}(k,k_b) = \frac{\phi^{\infty}_{-,k}(x')\phi^{\infty}_{+,k_b}(x)}{\sqrt{g^2+k_b^2}} \frac{kk_b}{k+k_b} e^{-\frac{i}{2}(k^2-k_b^2)t} , \tag{2.147}$$

where $\phi^{\infty}_{\pm,k}(x)$ is defined in (2.121). Taking the limit $\ell \to \infty$ of (2.146) to obtain a double integral is very delicate due to the presence in the sum of a pole $\frac{1}{k-k_b}$ and the fact that the two lattices Λ_- and Λ_+ are intertwined (see Fig. 2.9). However, thanks to the method introduced in Appendix A, D can be written as the following contour integral

$$D(x,x',t) = \frac{4}{\ell^2} \sum_{k_b \in \Lambda_+} \int_{\Gamma_0} \frac{dk}{2\pi} \frac{\ell}{e^{i\ell k}-1} \frac{h_{x,x',t}(k,k_b)}{k-k_b} , \tag{2.148}$$

where the contour Γ_0 is a union of very small circles centered around the points $k = \frac{2\pi n}{\ell}$ with $N_L+1 \leq n \leq N_R$ and oriented clockwise (see Fig. 2.10). This equality (2.148) is valid because the factor $\frac{\ell}{e^{i\ell k}-1}$ has poles at points $k = \frac{2\pi n}{\ell}$, hence, the equality results from the residue theorem. The circles should be small enough so that the contour does not enclose any point $k = k_b \in \Lambda_+$. We now deform the contour Γ_0 into the closed clockwise contour γ_δ which is the rectangle with the four corners $k_L^+ - \frac{2\pi\delta}{\ell} - i\epsilon$, $k_L^+ - \frac{2\pi\delta}{\ell} + i\epsilon$, $k_R + \frac{2\pi\delta}{\ell} + i\epsilon$, $k_R + \frac{2\pi\delta}{\ell} - i\epsilon$, represented in Fig. 2.10. The parameter $0 < \delta < 1$ is chosen small enough so that the contour does not contain any point k_b of Λ_+ located to the left of k_L^+ and to the right of k_R. During this deformation one encounters only the poles at $k = k_b \in \Lambda_+ \cap]k_L^+, k_R[$. Taking into account the residues associated to these poles one obtains

$$\begin{aligned} D(x,x',t) = \frac{4}{\ell^2} \Bigg(& \sum_{k_b \in \Lambda_+} \oint_{\gamma_\delta} \frac{dk}{2\pi} \frac{\ell}{e^{-i\ell k}-1} \frac{h_{x,x',t}(k,k_b)}{k-k_b} \\ & + 2\pi i \sum_{k_b \in \Lambda_+ \cap]k_L^+, k_R[} \frac{\ell}{2\pi} \frac{1}{e^{-i\ell k_b}-1} h_{x,x',t}(k_b,k_b) \Bigg) . \end{aligned} \tag{2.149}$$

Where the second line are the residue. Until now this is an exact rewriting of $D(x,x',t)$ in Eq. (2.146) valid for any ℓ. For any $k_b \in \Lambda_+$, using the second relation in (2.134), or equivalently using the result (A.10), one can evaluate the factor

$$\frac{1}{e^{-i\ell k_b}-1} = -(\frac{k_b + ig}{2k_b}) . \tag{2.150}$$

[1] Since we are eventually interested in the large ℓ limit we omitted in (2.147) the unimportant extra factor $2g/\ell$ in the denominator in (2.143), which should be restored to obtain finite ℓ formula.

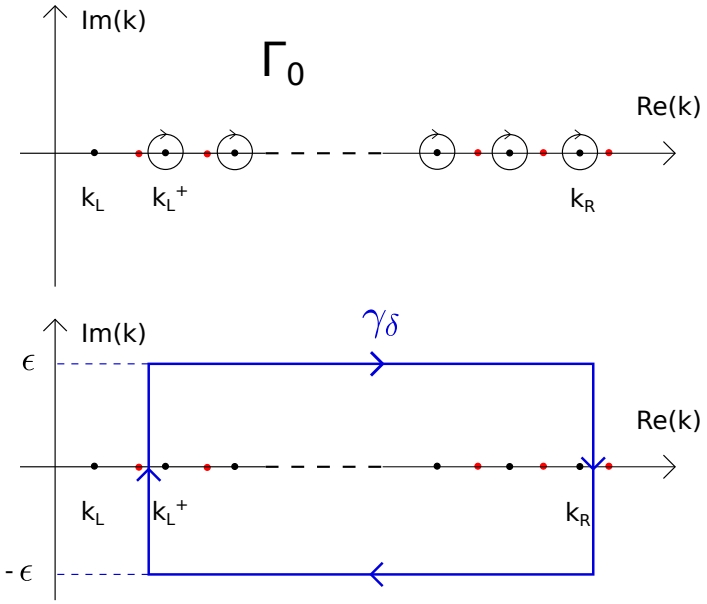

FIGURE 2.10: Illustration of the contours Γ_0 (upper panel) and γ_δ (lower panel) used in Eqs. (2.148) and (2.149) respectively. In red we represent the poles of $D(x,x',t)$ in (2.148) at $k=k_b$.

We now take the large ℓ and large time limit successively on Eq. (2.149). We already argued in Section A that the integral over γ_δ vanishes in that limit because the factor

$$\frac{e^{-i\frac{k^2}{2}t}}{e^{-i\ell k}-1}, \tag{2.151}$$

contained in the integral decays in the double limit when it is evaluated on γ_δ. In fact, the decay of the integral over γ_δ in (2.149) is more complex, this decay is explained in details in Appendix B. In the end, only the residue part of (2.149) remains in the double limit $\ell \to +\infty$, and $t \to +\infty$. Together, the double limit of D and C yields the second line of (2.120) (we recall that $C(x,x',t) = D^*(x,x',t)$ such that we also know the double limit of $C(x,x',t)$).

The term $B(x,x',t)$: We now give the double limit limit of $B_L(x,x')$ and $B_R(x,x')$ defined in (2.143). Each term can be decomposed as the sum of two terms

$$B_{R/L}(x,x',t) = B^{\text{off-diag}}_{R/L}(x,x',t) + B^{\text{diag}}_{R/L}(x,x') \tag{2.152}$$

where the first term comes from the terms $k_a \neq k_b$ in the triple sum in (2.143), this part decays to zero in the large system size and large time limit,

$$B^{\text{off-diag}}_{R/L}(x,x',t) \underset{\substack{\ell\to\infty \\ t\to\infty}}{\to} 0 \tag{2.153}$$

while the second one comes from the terms $k_a = k_b$ and does not depend on time.

The second term in (B.8) that is the diagonal part is equal to

$$B^{\text{diag}}_{R/L}(x,x') = \int_0^{k_{R/L}} \frac{dk}{2\pi} \phi^\infty_{+,k}(x)\phi^\infty_{+,k}(x') \ , \tag{2.154}$$

where the $\phi^{\infty}_{+,k}(x)$ are defined in (2.121). The equation (B.12) yields the second term of the first line of (2.120). Again, we refer to Appendix B for details on the decay of $B^{\text{off-diag}}_{R/L}(x,x',t)$ which is a non trivial task.

In summary we have considered all term A, B, C, D of (2.144) and proven the relaxation to the NESS described by the kernel (2.120) in the double limit $\ell \to +\infty$, and $t \to +\infty$. Now, we are going to discuss the case where the system relaxes to a GGE after a quench with identical initial conditions but in a different limit.

2.4.4 NESS from finite temperature initial state

Now we want to generalize this result to a wider initial condition. We choose the left and right initial state to be in a thermal state with different temperatures $T_{R/L}$ on both sides of the impurity and with associated chemical potential $\mu_{R/L}$. We will see that the NESS kernel (2.120) has a simple generalisation in term of Fermi-Dirac statistics. A difference also lies in the large-time decay to the NESS, which will be discussed in a later section.

Initial condition at finite temperature. The described initial state is a thermal product state, i.e. is is associated to a density matrix that is the density matrix of two thermal state density matrix $\hat{\rho} = \hat{\rho}_L \otimes \hat{\rho}_R$, such that both half system are independent. This amounts to take the initial kernel at $t = 0$

$$K(x,x',t=0) = K_L(x,x') + K_R(x,x'), \tag{2.155}$$

with,

$$\begin{aligned} K_L(x,x') &= \Theta(-x)\Theta(-x') \textstyle\sum_{n=1}^{\infty} \frac{4}{\ell} f_L\left(\frac{2\pi n}{\ell}\right) \sin\left(\frac{2\pi n x}{\ell}\right) \sin\left(\frac{2\pi n x'}{\ell}\right), \\ K_R(x,x') &= \Theta(x)\Theta(x') \textstyle\sum_{n'=1}^{\infty} \frac{4}{\ell} f_R\left(\frac{2\pi n'}{\ell}\right) \sin\left(\frac{2\pi n' x}{\ell}\right) \sin\left(\frac{2\pi n' x'}{\ell}\right) , \end{aligned} \tag{2.156}$$

and where

$$f_{R/L}(k) = \frac{1}{\exp(\beta_{R/L}(\frac{k^2}{2} - \mu_{R/L})) + 1} , \tag{2.157}$$

is the Fermi factor with $\beta_{R/L} = 1/T_{R/L}$. The density of fermions in the initial state is now related to the chemical potentials via

$$\rho_{R/L} = \int_0^{+\infty} \frac{dk}{\pi} f_{R/L}(k) . \tag{2.158}$$

The calculation proceeds in the same way as for $T_{R/L} = 0$ but with some integral contour modification. For example, when computing the large time behavior of D in (2.143), the integral contours Γ_0 in Eq. (2.148) and $\gamma_{\delta'}$ in (2.149) are changed (see Fig. 2.12). Notice that this change in the contours will affect the large time decay. We present here only the result for $g > 0$.

Results at finite temperature. In the NESS regime $x = O(1)$ the full kernel is given by

$$\boxed{\begin{aligned} K_\infty(x,x') &= \int_0^\infty \frac{dk}{2\pi}(f_R(k)+f_L(k))\left[\phi^\infty_{-,k}(x)\phi^\infty_{-,k}(x')+\phi^\infty_{+,k}(x)\phi^\infty_{+,k}(x')\right] \\ &+ (f_R(k)-f_L(k))\left[\frac{(g+ik)}{\sqrt{g^2+k^2}}\phi^\infty_{-,k}(x)\phi^\infty_{+,k}(x')+\frac{(g-ik)}{\sqrt{g^2+k^2}}\phi^\infty_{-,k}(x')\phi^\infty_{+,k}(x)\right] . \end{aligned}} \tag{2.159}$$

This result is very similar to the kernel at zero temperature (2.120) but with the corresponding Fermi factors. From this one can extract the density, which retains a cusp at $x = 0$ even at finite temperature. The current in the NESS at finite temperature is obtained as

$$\boxed{J_\infty = -\int_0^\infty dk \frac{f_R(k)-f_L(k)}{2\pi} k\, T(k)\ .} \tag{2.160}$$

We display its low temperature expansion in the case $\mu_L = \mu_R = \frac{k_F^2}{2}$

$$J_\infty = \frac{\pi}{6}(T_L^2 - T_R^2)\frac{g^2}{(g^2+k_F^2)^2} + \frac{7\pi^3}{15}\frac{g^2}{(g^2+k_F^2)^4}(T_L^4 - T_R^4) + O(T_R^6, T_L^6). \tag{2.161}$$

Note that in the absence of impurity, for $g = 0$, one has instead (for any $\mu_{R/L}$)

$$J_\infty|_{g=0} = \frac{\mu_L - \mu_R}{2\pi} + \frac{1}{2\pi}(T_L e^{-\mu_L/T_L} - T_R e^{-\mu_L/T_R}), \tag{2.162}$$

which generalizes the standard zero temperature result. Reversely, one can show that the current is proportional to $T_R \sim T_L$ at high temperature, which is consistent with the case $g = 0$ performed in [134].

In the ray regime $\xi = x/t = O(1)$ the kernel is obtained from Eqs. (2.129), (2.130), and (2.131) by replacing the integrals over finite intervals to integral on half infinite line with adequate Fermi factors

$$\begin{aligned} \int_0^{k_{R/L}} \frac{dk}{2\pi} &\to \int_0^{+\infty} \frac{dk}{2\pi} f_{R/L}(k) \\ \int_{k_L}^{k_R} \frac{dk}{2\pi} &\to \int_0^{+\infty} \frac{dk}{2\pi}\left(f_R(k) - f_L(k)\right). \end{aligned} \tag{2.163}$$

For simplicity, we only give the resulting current which is given by

$$\boxed{\tilde{J}(\xi) = -\int_0^\infty dk \frac{f_R(k)-f_L(k)}{2\pi} kT(k)\Theta(k-|\xi|),} \tag{2.164}$$

and it is plotted with the density in Fig. 2.11.

Remark: Note that the above initial state is quite different from the one considered in the lattice model in Ref. [143] which has purely local correlations. These correspond to two independent systems of free lattice fermions on a ring (as can be seen by writing the Fourier decomposition of $\delta_{xx'}$) while the initial kernel considered here

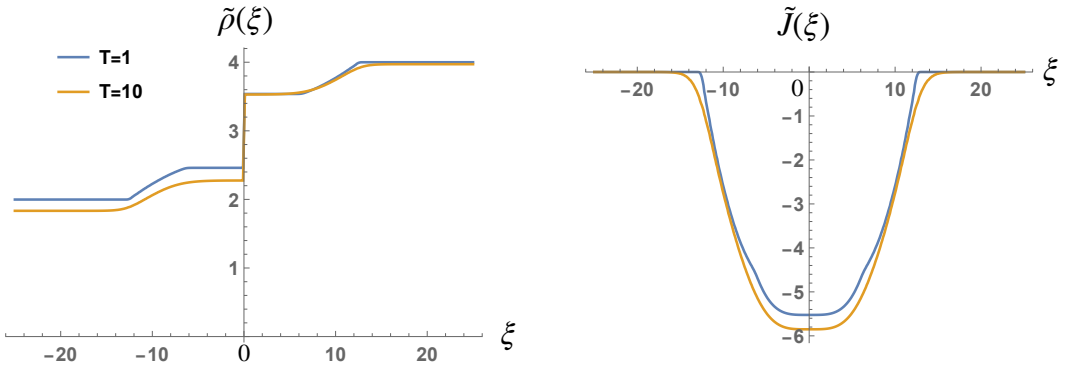

FIGURE 2.11: Plot of the asymptotic density $\tilde{\rho}(\xi)$ and current $\tilde{J}(\xi)$ in the ray regime as a function of $\xi = x/t$ for non zero temperature as given by Eq. (2.164) for $\rho_R = 4$, $\rho_L = 2$ and $g = 10$. The temperatures are identical on both sides with $T_L = T_R$ equal to 1 (orange curve) and 10 (blue curve). We notice that the singularities at the light cones $\xi = \pm k_{R/L}$ are rounded compared to the zero temperature case shown in Fig. 2.8.

corresponds instead to two independent systems of fermions in hard boxes. It is however possible to match the two sets of results (lattice and continuum) but only in the double limit $\beta_{R/L} \to 0$ with $\mu_{R/L} \to +\infty$ of our kernel with $\beta_{R/L}\mu_{R/L} = \alpha_{R/L}$ where $\nu \pm \mu = \frac{1}{1+e^{\alpha_{L,R}}}$ are the initial densities on each side of the origin.

Matching between finite and zero temperature. Here, we give some details of the finite temperature calculation. The process is very close to the zero temperature computation. One starts from the initial kernel defined in (2.156). Again, the kernel can be decomposed into terms A, B, C, and D (2.143), but the sums are slightly different. Let us take the example of D. Instead of having a sum over k as in (2.146), where $k \in]k_L, k_R]$, the sum runs over the complete set Λ_- and contains a Fermi factor. In other words, we have the following transformation $\sum_{k\in\Lambda_-,k=k_L^+}^{k_R} \to \sum_{k\in\Lambda_-} (f_R(k) - f_L(k))$.

The contour γ_δ in Fig. 2.10 is now replaced by the semi-infinite rectangular contour $\gamma_{\delta'}$ with horizontal width 2ϵ shown in Fig. 2.12 (top right panel). A formula analogous to (2.149) can be written where the integrand in the first term now contains the additional factor $f_R(k) - f_L(k)$ while the sum in the second term contains the additional factor $f_R(k_b) - f_L(k_b)$ and k_b is now summed over the whole lattice Λ_+. This formula is valid however only provided the contour $\gamma_{\delta'}$ does not enclose a pole of the Fermi factors. Recall that the Fermi factor $f_{R/L}(k)$ has poles at $k = \pm k_n^{R/L}$ with

$$k_n^{R/L} = \sqrt{k_{R/L}^2 + 2(2n+1)i\pi T} \quad , \quad n \in \mathbb{Z}\,. \tag{2.165}$$

Hence we need to choose

$$\epsilon < \sqrt{k_{R/L}^2 + 2i\pi T}\,, \tag{2.166}$$

which we will assume from now on. The limit $\ell \to +\infty$ can now be performed and as before (see Appendix A) the contribution of the upper half of γ'_δ (i.e., for $\mathrm{Im}(k) > 0$) vanishes in that limit. Then in the large time limit, it is the lower half of γ'_δ that will decay, resulting in the last of the fourth term of (2.159).

Now we want to understand what happens to the integral contour if we take the

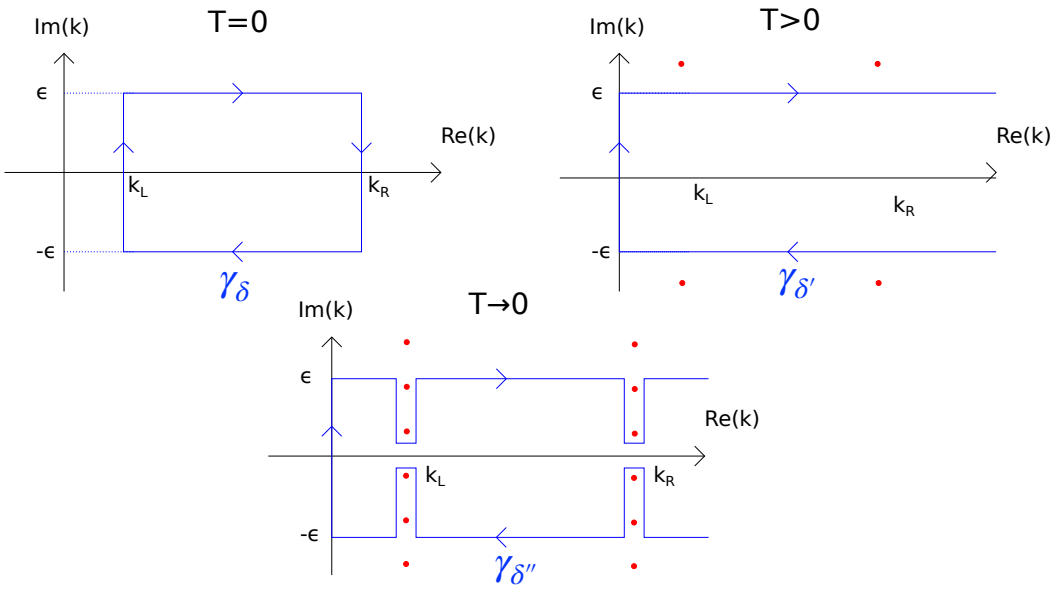

FIGURE 2.12: Modification of the contour of integration for nonzero temperature. The top left part shows the zero temperature contour γ_δ, while the top right panel shows the contour $\gamma_{\delta'}$ used at finite temperature. The red dots are the poles of the Fermi functions which, at low temperature, are located approximately along two vertical lines going through k_L and k_R. As explained in the text the residues at these poles can be used to recover the results in the $T \to 0$ limit, using the contour $\gamma_{\delta''}$ shown on the lower panel.

temperature to zero. In the above formula we have assumed that ϵ satisfies the bound in (2.166) such that the contour γ'_δ does not enclose any pole of the Fermi factors. However these poles get closer to the real axis when the temperature goes to zero. In other words the bound (2.166) becomes $\epsilon < \frac{\pi T}{k_R}$ at low T. So one can ask how is the $T = 0$ recovered. The answer is illustrated in the Fig. 2.12. The contour $\gamma_{\delta'}$ can be deformed into the contour $\gamma_{\delta''}$ as shown in the third panel in Fig. 2.12. Consider for instance the term C. One notes that as $T \to 0$ the contribution of the part of the contour to the left of k_L and the part of the contour to the right of k_R vanishes. Hence the result is indentical in that limit to the one obtained from the previously considered contour γ_δ (see first panel in Fig. 2.12), and to the $T = 0$ result.

2.4.5 Large time decay to the NESS

One of the main advantages of considering a quench is that it encompasses the dynamics. In this section, we will discuss how the NESS is reached at large times and how this dependence is influenced by the initial state having zero or non-zero left and right temperatures $T_{R/L}$.

Zero Temperature. We have also obtained the large time decay at zero temperature of the kernel $K(x, x', t)$ towards its value in the NESS for $g > 0$. It yields a

power law decay modulated by time oscillations

$$\boxed{\Delta K(x,x',t) = K(x,x',t) - K_\infty(x,x') \underset{t\to\infty}{\simeq} \frac{1}{t^{5/2}}}. \tag{2.167}$$

From it one extract the density and the current. The detailed decay of the density is found to be

$$\begin{aligned}\rho(x,t) - \rho_\infty(x) \simeq & -\frac{1}{\pi^2 g^4}(1+g|x|)^2 \frac{1}{t^3}\left(\frac{1}{k_L}+\frac{1}{k_R}\right) \\ & -\frac{4(1+g|x|)}{g(2\pi)^{3/2}t^{5/2}}\Big(\frac{k_R\cos(k_R x)+g\sin(k_R|x|)}{k_R^2(g^2+k_R^2)}\cos(\frac{k_R^2 t}{2}-\frac{\pi}{4}) \\ & +\frac{k_L\cos(k_L x)+g\sin(k_L|x|)}{k_L^2(g^2+k_L^2)}\cos(\frac{k_L^2 t}{2}-\frac{\pi}{4})\Big) \\ & +\frac{4(1+g|x|)}{g^2(2\pi)^{3/2}t^{5/2}}\left(\frac{\sin(k_L x)}{k_L^2}\cos(\frac{k_L^2 t}{2}-\frac{\pi}{4}) - \frac{\sin(k_R x)}{k_R^2}\cos(\frac{k_R^2 t}{2}-\frac{\pi}{4})\right) .\end{aligned} \tag{2.168}$$

Hence the leading decay is $t^{-5/2}$ modulated by oscillations, together with a $1/t^3$ term which is non oscillating. We also find that the current has also a leading algebraic decay as $t^{-5/2}$ modulated by oscillations. Note that power law decays with oscillations have been obtained in other systems of noninteracting fermions [31, 133].

Notice that this results are not valid in the ray regime, at finite temperature and for $g = 0$.

Finite Temperature. The decay in time to the NESS is different at finite T. It follows a power law together with time oscillations:

$$\Delta K(x,x',t) = \Delta K = K - K_\infty \simeq t^{-2} . \tag{2.169}$$

It is slower that the result obtained at zero temperature, where we found an oscillating $t^{-5/2}$ decay dominated by $k = k_{R/L}$ (see Eq. (2.167)).

2.4.6 Energy current and CFT in the NESS

Conformal Field Therory (CFT) has been widely used to make prediction for quantum quenches [125, 184]. In the case of partitioning protocol with a defect between the two systems, the CFT prediction for the energy current was given in [123]. Let us compute the energy current in the NESS, first we recall the definition of the energy current in quantum mechanics for a single particle with a Hamiltonian $\hat{H} = -\frac{1}{2}\partial_x^2 + V(x)$ and described by the wavefunction $\psi(x,t)$, see e.g. [185]. The local energy $q(x,t)$ and energy current $j_q(x,t)$ are given by

$$q(x,t) = \frac{1}{2}(\partial_x\psi(x,t)^*)(\partial_x\psi(x,t)) + \psi(x,t)^* V(x)\psi(x,t) , \tag{2.170}$$

$$j_q(x,t) = -\mathrm{Re}\left(i(\hat{H}\psi)(x,t)^*\partial_x\psi(x,t)\right) . \tag{2.171}$$

The total averaged energy is recovered from $\int dx\, q(x,t) = \langle\psi|\hat{H}|\psi\rangle$ while $q(x,t)$ and $j_q(x,t)$ obey the conservation equation (from the Schrödinger equation)

$$\partial_t q(x,t) + \partial_x j_q(x,t) = 0 . \tag{2.172}$$

For noninteracting fermions with the initial condition considered here (see Section 2.4), each state $\psi^n_{L/R}(x,t)$ evolves independently, hence the total local energy $Q(x,t)$ and energy current $J_Q(x,t)$ are given by the corresponding sums of the one-body contributions weighted by the Fermi factors. The time dependent energy current is thus given by

$$J_Q^{L/R}(x,t) = \sum_{n=1}^{\infty} f_{L/R}(k_n) \mathrm{Im}\left((\hat{H}_g \psi^n_{L/R})(x,t)^* \partial_x \psi^n_{L/R}(x,t) \right) , \tag{2.173}$$

where $k_n = \frac{2\pi n}{\ell}$ and $\hat{H}_g$ is the single-particle Hamiltonian with a delta-impurity in Eq. (2.96). This can also be written in term of the kernel

$$\boxed{J_Q(x,t) = \mathrm{Im}\left(\hat{H}_{g,x} \partial_y K(x,y)|_{x=y} \right) ,} \tag{2.174}$$

where $\hat{H}_{g,x}$ is the Hamiltonian applied with respect to the variable x. In the case where there is no potential (which is true here if $x \neq 0$), then

$$J_Q(x,t) = \frac{1}{4i} (\partial_x \partial_y^2 - \partial_x^2 \partial_y) K(x,y)|_{x=y}. \tag{2.175}$$

Thus, the explicit calculation can be performed either from (2.173) using the contour integral method A, or directly from the exact stationary kernel (2.120), and (2.159). Both paths yield the same result, i.e. in the large time limit the energy current $J_Q(x,t)$ converges to an asymptotic constant value $J_{Q,\infty}$ which reads

$$\boxed{J_{Q,\infty} = -\int_0^\infty \frac{dk}{2\pi} (f_R(k) - f_L(k)) k E(k) T(k) \quad , \quad E(k) = \frac{k^2}{2} .} \tag{2.176}$$

In the low temperature limit, using Sommerfeld expansion, one obtains the current expansion (in the case $\mu_L = \mu_R = \frac{k_F^2}{2}$)

$$\boxed{J_{Q,\infty} = \frac{\pi}{12} \frac{k_F^2 (2g^2 + k_F^2)}{(g^2 + k_F^2)^2} (T_L^2 - T_R^2) - \frac{7\pi^3}{30} \frac{g^4}{(g^2 + k_F^2)^4} (T_L^4 - T_R^4) + O(T_R^6, T_L^6) .} \tag{2.177}$$

It is interesting to compare the first term in this low-temperature expansion with a result for the energy current obtained in [123]. In that case, the current is obtained for a quantum quench where two systems represented by two different CFT are glued together at initial time with a defect at the junction

$$J_{Q,\infty}^{\mathrm{CFT}} = c \frac{\pi}{12} \cos^2 \alpha (T_L^2 - T_R^2) , \tag{2.178}$$

where c is the central charge. A simple derivation of this result was given in [123] for free Majorana fermions (corresponding to $c = 1/2$). In that work $\cos^2 \alpha$ is the transmission coefficient of the defect, i.e. the analog of $T(k_F)$ here. However the coefficient of $T_L^2 - T_R^2$ that we obtain here in (2.177) is not equal to $\frac{\pi}{12} T(k_F)$ as would be predicted by the model of [123] taking into account that here $c = 1$. The discrepancy can be understood as follows. One can show that for a general dispersion

relation $E(k)$ our formula (2.177) becomes to leading order for small T_L and T_R

$$J_{Q,\infty} \simeq \frac{\pi}{12}\frac{1}{k_F}\left(\partial_k(E(k)T(k))\right)|_{k=k_F}(T_L^2 - T_R^2)\,. \tag{2.179}$$

Performing the derivative with respect to k in (2.179) we obtain two terms. The first one is $\propto E'(k_F)T(k_F)/k_F = T(k_F)$ and coincides with the result of [123]. The additional term $\propto E(k_F)T'(k_F)/k_F$ is non zero when the transmission coefficient depends on the momentum k, which is not the case in [123] as they consider a conformal defect i.e. a defect that acts similarly for any k. In our case, the defect is not a conformal defect, this explains the discrepancy (see Appendix C for an example of a conformal defect). This additional term is negligible compared to the first one only when the impurity strength is small, i.e., $g \ll k_F$.

Note that in the absence of the impurity, i.e. for $g = 0$, the low-temperature expansion of $J_{Q,\infty}$ reads for arbitrary $\mu_{L/R}$

$$\begin{aligned} J_{Q,\infty}|_{g=0} =& \frac{\mu_L^2 - \mu_R^2}{4\pi} + \frac{\pi}{12}(T_L^2 - T_R^2) \\ &- \frac{1}{2\pi}(T_L^2 e^{-\mu_L/T_L} - T_R^2 e^{-\mu_R/T_R}) + O(e^{-2\mu_L/T_L}, e^{-2\mu_R/T_R}). \end{aligned} \tag{2.180}$$

Note that the second term agrees with the formula (2.178) with full transmission. After characterizing the NESS reached in the double limit $\ell \to \infty$ followed by $t \to \infty$, we now give a description of what happens when the particles start interacting with the boundaries.

2.5 Partitioning protocol with a delta Dirac defect: relaxation to a GGE

Again, we consider N noninteracting fermions in one dimension and in the presence of a delta impurity as in (2.4). This time, instead of taking the large time limit after the thermodynamic limit, which led in the previous section to the emergence of a NESS, we simultaneously take both limits such that the particles are reflected at the boundaries. This is done following the discussion in (2.3), where we let $\frac{t}{\ell} \to \infty$ and $\frac{t}{\ell^2} \to 0$. It was argued numerically in [134] to yield a GGE (in the absence of a defect). As we have not discussed this regime in our paper [2], we want to give here a theoretical argument, explaining why the GGE should persist in the presence of the delta defect. We define the limit as follows

$$\ell \to \infty, \quad \begin{cases} t = \ell^a \text{ if } a \neq 1 \\ t = \frac{\ell}{k^*} \text{ if } a = 1 \end{cases} . \tag{2.181}$$

We begin with the expression Eq. (2.143) where the kernel is is divided in terms A, B, C, and D. We claim that depending on the value of a, this leads to the different regimes

- If $a \in]0, 1[$, we recover the NESS regime, and the limit (2.181) leads to a stationary kernel equal to Eq. (2.120). The kernel is the sum of the non-zero large time limit terms A, B, C, and D from the previous section (2.143). We stress that while A and B correspond to the diagonal ensemble (2.17) in the eigenbasis

of the Hamiltonian $\hat{H}_g$, C and D, which contain the current, are off-diagonal terms, this means that the kernel does not match the diagonal ensemble (2.17). We also stress that this kernel does not correspond to the kernel given by GGE (2.26) with initial condition (2.99).

- If $a \in]1,2[$, the limit (2.181) leads to a GGE (2.26) obtained from the initial state (2.99). It is characterised by the kernel

$$\boxed{K_{\text{eq}}(x,x') = \left(\int_0^{k_L} \frac{dk}{2\pi} + \int_0^{k_R} \frac{dk}{2\pi}\right) \left(\phi^{\infty}_{-,k}(x)\phi^{\infty}_{-,k}(x') + \phi^{\infty}_{+,k}(x)\phi^{\infty}_{+,k}(x')\right),} \tag{2.182}$$

where, $\phi^{\infty}_{\pm,k}(x)$ are defined in (2.121). It has no current (2.7) because it has no imaginary part. This time the kernel is equal to the large time limit of A, B, in this limit, we see that only the diagonal elements survive, hence the kernel matches with the diagonal ensemble (2.17). Note that this kernel (2.182) is the mean of two equilibrium kernels in presence of a delta impurity found in [164]; one with Fermi momentum k_L and one with Fermi momentum k_R.

- If $a = 1$, even if we have no proof yet, we believe that this limit leads to a crossover regime between the NESS regime and the GGE regime. More precisely, when $k^* = 0$, it corresponds to the GGE regime, while as $k^* \to \infty$, it corresponds to the NESS. The intuition behind this is that waves with wave number k have a velocity $v(k) = k$, hence they will bounce on the boundaries a number of time of order $\sim \frac{k}{k^*}$. This implies that waves with $k < k^*$ will not be affected by the boundaries, leading to NESS physics. On the other hand, waves with $k \gg k^*$ will bounce multiple times on the boundary, getting dephased, and leading to the GGE. Note that this regime can be described by the GHD extension given in Section 2.7.3; however, this predicts local correlations only, whereas in this system, we also expect non-local correlations.

- If $a = 2$: This case leads to possible revivals such that there is no observed NESS or GGE in this limit. A quantum revival is a phenomenon where the wave function periodically comes back to its initial form [186].

2.5.1 The NESS regime is still observed for $a < 1$

If $a \in]0,1[$, we argue that one can proceed as in Section (2.4.3.2). The term $A(x,x')$ in (2.143) is independent of time so it will converge to the same value. For the terms B, C, and D of (2.143) we will still use the method from Appendix A used in Section 2.4.3.2 and nothing is changed. Indeed, let us consider the term D. We can still express it as a contour integral, similar to (2.149). However, this time the factor (2.151) of the integrand of (2.149) is given by

$$\frac{e^{-i\frac{k^2}{2}t}}{e^{-ik\ell}-1} = e^{-i\frac{k_1^2-k_2^2}{2}\ell^a} \frac{e^{k_1k_2\ell^a}}{e^{-ik_1\ell}e^{\ell k_2}-1}, \tag{2.183}$$

with $k = k_1 + ik_2$, $k_1 > 0$ and $t = \ell^a$. Now, we recall that in the Appendix A, a key-point was the decay to zero of the factor (2.183) in the double limit $\lim_{t\to\infty} \lim_{\ell\to\infty}$ for $\text{Im}[k] = k_2 \neq 0$. Therefore, the method will be valid if this factor also goes to zero in

the limit (2.181). In this limit, the factor is equivalent to

$$\frac{e^{-i\frac{k^2}{2}t}}{e^{-ik\ell}-1} \underset{\ell\to\infty}{\simeq} \begin{cases} e^{-i\frac{k_1^2-k_2^2}{2}\ell^a} e^{ik_1\ell} e^{k_2\ell(k_1\ell^{a-1}-1)} \text{ if } k_2>0 \\ -e^{-i\frac{k_1^2-k_2^2}{2}\ell^a} e^{k_1k_2\ell^a} \text{ if } k_2<0 \end{cases} . \tag{2.184}$$

From this it is easy to see that if $k_2 \neq 0$ the factor (2.183) goes to zero

$$\lim_{\ell\to\infty} \frac{e^{-i\frac{k^2}{2}t}}{e^{-ik\ell}-1} = 0 \text{ if } a \in]0,1[. \tag{2.185}$$

As a consequence, we recover the NESS regime (2.120) for $a \in]0,1[$. However, if $a>1$ the behaviour of the factor (2.183) is different and

$$\text{for } a \in]1,2[, \quad \lim_{\ell\to\infty} \frac{e^{-i\frac{k^2}{2}t}}{e^{-ik\ell}-1} = \begin{cases} +\infty \text{ if } k_2>0 \\ 0 \text{ if } k_2<0 \end{cases} , \tag{2.186}$$

the factor does not decay to zero, indicating that the result from the Appendix A cannot be used anymore. Therefore, we expect to encounter a new regime for which we will need a new method.

Critical value $t=\frac{\ell}{k^*}$. Before explaining how the system reaches the GGE regime when $a \in]1,2[$, let us give details on the critical value $a=1$, $t=\frac{\ell}{k^*}$. In that case, (2.184) has the following limit

$$\lim_{\ell\to\infty} \frac{e^{-i\frac{k^2}{2}t}}{e^{-ik\ell}-1} = \begin{cases} +\infty \text{ if } k_2>0 \text{ and } k_1>k^* \\ 0 \text{ if } k_2>0 \text{ and } k_1<k^* \\ 0 \text{ if } k_2<0 \end{cases} , \tag{2.187}$$

such that the method from the Appendix A can be applied only to a part of the sums (that is $k<k^*$) in terms B, C, and D. Indeed if $k<k^*$ then in the integral contour γ_δ from Fig. 2.10, the real part of k verifies $\mathrm{Re}[k]<k^*$ such that the factor (2.183) decays. For the rest of the sum (that is $k>k^*$), the method from Appendix A cannot be applied, therefore we expect a new regime.

Note that the local part of the kernel can be described in terms of GHD (see Section 2.7.3). However, the full kernel $K(x,x',t=\frac{\ell}{k^*})$ remains unknown, whether it is obtained from an extension of GHD or an exact computation.

2.5.2 An argument for the GGE regime for $1<a<2$

Now we will give an argument for the emergence of the GGE regime (2.182) when $1<a<2$. We start from the exact finite time finite system size decomposition of the kernel (2.143). A and B^{diag} are time independent, so they have the same behaviour as for $0<a<1$ and relax to the same stationary non zero component. Additionally, we already explained why we cannot use the method from the Appendix A to compute C, D and $B^{\text{off-diag}}$. We want to argue why each of them decay to zero . We recall that $D(x,x',t)=C^*(x',x,t)$ such that we restrict to the study of D, concerning $B^{\text{off-diag}}$ its decay is shown with similar methods. First we give $D(x,x',t=\ell^a)$ from (2.146)

$$D(x,x',t=\ell^a)=\frac{4}{\ell^2}\sum_{k_b\in\Lambda_+}\sum_{k\in\Lambda_-,k=k_L^+}^{k_R}\frac{h_{x,x',t=0}(k,k_b)e^{-\frac{i\ell^a}{2}(k^2-k_b^2)}}{k-k_b} \tag{2.188}$$

where the function $h_{x,x',t}(k,k_b)$ is defined in (2.147), and the lattice $\Lambda_\pm$ are defined in (2.135), (2.132). Here we just took the time dependent exponential factor out of $h_{x,x',t}(k,k_b)$. The remaining $h_{x,x',t=0}(k,k_b)$ is a continuous function that is irrelevant for the rest of the argument. The sum can also be performed over the index n and m such that $k=k_n=\frac{2\pi n}{\ell}\in\Lambda_-$ and $k_b=q_m\in\Lambda_+$. From (2.135), with a repulsive potential $g\geq 0$, it is possible to show that (see also Fig. 2.9)

$$q_m=\frac{(2m+1)\pi}{\ell}+\frac{\phi_m}{\ell},\quad \phi_m\in[0,\pi]. \tag{2.189}$$

Furthermore, $\{\phi_m\}_{m\in\mathbb{N}}$ is a decreasing sequence such that $\lim_{m\to\infty}\phi_m=0$, and $\phi_m=0$ if $g=0$ which means that ϕ_m is non zero only in presence of the defect. For convenience, we also define

$$\theta_{n,m}=\ell(q_m-k_n), \tag{2.190}$$

such that $\theta_{n,n+p}=(2p+1)\pi+\phi_{n+p}$. Using (2.135) the definition of Λ_+, we obtain the large ℓ behaviour

$$\theta_{n,n+p}\underset{\ell\to\infty}{\simeq}2(p+1)\pi-2\arctan(\frac{k_n}{g})=f_p(k_n). \tag{2.191}$$

Now, we proceed with a variable manipulation in the sum (2.188), where we enforce the constraint $m=n+p$ and run the sum over p instead of m. This yields

$$D(x,x',t=\ell^a)=\sum_{p=-N_R}^{+\infty}D_p, \tag{2.192}$$

$$D_p=\sum_{n=N_L+1}^{N_R}\theta(n+p)\frac{4}{\ell^2}\frac{h_{x,x',t=0}(k_n,q_{n+p})e^{-\frac{i\ell^a}{2}(k_n^2-q_{n+p}^2)}}{k_n-q_{n+p}}.$$

Inserting (2.190) leads to

$$D_p=-\sum_{n=N_L+1}^{N_R}\theta(n+p)\frac{4}{\ell}\frac{h_{x,x',t=0}(k_n,q_{n+p})e^{i(k_n\theta_{n,n+p}\ell^{a-1}+\theta_{n,n+p}^2\ell^{a-2})}}{\theta_{n,n+p}}. \tag{2.193}$$

The important part of this step is that now, according to (2.191), in the large ℓ limit, and for a fixed p, $\theta_{n,n+p}$ will not change sign and will remain outside of an interval $[-\epsilon,\pi]$ containing zero ($\epsilon>0$), as n goes from N_L+1 to N_R, or equivalently $k_n\in]k_L,k_R]$. In simpler terms, we find that D_p does not have any poles along n. However, the trade-off for this result is that we now have a double sum with only one factor of $\frac{1}{\ell}$, which means that we cannot rewrite it as a double integral in the limit of large ℓ.

Let us focus on D_p, in the large ℓ limit with fixed p. The reason why we can restrict to p fixed, is because the part of the sum (2.188) with p of order ℓ (or equivalently $\frac{1}{k-k_b}=O(1)$) contains no pole, and therefore can be treated as a double integral which

decays to zero in the large ℓ limit whether $a \in]0,1[$ or $a \in]1,2[$. Now it appears that for $a \in]1,2[$

$$D_p \underset{\ell\to\infty}{\simeq} -\int_{k_L}^{k_R} \frac{2dk}{f_p(k)\pi} h_{x,x',t=0}(k,k) e^{i f_p(k) k_n \ell^{a-1}}, \tag{2.194}$$

which is just the Fourier transform $\hat{F}(\xi)$ with a large argument $\xi = f_p(k_n)\ell^{a-1}$ of a discontinuous compactly supported function $F(k)$ with hard edges at k_L and k_R. The Fourier transform of such a function decrease at least as $\hat{F}(\xi) \underset{\xi\to\infty}{\simeq} \xi^{-1}$. In order to conclude the argument, we recall that $f_p(k)$ doesn't approach 0 and varies slowly with k such that we roughly replace it by $f_p(k) \sim 2(p+1)+1/2$. This yields

$$D \underset{\ell\to\infty}{\simeq} \sum_{p=-\infty}^{+\infty} \frac{\hat{F}(f_p(k_n)\ell^{a-1})}{f_p(k_n)} \lesssim \sum_{p=-\infty}^{+\infty} \frac{\ell^{1-a}}{(2(p+1)+1/2)^2} \simeq \ell^{1-a}. \tag{2.195}$$

At fixed ℓ the sum over p converges, and we obtain the decrease in ℓ. Note that this demonstration cannot be performed for the critical value $a = 1$, $t = \frac{\ell}{k^*}$ and $k > k^*$ as in this case, Fourier transform argument in (2.195) does not grow to infinity. Hence, another method needs to be introduced in order to obtain the kernel in that limit.

2.6 Quench with a General Defect

From the previous sections, while the formulae for the kernel (Eqs. (2.118) and (2.119)) may appear somewhat cumbersome, they seem to have dependencies on the reflection and transmission coefficients of the delta impurity. To clarify these dependencies, we introduce a more general setup, which was the focus of the third article [3]. In The first Section 2.6.1 we will present a quench with a general defect characterised by its reflection and transmission coefficients. Such a general defect also comes with bound states whose effect is discussed in Section 2.6.4. In Section 2.6.2, we extend our computation to the space-time extended kernel which allows computations of multi-time correlations. Then, in Section 2.6.5 we apply this to the computation of density-density space-time correlations for which algebraic decay are found. In Section 2.6.3 we present another way to compute the kernel by using the method from Appendix A directly on the wave function instead of using it on the kernel. This method is simpler to implement and provides a better physical intuition of the result.

2.6.1 Model

The defect We consider N noninteracting fermions in one dimension in the presence of a finite size impurity modeled by a potential. The evolution at $t > 0$ is governed by the single particle Hamiltonian

$$\hat{H} = -\frac{1}{2}\partial_x^2 + V(x)\ . \tag{2.196}$$

For simplicity, the potential $V(x)$ is localized in the region $[-\frac{a}{2}, \frac{a}{2}]$ and does not possess any bound state (i.e., a repulsive impurity). Outside of this region the eigenfunctions of $\hat{H}$ are plane waves $\sim e^{\pm ikx}$ with amplitudes related through a scattering matrix

similar to (2.74)

$$\mathbf{S}(k) = \begin{pmatrix} \mathsf{t}_L(k) & \mathsf{r}_R(k) \\ \mathsf{r}_L(k) & \mathsf{t}_R(k) \end{pmatrix} , \tag{2.197}$$

where $\mathsf{r}_{R/L}(k)$ and $\mathsf{t}_{R/L}(k)$ are right and left momentum dependent reflection and transmission coefficients. The current conservation and time reversal symmetry leads to the following constraint

$$\begin{gathered} \mathsf{r}_L(k) = e^{i\varphi_L(k)} \cos\theta(k) \quad , \quad \mathsf{r}_R(k) = e^{i\varphi_R(k)} \cos\theta(k) \\ \mathsf{t}_R(k) = \mathsf{t}_L(k) = \mathsf{t}(k) = ie^{\frac{i}{2}(\varphi_R(k)+\varphi_L(k))} \sin\theta(k). \end{gathered} \tag{2.198}$$

Examples of scattering potentials together with the expression of their transmission and reflection coefficients can be found in Appendix C. Similarly to (2.132) and (2.133), the eigenstates of $\hat{H}$ form a two component family $\phi_{\pm,k}(x)$ with $k \in \Lambda^{\pm}$. The fermions are confined in a hard box of size ℓ with $\ell > a$ such that $\Lambda^{\pm}$ is defined by the hard-box boundary condition

$$\Lambda^{\pm} = \{k \in \mathbb{R}^{+} | \phi_{\pm,k}(\frac{\ell}{2}) = 0\} . \tag{2.199}$$

In the simpler case of a symmetric potential $\mathsf{r}_R(k) = \mathsf{r}_L(k) = \mathsf{r}(k)$, and the eigenstates of $\hat{H}$ are either odd $(-)$ or even $(+)$, they take the form

$$\begin{aligned} \phi_{-,k}(x) &= \mathrm{sgn}(x) c_{\ell,-,k} \cos(k(|x| - \delta_k^-)) \quad k \in \Lambda^-, \\ \phi_{+,k}(x) &= c_{\ell,+,k} \cos(k(|x| - \delta_k^+)) \quad k \in \Lambda^+, \end{aligned} \tag{2.200}$$

where the phase shifts $k\delta_k^{\pm}$ are related to the scattering coefficients as

$$\mathsf{r}(k) + \mathsf{t}(k) = e^{-2ik\delta_k^+} \quad , \quad \mathsf{r}(k) - \mathsf{t}(k) = e^{-2ik\delta_k^-} . \tag{2.201}$$

These eigenfunctions are normalized on $[-\frac{\ell}{2}, \frac{\ell}{2}]$ and the normalization prefactor $c_{\ell,\pm,k}$ becomes k-independent and $\pm$-independent at large ℓ with $c_{\ell,\pm,k} \simeq \sqrt{\frac{2}{\ell}}$.

The initial condition. We also give a more general initial condition. We describe the initial state with an impenetrable defect such that both left and right system are independent at initial time. This defect is described by the single particle Hamiltonian $\hat{H}_0$

$$\hat{H}_0 = -\frac{1}{2}\partial_x^2 + V_0(x) , \tag{2.202}$$

where $V_0(x)$ is another potential localized in the region $[-\frac{a}{2}, \frac{a}{2}]$ and characterized by a scattering matrix

$$\mathbf{S}_0 = \begin{pmatrix} 0 & \mathsf{r}_0^R(k) \\ \mathsf{r}_0^L(k) & 0 \end{pmatrix} \quad , \ |\mathsf{r}_0^L(k)|^2 = |\mathsf{r}_0^R(k)|^2 = 1 . \tag{2.203}$$

The potential $V_0(x)$ is sufficiently divergent at $x = 0$ so that the system is cut in two halves with $\mathsf{t}_0^R(k) = \mathsf{t}_0^L(k) = 0$. The initial N-body density matrix $\hat{\rho} = \hat{\rho}_L \otimes \hat{\rho}_R$ is the tensor product of left and right density matrices $\hat{\rho}_{L/R}$, each describing equilibrium at temperature $T_{L/R}$ with chemical potentials $\mu_{L/R}$. In the zero temperature case, this amounts to consider the ground state with a fixed number of fermions $N_{L/R}$ on each side.

The normalized eigenfunctions $\phi_k^{R/L}(x)$ of the initial Hamiltonian $\hat{H}_0$ vanish for $x \in \mathbb{R}^{-/+}$ and can be written outside the interval $[-\frac{a}{2}, \frac{a}{2}]$

$$\begin{aligned}\phi_k^R(x) &= c_\ell^0 \cos(k(|x| - \delta_k^R))\theta(x - \frac{a}{2}),\ k \in \Lambda^R \\ \phi_k^L(x) &= c_\ell^0 \cos(k(|x| - \delta_k^L))\theta(-\frac{a}{2} - x),\ k \in \Lambda^L\end{aligned} \tag{2.204}$$

with $c_\ell^0 \simeq \sqrt{\frac{4}{\ell}}$ at large ℓ. The phase shifts $\delta_k^{R/L}$ are related to the reflection coefficients as

$$\mathsf{r}_0^{R/L}(k) = e^{-2ik\delta_k^{R/L}}\ , \tag{2.205}$$

while the lattices Λ^R and Λ^L are defined as follows

$$\Lambda^{R/L} = \left\{ k \in \mathbb{R}^+ | \phi_k^{R/L}(\pm\frac{\ell}{2}) = 0 \right\}\ . \tag{2.206}$$

In the quench with a delta defect, the initial state (2.99) (or (2.156) at finite temperature) was characterised only by the left and right inverse temperature $\beta_{R/L}$, and chemical potential $\mu_{R/L}$. This time, in addition to those, the initial state also depends on the reflection coefficients $\mathsf{r}_0^{R/L}(k)$ or equivalently the phase shifts $\delta_k^{R/L}$ of the initial defect.

2.6.2 Space-time extended kernel

We want to extend our result to the space-time m point density correlation functions, defined for $0 \le t_1 \le \cdots \le t_m$ and all distinct space time points (x_i, t_i) as

$$\mathcal{R}_m(x_1, t_1; ...; x_m, t_m) = \mathrm{Tr}(\hat{\rho}\hat{d}(x_m, t_m) \dots \hat{d}(x_1, t_1)), \tag{2.207}$$

where $\hat{d}(x,t) = \hat{c}^\dagger_{x,t}\hat{c}_{x,t}$ is the density operator in the Heisenberg representation, and $\hat{c}_{x,t}$, $\hat{c}^\dagger_{x,t}$, are the fermionic creation and annihilation field operators in the Heisenberg picture. This object generalise the correlation function (1.49). For noninteracting fermions they can be expressed as an $m \times m$ determinant involving the so-called space-time extended kernel (see [187])

$$\mathcal{R}_m(x_1, t_1; ...; x_m, t_m) = \det_{1 \le i,j \le m} K(x_i, t_i; x_j, t_j)\ . \tag{2.208}$$

The space-time extended kernel is defined as follow

$$\begin{aligned}&K(x,t;x',t') = \mathrm{Tr}\hat{\rho}T\hat{c}^\dagger_{x,t}\hat{c}_{x',t'}, \\ &T\hat{c}^\dagger_{x,t}\hat{c}_{x',t'} = \hat{c}^\dagger_{x,t}\hat{c}_{x',t'}\theta(t \ge t') - \hat{c}_{x',t'}\hat{c}^\dagger_{x,t}\theta(t' > t).\end{aligned} \tag{2.209}$$

It is a generalisation of the time dependent kernel (2.5) such that $K(x,t;x',t) = K(x,x';t)$. In addition to density-density correlation, the current correlations can also be extracted from the space-time extended kernel [188]. The space-time extended kernel can be written as a generalisation of the kernel (2.104), such that

$$K(x,t;x',t') = K_R(x,t;x',t') + K_L(x,t;x',t')\ , \tag{2.210}$$

where

$$K_{R/L}(x,t;x',t') = \sum_{k\in\Lambda^{R/L}} (f_{R/L}(k) - \theta(t'>t))\psi_k^{R/L,*}(x,t)\psi_k^{R/L}(x',t') \,. \quad (2.211)$$

we recall that $f_{R/L}(k) = 1/(1+e^{\beta_{R/L}(\mu_{R/L}-\frac{k^2}{2})})$ are the right and left Fermi factors, and $\psi_k^{R/L}(x,t)$ is the solution of the Schrödinger equation $i\partial_t\psi_k^{R/L}(x,t) = \hat{H}\psi_k^{R/L}(x,t)$ with the initial condition $\psi_k^{R/L}(x,0) = \phi_k^{R/L}(x)$, where $\phi_k^{R/L}(x)$ are given in Eq. (2.204).

2.6.3 The limit wave function

NESS regime. Now we want to obtain the kernel (2.210) in the large system size limit followed by the large time limit. In the case of the delta defect, we demonstrated how the contour integral method presented in Appendix A could be directly applied to the kernel, for example to compute the term D, or B (2.143). For the latter, this required the method to be applied twice in a row (see Appendix B), or to be generalised to higher order poles. Here we present an alternative method that not only provides an intuitive interpretation of the computation in term of scattering, but also significantly simplify it. This method involves applying the contour integral method of Appendix A directly to the single-particle time evolved initial eigenfunctions $\psi_k^{R/L}(x,t)$ of the kernel Eq. (2.211) as explained below.

The exact formula for $\psi_k^{R/L}(x,t)$ is an infinite superposition which involves the overlaps of the eigenstates $\phi_k^{R/L}(x) = \psi_k^{R/L}(x,t=0)$ of the pre-quench Hamiltonian $\hat{H}_0$ with the eigenstates $\phi_{\sigma,k}(x)$ of the post-quench Hamiltonian $\hat{H}$

$$\psi_k^{R/L}(x,t) = \sum_{\sigma=\pm1,k'\in\Lambda^\sigma} \phi_{\sigma,k'}(x)e^{-i\frac{k'^2}{2}t}\langle\phi_{\sigma,k'}|\phi_k^{R/L}\rangle \,. \quad (2.212)$$

The asymptotic form of this superposition is obtained using a contour-integral representation which leads to

$$\boxed{\begin{aligned}&\psi_k^{R/L}(x,t) = \frac{1}{\sqrt{\ell}}(e^{-i\frac{k^2}{2}t}\chi_k^{R/L}(x) + \delta\chi_{k,\ell}^{R/L}(x,t)),\\ &\lim_{\ell\to\infty}\delta\chi_{k,\ell}^{R/L}(x,t) = \delta\chi_k^{R/L}(x,t),\\ &\lim_{t\to\infty}\delta\chi_k^{R/L}(x,t) = 0.\end{aligned}} \quad (2.213)$$

See [188] for expressions of $\delta\chi_{k,\ell}^{R/L}(x,t)$, $\delta\chi_k^{R/L}(x,t)$, and details of the proof including how we deal with the fact that the potential has a non zero size (which was not the case of the delta defect). The result (2.213) can be interpreted as follows, the first term of the first line $\frac{1}{\sqrt{\ell}}e^{-i\frac{k^2}{2}t}\chi_k^{R/L}(x)$ is the only relevant part in the NESS reached in the double limit $\ell\to\infty$, $t\to\infty$, while the second term $\frac{1}{\sqrt{\ell}}\delta\chi_{k,\ell}^{R/L}(x,t)$ contains information on finite system size corrections and large time decay to the

NESS. Additionally, the leading contributions $\chi_k^{R/L}(x)$ are given by

$$\chi_k^R(x) = \begin{cases} (e^{-ikx} + \mathsf{r}_R(k)e^{ikx})e^{ik\delta_k^R} & \text{if } x > \frac{a}{2} \\ \mathsf{t}_R(k)e^{-ikx}e^{ik\delta_k^R} & \text{if } x < -\frac{a}{2} \end{cases} \tag{2.214}$$

$$\chi_k^L(x) = \begin{cases} \mathsf{t}_L(k)e^{ikx}e^{ik\delta_k^L} & \text{if } x > \frac{a}{2} \\ (e^{ikx} + \mathsf{r}_L(k)e^{-ikx})e^{ik\delta_k^L} & \text{if } x < -\frac{a}{2} \end{cases} \tag{2.215}$$

where we recall that $\mathsf{r}(k)$ and $\mathsf{t}(k)$ are the reflection and transmission coefficients (2.197). In this result (2.213) the time-dependence $\propto e^{-i\frac{k^2}{2}t}$ is simply the one of a free particle of energy $\frac{k^2}{2}$, while the factor $\frac{1}{\sqrt{\ell}}$ ensures the normalization of $\psi_k^{R/L}(x,t)$. The form of $\chi_k^{R/L}(x)$ in (2.214) and (2.215) can be qualitatively understood in term of particle scattering as follows. Away from the impurity, at time $t = 0$, from (2.204) a particle can have momentum k or $-k$ (everywhere $k > 0$). Consider a space time point (x,t) with $x = O(1) > 0$ and t large and first ask how a particle starting *from the left* of the impurity can reach (x,t). As shown in Fig. 2.13 a), there is a single possible initial position such that a particle with initial momentum k reaches (x,t). Since it crosses the barrier, it collects a factor $\mathsf{t}(k)$. This accounts for the first line in (2.215). It contains a single term, with phase factor $e^{ik\delta_k^L}$, since particles with initial momentum $-k$ escape to $-\infty$ (the phase factor information they carry $e^{-ik\delta_k^L}$ is lost). For particle starting *from the right* of the impurity, one similarly interprets the two terms in the first line in (2.214). Indeed, one sees from Fig. 2.13 b) that there are two possible initial positions such that a particle with initial momentum $-k$ reaches (x,t) either (i) directly (leading to the factor e^{-ikx}) or after one reflection (which changes $-k$ into k leading to the factor $\mathsf{r}(k)e^{ikx}$). Of course this semi-classical argument is deceptively simple, since in reality momentum is not a quantum number here and the true wave function is a complicated superposition. However we show here that it becomes exact at large time. Thus, although the final result is intuitively simple, the convergence to the large time limit is nontrivial. It can be extracted from the exact expression for the subleading part $\delta\chi_{k,\ell}^{R/L}(x,t)$ (see [188]). Although we did not perform an exhaustive analysis it is easy to see that the decay is generically algebraic in time (with possible oscillations).

Remark: The above arguments were made for $|x| > a/2$, i.e., outside the defect, where the wave-functions and their analytic continuations are controlled. However we also concluded that the asymptotic formulae Eqs. (2.214), and (2.215) generalize to any $x = O(1)$ (including inside the impurity) but with an extended formula for $\chi_k^{R/L}$

$$\tfrac{1}{\sqrt{\ell}}\chi_k^{R/L}(x) = \tfrac{1}{\sqrt{2}}\left(\phi_{+,k}(x)e^{ik(\delta_k^{R/L}-\delta_k^+)} + \sigma_{R/L}\phi_{-,k}(x)e^{ik(\delta_k^{R/L}-\delta_k^-)}\right) \tag{2.216}$$

where $\sigma_R = 1$ and $\sigma_L = -1$. Here $k \in \mathbb{R}^+$ and $\phi_{\pm,k}(x)$ denote the two eigenstates of $\hat{H}$ (2.200) which become degenerate in the infinite size limit with eigenenergy $\frac{k^2}{2}$.

Kernel. By definition of the space-time extended kernel is given by Eq. (2.211) Since we have already obtained the large ℓ limit of the individual wave-functions $\psi_k^{R/L}(x,t)$, see (2.213), it is natural to inject their expressions into the formula (2.211). Indeed, as $\ell \to \infty$, it turns out that one can safely replace $\frac{1}{\ell}\sum_{k\in\Lambda^{R/L}}$ by $\int_0^{+\infty}\frac{dk}{2\pi}$, i.e.,

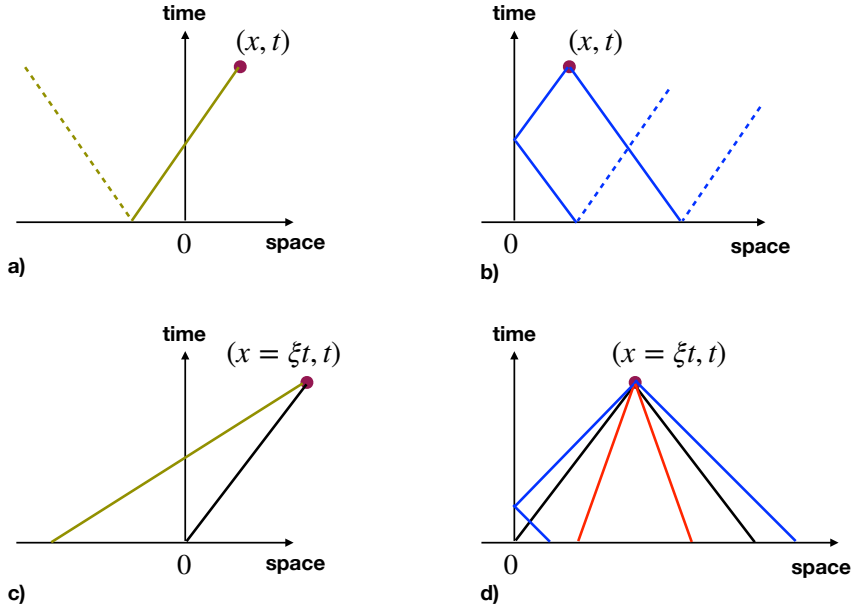

FIGURE 2.13: Interpretation of (2.214)-(2.215), see text for details. a) A particle starts from the left with momentum k and reaches $(x > 0, t)$ after being transmitted (solid green), while the $-k$ component (dotted red) get lost at $-\infty$. b) Starting from the right with $-k$ it reaches (x, t) either directly, or after one reflection. c) Same as top left for the ray regime, the ray $x/t = \xi$ is black solid line. d) The trajectories (in red) inside the black "hat" shape have $k < |\xi|$: they do not meet the impurity and carry the memory of the initial state (2.229). The other trajectories (in blue) have $k > |\xi|$ and are similar to those in the subfigure b) leading to (2.230).

there is no singularity in this summation. This leads to

$$\lim_{\ell\to\infty} K_{R/L}(x,t;x',t') = \int_{R/L,\tau} \tfrac{dk}{2\pi}(e^{-i\frac{k^2}{2}t}\chi_k^{R/L}(x) + \delta\chi_k^{R/L}(x,t))^* \times(e^{-i\frac{k^2}{2}t'}\chi_k^{R/L}(x') + \delta\chi_k^{R/L}(x',t')) \quad (2.217)$$

$$= K_{\infty,R/L}(x,t;x',t') + \delta K_{R/L}(x,t;x',t'), \quad (2.218)$$

where we have split the limiting kernel in two parts, defined as

$$K_{\infty,R/L}(x,t;x',t-\tau) = \int_0^\infty \frac{dk}{2\pi}\left(f_{R/L}(k) - \theta(-\tau)\right) e^{i\frac{k^2}{2}\tau}\chi_k^{R/L}(x)^*\chi_k^{R/L}(x') \quad (2.219)$$

and $\delta K_{R/L}(x,t;x',t-\tau)$ is an integral containing products of $\chi_k^{R/L}(x)$ and $\delta\chi_k^{R/L}(x,t)$. Note that we have set $t' = t - \tau$. Let us consider now the limit $t, t' \to +\infty$ with fixed τ. We claim that

$$\lim_{t\to\infty} \delta K_{R/L}(x,t;x',t-\tau) = 0. \quad (2.220)$$

Since we have shown (2.213) in the previous section that $\delta\chi_k^{R/L}(x,t)$ decays to zero in the large time limit it would be natural to arrive at this conclusion. However this simple information is not enough to obtain (2.220). In fact, showing this decay is not a trivial task and has to be performed with much care similarly to the case of the delta defect quench treated in Appendix B. The present final result agrees perfectly

with the conclusions of Ref. [2], which indicates that our simpler method works.

Finally, this yields $\lim_{t\to\infty}\lim_{\ell\to\infty} K(x,t;x',t-\tau) = K_\infty(x,x',\tau)$ with

$$\boxed{\begin{aligned} K_\infty(x,x',\tau) &= \int_0^\infty \frac{dk}{2\pi}\,(f_L(k)-\theta(-\tau))\,e^{i\frac{k^2}{2}\tau}\chi_k^L(x)^*\chi_k^L(x') \\ &+ \int_0^\infty \frac{dk}{2\pi}\,(f_R(k)-\theta(-\tau))\,e^{i\frac{k^2}{2}\tau}\chi_k^R(x)^*\chi_k^R(x')\;. \end{aligned}} \tag{2.221}$$

We use the convention $\theta(0)=0$. Substituting the explicit form of the function $\chi_k^{R/L}(x)$ from (2.214) and (2.215) in (2.221) we find

$$\begin{aligned} &K_\infty(x>\tfrac{a}{2},x'>\tfrac{a}{2},\tau) = \textstyle\int_0^\infty \frac{dk}{2\pi}(f_L(k)-f_R(k))e^{i(\frac{k^2}{2}\tau-k(x-x'))}|\mathsf{t}(k)|^2 \\ &+\textstyle\int_0^\infty \frac{dk}{\pi}\,(f_R(k)-\theta(-\tau))\,e^{i\frac{k^2}{2}\tau}\left(\cos(k(x-x'))+\mathrm{Re}[\mathsf{r}_R(k)e^{ik(x+x')}]\right) \\ &K_\infty(x>\tfrac{a}{2},x'<\tfrac{-a}{2},\tau) = \textstyle\int_0^\infty \frac{dk}{2\pi}\,(f_R(k)-\theta(-\tau))\,e^{i\frac{k^2}{2}\tau}\mathsf{t}_R(k)e^{ik(x-x')} \\ &\qquad+\textstyle\int_0^\infty \frac{dk}{2\pi}\,(f_L(k)-\theta(-\tau))\,e^{i\frac{k^2}{2}\tau}\mathsf{t}_L^*(k)e^{-ik(x-x')} \\ &+\textstyle\int_0^\infty \frac{dk}{2\pi}(f_L(k)\mathsf{r}_L(k)\mathsf{t}_L(k)^*+f_R(k)\mathsf{r}_R(k)^*\mathsf{t}_R(k))e^{i\frac{k^2}{2}\tau}e^{-ik(x+x')}\;, \end{aligned} \tag{2.222}$$

together with the other regions obtained using the symmetry $K_\infty(x,x',\tau)|_{L,R} = K_\infty(-x,-x',\tau)|_{R,L}$ (we recall that $\mathsf{r}_L(k)\mathsf{t}_L(k)^*+\mathsf{r}_R(k)^*\mathsf{t}_R(k)=0$). Note that the initial phase shifts $e^{ik\delta^{R/L}}$ cancel in the kernel. As expected $K_\infty(x,x',\tau)$ vanishes at large $|\tau|$, with algebraic decay see [3]. In particular, from (2.222), one obtains the density $\rho_\infty(x)=K_\infty(x,x,0)$ in the NESS, which reads, for $|x|>a/2$

$$\boxed{\begin{aligned} \rho_\infty(x) &= \int_0^\infty \frac{dk}{2\pi}(f_L(k)-f_R(k))|\mathsf{t}(k)|^2 \\ &+\int_0^\infty \frac{dk}{\pi} f_R(k)\left(1+\mathrm{Re}[\mathsf{r}(k)e^{i2kx}]\right)\;. \end{aligned}} \tag{2.223}$$

Similarly, from (2.222) one also obtains the current in the NESS using (2.7), which yields

$$\boxed{J_\infty = \int_0^\infty \frac{dk}{2\pi}(f_L(k)-f_R(k))k|\mathsf{t}(k)|^2\;.} \tag{2.224}$$

Again, this result agrees with the current in the Landauer-Bütikker formalism (2.79). For $f_L(k)=f_R(k)$ the first and fourth line in (2.222) vanish and one can check that one recovers the thermal equilibrium (in the absence of bound states).

To summarize, one of the advantages of limit wavefunction method is its computational efficiency, as it directly yields the time-independent part of the kernel (2.221) using only the limit wave function (2.214). However, when studying the decay towards this time-independent part, it is necessary to consider the complete kernel (as the decay (2.213) of the wave function alone is not a sufficient information). This involves proving the large time decay of multiple singular and oscillating integrals, similar to those discussed in the Appendix B.

Remark: Following the remark (2.216), the kernel in the NESS takes the general form for any $x,x',\tau = O(1)$ (including in the support of the defect), in terms of the eigenfunctions of the evolution Hamiltonian $\hat{H}$ considered here (which does not

possess any bound state)

$$\lim_{\substack{\ell\to\infty\\ t\to\infty}} K_{R/L}(x,t;x',t-\tau) = \int_{R/L,\tau} \frac{dk}{2\pi} e^{i\frac{k^2}{2}\tau} \big(\phi_{-,k}(x)^*\phi_{-,k}(x') + \phi_{+,k}(x)^*\phi_{+,k}(x') \\ \pm(\phi_{+,k}(x)^*\phi_{-,k}(x')e^{ik(\delta_k^+-\delta_k^-)} + \phi_{-,k}(x)^*\phi_{+,k}(x')e^{-ik(\delta_k^+-\delta_k^-)})\big). \qquad (2.225)$$

Comparing with our previous work in the case of a delta impurity and $\tau = 0$, this is the decomposition from (2.143) and (2.120) in term A, B, C, and D. We see that the "diagonal terms" called A and B there (which are real and do not carry current) correspond to the first two terms respectively in (2.225), while the terms noted C and D (which carry the current in the NESS) correspond to the last two terms in (2.225).

The ray regime. We also computed the asymptotic kernel at large time when distances are scaled with time $x = O(t)$, i.e., setting $x = \xi t + y$ with $\xi, y = O(1)$. Again we first obtain the asymptotic form of the wave function [188]

$$\boxed{\psi_k^{R/L}(x = \xi t + y, t) \underset{\substack{\ell\to\infty\\ t\to\infty}}{\simeq} \frac{1}{\sqrt{\ell}} e^{-i\frac{k^2}{2}t} \chi_{\xi,k}^{R/L}(x = \xi t + y)\ ,} \qquad (2.226)$$

where we have defined

$$\chi_{\xi,k}^{R}(x) = \begin{cases} \theta(k > -\xi)\mathsf{t}(k)e^{-ikx}e^{ik\delta_k^R} & \text{if } \xi < 0 \\ \theta(k < \xi)e^{ikx}e^{-ik\delta_k^R} & \text{if } \xi > 0 \\ +(e^{-ikx} + \theta(k > \xi)\mathsf{r}(k)e^{ikx})e^{ik\delta_k^R} & \end{cases} \qquad (2.227)$$

$$\chi_{\xi,k}^{L}(x) = \begin{cases} \theta(k > \xi)\mathsf{t}(k)e^{ikx}e^{ik\delta_k^L} & \text{if } \xi > 0 \\ \theta(k < -\xi)e^{-ikx}e^{-ik\delta_k^L} & \text{if } \xi < 0 \\ +(e^{ikx} + \theta(k > -\xi)\mathsf{r}(k)e^{-ikx})e^{ik\delta_k^L}\ . & \end{cases} \qquad (2.228)$$

Since $x = \xi t + y$ (2.226) exhibits fast oscillations in time $\propto e^{-i\frac{k^2}{2}t \pm i\xi k t}$. The forms (2.227) and (2.228) can be understood by an extension to the ray regime of the argument given in the NESS, see Fig. 2.13 c) and d). It can also be summarized by considering the "light cone" with slopes $\pm k$ originating from the impurity, see Fig. 2.14. Outside of it, i.e., for $|\xi| > k$, $\psi^{R/L}(x,t)$ recovers the initial condition up to a time propagation phase $e^{-i\frac{k^2}{2}t}$, i.e.,

$$\frac{1}{\sqrt{\ell}}\chi_{\xi,k}^{R/L}(x) = \phi_k^{R/L}(x) \quad \text{for} \quad |\xi| > k\ . \qquad (2.229)$$

Inside the cone, i.e., for $|\xi| < k$, $\psi^{R/L}(x,t)$ is given by the extrapolation to the ray regime (with $x = \xi t + y$) of the form obtained above in the NESS (for $x = O(1)$), in Eqs. (2.227) and (2.228), i.e.,

$$\chi_{\xi,k}^{R/L}(x) = \chi_k^{R/L}(x) \quad , \quad \text{for} \quad |\xi| < k\ . \qquad (2.230)$$

We now compute the kernel in the ray regime from Eqs. (2.210) and (2.211). Again, [188] it turns out that in the limit $\ell \to \infty$ followed by $t \to \infty$ with $x, x' = O(t)$, one can simply inject the asymptotic forms (2.226) in the formula for the kernel (2.210) as was done in (2.211), and replace the discrete sums by integrals . We thus use the same procedure that brought us from (2.211) to (2.221), but here using $\chi_{\xi,k}^{R/L}$ instead

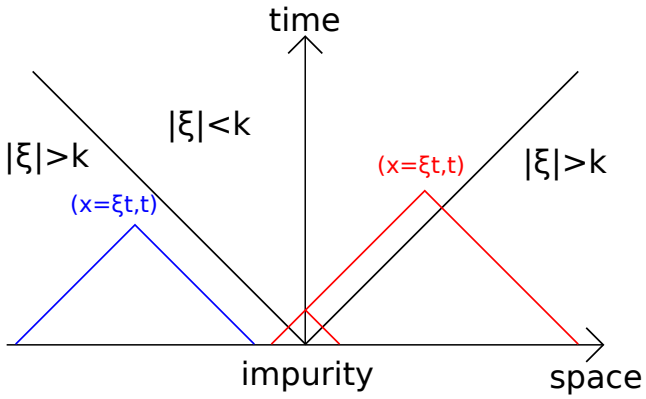

FIGURE 2.14: For a given initial momentum k, the space-time is divided in two regions (at large time). If $|\xi| > k$ the initial condition is unaffected by the impurity. In blue: the two trajectories arriving at (x,t) with phase factors $e^{\pm ik(x-\delta_k^L)}$, explaining (2.229). However for $|\xi| < k$ the possible trajectories (red) are affected by the impurity, giving back the bottom part of Fig. 2.13.

of $\chi_k^{R/L}$. When scaling[2] $x = \xi t + y$, and $x' = \xi' t + y'$, because of oscillatory behaviors of $\chi_{\xi,k}^{R/L}$, the kernel has a non zero limit only if $\xi = \pm\xi'$. For these two cases, we obtain

$$\boxed{\lim_{\substack{\ell\to\infty\\ t\to\infty}} K(\xi t + y, t; \xi' t + y', t-\tau) = \begin{cases} 0 \text{ if } \xi \neq \pm\xi' \\ K_\xi^+(y,y',\tau), \xi' = \xi \\ K_\xi^-(y,y',\tau), \xi' = -\xi \end{cases}} \tag{2.231}$$

with the following explicit expressions

$$\boxed{\begin{aligned} K_\xi^+(y,y',\tau) &= \int_0^\infty \frac{dk}{\pi} \left(f_R(k)\theta(\xi) + f_L(k)\theta(-\xi) - \theta(-\tau)\right) e^{i\frac{k^2}{2}\tau} \cos(k(y-y')) \\ &\quad + \int_0^\infty \frac{dk}{2\pi} \mathrm{s}(\xi)(f_L(k) - f_R(k)) e^{i\frac{k^2}{2}\tau} |\mathsf{t}(k)|^2 e^{-i\mathrm{s}(\xi)k(y-y')}\theta(k-|\xi|), \\ K_\xi^-(y,y',\tau) &= \int_0^\infty \frac{dk}{2\pi} \mathrm{s}(\xi)(f_L(k) - f_R(k)) e^{i\frac{k^2}{2}\tau} \mathsf{r}(k)\mathsf{t}(k)^* e^{-i\mathrm{s}(\xi)k(y+y')}\theta(k-|\xi|), \end{aligned}}$$

where $\mathrm{s}(\xi) = \theta(\xi) - \theta(-\xi)$ is the sign of ξ. For simplicity, we give the result only for a symmetric potential such that $\mathsf{r}_R(k) = \mathsf{r}_L(k)$. One can check that the ray regime matches the large distance behavior of the NESS in the following sense

$$\lim_{\substack{|y|,|y'|\to\infty\\ y\mp y' = O(1)}} K_\infty(y,y',\tau) = \lim_{\xi\to 0^+} K_\xi^\pm(y,y',\tau)\ . \tag{2.232}$$

Interestingly, while the above formula for K^+ can also be obtained from a semi-classical argument based on the Wigner function [2, 143] or Section 2.7, this is not the

[2] Alternatively one could define the large t limit of $K(\xi t + y, t; \xi'(t-\tau) + y', t-\tau)$ which amounts to a simple shift $y' \to y' - \xi'\tau$ in our formula.

case for K^-. [3] Instead, in the present framework, the correlations between $(-x,t)$ and (x,t) arise naturally from trajectories which start from the same point (e.g. from the right with momentum $-k$) and are either reflected or transmitted. In the kernel, the interferences between these two trajectories result from the product of the first and the third line in (2.227) when computing $\chi^R_{-\xi,k}(x,t)^*\chi^R_{\xi,k}(x,t)$ [see (2.221)].

At large time the mean density along rays thus converges $\rho(\xi t,t)\to\tilde\rho(\xi)$ given by

$$\boxed{\tilde\rho(\xi>0)=\rho_R+\int_0^\infty\frac{dk}{2\pi}(f_L(k)-f_R(k))|\mathtt{t}(k)|^2\theta(k-|\xi|)\ ,} \tag{2.233}$$

and the same for $\xi<0$ exchanging R and L. Here $\rho_{R/L}=\int_0^\infty\frac{dk}{\pi}f_{R/L}(k)$ are the initial mean densities. The function $\tilde\rho(\xi)$ exhibits a jump discontinuity at $\xi=0$, $\tilde\rho(0^+)-\tilde\rho(0^-)=\int_{L,R}\frac{dk}{\pi}|\mathtt{t}(k)|^2$. Similarly the current along rays converges to $J(\xi t,t)\to\tilde J(\xi)$ with

$$\boxed{\tilde J(\xi)=\int_0^\infty\frac{dk}{2\pi}(f_L(k)-f_R(k))k|\mathtt{t}(k)|^2\theta(k-|\xi|)\ .} \tag{2.234}$$

2.6.4 Defect with bound states

In order to have a completely general defect, one has to take into account a defect with bound states. We will see that the effect of such defect is to destroy the NESS as it produces permanent time oscillations. We consider the NESS regime when $V(x)$ admits a sequence of bound states $\phi_\kappa(x)$, $\kappa\in\Lambda_b$ of energies $-\frac{\kappa^2}{2}$. In that case the asymptotic large time kernel $K=K_s+K_b$ is the sum of two pieces: (i) one due to scattering states, K_s, identical to the one obtained above (ii) one due to bound states, $K_b=K_b^R+K_b^L$, where

$$\boxed{K_b^{R/L}(x,t;x',t')=\sum_{\kappa',\kappa''\in\Lambda_b}\phi_{\kappa'}(x)\phi_{\kappa''}(x')e^{-i(\frac{\kappa'^2}{2}t-\frac{\kappa''^2}{2}t')}C^{R/L}_{\kappa',\kappa''}\ ,} \tag{2.235}$$

with

$$\boxed{C^{R/L}_{\kappa',\kappa''}=\langle\phi_{\kappa'}|(1+e^{\beta_{R/L}(\hat H_0^{R/L}-\mu_{R/L})})^{-1}|\phi_{\kappa''}\rangle.} \tag{2.236}$$

In the particular case $V(x)=g\delta(x)$ ($g<0$ in order to have a bound state) and $V_0(x)=\lim_{g\to\infty}g\delta(x)$, there is one bound state for $\kappa'=-g$ and the overlap is

$$\langle\phi_{-g}|\phi_k^{R/L}\rangle\underset{\ell\to\infty}{\simeq}\sqrt{-g}\sqrt{\frac{4}{\ell}}\frac{k}{k^2+g^2}, \tag{2.237}$$

which leads to

$$C^{R/L}_{-g,-g}=-2g\int_0^\infty\frac{dk}{\pi}\left(f_{R/L}(k)-\theta(t'-t)\right)\frac{k^2}{(k^2+g^2)^2}, \tag{2.238}$$

[3] Indeed an exact calculation of the Wigner function $W(x,p)$, see [3], unveils the existence of a $\delta(p)$ peak, which is shown to be a quantum signature of the finite limit of the correlations along opposite rays.

and we recover the kernel

$$K_b^{R/L}(x,t;x',t') = 2g^2 e^{g(|x|+|x'|)} e^{-i\frac{g^2}{2}(t-t')} \int_0^\infty \left(f_{R/L}(k) - \theta(t'-t)\right) \frac{dk}{\pi} \frac{k^2}{(k^2+g^2)^2} , \tag{2.239}$$

which coincides with the result obtained in [2].

When there are at least two bound states the total NESS kernel exhibits permanent oscillations in time. These oscillations also occur in the density and current. Note that these oscillations contain information about the overlap of the initial wave functions with the post-quench bound states (and about the fact that V_0 has or not bound states), while in the absence of bound states of $V(x)$, only the scattering coefficients remains relevant at large time. In particular one finds that the post-quench bound states are always partially empty in the NESS. See [189] for the relation between the scattering coefficients and the bound states. Finally, bound states do not contribute to the kernel in the ray regime since their wave-functions decrease exponentially at large $|x|$ (see [2, 3] for details). For related results in the presence of bound states see [29, 143, 190].

2.6.5 Density-density time correlation

Finally, we apply our result for the time extended kernel (2.221) to the study of the connected correlation function of the density at two distinct space-time points in the NESS with initial zero temperature $T_{R/L} = 0$ in left and right systems. It is obtained from the kernel in the NESS using (2.207)-(2.208) as

$$\lim_{t\to+\infty} \langle \hat{\rho}(x', t+\tau)\hat{\rho}(x,t)\rangle^c = -K_\infty(x,x';-\tau)K_\infty(x',x,\tau) . \tag{2.240}$$

In the large τ limit the behavior of this correlation depends on the ratios $\zeta = \frac{x}{\tau}$ and $\zeta' = \frac{x'}{\tau}$. As shown in Fig. 2.15 there are several sectors in the (ζ, ζ') plane, where the decay of the correlation at large time is of the form $\sim \tau^{-\alpha} C(\zeta, \zeta')$ where α depends on the sector.(see [188] for details). As compared to the equilibrium case in the absence of a defect for which $\alpha = 3/2$ for all (ζ, ζ') [191], the stationary temporal correlations in the NESS in the presence of an impurity exhibits a richer behavior, in particular regions with a slower decay. In addition, we have shown that the response function reaches a stationary limit $\lim_{t\to+\infty} \frac{\delta\langle\hat{\rho}(x,t)\rangle}{\delta f(x',t-\tau)}|_{f=0}$ which we have expressed in terms of the kernel $K_\infty(x,x',\tau)$ [188].

2.7 A GHD approach to scattering

In this section, we will review the possibility of describing the partitioning protocols discussed in Sections 2.4 and 2.6 using GHD. We will start by explaining the predictions of semiclassical 2.7.1 or naive GHD 2.7.2 and why they fail to describe correlations in the ray regime Eq. (2.231). Then, in Section 2.7.3 we discuss a generalization of GHD for scattering defects. We will notice that while this generalization can provide the kernel on equal rays $K_\xi^+(y,y')$ Eq. (2.231), it cannot predict the kernel on opposite rays, denoted as $K_\xi^-(y,y')$ Eq. (2.231). Finally, in Section 2.7.4 we expose a work in progress. We examine a field $\overline{\rho}$ derived from a rescaling of the Fourier-transformed Wigner function, similar to the Euler scaling limit Eq. (2.67). Then, we explain how this field can be incorporated into the generalization of GHD to reproduce the kernel on opposite rays $K_\xi^-(y,y')$.

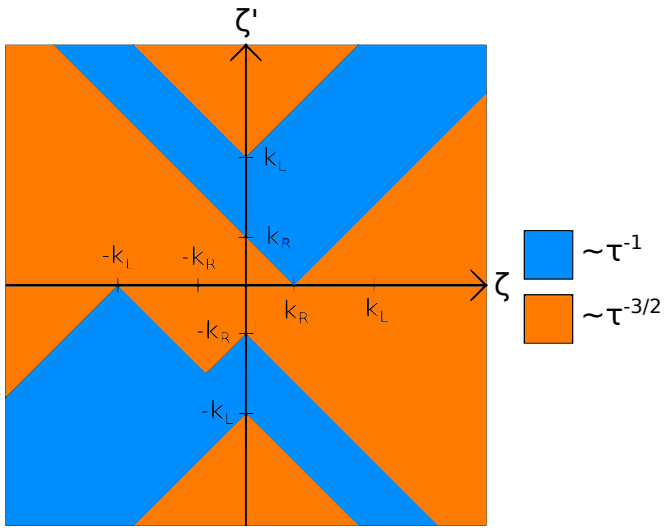

FIGURE 2.15: The density-density correlation in the NESS (2.240) at zero temperature exhibits different power law regimes for large $\tau = t' - t$ and $x = \zeta\tau, \quad x' = \zeta'\tau$. The figure is plotted for $k_R < k_L$, where $k_{R/L} = \sqrt{2\mu_{R/L}}$ are the initial left and right Fermi momentum.

2.7.1 Wigner function semiclassical dynamics

We consider noninteracting fermions evolving within a potential $V(x)$. In the case of a partitioning protocol with a defect, we want to explore the possibility of predicting the kernel Eq. (2.231) at $\tau = 0$ without performing exact computations, but instead, using a semiclassical approximation.

When looking for semiclassical approximation, we prefer working with the Wigner function Eq. (1.83) rather than with the kernel. The initial step involves writing the propagation equation of the Wigner function for noninteracting fermions with a potential $V(x)$, it is derived directly from the Schrödinger equation

$$\partial_t W(x,p,t) + p\partial_x W(x,p,t) = \frac{i}{\hbar}\left(V(x - \frac{i\hbar}{2}\partial_p) - V(x + \frac{i\hbar}{2}\partial_p)\right) W(x,p,t). \quad (2.241)$$

From here, it is common to expand the potential in a power series such that

$$\partial_t W(x,p,t) + p\partial_x W(x,p,t) = \frac{2}{i\hbar}\sum_{n=0}^{\infty} \frac{V^{(2n+1)}(x)}{(2n+1)!}(\frac{i\hbar\partial_p}{2})^{2n+1} W(x,p,t), \quad (2.242)$$

where $V^{(n)}(x)$ is the n-th derivative of the potential at point x. The semiclassical dynamics result directly from retaining the first-order term in $\hbar$ of the power expansion, resulting in:

$$\partial_t W(x,p,t) + p\partial_x W(x,p,t) = V'(x)\partial_p W(x,p,t). \quad (2.243)$$

Note that considering the next order was also explored in [187]. However, if we retain only the first term, we have the Liouville propagation, which can be solved by considering the dynamics of classical particles in the presence of the potential

$V(x)$. Consequently, particles with energy higher than the potential barrier will pass through it entirely, experiencing full transmission, while particles with lower energy will be reflected back, resulting in complete reflection (see Fig. 2.16). In other words, this equation cannot capture the tunneling effect that leads to partial scattering i.e. we have either $R(k) = 0$, and $T(k) = 1$, or $R(k) = 1$, and $T(k) = 0$. It is worth noting that similar results can be obtained when employing the Van Vleck-Gutzwiller propagator [192, 193] which can be used to study the semiclassical behavior of the Wigner function [194].

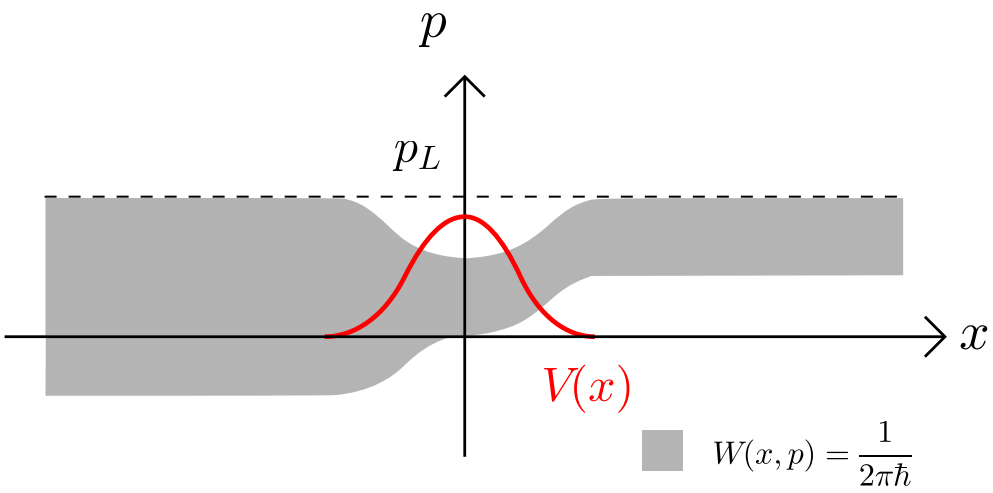

FIGURE 2.16: Illustration of the semiclassical evolution of the Wigner function. The system is initialized in the ground state, where only the left half of the system is filled up to momentum p_L. The illustration represents the NESS that emerges at large times. The part of the Wigner function with an energy higher than the maximum of the potential, $\frac{p^2}{2m} > \max_x V(x)$, experiences full transmission, while the part of the Wigner function with lower energy, $\frac{p^2}{2m} < \max_x V(x)$, undergoes complete reflection. Consequently, the Wigner function is always either equal to 0 or $\frac{1}{2\pi\hbar}$ and never takes an intermediate value between the two. Note that this behavior will change later when we consider a GHD extension, as shown, in Fig. 2.17.

This is not surprising, considering that at zero temperature, the self-reproducing property of the kernel Eq. (1.2.1), which can be shown to hold true for the time-dependent kernel Eq. (2.5), implies that the Wigner function takes values of either zero or $\frac{1}{2\pi\hbar}$ in the semiclassical limit

$$\lim_{\hbar\to 0} 2\pi\hbar W(x,p,t) = 0 \text{ or } 1. \tag{2.244}$$

Whereas, we would imagine this function to take value between zero and one in presence of scattering, for example it could be equal to the reflection $R(p) = |\mathsf{r}(p)|^2$ or the transmission $T(p) = |\mathsf{t}(p)|^2$ coefficient after getting through the potential.

2.7.2 GHD and scattering

One might wonder what the prediction of GHD is within this framework. Interestingly, it turns out that GHD yields the same prediction as the semiclassical limit $\hbar \to 0$. Let us first consider the evolution of the conserved charge $\hat{Q}_j$ from Eq. (2.32), in the presence of a potential $V(x)$. In this dynamics, the charges are no longer conserved. Instead, they follow continuity equations that couple the charges together, resulting in:

$$\forall n \in \mathbb{N}, \quad \partial_t \hat{Q}_n(x,t) = -\partial_x \hat{J}_n(x,t) - i \sum_{j=1}^{n} (-i)^j \binom{n}{j} \hat{Q}_{n-j}(x) V^{(j)}(x) \tag{2.245}$$

with $\binom{n}{j} = \frac{n!}{(n-j)!j!}$ the binomial coefficients and $\hat{J}_n(x,t)$ the charge current (2.35). Now using the procedure which yields the GHD equations in Section 2.1.4 results in the following equation [37]

$$\partial_t \rho_{x,t}(p) + \epsilon'(p) \partial_x \rho_{x,t}(p) = V'(x) \partial_p \rho_{x,t}(p), \tag{2.246}$$

which yields results similar to those of the semiclassical limit Eq. (2.243), where particles are either fully transmitted if their energy is higher than the height of the potential barrier or fully reflected otherwise.

We want to gain a more intuitive understanding of why GHD produces this type of physics. This effect arises due to the condition that GHD is valid when the potential is taken in the infinitely smooth limit, meaning that the variations in the potential occur on a significantly larger scale than the microscopic scale. Specifically, when we take the Euler scaling limit Eq. (2.67), the potential is rescaled as:

$$V_\Lambda(x) = V(\frac{x}{\Lambda}) = V(\tilde{x}). \tag{2.247}$$

From here, one can provide a heuristic argument by comparing the length of the potential with the tunneling length in the large Λ limit. This can be formalized using the WKB approximation as follows. The WKB approximation gives the transmission probability of an incoming wave with energy E smaller than the height of the potential barrier as [195]

$$\begin{aligned} T(E) &\sim \exp\left(-2 \int_{x_1}^{x_2} dx \sqrt{\frac{2m}{\hbar^2}(V_\Lambda(x) - E)}\right) \\ &\sim \exp\left(-\frac{2\Lambda}{\hbar} \int_{\tilde{x}_1}^{\tilde{x}_2} d\tilde{x} \sqrt{2m(V(\tilde{x}) - E)}\right), \end{aligned} \tag{2.248}$$

where x_1, x_2 (respectively $\tilde{x}_1$, $\tilde{x}_2$) are the two turning points of the barrier $V_\Lambda(x)$ (respectively $V(\tilde{x})$) for a wave of energy E. Hence, we observe that in the limit of a smooth potential ($\Lambda \to \infty$), the transmission coefficient is either zero or one. This is also true in the semiclassical limit ($\hbar \to 0$), unless the potential and energy are rescaled by a factor of $\hbar^2$. This can also be observed at the level of the series expansion in Eq. (2.242). The truncation of the first term, which leads to total reflection or total transmission, can only be performed when $\hbar$ is small or when Λ is large (as $V_\Lambda^{(2n+1)} = \frac{V^{2n+1}(x)}{\Lambda^{2n+1}}$).

Therefore, neither a direct application of the semiclassical limit nor the GHD with a smooth potential can effectively describe the physics of partial scattering.

2.7.3 Euler scaled dynamics

Here, we present an extension to GHD [142, 143, 196] that allows for better results than the direct application of semiclassical approximation or GHD presented in the previous section. Specifically, it provides the kernel $K^+_\xi(y,y',\tau=0)$ in the ray regime along equal rays ($\xi=\xi'$) as given in Eq. (2.129). However, it cannot predict the kernel along different rays ($\xi\neq\xi'$), particularly $K^-_\xi(y,y',\tau=0)$, which represents the kernel along opposite rays ($\xi=-\xi'$). These correlations where proven to be essential in the computation of Renyi entropies (1.96), for example the entropy of a subsystem $\mathcal{I}$ far away from the defect was found in [197] to be a functional of the equal rays correlation $K^+_\xi(y,y')$. However, it was shown [198] that the correlation on opposite rays $K^-_\xi(y,y')$ contributes to the entanglement entropy or mutual information $\mathcal{M}_{\mathcal{I}_1,\mathcal{I}_2}=\mathcal{S}_{\mathcal{I}_1}+\mathcal{S}_{\mathcal{I}_2}-\mathcal{S}_{\mathcal{I}_1\cap\mathcal{I}_2}$ between two subsystems $\mathcal{I}_1$ and $\mathcal{I}_2$ far away from the defect and symmetric with respect to the defect.

This approximation yields the dynamics of $\rho_{\mathbf{x},\mathbf{t}}(p)$, i.e. the Wigner function in the Euler scaling limit (2.67), with a potential of fixed size (in contrast to the smooth potential required for GHD, as indicated in Eq. (2.247)). Consequently, we can consider the potential to have a compact support of size zero once the Euler limit is taken. For simplicity, we will now denote the Euler position $\mathbf{x}=\frac{x}{\Lambda}$ and time $\mathbf{t}=\frac{t}{\Lambda}$ as just x and t. In Euler limit, the Wigner function corresponding to the initial kernel (Eq. (2.210)) can be expressed as:

$$\rho_{x,t=0}(p)=\frac{1}{2\pi\hbar}f_L(p)\theta(-x)+\frac{1}{2\pi\hbar}f_R(p)\theta(x) \tag{2.249}$$

where $f_{R/L}(p)$ are the left and right Fermi factors corresponding to the associated initial thermal states (see Fig. 2.17 for a representation at temperature zero). Notice that while the Euler limit of the Wigner function is quite simple and has a discontinuity as a function of the position, the full Wigner function would exhibits complex oscillations close to the impurity and remains continuous in the position varible for most conventional defects. Once the system is prepared with (2.249), we let the system evolve according to the following two rules:

- For $x\neq 0$ i.e. outside of the trap (we recall that in the Euler limit, the trap has no size), the Wigner function follows the free evolution, which corresponds to the Liouville dynamics

$$(\partial_t+p\partial_x)\rho_{x,t}(p)=0. \tag{2.250}$$

  In simple terms, a patch of the Wigner function moves with a velocity of p along the x-axis.

- During the free evolution of the Wigner function, when a patch of the Wigner function crosses the potential at $x=0$, it undergoes transmission (retaining its free evolution but multiplied by a factor $T(p)$) or reflection (multiplied by a factor $R(p)$ and changing momentum from p to $-p$) (see Fig. 2.17).

In [196], this evolution was written in term of the following equation:

$$(\partial_t+p\partial_x)\rho_{x,t}(p)=\delta(x)|p|R(p)\left(\rho_{x=0^\sigma,t}(-p)-\rho_{x=0^{-\sigma},t}(p)\right), \tag{2.251}$$
$$\sigma=\begin{cases}+\text{ if } p>0\\ -\text{ if } p<0\end{cases},$$

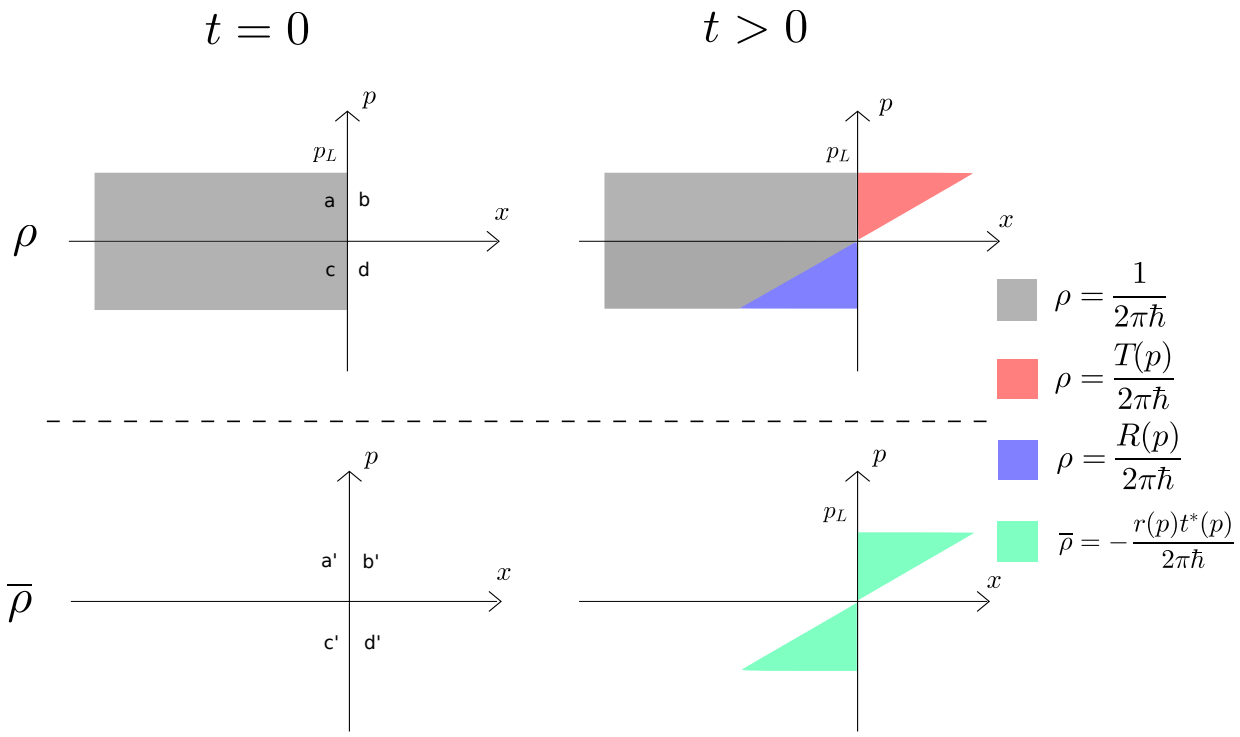

FIGURE 2.17: Illustration of the Euler limit of the Wigner function ρ (Eq. (2.67)) (top) and the Euler limit of the Fourier-transformed Wigner function $\overline{\rho}$ (Eq. (2.257))(bottom). Both are given at the initial time $t = 0$ (left) in the ground state, where only the left half-space is filled up to momentum p_L (in this case, $\overline{\rho}$ is equal to zero). Additionally, we represent their time evolution (right), which involves reflection and transmission coefficients. We choose a symetric potential such that $\mathsf{r}_L(p) = \mathsf{r}_R(p)$ and $\mathsf{t}_L(p) = \mathsf{t}_R(p)$. Additionally, we indicated the sectors a, d, a' and d' where ρ and $\overline{\rho}$ are moving towards the defect at $x = 0$, and the sectors b, c, b' and c' where ρ and $\overline{\rho}$ are moving away from the defect at $x = 0$.

where $\rho_{x=0^{\pm},t}(p)$ is understood as $\lim_{x\to 0^{\pm}} \rho_{x,t}(p)$ (i.e., the left or right limit of ρ, since it is discontinuous in x at $x = 0$). In the equation (2.251), the first term on the right-hand side represents the positive flux of particles reflected from momentum $-p$ to momentum p, while the second term represents the negative flux of particles reflected from momentum p to momentum $-p$. Note that the source terms depends only on particle coming towards the defect (that is on ρ in sectors a and d of Fig. 2.17).

This evolution of ρ can be solved and yields for $x > 0$

$$2\pi\hbar\rho_{x,t}(p) = (f_L(p)T(p) + f_R(p)R(p))\theta(k > \frac{x}{t}) + f_R(p)\theta(k < \frac{x}{t}), \tag{2.252}$$

and for $x < 0$

$$2\pi\hbar\rho_{x,t}(p) = (f_R(p)T(p) + f_L(p)R(p))\theta(k < \frac{x}{t}) + f_L(p)\theta(k > \frac{x}{t}), \tag{2.253}$$

Substituting this into the formula for the kernel Eq. (1.87) enables us to recover

the equal rays part of the kernel $K_\xi^+(y,y',\tau=0)$ in the ray regime Eq. (2.231). However, as previously mentioned, it does not predict the kernel for opposite rays $K_\xi^-(y,y',\tau=0)$, nor does it capture the microscopic details, i.e., the full kernel (Eq. (2.222)).

2.7.4 Another Euler scaled field

Now, we aim to propose an extension of the previous Section 2.7.3 that predicts the non-local correlations i.e. the kernel for opposite rays $K_\xi^-(y,y',\tau=0)$. We would like to emphasize that this is still a work in progress. The first step is to understand which part of the Wigner function contains this information. From the exact kernel Eq. (2.222) and the Kernel ray regime Eq. (2.231), one can compute the Wigner function exactly (see [188] for exact expression of the Wigner function), and its Euler limit precisely matches Eqs. (2.252-2.253). While it is evident that the microscopic details vanish when we take the Euler limit, it is not apparent why the opposite rays should also vanish. In fact, in the exact Wigner function, the opposite rays K_ξ^- correspond to a delta Dirac component $W^-(x,p)=\delta(p)f(x)$, where $f(x)$ is a function localized around the impurity. This function $f(x)$ vanishes in the Euler limit, i.e., $\lim_{|x|\to\infty} f(x)=0$. Thus, when the Euler scaling limit is taken, the information concerning the opposite rays is lost.

In order to isolate the information describing the opposite rays K_ξ^-, we need to isolate this $\delta(p)$ in the Wigner function. Hence, we consider the Fourier transform of the following Wigner function (this will spread the $\delta(p)$ in Fourier space)

$$\begin{aligned}\overline{W}(\overline{x},\overline{p},t) &= \int \frac{dxdp}{\pi\hbar} W(x,p,t) e^{-\frac{2i}{\hbar}(\overline{p}x-\overline{x}p)} \\ &= \int \frac{dx}{\pi\hbar} K(x-\overline{x},x+\overline{x},t) e^{-\frac{2i}{\hbar}\overline{p}x}.\end{aligned} \tag{2.254}$$

We also provide the kernel as a functional of $\overline{W}$:

$$K(x,x',t) = \int d\overline{p} e^{\frac{i\overline{p}}{\hbar}(x+x')} \overline{W}(\frac{x'-x}{2},\overline{p},t). \tag{2.255}$$

Interestingly, this functions obeys the equation

$$(\partial_t + p\partial_{\overline{x}})\overline{W}(\overline{x},\overline{p},t) = \frac{i}{\hbar}(V(-\overline{x}-\frac{i\hbar\partial_{\overline{p}}}{2}) - V(\overline{x}-\frac{i\hbar\partial_{\overline{p}}}{2}))\overline{W}(\overline{x},\overline{p},t). \tag{2.256}$$

It has similarities to Eq. (2.241), where the left-hand side corresponds to the Liouville dynamics (now in Fourier space), and the right-hand side arises from the interaction with the potential. Analogously to Eq. (2.67), we can define a new Euler limit by scaling the Fourier space position variable instead of the real space position variable. This can be accomplished as follows:

$$\overline{\rho}_{\overline{\mathbf{x}},\mathbf{t}}(\overline{p}) = \lim_{\Lambda\to\infty} \overline{W}(\overline{x}=\overline{\mathbf{x}}\Lambda,\overline{p},t=\mathbf{t}\Lambda). \tag{2.257}$$

Because we know the exact kernel, and hence, the exact Wigner function, we can compute exactly $\overline{\rho}$, this leads to (for simplicity, we have omitted the Euler limit i.e.

made the replacement $\begin{cases} \overline{\mathbf{x}} \to \overline{x} \\ \mathbf{t} \to t \end{cases}$ in the following equation and in Fig. 2.17)

$$2\pi\hbar\overline{\rho}_{\overline{x},t}(\overline{p}) = (\mathsf{r}_R(\overline{p})\mathsf{t}_R^*(\overline{p})f_R(\overline{p}) + \mathsf{r}_L^*(\overline{p})\mathsf{t}_L(\overline{p})f_L(\overline{p}))\theta\left((t\overline{p} - \overline{x})\mathrm{sgn}(\overline{x})\right). \tag{2.258}$$

Here, it is crucial to remark that this evolution is surprisingly simple (see Fig. 2.17). It seems to follow the Liouville dynamics away from the defect $\overline{x} \neq 0$. Near the defect, it is coupled to ρ which act as a source. Hence we propose the following dynamic for the two fields ρ and $\overline{\rho}$:

- For $x \neq 0$ and $\overline{x} \neq 0$ i.e. outside of the trap (we recall that in the Euler limit, the trap has no size), the ρ and $\overline{\rho}$ follow the free evolution, which corresponds to the Liouville dynamics

$$(\partial_t + p\partial_x)\rho_{x,t}(p) = 0, \tag{2.259}$$
$$(\partial_t + \overline{p}\partial_{\overline{x}})\overline{\rho}_{\overline{x},t}(\overline{p}) = 0. \tag{2.260}$$

- During the free evolution, when a patch of $\rho_{x,t}(p)$ crosses the potential at $x = 0$, it undergoes transmission (retaining its free evolution but multiplied by a factor $T(p)$) or reflection (multiplied by a factor $R(p)$ and changing momentum from p to $-p$).

- Additionally, when a patch of ρ crosses the potential at $x = 0$ and momentum p, it acts as a source for $\overline{\rho}$ at position $\overline{x} = 0$ and momenta $\overline{p} = \pm p$. To be more precise, $\rho_{x=0^-,t}(\overline{p} > 0)$ generates a flux $\rho_{x=0^-,t}(\overline{p} > 0)\mathsf{r}_L^*(\overline{p})\mathsf{t}_L(\overline{p})$ for $\overline{\rho}_{\overline{x}=0,t}(\overline{p})$ and another flux $\rho_{x=0^-,t}(\overline{p} > 0)\mathsf{r}_L^*(-\overline{p})\mathsf{t}_L(-\overline{p})$ for $\overline{\rho}_{\overline{x}=0,t}(-\overline{p})$. Similarly, $\rho_{x=0^+,t}(\overline{p} < 0)$ generates a flux $\rho_{x=0^+,t}(\overline{p} < 0)\mathsf{r}_R(\overline{p})\mathsf{t}_R^*(\overline{p})$ for $\overline{\rho}_{\overline{x}=0,t}(\overline{p})$ and another flux $\rho_{x=0^+,t}(\overline{p} < 0)\mathsf{r}_R(-\overline{p})\mathsf{t}_R^*(-\overline{p})$ for $\overline{\rho}_{\overline{x}=0,t}(-\overline{p})$ (see Fig. 2.17).

In the spirit of (2.251), we propose the following equation summing up the dynamics and coupling of ρ and $\overline{\rho}$:

$$\begin{aligned}(\partial_t + p\partial_x)\rho_{x,t}(p) &= \delta(x)|p|R(p)\left(\rho_{x=0^\sigma,t}(-p) - \rho_{x=0^{-\sigma},t}(p)\right), \\ (\partial_t + \overline{p}\partial_{\overline{x}})\overline{\rho}_{\overline{x},t}(\overline{p}) &= \delta(\overline{x})\left(\mathsf{r}_L^*(\overline{p})\mathsf{t}_L(\overline{p})\rho_{x=0^-,t}(|\overline{p}|) + \mathsf{r}_R(\overline{p})\mathsf{t}_R^*(\overline{p})\rho_{x=0^+,t}(-|\overline{p}|)\right),\end{aligned} \tag{2.261}$$

where we recall that $\sigma = \begin{cases} + \text{ if } p > 0 \\ - \text{ if } p < 0 \end{cases}$ and $\rho_{x=0^\pm,t}(p)$ is understood as $\lim_{x\to 0^\pm} \rho_{x,t}(p)$. Once this is done, the solution of the differential equations (2.261) is given by Eqs. (2.252), (2.253) and (2.258). Then, we can reconstruct the equal rays correlations $K_\xi^+(y, y', \tau = 0)$ by plugging ρ in the appropriate expression (1.87) of the kernel as a functional of the Wigner function. We also reconstruct the opposite rays correlations $K_\xi^-(y, y', \tau = 0)$ by plugging $\overline{\rho}$ in the appropriate expression (2.255) of the kernel as a functional of the Fourier transform of Wigner function.

From here multiple remarks and questions arise:

- Does the kernel $K(x, x', t)$ admits a similar equation to (2.261) in the Euler scaling limit?

- We know that the two equations (2.261) are correct in our quench with a non-interacting defect and free fermions, but we are uncertain if they remain valid in a more general setup.

- One relevant question to ask is whether there are any additional coupling terms from $\overline{\rho}$ to ρ in the equations (2.261). On the mathematical side, a hint comes from the fact that the two equations for the dynamics of W and $\overline{W}$ (2.241-2.256) are exactly the same for a symmetric potential $V(x) = V(-x)$. This implies that the two equations (2.261) must be symmetric if the potential is symmetric. Hence, there must be two additional terms to the equation, one of them being a coupling from $\overline{\rho}$ to ρ. However, on the physical side, it is unclear how to create an initial condition where $\overline{\rho}$ is nonzero in the sector of phase space where $\overline{\rho}$ is moving towards the defect (that is, the sectors b' and c' of Fig. 2.17). Hence, even if this coupling term exists mathematically, the question of finding a physical setting where it is nonzero remains open.

- Multiple generalizations can be considered; for example, in a quench with multiple defects far away from each other. This includes the case of a defect in the middle of a hard box (the two hard walls can be seen as totally reflecting defects) discussed in Section 2.5. In particular, for the critical regime $a = 1$ whose kernel is unknown.

- Of course, another generalization is the quench of an interacting gas and interacting defect. In that case, it could be that particles are scattered by the defect with different momenta (in our case, the momenta of scattered particles are just opposite).

Article 2

Quench dynamics of noninteracting fermions with a delta impurity [2]

Abstract We study the out-of-equilibrium dynamics of noninteracting fermions in one dimension and in continuum space, in the presence of a delta impurity potential at the origin whose strength g is varied at time $t = 0$. The system is prepared in its ground state with $g = g_0 = +\infty$, with two different densities and Fermi wave-vectors k_L and k_R on the two half-spaces $x > 0$ and $x < 0$ respectively. It then evolves for $t > 0$ as an isolated system, with a finite impurity strength g. We compute exactly the time dependent density and current. For a fixed position x and in the large time limit $t \to \infty$, the system reaches a non-equilibrium stationary state (NESS). We obtain analytically the correlation kernel, density, particle current, and energy current in the NESS, and characterize their relaxation, which is algebraic in time. In particular, in the NESS, we show that, away from the impurity, the particle density displays oscillations which are the non-equilibrium analog of the Friedel oscillations. In the regime of "rays", $x/t = \xi$ fixed with $x, t \to \infty$, we compute the same quantities and observe the emergence of two light cones, associated to the Fermi velocities k_L and k_R in the initial state. Interestingly, we find non trivial quantum correlations between two opposite rays with velocities ξ and $-\xi$ which we compute explicitly. We extend to a continuum setting and to a correlated initial state the analytical methods developed in a recent work of Ljubotina, Sotiriadis and Prosen, in the context of a discrete fermionic chain with an impurity. We also generalize our results to an initial state at finite temperature, recovering, via explicit calculations, some predictions of conformal field theory in the low energy limit.

Article 3

Stationary time correlations for fermions after a quench in the presence of an impurity [3]

Abstract We consider the quench dynamics of non-interacting fermions in one dimension in the presence of a finite-size impurity at the origin. This impurity is characterized by general momentum-dependent reflection and transmission coefficients which are changed from $\mathsf{r}_0(k), \mathsf{t}_0(k)$ to $\mathsf{r}(k), \mathsf{t}(k)$ at time $t = 0$. The initial state is at equilibrium with $\mathsf{t}_0(k) = 0$ such that the system is cut in two independent halves with $\mathsf{r}_0^R(k)$, $\mathsf{r}_0^L(k)$ respectively to the right and to the left of the impurity. We obtain the exact large time limit of the multi-time correlations. These correlations become time translationally invariant, and are non-zero in two different regimes: (i) for $x = O(1)$ where the system reaches a non-equilibrium steady state (NESS) (ii) for $x \sim t$, i.e., the ray-regime. For a repulsive impurity these correlations are independent of $\mathsf{r}_0^R(k)$, $\mathsf{r}_0^L(k)$, while in the presence of bound states they oscillate and memory effects persist. We show that these nontrivial relaxational properties can be retrieved in a simple manner from the large time behaviour of the single particle wave functions.

Chapter 3

Quantum propagating front and the edge of the Wigner Function

The phenomenon we want to highlight here was inspired by the result of [40]. This article consider fermions on a lattice introduced in (2.46) with $J = 1/2$. Initially, the system is prepared in a step like condition filling every sites of the left system half

$$\langle c_m^\dagger c_n \rangle = \begin{cases} \delta_{i,j} & n, m \leq 0 \\ 0 & \text{else} \end{cases} . \tag{3.1}$$

Now we are interested in the observable equivalent to the time-dependent kernel for lattice fermions, i.e. $C_{m,n}(t) = \langle c_m^\dagger(t) c_n(t) \rangle$ where $c_n(t)$ is the time evolved fermionic creation operator in the Heisenberg picture. More precisely, a propagating front moving from left to right emerges, and we are interested in the correlation around this front. It can be shown that the density in the large time limit takes a scaling form (see Fig. 3.1)

$$\rho_n(t) \simeq \begin{cases} 1 \text{ if } x/t < -1 \\ \frac{\arccos(x/t)}{\pi} \text{ if } -1 < x/t < 1 \\ 0 \text{ if } 1 < x/t \end{cases} . \tag{3.2}$$

The correlations can be computed in large time with a saddle point approximation. However, near the quantum front, the saddle point is by definition located at the maximum of the velocity $v(k) = \epsilon'(k)$ (the dispersion relation is $\epsilon(k) = -\cos(k)$) that is the saddle point is at $v(k^*) = \sin(k^*) = 1$. This implies that the expansion around the saddle point at the quantum front involves a third order term $\sim k^3$ which eventually leads to the emergence of the Airy kernel [40]

$$C_{m,n}(t) \simeq i^{n-m} (\frac{2}{t})^{1/3} K_{Ai}(\frac{m-t}{(\frac{t}{2})^{1/3}}, \frac{n-t}{(\frac{t}{2})^{1/3}}). \tag{3.3}$$

We see that $t^{1/3}$ emerge as a characteristic length. Note that Wick theorem implies that the phase factor i^{n-m} in front of the kernel is irrelevant for the density-density correlations.

Now we compare this with fermions in the continuum. In that case, the dispersion relation is $\epsilon(k) = \frac{k^2}{2}$, therefore the velocity $v(k) = k$ has no extremum. This implies that we will never witness the emergence of the Airy kernel as it is the case for fermions in the lattice [40]. Despite this, we propose a quench protocol for fermions in the continuum where the Airy kernel Eq. (1.77) arises at the edge of the quantum front. The main trick is to change the initial condition. Instead of a domain wall initial condition, we prepare the system in the ground state of the inverse power-law

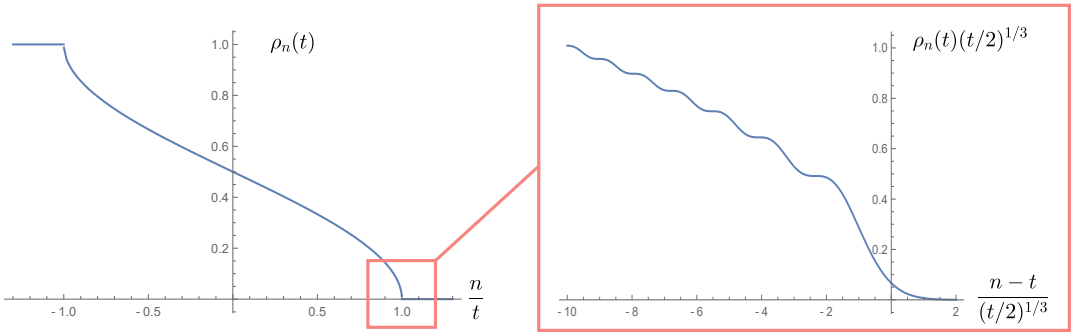

FIGURE 3.1: Illustration of the density $\rho_n(t) = C_{n,n}(t)$. On the left panel, we plot the large time scaling form of the density (3.2). We observe the propagation of a front in the density. On the right panel, we show the density rescaled around the front which follows Eq. (3.3). There is a staircase structure at the edge of the front.

potential $V(x) = \frac{c}{|x|^\gamma}$, such that only the left half-space is filled up to the Fermi momentum p_F. Then, at the initial time, we turn off the potential, allowing the fermions to freely propagate. From here, the statistics at the edge of the quantum front can be related to the Wigner function in the initial state. Therefore, following [199], we examine the initial state Wigner function corresponding to the ground state of the inverse power-law potential, and we demonstrate the emergence of the Airy kernel Eq. (1.77) at the edge of the quantum front.

This chapter is divided into two sections. The first section is dedicated to the study of the initial condition, that is the equilibrium properties of non interacting fermions in the inverse power law potential $V(x) = \frac{c}{|x|^\gamma}$. More precisely, our goal is to explore the properties of the semiclassical limit of the Wigner function introduced previously (1.83). In this limit, Berry [200] showed that the Wigner function for a single particle within a potential could be expressed in term of Airy function. Latter, this result was generalised to the ground state of N particles [199, 201]. In that case, the Wigner function has an edge called the "Fermi surf", which is completely characterized by the classical one-particle Hamiltonian of the system. In one dimension, the Fermi surf is a closed curve that separates the phase space in two parts, the Wigner function being equal to zero outside and $\frac{1}{2\pi\hbar}$ inside. Note that this result is the starting point of the LDA (1.2.4). It turns out that, for large but finite N fermions in a smooth potentials, close to generic points on the Fermi surf, the Heaviside theta function of the LDA (1.88) is smoothed around the Fermi surf. Furthermore, in these conditions, the Wigner function can be expressed in terms of Airy functions (3.5) in a way such that the kernel at the edge of the gas is none other than the Airy kernel. The result of the first section is the study of the Wigner function around the Fermi surf in the particular case of the inverse power law potential $V(x) = \frac{c}{|x|^\gamma}$, which turns out to exhibit different behaviors.

In the second part, we introduce a quench where noninteracting fermions are prepared in the ground state of the inverse power law potential $V(x) = \frac{c}{|x|^\gamma}$, occupying only the left half of the system. This way the initial condition corresponds to the Wigner function studied in the first section. Then, the potential is quenched to zero, allowing the fermions to evolve freely. Consequently, a quantum front (or the edge of the gas) propagates from left to right. The result of this second section, which is a consequence of the first section, lies in the emergence of the Airy kernel around the

quantum front.

3.1 Airy statistics and the Wigner function

First, let us provide a detailed justification for the LDA and the assumption made for the Wigner function in (1.88). By doing so, we will also refine this assumption beyond the LDA.

3.1.1 Short time expansion of the propagator and the semiclassical Limit

In this section, we will refer to the "semiclassical limit" as the large $N \to \infty$ limit. We will later establish a connection between this limit and the $\hbar \to 0$ limit, justifying the chosen terminology. Before going further, let us introduce the "Fermi surf" [201], that is the edge of the Wigner function in the semiclassical limit defined by

$$H(x_e, p_e) = \mu. \tag{3.4}$$

We recall that the Fermi surf is the separation between the bulk and the exterior of the Wigner function in the classical limit (1.88). Moving to the semiclassical limit means that we consider first order finite N correction. As a consequence, the Fermi surf of the "classical" Wigner function Eq. (1.88) softens up with the following universal scaling [199]

$$W_N(x,p) \underset{N\to\infty}{\simeq} \frac{\mathcal{W}(a)}{2\pi\hbar} = \frac{1}{2\pi\hbar}\int_{2^{2/3}a}^{\infty} dz Ai(z), \tag{3.5}$$

$$a = \frac{H(x,p)-\mu}{e_N}, \quad e_N = (\frac{\hbar^2}{2}(p_e^2 V''(x_e) + (V'(x_e))^2)^{1/3}, \tag{3.6}$$

where Ai is the Airy function. We say this scaling is universal in the sense that it is valid for any smooth potential as long as $e_N \neq 0$. Note that we called "classical" the result (1.88) which does not consider the first order corrections, i.e. corresponds to $\hbar = 0$, while we call "semiclassical" the small but finite $\hbar$ (respectively large but finite N) regime Eq. (3.5). Note that

$$\mathcal{W}(a) \simeq \begin{cases} 1 & \text{if } a \to -\infty \\ (8\pi)^{-1/2} a^{-3/4} \exp\left(-\frac{4}{3}a^{3/2}\right) & \text{if } a \to +\infty \end{cases} \tag{3.7}$$

such that the Wigner function is equal to $\frac{1}{2\pi\hbar}$ within the bulk, and zero outside, giving a first order smooth version of the classical limit (1.88). Furthermore, using the formula from the book [202]

$$\int \frac{dk}{\pi} e^{-ik(p-q)} Ai(k^2+p+q) = 2^{2/3} Ai(2^{1/3}p) Ai(2^{1/3}q), \tag{3.8}$$

together with the formula (1.87) and some smart changes of variables, one can show that the kernel at the edges of the gas is the Airy kernel (1.77) for any smooth potential

$$K_\mu(x,x') \underset{N\to\infty}{\simeq} K_{Ai}(\frac{x-x_{edge}}{w_N}, \frac{y-x_{edge}}{w_N}), \quad w_N = \left(\frac{\hbar^2}{2mV'(x_{edge})}\right)^{1/3}. \tag{3.9}$$

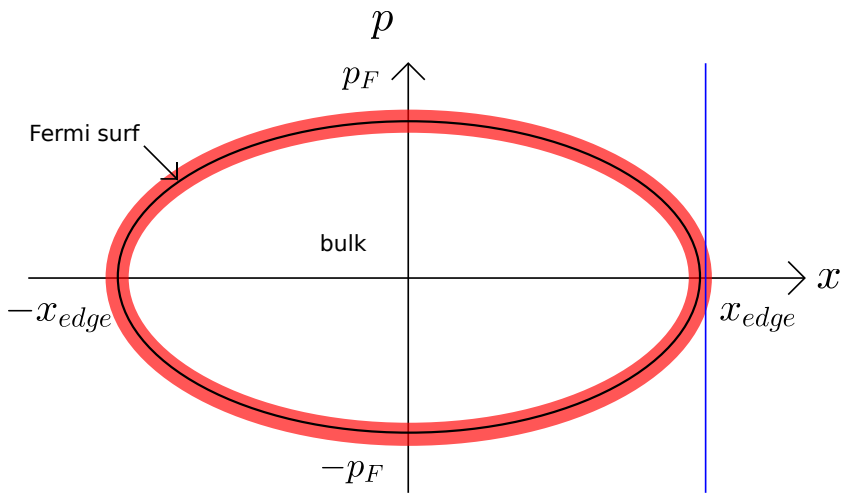

FIGURE 3.2: Representation of the Fermi surf for the harmonic potential. We also represent in red, the width of the Wigner function in the semiclassical limit around the Fermi surf. Additionally, the vertical line in blue is the integral contour of the formula (1.87) which leads to the recovery of the Airy kernel at the edge of the gas (3.9).

where x_{edge} is the particle density edge defined by $V(x_{edge}) = \mu$, not to be confused with the Fermi surf (x_e, p_e) (see Fig. 3.2).

Imaginary Time Propagator. In order to prove this to be true, We consider a system of noninteracting trapped fermions with a single-particle Hamiltonian $\hat{H}$, wave functions, and eigenenergy family ϕ_k, ϵ_k, in the ground state with chemical potential μ (or equivalently a finite number of N fermions). We note K_μ the kernel

$$K_\mu(x, x') = \sum_{k=0}^{\infty} \phi_k^*(x)\phi_k(x')\Theta(\mu - \epsilon_k). \tag{3.10}$$

Note that in the case of a non-trapping potential the family $\{\phi_k, \epsilon_k\}$ have a continuously indexed component, and the previous sum turns into an integral. Our method relies on the imaginary quantum propagator

$$G(x, x', t) = \langle x'|e^{-\frac{\hat{H}t}{\hbar}}|x\rangle = \frac{t}{\hbar}\int_0^\infty d\mu e^{-\frac{\mu t}{\hbar}} K_\mu(x, x'). \tag{3.11}$$

The last formula can be inverted to give the kernel as

$$K_\mu(x, x') = \int_C \frac{dt}{2\pi i t} e^{\frac{\mu t}{\hbar}} G(x, x', t), \tag{3.12}$$

where C is the Bromwich contour in the complex plane. Hence putting together Eq. (3.12), and (1.86), yields the expression for the Wigner function of N fermions in the ground state

$$W_N(x, p) = \frac{1}{2\pi\hbar}\int_C \frac{dt}{2\pi i t} e^{\frac{\mu t}{\hbar}} \int_{-\infty}^{+\infty} dy e^{\frac{ipy}{\hbar}} G(x + \frac{y}{2}, x - \frac{y}{2}, t). \tag{3.13}$$

The propagator obeys the following equation

$$\hbar\partial_t G(x,x',t) = \left(\frac{\hbar^2}{2m}\partial_x^2 - V(x)\right) G(x,x',t), \quad G(x,x',0) = \delta(x-x'). \tag{3.14}$$

Now, using the Feynamnn-Kac formula, the solution of this equation can be written as a path integral [203]. This can then be written in term of a Brownian bridge [17]

$$G(x+\frac{y}{2}, x-\frac{y}{2}, t) = \sqrt{\frac{m}{2\pi\hbar t}} e^{-\frac{my^2}{2\hbar t}} \langle \exp(-\frac{t}{\hbar}\int_0^1 du V(x+y(\frac{1}{2}-u) + \sqrt{\frac{\hbar t}{m}}B_u))\rangle_B.$$

Here B is a Brownian bridge that is a Brownian process on $u \in [0,1]$ with zero mean and correlation $\langle B_u B_{u'}\rangle_B = \min(u,u') - uu'$, hence $B_0 = B_1 = 0$. From here, the argument is that in the semiclassical limit (where μ is large), the Wigner function, given by Eq. (3.13), will be dominated by short-time contributions. Therefore, we proceed with the short-time expansion of the propagator. There is a saddle point at $y = itp$, so we make the change of variable $y = \frac{itp}{m} + \sqrt{\frac{\hbar t}{m}}\tilde{y}$ which yields (appendix of [199])

$$W_N(x,p) = \frac{1}{2\pi\hbar}\int_C \frac{dt}{2\pi i t} e^{(\mu - \frac{p^2}{2m} - V(x))\frac{t}{\hbar} + S(x,p)} \tag{3.15}$$

$$S(x,p) = \ln\langle \exp\left(-\frac{t}{\hbar}\int_0^1 du \left[V(x + \frac{itp}{m} + \sqrt{\frac{\hbar t}{m}}\tilde{y}(\frac{1}{2}-u) + \sqrt{\frac{\hbar t}{m}}B_u) - V(x)\right]\right)\rangle_{B,\tilde{y}},$$

with $\langle ... \rangle_{B,\tilde{y}} = \int \frac{d\tilde{y}}{\sqrt{2\pi}} e^{-\frac{\tilde{y}^2}{2}} \langle ... \rangle_B$.

Recovering the LDA/classical limit. Now, our goal is to justify the LDA (1.88). In order to do so, we expand V in (3.15) around x_e at small time t and we stop to the zeroth order in time. The two potentials V in (3.15) cancels, which yields $S(x,p) \simeq 0$, and therefore

$$W_N(x,p) = \frac{1}{2\pi\hbar}\int_C \frac{dt}{2\pi i t} e^{(\mu - \frac{p^2}{2m} - V(x))\frac{t}{\hbar}} = \frac{1}{2\pi\hbar}\Theta(\mu - H(x,p)). \tag{3.16}$$

This is the ansatz of the LDA (1.88). The only missing part in our argument is a justification for the short time expansion. In the large chemical potential μ limit, this expansion was justified in [199].

The semiclassical limit. Now, we want to push this method to higher order expansion. We choose a point close to the edge, $(x,p) \simeq (x_e, p_e)$, and we want to expand V in (3.15) around x_e. The expansion is achieved in detail in the Appendix D considering the fluctuations of the Brownian bridge B_u. The expansion is found to be valid under the conditions given in the Appendix in Eqs. (D.1), and (D.5). For now let us assume that those conditions are satisfied, then, the expansion yields the following result

$$\begin{aligned} W_N(x,p) &\underset{N\to\infty}{\simeq} \frac{1}{2\pi\hbar}\int_C \frac{dt}{2\pi i t} e^{(\mu - H(x,p))\frac{t}{\hbar} + \frac{t^3}{24\hbar}(p_e^2 V''(x_e) + V'(x_e)^2)}, \\ &= \frac{1}{2\pi\hbar}\int_C \frac{d\tau}{2\pi i\tau} e^{-2^{2/3}a\tau + \frac{\tau^3}{3}} = \frac{\mathcal{W}(a)}{2\pi\hbar}, \end{aligned} \tag{3.17}$$

where a was defined in Eq. (3.5). This is the Airy scaling discussed above in Eq.

Limit	Near the gas edge	Away from the gas edge
$\mu \to +\infty$	$\gamma > 2$	$\emptyset$
$\hbar \to 0$	$\forall \gamma$	$\forall x$ if $\gamma < 1$ or if $x^{\gamma-1} \ll \frac{\sqrt{mc}}{\hbar\sqrt{\mu}}$

TABLE 3.1: Summary of the conditions under which the Wigner function exhibits the Airy scaling (3.5) along the Fermi surf (see Fig. 3.3) for the ground state in the inverse power law potential.

(3.5). The authors of [199] then argue that in most generic confining potential, the condition Eqs. (D.1) and (D.5) are verified in the large $\mu \to \infty$ limit, which allows to recover the universal scaling Eq. (3.5) and (3.9). From now on, the conditions Eqs. (D.1) and (D.5) will be essential if one wants to know whether the Wigner functions follows the Airy scaling (3.5) in a specific region of the Fermi surf.

While the Airy scaling (3.5) is generally valid for generic points, it has been found to be absent at certain specific points for certain potentials. For instance, when examining the Wigner function of potentials $V(x) \sim x^{2n}$ with $2 \leq n$, it is clear that e_N defined in (3.5) becomes zero at $x_e = 0$, such that, the Airy scaling is not valid. This phenomenon is discussed in [65], where the authors obtained the momentum coordinate kernel at the edge of the momentum density and found it to differ from the Airy kernel. Another example is provided by the inverse power law potential $V(x) = \frac{\hbar^2(\nu^2-\frac{1}{4})}{2m|x|^\gamma}$, for which the kernel at the edge of the density was determined in [182]. This analysis shows the emergence of the Airy kernel if $\gamma > 2$. Knowing this, we aim to extend the analysis to the full Wigner function and investigate the conditions under which the Wigner function exhibits the Airy scaling (3.5) for the inverse power law potential.

Remark. It is interesting to note that the expansion of the propagator can be obtained from an expansion around the classical path, as demonstrated in [204]. In the case of an inverse power law potential $V(x) = \frac{c}{x^\gamma}$, there are two such paths: a direct path and an indirect path with a turning point [205, 206]. However, when using the imaginary time propagator in the small $\hbar$ limit, the contribution from the indirect path is subleading such that the two different methods yield identical results.

3.1.2 The Inverse Repulsive Power Law Potential $V(x) = \frac{c}{|x|^\gamma}$

Here for purpose that will become clear in the next section 3.2 we want to extend the previous analysis to the special case of the non-confining potential $V(x) = \frac{c}{|x|^\gamma}$ with $c > 0$. We show that for this potential, the Airy scaling Eq. (3.5) in the large μ limit is valid only under tight conditions, that is for $\gamma > 2$ and close to the edge of the gas (or equivalently on the part of the Fermi surf Eq. (3.4) where $p_e \simeq 0$). Our main result lies in the fact that the Airy scaling remains valid on a wider part of the Fermi surf under the small $\hbar$ limit. More precisely in the small $\hbar$ limit, the Airy scaling is valid on the complete Fermi surf if $\gamma \leq 1$, and only for $\hbar x_e^{\gamma-1} \ll 1$ if $\gamma > 1$. Our results are summarized in the table 3.1 and figure 3.3.

In the article [199], the analysis was carried out with $\hbar = 1$. Here, we reintroduce $\hbar$ specifically in conditions Eq. (D.1) and (D.5). We realize that the limit $\hbar \to 0$ leads to the Airy scaling (3.5) on a wider part of the Fermi surf than in the large μ limit. Before diving into the details, let us briefly review some known facts about

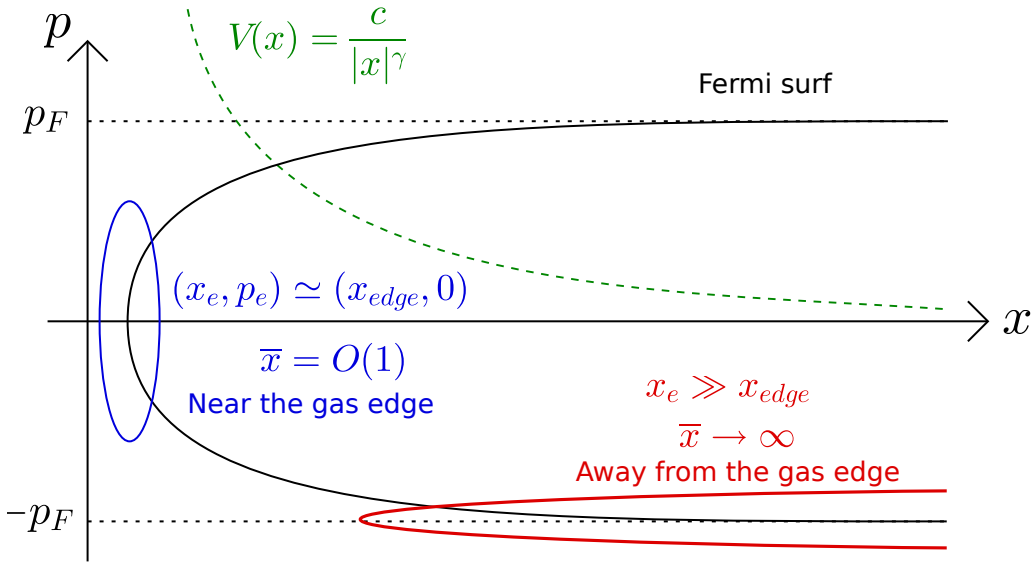

FIGURE 3.3: Illustration of the Fermi surf of the Wigner function for the ground state of the repulsive inverse power law potential $V(x) = \frac{c}{|x|^\gamma}$. We specify the two region of the Fermi surf defined in terms of $\overline{x}$ of order one or taken large where $\overline{x}$ is defined in (3.23).

noninteracting fermions in the presence of the inverse power law potential $V(x) = \frac{c}{|x|^\gamma}$, when $c \sim \hbar^2$.

The $c = \frac{\hbar^2(\nu^2-\frac{1}{4})}{2m}$ barrier. First, in [182], the case where $c = \frac{\hbar^2(\nu^2-\frac{1}{4})}{2m}$ was studied. Notice that if $\gamma = 2$, the potential is equivalent to a centrifugal barrier, which corresponds to the effective potential generated by the angular decomposition introduced in Eq. (1.126) in the absence of a background potential $V(r)$. First, let us mention that if the potential is scaled like this to be proportional to $\hbar^2$, taking the limit $\mu \to \infty$ and taking the limit $\hbar \to 0$ yields identical results. This will not be true when we will consider c of order one. In both limits of large μ or small $\hbar$, we have the same behaviour depending on the value of γ:

- $0 < \gamma < 1$: In that case, the barrier is penetrable, meaning that there exist eigenstates that do not vanish at $x = 0$.
- $1 \leq \gamma < 2$: The barrier is impenetrable (and it is for all $1 \leq \gamma$). By rescaling the Schrödinger equation, the potential can be neglected and the kernel is similar to the hard-wall kernel

$$\begin{aligned} K(x,x') &\sim K_{hw}(k_F x, k_F, x'), \\ K_{hw}(u,u') &= \frac{\sin(u-u')}{\pi(u-u')} - \frac{\sin(u+u')}{\pi(u+u')}, \end{aligned} \tag{3.18}$$

  with $k_F = \frac{\sqrt{2m\mu}}{\hbar}$ the Fermi wavenumber.
- $\gamma > 2$: On the contrary, in that case, the potential cannot be neglected and, the kernel is the Airy kernel.

- $\gamma = 2$: In this case, we already mentioned that the kernel is the Bessel kernel. This case connects $1 \leq \gamma < 2$ with $\gamma > 2$. Indeed, for $\nu = \frac{1}{2}$ the Bessel kernel is identical to the hard wall kernel, this can be seen at the level of the wave function as $J_{1/2}(x) = \sqrt{\frac{2}{\pi x}} \sin x$. On the other side, for $\nu \to \infty$, if properly rescaled, the Bessel kernel converges to the Airy kernel. Again this can be seen as a consequence of $(\nu/2)^{1/3} J_\nu(\nu + (\nu/2)^{1/3} x) = Ai(-x)$.

Now we want to address the following questions:

- What happens if we keep c fixed while taking the limit $\hbar \to 0$ and $\mu \to \infty$?
- Does the Wigner function exhibits the Airy scaling in one of those limits? If it does, on which part of the Fermi surf? We will distinguish two regions, close to the edge of the gas and away from the edge of the gas (see Fig. 3.3).

For the part of the Fermi surf close to the edge of the gas, looking at the Schrödinger equation for the propagator (3.14), one concludes that the potential term is not negligible if and only if $\hbar^2 \mu^{\frac{2-\gamma}{\gamma}} \ll 1$. Hence, we expect to recover the Airy kernel under this condition. The conditions under which the Fermi surf exhibits the Airy scaling (3.5) are summarised in the table (3.1).

The inverse square potential, $\gamma = 2$. Now, we want to study the Wigner function close to the Fermi surf in the inverse power law potential. Before examining the general inverse power law potential, we start with a particular case, the inverse squared potential. For $\gamma = 2$, the eigenfunctions are known such that one can compute exactly the Wigner function. We know that the Airy kernel is recovered when $\nu \to \infty$, for fixed c, which is equivalent to taking the $\hbar \to 0$ limit, as $\nu = \sqrt{\frac{1}{4} + \frac{2mc}{\hbar^2}}$. Therefore, we consider the Wigner function in the latter limit and prove that is exhibits the Airy scaling (3.5). In this case, the single-particle eigenfunctions ϕ_p form a continuously indexed family, and they are related to the Bessel function through the following expression

$$\phi_p(x) = \sqrt{\frac{px}{\hbar}} J_\nu\left(\frac{px}{\hbar}\right), \tag{3.19}$$

with $\nu \underset{\hbar \to 0}{\simeq} \frac{\sqrt{2mc}}{\hbar}$. This leads to the following expression for the Wigner function [207]

$$\begin{aligned} W(x,p) &= \frac{1}{2\pi\hbar^3} \int_0^{p_F} p' dp' \int_{-2x}^{2x} dy e^{\frac{i\nu y}{x_\alpha(p)}} \sqrt{(x + \frac{y}{2})(x - \frac{y}{2})} \\ &\times J_\nu(\nu \frac{x + y/2}{x_\alpha(p')}) J_\nu(\nu \frac{x - y/2}{x_\alpha(p')}), \end{aligned} \tag{3.20}$$

where $x_\alpha(p') = \frac{\sqrt{2mc}}{p'}$ is the turning point (i.e. the point where $\frac{p'^2}{2} = V(x_\alpha)$) for a wave of impulsion p'. Using the integral representation for the Bessel function $J_\nu(x) = \frac{1}{2\pi} \int_{-\pi}^{\pi} d\tau e^{i(\nu\tau - x\sin(\tau))}$ in (3.20) leads to

$$\begin{aligned} W(x,p) &= \frac{1}{(2\pi\hbar)^3} \int_0^{p_F} p' dp' \int_{-2x}^{2x} dy \int_{-\pi}^{\pi} d\tau_1 d\tau_2 \sqrt{x^2 - \frac{y^2}{4}} e^{i\nu F(\tau_1, \tau_2, p', y)} \\ F(\tau_1, \tau_2, p', y) &= \tau_1 + \tau_2 - \frac{x + \frac{y}{2}}{x_\alpha(p')} \sin(\tau_1) - \frac{x - \frac{y}{2}}{x_\alpha(p')} \sin(\tau_2) + \frac{y}{x_\alpha(p)} \end{aligned} \tag{3.21}$$

In the small $\hbar$ limit, $\nu \to \infty$, hence, Eq. (3.21) is a four-dimensional saddle point integral. We notice that the y dependent integral converges towards a delta Dirac function in the small $\hbar$ limit. including a delta function. When expanding the function F to second order, the delta Dirac part, that is the term proportional to y constrain τ_1 and τ_2 such that their second derivative contributions cancels out. Therefore one has to push the expansion to third order resulting, for a phase space point taken close to the Fermi surf $(x, p) \simeq (x_e, p_e)$, in the Airy scaling limit Eq. (3.5). However, we find that the following additional condition must be satisfied

$$\boxed{\frac{xp\hbar}{mc} \ll 1}. \tag{3.22}$$

A few remarks are in order:

- Notice that if the Airy scaling was given by the semiclassical limit $\hbar \to 0$, it would not be possible to obtain it solely from the large μ limit.
- The condition Eq. (3.22) results from two phenomena. First, the higher-order term in the expansion of the saddle point function $F(\tau_1, \tau_2, p', y)$ contains powers of $\frac{xp\hbar}{c}$ such that the expansion cannot be performed if the aforementioned condition is violated. Second, the integration space in the saddle point integral is constrained by the aforementioned delta function in the small $\hbar$ limit. This delta function restricts the integration space to a two dimensional subspace. This subspace has a characteristic width $\Delta \simeq (\frac{xp\hbar}{c})^{-1/3}$ along one integration axis, such that the saddle point can not be performed when the condition is not valid, i.e. when $\Delta \ll 1$.
- Typically p is lower or close to $\sqrt{2m\mu}$ and the condition (3.22) is not satisfied away from the potential that is for large $x \sim \hbar^{-1}$.

The inverse power law potential, $\gamma \geq 0$. In order to generalise the result obtained for $\gamma = 2$, we apply the short time propagator expansion (3.1.1) method to the inverse power law potential. Note that one could worry about the fact that the potential is not smooth anymore and exhibits a diverging singularity eventually invalidating the previous analysis. In fact, this is not a problem, as long as the singularity is repulsive, in this case the propagator from (3.15) is still well defined.

Near the gas edge. We want to look at the Wigner function near the gas edge that is where the particle density vanishes i.e. when $p_e = 0$, and $x_e = x_{edge} = (\frac{c}{\mu})^{1/\gamma}$ (see Fig. 3.3). This is done by rescaling the Fermi surf as

$$\begin{aligned} x_e &= \overline{x} x_{edge}, \\ p_e &= \sqrt{2m\mu(1 - \overline{x}^{-\gamma})}, \end{aligned} \tag{3.23}$$

where $\overline{x} \in [1, +\infty[$. Then we consider the different limits (large μ or small $\hbar$) with $\tilde{x}$ fixed. This case turns out to be simple as the conditions Eqs. (D.1), and (D.5) depend only on one dimensionless parameter and the expansion of the propagator is valid if

$$\boxed{\frac{\hbar^2 \mu^{\frac{2-\gamma}{\gamma}}}{mc^{\frac{2}{\gamma}}} \ll 1}. \tag{3.24}$$

Hence, we find the Airy scaling Eq. (3.5) in two different limits, for $\mu \to \infty, \quad \gamma > 2$, or for $\hbar \to 0$ with any $\gamma > 0$. In other words, the limit $\hbar \to 0$ is more universal as it

works for any value of γ. Notice that if we set $c = \frac{\hbar^2(\nu^2-\frac{1}{4})}{2m}$, the previous condition becomes

$$\frac{1}{m(\nu^2-\frac{1}{4}))^{\frac{2}{\gamma}}}(\frac{\hbar^2}{\mu})^{\frac{\gamma-2}{\gamma}} \ll 1. \tag{3.25}$$

This is consistent with the discussion on the small $c \sim \hbar^2$ barrier (3.1.2) where the small $\hbar$ and the large μ limit where equivalent.

Away from the gas edge. We look at the Wigner function for $x_{edge} \ll x_e$ and $p_e \simeq \sqrt{2m\mu}$ (see Fig. 3.3) or equivalently $\overline{x} \to \infty$ in (3.23). This time the conditions Eqs. (D.1) and (D.5) yield Eq. (D.11) (see Appendix D), such that, in the limits of interest, the Airy scaling is correct only if the following condition is satisfied

$$\boxed{\frac{\hbar\sqrt{\mu}x_e^{\gamma-1}}{\sqrt{m}c} \ll 1} \tag{3.26}$$

Let us make a few remarks on this condition:

- The large μ limit does not satisfy the condition (3.26), hence, there is no Airy scaling at large μ, and large x_e.
- In the case of the small $c = \frac{\hbar^2(\nu^2-\frac{1}{4})}{2m}$ barrier, again, the large μ and small $\hbar$ limit play the same role and there is no Airy scaling at large x_e.
- The condition matches (3.22) for $\gamma = 2$.
- There is a change of behavior at $\gamma = 1$. For $\gamma > 1$ the Airy scaling is recovered for small $\hbar$ as long as x_e is small enough to verify Eq. (3.26). For $\gamma \leq 1$ the Airy scaling is recovered for any x_e.
- The question that remains open is how the Wigner function behaves near the Fermi surf when the condition Eq. (3.26) is broken as x is taken large.

3.2 Airy kernel at the quantum front

Now let us give details on the chosen quench protocol.

Initial condition. Instead of having a domain wall release like in [40]. The system is prepared in the ground state of noninteracting fermions with the impenetrable barrier $V(x) = c/|x|^\gamma$, studied in Section 3. This ground state is such that only the left half space is filled up to Fermi momentum p_F or chemical potential $\mu_F = \frac{p_F^2}{2}$. We will study the dynamics of the Wigner function introduced in Eq. (1.83). Equation (3.4) allows us to define the "Fermi surface". For the inverse power law potential (see Fig. 3.3), this gives

$$\begin{aligned} \frac{p_e^2}{2} + \frac{c}{|x_e|^\gamma} &= \frac{p_F^2}{2}, \\ p_e(x) &= \sqrt{p_F^2 - \frac{2c}{|x|^\gamma}}, \\ x_e(p) &= -(\frac{2c}{p_F^2 - p^2})^{\frac{1}{\gamma}}. \end{aligned} \tag{3.27}$$

We have already discussed the fact that around the Fermi surf, for small $\hbar$, the Wigner function exhibits the Airy scaling Eq. (3.5).

Quench. Later, we will quench the trap and consider the free evolution of fermions, producing a positive current (from left to right). For free fermions, the dynamical evolution of the Wigner function (2.241) is reduced to the Liouville dynamics (2.259) such that

$$W(x,p,t) = W(x-pt,p,t=0) = W_0(x-pt,p) \tag{3.28}$$

where $W_0(x,p)$ is the Wigner function at initial time. This implies that the Fermi surf will be deformed with time as in Fig. 3.4 following

$$x(p,t) = x_e(p) + pt. \tag{3.29}$$

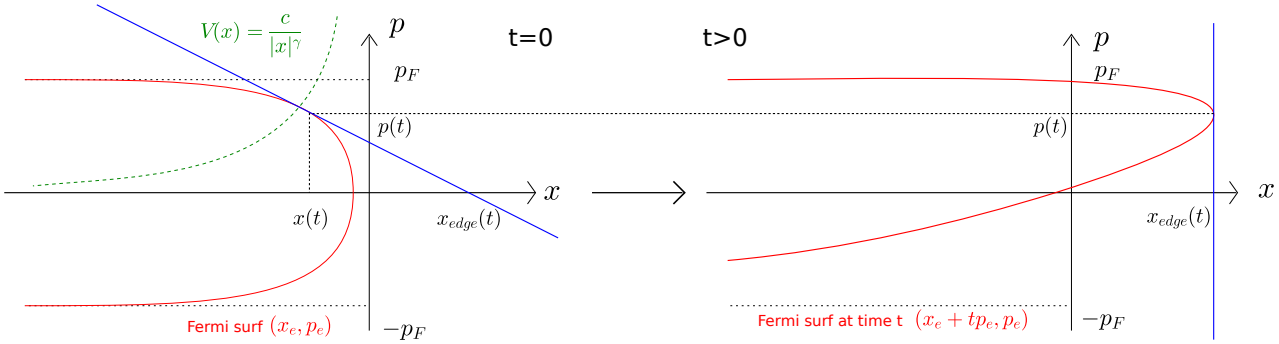

FIGURE 3.4: Plot of the Fermi surf for the inverse power law potential (red line, left) and its free evolution at time t (red line, right). We also plot the line tangent to the Fermi surf at the quantum front $(x_{\rm edge}(t), p(t))$ (blue, right) and its backward time propagation, i.e., the tangent to the point $(x(t), p(t))$ (blue, left). These two tangent lines appear in (3.35), where in the first line of the equation the integral is performed over a line parallel to the right tangent line, and in the second line of the equation, the integral is performed over a line parallel to the left tangent line. Thus, in the large time limit, the computation of the kernel (3.35) probes the edge properties of the Wigner function in the inverse power law potential away from the center of the potential ($x_e \to -\infty$), leading to the Airy kernel at the quantum front (3.36).

Therefore, we will observe a quantum front, i.e., the point where the density vanishes in the classical limit, propagating to the right. We look for the position $x_{\rm edge}(t)$ of the propagating quantum front, which is given by $x_{\rm edge}(t) = \max_p x(p,t)$. This obeys the equation $\partial_p x(p(t),t) = 0$, defining the corresponding point $p(t)$ and $x(t) = x_e(p(t))$, which is the projection of the quantum front on the Fermi surface of the initial Wigner function

$$x_e'(p(t)) + t = 0, \tag{3.30}$$

$$p_e'(x(t)) + \frac{1}{t} = 0. \tag{3.31}$$

Because the front is moving to the right, $x_{\rm edge}(t)$ is a monotonous function of t, hence by construction $x(t)$ and $p(t)$ are also monotonous, they have the following large time

limit (see Fig. 3.4)

$$\begin{aligned}\lim_{t\to\infty} x_{\rm edge}(t) &= +\infty,\\ \lim_{t\to\infty} x(t) &= -\infty,\\ \lim_{t\to\infty} p(t) &= p_F,\end{aligned} \tag{3.32}$$

and the three of them are linked by the relation

$$x_{\rm edge}(t) = x(t) + tp(t). \tag{3.33}$$

Their large time asymptotics are

$$\begin{aligned}p(t) &\underset{t\to\infty}{\simeq} p_L - \frac{1}{(\gamma t)^{\frac{\gamma}{\gamma+1}}}(\frac{c}{p_L})^{\frac{1}{\gamma+1}}\\ x(t) &\underset{t\to\infty}{\simeq} -(\frac{\gamma c t}{p_L})^{\frac{1}{1+\gamma}}\end{aligned} \tag{3.34}$$

The Liouville dynamics gives the time dependent kernel at time t as a functional of the initial Wigner function

$$\begin{aligned}K(x,x',t) &= \int dp e^{-i\frac{p}{\hbar}(x-x')} W(\frac{x+x'}{2},p,t)\\ &= \int dp e^{-i\frac{p}{\hbar}(x-x')} W_0(\frac{x+x'}{2}-pt,p)\end{aligned} \tag{3.35}$$

As illustrated in Fig. 3.4, the integral (3.35) giving the kernel at the quantum front $x_{edge}(t)$ is performed over a line parallel to the Fermi surf at the quantum front of the Wigner function at time t. In the second line of (3.35), the integral is now performed on a line parallel to the line tangent to the Fermi surf of the initial Wigner function at the point $(x(t),p(t))$. Thus, using the Airy scaling (3.5) demonstrated in the first section to be valid for the inverse power law potential under the condition (3.26), it is possible to show that along the quantum front, the kernel can be expressed in term of Airy as

$$\boxed{\begin{aligned}K(x,x',t) \simeq -\frac{1}{w(t)} e^{-\frac{i}{\hbar}(p(t)(x-x')+\frac{(x-x_{\rm edge}(t))^2}{2t}-\frac{(x'-x_{\rm edge}(t))^2}{2t})}\\ \times K_{Ai}(\frac{x-x_{\rm edge}(t)}{w(t)},\frac{x'-x_{\rm edge}(t)}{w(t)}),\\ w(t) = t(\frac{\hbar^2|p_e''(x(t))|}{2})^{1/3} = (\hbar^2\frac{\gamma+1}{2}(\frac{p_L}{\gamma c})^{1/(\gamma+1)})^{1/3} t^{\frac{2\gamma+1}{3(\gamma+1)}}.\end{aligned}} \tag{3.36}$$

- Notice that the phase in front of the kernel is not relevant for a determinantal process (1.46) as $\det|e^{f(x_i)-f(x_j)}K(x_i,x_j)]_{i,j} = \det|K(x_i,x_j)|_{i,j}$. However in the case of non-equilibrium dynamics of fermions, observables like the current are affected. Indeed, we recal that the current is a functional of the kernel as

$$J\left[K(x,y,t)\right](x,t) = \frac{1}{2i}(\partial_y - \partial_x)K(x,y,t)|_{x=y}. \tag{3.37}$$

This implies that the phase modify the current as

$$J\left[e^{f(x)-f(y)}K(x,y,t)\right](x,t) = J\left[K(x,y,t)\right](x,t) + if'(x)\rho(x,t), \tag{3.38}$$

where $\rho(x,t) = K(x,x,t)$. In our specific case, because the Airy kernel alone produce no current this yields

$$J(x,t) = \left(p(t) + \frac{x - x_{edge}(t)}{t}\right)\rho_{Ai}\left(\frac{x - x_{\text{edge}}(t)}{w(t)}\right) \tag{3.39}$$

where we used the notation $\rho_{Ai}(x) = K_{Ai}(x,x)$. Notice that the first term can be interpreted as a consequence of the motion of the quantum front with velocity $p(t)$.

- Here, the Airy kernel at the quantum front is already present at initial time. This does not have to be the case, for example if the initial potential behaves like the power law potential for large x but has a derivative that cancels precisely at the edge of the gas ($V'(x_{edge}) = 0$). Then, the Wigner function at initial time exhibits the Airy scaling (3.5) only far away from edge of the gas, such that we expect the Airy kernel to appear only in the large time limit.

- In [187], a small $\hbar$ analysis of the Wigner function propagation within a potential is done. The conclusion is that if present at initial time, the Airy scaling (3.5) would persist at short time (up to some rescaling of the width e_N).

- The Airy kernel (3.36) is valid only if the initial time Wigner function exhibits the Airy scaling at position $x(t)$, that is if $x(t)$ verifies the condition (3.26) from the first section.

- This quench set up appears as possible experimental protocol to probe the edge of the ground state Wigner function for x_e away from the edge of the gas, within potentials with power law decay at infinity like the inverse power law potential.

Conclusion and Perspectives

In this thesis, we have aimed to highlight the utilization of noninteracting fermions as an exactly solvable model, allowing for the exploration of nontrivial many-body statistics both in-equilibrium and out-of-equilibrium scenarios. On the side of equilibrium statistics, we discussed how the mathematical tool box of Random Matrix Theory could be used to obtain the hole probability in ground state and in any dimensions. Remarkably, this investigation revealed an intriguing connection (1.140) between Fredholm determinants of kernels that were initially unrelated. A natural research direction would be to extend our results to the Full Counting Statistics and the finite temperature properties. This would eventually lead to a generalisation of the aforementioned connection between Fredholm determinants.

On the side of out-of-equilibrium statistics, we have explored various quench protocols. We investigated the ground state statistics of a noninteracting fermionic gas in a slowly decaying potential (such as the inverse power law potential). We paid particular attention to the edge of the Wigner function, which led in large time to the emergence of the Airy kernel at the edges of propagating front for fermions in the continuum. It would be interesting to investigate whether these phenomena can be observed in the context of cold atoms experiments.

Additionally, we have conducted a detailed study on the dynamics of noninteracting fermions in the presence of a defect, which refers to a potential that varies on a microscopic scale. Depending on the time scales involved, we have observed relaxation to either a Non Equilibrium Steady State or a Generalized Gibbs Ensemble. In our investigations, we have obtained space-time multi-point correlations and have observed power-law relaxation towards the Non Equilibrium Steady State. Furthermore, we have compared our findings with Conformal Field Theory. In the presence of bound states of the defect, we have characterized persistent oscillations at large timescales. Interestingly, we have also uncovered non-local correlations between distant points located symmetrically across the defect. These correlations fall beyond the scope of the current Generalized Hydrodynamics (GHD) theory in the presence of a defect. Therefore, we have proposed a potential extension or an alternative Euler scaling limit to describe the propagation of these correlations. In this extension, the gas is described by the usual root density from GHD along with an additional field. These two objects are coupled only in the vicinity of the defect, while they propagate freely elsewhere. This raises several intriguing questions. On the theoretical front, it is not clear how to prove the evolution of the two fields. It can also be asked, how does the additional field behave in the presence of multiple far away defects. Additionally, one may wonder how this generalization applies to interacting integrable gas. Indeed, while it is expected that the root density will evolve according to the GHD equations away from the defect, the behavior of the additional field remains uncertain. Similar questions arise regarding the interpretation of this field in terms of the so-called "quasi-particle". Finally, the alternative Euler scaling limit can be used to investigate correlations between particles that spread out from the defect with different momenta, rather than just opposing momenta. This could potentially prove useful for studying defects that are more sophisticated than those considered in this thesis.

Appendix A

A trick for Sum with Poles on a Lattice.

The goal of this appendix is to explain clearly and in a full general form the trick used to prove the relaxation to the NESS in Sections 2.4.3 and 2.6.3.

Typically, we will want to compute the thermodynamic limit followed by the large time limit of sums defined as (for example $D(x,x',t)$ in (2.146))

$$S_k = \sum_{k'\in\Lambda'} \frac{1}{\ell}\frac{F(k,k')}{k-k'} e^{-i\frac{k'^2}{2}t}, \tag{A.1}$$

where $F(k,k')$ is a continuous function. The sum is performed over the lattice Λ' defined by

$$\Lambda' = \{k' \in \mathbb{R} | e^{2ik'(\frac{\ell}{2}-\delta'_{k'})} + 1 = 0, k' > 0\}, \tag{A.2}$$

with $k'\delta'_{k'}$ typically a continuous function of k'. Similarly, k belongs to a lattice Λ defined as

$$\Lambda = \{k \in \mathbb{R} | e^{2ik(\frac{\ell}{2}-\delta_k)} + 1 = 0, k' > 0\}. \tag{A.3}$$

δ and δ' are two different functions such that, both lattices have no common elements, ensuring that there is no division by zero. The role of the function $k\delta_k$ and $k'\delta'_{k'}$ will latter be related to the transmission and reflection coefficient of the scattering potential. Latter we might be interested in double or triple sums running over both lattices Λ and Λ' such as

$$\sum_{k\in\Lambda, k'\in\Lambda'} \frac{1}{\ell^2}\frac{F(k,k')}{k-k'} e^{-i\frac{k'^2-k^2}{2}t}, \tag{A.4}$$

But most of the main ingredient can be understood by examining only the original sum (A.1), the main point is that it contains a pole such that, one cannot replace (in the limit $\ell \to \infty$) the discrete sum over $k' \in \Lambda'$ by an integral. Instead we introduce a contour integral method which is a generalisation of the one used in [143] which allows us to take this limit. To be precise, the method used in [143] would allow to compute the sum (A.4) only if at least one of the two lattices Λ and Λ' was the periodic lattice $\{\frac{2\pi n}{\ell}, \quad n \in \mathbb{N}^*\}$.

Now we will write the sum over k' as a contour integral in the complex plane for k'. With this goal in mind we introduce the function

$$g_{\delta',\ell}(k') = \frac{-1}{e^{-ik'(\ell-2\delta'_{k'})}+1}, \tag{A.5}$$

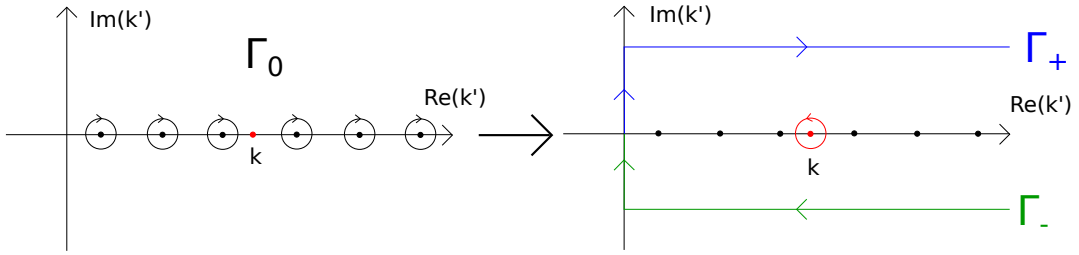

FIGURE A.1: Illustration of the contour Γ_0 in the complex k' plane, and its deformation into the union of three different contours, i.e., Γ_+, Γ_- and the small counter-clockwise red circle around $k' = k$.

The Eq. (A.2) implies that $g_{\delta',\ell}(k')$ has poles on each element k' of the lattice Λ' with residue

$$-\frac{1}{\partial_{k'} e^{-ik'(\ell-2\delta'_{k'})}} = \frac{1}{(i\ell - 2\partial_{k'}(k'\delta'_{k'}))e^{-ik'(\ell-2\delta'_{k'})}} = -\frac{1}{i\ell - 2i\partial_{k'}(k'\delta'_{k'})} = -\frac{1}{i\ell}(1+O(1/\ell)), \tag{A.6}$$

This allow us to write the discrete sum in the expression (A.1) as an integral over a contour Γ_0 equal to the union of small clockwise circular contours around each element of Λ' as shown in Fig. A.1

$$\frac{1}{\ell}\sum_{k'\in\Lambda'} \cdots = \int_{\Gamma_0} \frac{dk'}{2\pi} g_{\delta',\ell}(k') \ldots \tag{A.7}$$

leading to

$$S_k = \int_{\Gamma_0} \frac{dk'}{2\pi} g_{\delta',\ell}(k') \frac{F(k,k')}{k-k'} e^{-i\frac{k'^2}{2}t}. \tag{A.8}$$

Assuming that the integrand has a singularity only at $k' = k$ (within a strip around the positive real axis) we can now deform this contour into the union of a larger contour $\Gamma = \Gamma_- \cup \Gamma_+$ (see Fig. A.1)that encloses all the previous ones, and of a tiny contour around k. Computing the residue associated to this pole at $k' = k$ we obtain

$$S_k \quad = -ig_{\delta^\pm,\ell}(k)F(k,k)e^{-i\frac{k^2}{2}t} + \textstyle\int_{\Gamma_-\cup\Gamma_+} \frac{dk'}{2\pi} g_{\delta',\ell}(k') \frac{F(k,k')}{k-k'} e^{-i\frac{k'^2}{2}t}. \tag{A.9}$$

Using the quantification condition for $k \in \Lambda$ from Eq. (A.3) we can eliminate ℓ and obtain

$$-2ig_{\delta',\ell}(k) = \frac{e^{ik(\delta_k - \delta'_k)}}{\sin(k(\delta_k - \delta'_k))} = (\cot(k(\delta_k - \delta'_k)) + i), \tag{A.10}$$

such that

$$S_k = \frac{e^{ik(\delta_k-\delta'_k)}}{\sin(k(\delta_k-\delta'_k))}\frac{F(k,k)}{2}e^{-i\frac{k^2}{2}t} + \int_{\Gamma_-\cup\Gamma_+} \frac{dk'}{2\pi} g_{\delta',\ell}(k') \frac{F(k,k')}{k-k'} e^{-i\frac{k'^2}{2}t}. \tag{A.11}$$

Under this form, we can now take the large $\ell \to +\infty$ limit. The limiting value of the function $g_{\delta^\pm,\ell}(k')$ for $k' \in \Gamma_- \cup \Gamma_+$ is (for $\mathrm{Im}(k') \neq 0$)

$$g_{\delta',\ell}(k') \underset{\ell\to\infty}{\to} \begin{cases} 0 \text{ if } k' \in \Gamma_+ \\ -1 \text{ if } k' \in \Gamma_- \end{cases}. \tag{A.12}$$

As a consequence, we are left with the residue part and the Γ_- integral part only

$$\lim_{\ell\to\infty} S_k = \frac{e^{ik(\delta_k^{R/L}-\delta_k^{\pm})}}{\sin(k(\delta_k-\delta'_k))}\frac{F(k,k)}{2}e^{-i\frac{k^2}{2}t} - \int_{\Gamma_-}\frac{dk'}{2\pi}\frac{F(k,k')}{k-k'}e^{-i\frac{k'^2}{2}t}, \tag{A.13}$$

while the Γ_+ integral part gives information on the finite size corrections (see Fig. A.1). Now we want to take the large time limit. The idea is that only the residue part will remain at large time, while the Γ_- integral gives information about finite time corrections. Indeed if we write $k' = k'_1 + ik'_2$, with $k'_2 \leq 0$ on Γ_-, then

$$e^{-i\frac{k'^2}{2}t} = e^{-i\frac{k'^2_1-k'_2}{2}t}e^{k'_1k'_2t} \underset{t\to\infty}{\to} 0. \tag{A.14}$$

Here we would like to conclude that the integral in (A.13) decays to zero in the large time limit $\lim_{t\to\infty}$ because the integrand of this same integral does decay to zero (A.14) on the contour Γ_-. However, we stress that this is not a sufficient information to conclude to the decay of the integral in (A.13). In fact when we will compute exactly double or triple sum like (A.4), the contour integral in (A.11) will turn in double or triple integral with singularities. Then, one needs to to carefully checke the decay of the integrals to zero using dominated convergence theorem. Note that the decay is dominated by the vertical part of Γ_+ and Γ_-, in the vicinity of $k = 0$. As a conclusion, in the double limit $\lim_{t\to\infty}\lim_{\ell\to\infty}$ only the residue part of (A.13) remains, while the integral part of (A.13) encodes the large time decay.

Appendix B

Convergence of B and D to the NESS

Here we present the exact decay of the kernel (2.104) to the NESS kernel (2.120) in the double limit $\ell \to \infty$, $t \to \infty$ starting from a quench with a delta Dirac impurity. Although most of the details presented here was present in the supplementary materials of our paper [2], we give here some slight modifications that allows for a better understanding of the existence of a limit for the kernel large time t.

The term $D(x, x', t)$: From (2.143) the term D is given by a double sum

$$D = D(x, x', t) = \frac{4}{\ell^2} \sum_{k_b \in \Lambda_+} \sum_{k \in \Lambda_-, k = k_L^+}^{k_R} \frac{h_{x,x',t}(k, k_b)}{k - k_b}, \tag{B.1}$$

with $k_L = 2\pi N_L/\ell$, $k_L^+ = 2\pi(N_L + 1)/\ell$ and $k_R = 2\pi N_R/\ell$ and we recall that the lattices Λ_- and Λ_+ are defined in Eqs. (2.132) and (2.135) respectively. We have also defined the function [1]

$$h_{x,x',t}(k, k_b) = \frac{\phi^\infty_{-,k}(x')\phi^\infty_{+,k_b}(x)}{\sqrt{g^2 + k_b^2}} \frac{k k_b}{k + k_b} e^{-\frac{i}{2}(k^2 - k_b^2)t}\ , \tag{B.2}$$

where $\phi^\infty_{\pm,k}(x)$ is defined in (2.121). Taking the limit $\ell \to \infty$ of (B.1) to obtain a double integral is very delicate due to the presence in the sum of a pole $\frac{1}{k-k_b}$ and the fact that the two lattices Λ_- and Λ_+ are intertwined (see Fig. 2.9). Let us first state the result and give its derivation below. One finds

$$\begin{aligned} \lim_{\ell \to \infty} D(x, x', t) = &\int_0^{+\infty} \frac{dk_b}{\pi} \left[\int_{\gamma_c} \frac{dk}{\pi} \frac{h_{x,x',t}(k, k_b)}{k - k_b} \right] \\ &+ \int_{k_L}^{k_R} \frac{dk_b}{\pi} \left(-i + \frac{g}{k_b} \right) h_{x,x',t}(k_b, k_b)\ . \end{aligned} \tag{B.3}$$

The first line of (B.3) is an integral over a contour that we denote γ_c consisting in straight lines in the complex k-plane, forming a half-rectangle as represented in Fig. B.1. Its value does not depend on the parameter $\epsilon > 0$ since $h_{x,x',t}(k, k_b)$ as a function of k does not have poles in the strip $[k_L, k_R] - i\mathbb{R}^+$. In addition to the derivation given below we have carefully checked numerically this formula (B.3) for a variety of function h which share the same properties.

[1] Since we are eventually interested in the large ℓ limit we omitted in (B.2) the unimportant extra factor $2g/\ell$ in the denominator in (2.143), which should be restored to obtain finite ℓ formula.

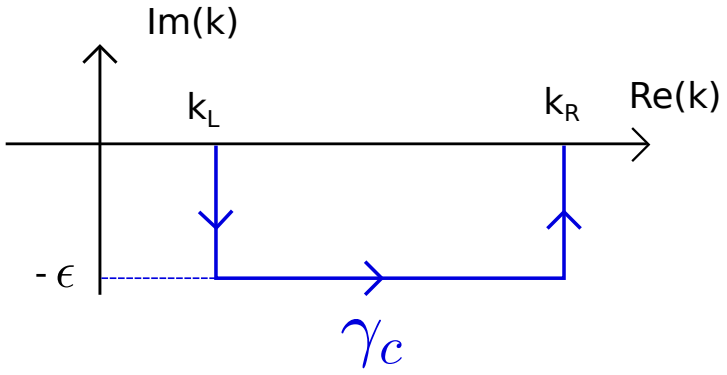

FIGURE B.1: Illustration of the contour γ_c over which the integral over k in the first line of (B.3) is performed.

Let us now give the derivation of this result in Eq. (B.3). This is done using the method introduced above (A), which reduces here to a simpler case. First, we notice that $\Lambda_- = \Lambda'$ through (A.2) if we set $e^{-2ik\delta'_k} = e^{-2ik\delta^-_k} = -1$, this does define the periodic lattice Λ_-. Similarly, Λ_+ can be defined as Λ through (A.3) by setting $e^{-2ik\delta_k} = e^{-2ik\delta^+_k} = \frac{k-ig}{k+ig}$, yielding a non periodic lattice Λ_+. Because the lattice $\Lambda' = \Lambda_-$ is periodic, the function $g_{\delta^-,\ell}(k')$ of (A.5) has the simple expression

$$g_{\delta^-,\ell}(k') = \frac{1}{e^{-ik'\ell} - 1}. \tag{B.4}$$

Now we can replace the discrete sum over k in (B.1) by a contour integral as follows

$$D(x,x',t) = \frac{4}{\ell^2} \sum_{k_b \in \Lambda_+} \int_{\Gamma_0} \frac{dk}{2\pi} \frac{\ell}{e^{i\ell k} - 1} \frac{h_{x,x',t}(k,k_b)}{k - k_b}\ , \tag{B.5}$$

where the contour Γ_0 is a union of very small circles centered around the points $k = \frac{2\pi n}{\ell}$ with $N_L + 1 \leq n \leq N_R$ and oriented clockwise (see Fig. 2.10). The circles should be small enough so that the contour does not enclose any point $k = k_b \in \Lambda_+$. We now deform the contour Γ_0 into the closed clockwise contour γ_δ which is the rectangle with the four corners $k_L^+ - \frac{2\pi\delta}{\ell} - i\epsilon$, $k_L^+ - \frac{2\pi\delta}{\ell} + i\epsilon$, $k_R + \frac{2\pi\delta}{\ell} + i\epsilon$, $k_R + \frac{2\pi\delta}{\ell} - i\epsilon$, represented in Fig. 2.10. The parameter $0 < \delta < 1$ is chosen small enough so that the contour does not contain any point k_b of Λ_+ located to the left of k_L^+ and to the right of k_R. During this deformation one encounters only the poles at $k = k_b \in \Lambda_+ \cap]k_L^+, k_R[$. Taking into account the residues associated to these poles one obtains

$$\begin{aligned} D(x,x',t) = \frac{4}{\ell^2} \Bigg(& \sum_{k_b \in \Lambda_+} \oint_{\gamma_\delta} \frac{dk}{2\pi} \frac{\ell}{e^{-i\ell k} - 1} \frac{h_{x,x',t}(k,k_b)}{k - k_b} \\ & + 2\pi i \sum_{k_b \in \Lambda_+ \cap]k_L^+, k_R[} \frac{\ell}{2\pi} \frac{1}{e^{-i\ell k_b} - 1} h_{x,x',t}(k_b,k_b) \Bigg)\ . \end{aligned} \tag{B.6}$$

Until now this is an exact rewriting of $D(x,x',t)$ in Eq. (B.1) valid for any ℓ. For any $k_b \in \Lambda_+$, using the second relation in (2.134), or equivalently using the result

(A.10), one can evaluate the factor

$$\frac{1}{e^{-i\ell k_b}-1} = -\frac{1}{2} - \frac{i}{2}\frac{g}{k_b} \,. \tag{B.7}$$

We now take the large ℓ limit on Eq. (B.6). The factor $\frac{1}{e^{-i\ell k}-1} \to 0$ for $\mathrm{Im}\, k > 0$ and $\frac{1}{e^{i\ell k}-1} \to -1$ for $\mathrm{Im}\, k < 0$. Hence the k integral in (B.6) over the clockwise closed contour γ_δ becomes the k integral over the clockwise half-rectangle in (B.3). In addition the sum over k_b becomes an integral in the large ℓ limit. This leads to the result (B.3).

The term $B(x,x',t)$: We now give the large ℓ limit of $B_L(x,x')$ and $B_R(x,x')$ defined in (2.143). Each term can be decomposed as the sum of two terms

$$B_{R/L}(x,x',t) = B^{\text{off-diag}}_{R/L}(x,x',t) + B^{\text{diag}}_{R/L}(x,x') \tag{B.8}$$

where the first term comes from the terms $k_a \neq k_b$ in the triple sum in (2.143), while the second one comes from the terms $k_a = k_b$ and does not depend on time. We obtain the first term in (B.8) as

$$\begin{aligned} B^{\text{off-diag}}_{R}(x,x',t) &= \int_0^\infty \int_0^\infty \frac{dk_a}{\pi}\frac{dk_b}{\pi} F_{x,x'}(k_a,k_b) e^{\frac{1}{2}i(k_a^2-k_b^2)t} \\ &\times \left[\frac{1}{2\pi}\left(\frac{k_b \log(\frac{k_b+k_R}{|k_b-k_R|}) - k_a \log(\frac{k_a+k_R}{|k_a-k_R|})}{k_a^2-k_b^2}) + \frac{g}{2(k_a^2-k_b^2)}\left(\Theta(k_R-k_a)-\Theta(k_R-k_b)\right)\right)\right] , \end{aligned} \tag{B.9}$$

where we have defined the function

$$F_{x,x'}(k_a,k_b) = 2\frac{\phi^\infty_{+,k_a}(x)}{\sqrt{g^2+k_a^2}}\frac{\phi^\infty_{+,k_b}(x')}{\sqrt{g^2+k_b^2}} k_a k_b \tag{B.10}$$

where the $\phi^\infty_{+,k}(x)$ are defined in (2.121). The second term in (B.8) is obtained in the large ℓ limit as

$$B^{\text{diag}}_{R}(x,x') = \int_0^{k_R} \frac{dk_a}{2\pi} F_{x,x'}(k_a,k_a)\frac{(g^2+k_a^2)}{2k_a^2} \,. \tag{B.11}$$

The terms $B^{\text{off-diag}}_{L}(x,x',t)$ and $B^{\text{diag}}_{L}(x,x')$ are simply obtained from $B^{\text{off-diag}}_{R}(x,x',t)$ and $B^{\text{diag}}_{R}(x,x')$ by substituting $k_R \to k_L$ in Eqs. (B.9) and (B.12) leading for the diagonal part to

$$B^{\text{diag}}_{R/L}(x,x') = \int_0^{k_{R/L}} \frac{dk}{2\pi}\phi^\infty_{+,k}(x)\phi^\infty_{+,k}(x') \,. \tag{B.12}$$

Let us gives a summary of the proof of Eqs. (B.9), and (B.12). This can be achieved in two ways that are useful for different reasons.

1. First, $B_{R/L}(x,x',t)$ in (2.143) is split into a diagonal $B^{\text{diag}}_{R/L}(x,x')$ and an off-diagonal $B^{\text{off-diag}}_{R/L}(x,x',t)$ part. For the off-diagonal part, one uses the method A on the sum $\sum_{k\in\Lambda_-, k\leq k_{R/L}}$ that has two single poles, one at $k=k_a$ and one at $k=k_b$, this yields (B.9). For the diagonal part, since $k_a = k_b$, we now have

a pole of order two at $k = k_a = k_b$, requiring a generalization of the method. This yields an integral part that decays in the thermodynamic limit, along with a residue part which is (B.12).

2. Starting from $B_{R/L}(x, x', t)$ in (2.143), instead of using the method (A) on the sum $\sum_{k\in\Lambda_-, k\leq k_{R/L}}$, one could apply this method twice, first to the sum $\sum_{k_a\in\Lambda_+}$, and then to the sum $\sum_{k_b\in\Lambda_+}$. This would result in the sum of four terms. One term is time independent and is equals $B^{\text{diag}}_{R/L}(x, x', t)$. This means that the three other terms yields a new expression of $B^{\text{off-diag}}_{R/L}(x, x')$. The difference is that they all contain at least one integral in the complex plane together with exponential factors decaying in the large time limit (Note that in (B.9) the exponential factors oscillate without decay). It is worth noting that this approach yields the desired result without requiring any generalization of an order two pole of the method from Appendix A.

Large Time Limit: Stationary state at fixed position x. In the previous section we have obtained the expression of the kernel in the thermodynamic limit $\lim_{\ell\to+\infty} K(x, x', t)$ in (2.144) together with (B.8), as a sum of several terms. Now we can take the limit $t \to +\infty$ of each term in this expression for fixed positions x and x' to obtain

$$K_\infty(x, x') = \lim_{t\to+\infty} \lim_{\ell\to+\infty} K(x, x', t) \, . \tag{B.13}$$

- In (2.144) and (B.8) the terms $A_{R/L}(x, x')$ and $B^{\text{diag}}_{R/L}(x, x')$ are independent of time.
- The term $D(x, x', t)$ goes to a finite limit $D_\infty(x, x')$ where only the last term in (B.3) (coming from the residues) survives at large time. Indeed, as already mentioned, the first integral of Eq. (B.3) contains a term $e^{-i\frac{k^2}{2}t}$. As $k \in \gamma_c$, one can write $k = k_1 + ik_2$ with $k_1 > 0$ and $k_2 < 0$, which yields $e^{-i\frac{k^2}{2}t} = e^{-i\frac{k_1^2-k_2^2}{2}t} e^{k_1 k_2 t}$, and thus the integrand decays in large time. Using this fact, together with the dominated convergence theorem, it can be shown that the integral decays to zero in the large time limit. The decay is found to follow a power law with oscillations, which is discussed in Section 2.4.5. From the last term in (B.3) we obtain

$$D_\infty(x, x') = \frac{1}{2}\int_{k_L}^{k_R} \frac{dk}{\pi}(g - ik)\frac{\phi^\infty_{-,k}(x')\phi^\infty_{+,k}(x)}{\sqrt{g^2 + k^2}} \, . \tag{B.14}$$

- Finally, it is possible to show that $B^{\text{off}-\text{diag}}_{R/L}(x, x', t)$ decays to zero. This is hard to see on the expression (B.9) obtained from (1), although one could guess that the oscillations coming from the exponential factors are the cause of the decay. A proper proof is obtained in a similar fashion to the decay of $D(x, x', t)$ using the decaying exponential factors obtained from the second path (2). However, the expression (B.9) obtained from the first path (1) is more convenient when it comes to showing that the decay of $B^{\text{off}-\text{diag}}_{R/L}(x, x', t)$ follows a power law (see Section 2.4.5).

Putting all terms together we find the result for $K_\infty(x, x')$ given in Eq. (2.120).

Appendix C

Some examples of impurity potentials and their scattering coefficients

Here we just list few examples of potentials for which the scattering coefficients are known

The delta barrier. In the case $V(x) = g\delta(x)$ one has

$$\mathsf{t}(k) = \frac{k}{k+ig} \quad , \quad \mathsf{r}(k) = \frac{-ig}{k+ig} \tag{C.1}$$

The double delta barrier. In the case $V(x) = g(\delta(x-\frac{a}{2})+\delta(x+\frac{a}{2}))$ [**doubledelta**] one has

$$\mathsf{t}(k) = \frac{k^2}{g^2(e^{2ika}-1)+k^2+2ikg} \quad , \quad \mathsf{r}(k) = -ig\frac{e^{ika}(k-ig)+e^{-ika}(k+ig)}{g^2(e^{2ika}-1)+k^2+2ikg} \tag{C.2}$$

Note that $\mathsf{r}(0) = -1$ unless $ag = -1$ in which case $\mathsf{r}(0) = 0$, and $\mathsf{t}(0) = -1$.

The square barrier potential. In the case $V(x) = V_0\theta(|x| < a/2)$, i.e., a square barrier of length a and height V_0 (which can be negative if the potential is an attractive well) with $k_1 = \sqrt{k^2 - 2V_0)}$, one has [195]

$$\mathsf{t}(k) = \frac{e^{-iak}}{\cos(k_1a)-i\frac{k_1^2+k^2}{2kk_1}\sin(k_1a)}, \qquad \mathsf{r}(k) = \frac{ie^{-ika}(k_1^2-k^2)\sin(ak_1)}{2kk_1\cos(ak_1)-i(k^2+k_1^2)\sin(ak_1)} \tag{C.3}$$

Note that $\mathsf{r}(0) = -1$ unless $\sin(ak_1) = 0$.

The delta derivative barrier. From [208] for the more general potential with no symmetry, $V(x) = g_1\delta(x) + g_2\delta'(x)$, one has

$$\mathsf{t}(k) = \frac{1-g_2^2}{1+g_2^2+i\frac{g_1}{k}}, \quad \mathsf{r}^R(k) = \frac{g_2-i\frac{g_1}{k}}{1+g_2^2+i\frac{g_1}{k}} \quad , \quad \mathsf{r}^L(k) = \frac{-g_2-i\frac{g_1}{k}}{1+g_2^2+i\frac{g_1}{k}} \tag{C.4}$$

If $g_1 = 0$, this is an example of a defect such that the scattering coefficients are independent on k. Defects with that property have been studied in the context of

conformal defects. Additionally we have $\mathsf{r}(0) \neq -1$.

Impurities in series. It is useful to consider the transfer matrix $\mathcal{M}$, which reads

$$\begin{pmatrix} C \\ D \end{pmatrix} = \mathcal{M} \begin{pmatrix} A \\ B \end{pmatrix} \quad , \quad \mathcal{M} = \begin{pmatrix} t_L - \frac{r_L r_R}{t_R} & \frac{r_R}{t_R} \\ -\frac{r_L}{t_R} & \frac{1}{t_R} \end{pmatrix} \tag{C.5}$$

Consider now two distinct symmetric impurities, the first one at $x = 0$, the second at $x = a$. The total transfer matrix is

$$\mathcal{M} = \begin{pmatrix} t_2 - \frac{r_2^2}{t_2} & \frac{r_2}{t_2} \\ -\frac{r_2}{t_2} & \frac{1}{t_2} \end{pmatrix} \begin{pmatrix} e^{ika} & 0 \\ 0 & e^{-ika} \end{pmatrix} \begin{pmatrix} t_1 - \frac{r_1^2}{t_1} & \frac{r_1}{t_1} \\ -\frac{r_1}{t_1} & \frac{1}{t_1} \end{pmatrix} \tag{C.6}$$

which leads to the scattering coefficients of the combined system

$$t_R = t_L = \frac{t_1 t_2 e^{iak}}{1 - r_1 r_2 e^{2iak}}, \quad r_R = \frac{r_2 - r_1 e^{2iak}\left(r_2^2 - t_2^2\right)}{1 - r_1 r_2 e^{2iak}}, \quad r_L = \frac{r_1 - r_2 e^{2iak}\left(r_1^2 - t_1^2\right)}{1 - r_1 r_2 e^{2iak}} \tag{C.7}$$

The most general case is

$$\begin{gathered} t_R = \frac{e^{iak} t_{\mathrm{R}1} t_{\mathrm{R}2}}{1 - e^{2iak} r_{\mathrm{L}2} r_{\mathrm{R}1}} \quad , \quad r_R = r_{\mathrm{R}2} + \frac{e^{2iak} t_{\mathrm{L}2} r_{\mathrm{R}1} t_{\mathrm{R}2}}{1 - e^{2iak} r_{\mathrm{L}2} r_{\mathrm{R}1}} \quad , \\ r_L = r_{\mathrm{L}1} + \frac{e^{2iak} t_{\mathrm{L}1} r_{\mathrm{L}2} t_{\mathrm{R}1}}{1 - e^{2iak} r_{\mathrm{L}2} r_{\mathrm{R}1}} \quad , \quad t_L = \frac{e^{iak} t_{\mathrm{L}1} t_{\mathrm{L}2}}{1 - e^{2iak} r_{\mathrm{L}2} r_{\mathrm{R}1}} \end{gathered} \tag{C.8}$$

Hence if $t_{\mathrm{R}1} = t_{\mathrm{L}1}$ and $t_{\mathrm{R}2} = t_{\mathrm{L}2}$ from time invariance, one has also $t_R = t_L$ as expected.

Remark. If one translates both impurities by δ the scattering matrix is multiplied by $e^{2ik\delta}$. This allows to check the case of two delta impurities given above.

Appendix D

Short time propagator expansion

Here we give some details on the short time propagator expansion presented in the appendix of [199]. We carefully restore the $\hbar$ factors in order to perform the small $\hbar$ analysis.

General smooth potential. We consider the Wigner function written as (3.15) at a point near the Fermi surf $(x,p) \simeq (x_e, p_e)$. The small time expansion of Eq. (3.15) is valid if the arguments of V in Eq. (3.13) are small compared to $x \simeq x_e$. In other words, we require that the following conditions hold:

$$\begin{cases} \frac{p_e t}{m x_e} \ll 1, \\ \frac{\hbar t}{m x_e^2} \ll 1. \end{cases} \tag{D.1}$$

Considering the Brownian bridge, the expansion to order 3 results in

$$\begin{aligned} S(x,p) \simeq & -\frac{t^2}{m}(\frac{1}{24}+\frac{1}{12})V''(x_e) + \frac{t^3}{24m\hbar}(V'(x_e))^2 \\ & -\frac{t^3}{m^2}[-\frac{1}{24\hbar}p_e^2 V''(x_e) + \hbar(\frac{1}{640}+\frac{1}{480}+\frac{1}{240})V''''(x_e)] + O(t^4). \end{aligned} \tag{D.2}$$

because we want to recover the Airy function, we want the second order to be negligible. Let us assume that, in the end, the only remaining term is

$$S(x,p) \simeq \frac{t^3}{24m\hbar}(\frac{p_e^2}{m}V''(x_e) + V'(x_e)^2). \tag{D.3}$$

Then we can make the change of variable $t = 2^{2/3}\hbar\tau/e_N$ in the integral (3.15), with

$$e_N = \hbar/t_N = \frac{\hbar^{2/3}}{(2m)^{1/3}}(\frac{p_e^2}{m}V''(x_e) + V'(x_e)^2)^{1/3}, \tag{D.4}$$

and the Airy scaling emerges (see Eq. (3.17)). If we assume that the integral is dominated by $t \sim t_N$, we obtain the condition for neglecting the discarded terms in (D.2) as

$$\frac{t^2}{m}V''(x_e) \simeq \frac{t_N^2 V(x_e)}{m x_e^2} \ll 1, \tag{D.5}$$

$$\hbar V''''(x_e) \ll \frac{1}{\hbar}p_e^2 V''(x_e) + \frac{m}{\hbar}V'(x_e)^2 \simeq t_N^{-3}. \tag{D.6}$$

Hence, the Airy sclaing is valid if the conditions (D.1) and (D.5) are satisfied.

Conditions for the inverse power law potential. Now we apply the short time expansion to the special case of the inverse power law potential. This is done by checking in which regime (D.1) and (D.5) are satisfied.

For the part of the Fermi surf near the edge of the gas (see Fig. 3.3) we parametrize the Fermi surf as

$$x_e = \overline{x} x_{edge} \tag{D.7}$$

$$p_e = \sqrt{2\mu(1-\overline{x}^{-\gamma})}, \tag{D.8}$$

where we recall that $x_{edge} = (\frac{c}{\mu})^{1/\gamma}$. With this scaling, the conditions (D.1), and (D.5) lead to

$$\begin{aligned}
&\frac{p_e t_N}{x_e} \simeq (\sqrt{\omega}\overline{x}^{\gamma-1})^{1/3} \ll 1, \\
&\frac{\hbar t_N}{x_e^2} \simeq (\omega^2 \overline{x}^{\gamma-4})^{1/3} \ll 1, \\
&t_N^2 V''(x_e) \simeq \left(\frac{\omega}{\overline{x}^{\gamma+2}}\right)^{1/3} \ll 1, \\
&\hbar V''''(x_e) t_N^3 \simeq \frac{\omega}{\overline{x}^2} \ll 1,
\end{aligned} \tag{D.9}$$

where $\omega = \frac{\hbar^2}{\mu^{\frac{2-\gamma}{\gamma}} c^{\frac{2}{\gamma}}}$ such that near the gas edge (that is $\overline{x}$ of order one), the expansion of Eq. (3.15) and hence the Airy scaling is valid if the single condition

$$\omega = \frac{\hbar^2}{\mu^{\frac{2-\gamma}{\gamma}} c^{\frac{2}{\gamma}}} \ll 1 \tag{D.10}$$

is satisfied, which yields (3.24). The main commentary to do here is that we need either $\hbar$ to be small or, if $\gamma > 2$, we need μ to be large.

Now, we examine the part of the Fermi surf, away from the edge of the gas (see Fig. 3.3), that is for $p \sim \sqrt{m\mu}$ and x_e as large as we want. First taking $\overline{x} \to \infty$ in (D.9) we see that the third and fourth line of (D.9) which corresponds to (D.5) are always satisfied. Therefore, we can focus on the two first line of (D.9), that is on (D.1). This yields

$$\begin{aligned}
&\frac{p_e t_N}{x_e} \simeq \left(\frac{\hbar \mu^{1/2} x_e^{\gamma-1}}{c}\right)^{1/3} \ll 1 \\
&\frac{\hbar t_N}{x_e^2} \simeq \left(\frac{\hbar^4 x_e^{\gamma-4}}{c\mu}\right)^{1/3} \ll 1
\end{aligned} \tag{D.11}$$

Because the first condition is more restrictive than the second one, in the limits of interest ($\hbar \to 0$ or $\mu \to \infty$ with x_e large), the Airy scaling is correct only if the second condition is satisfied

$$\boxed{\frac{\hbar\sqrt{\mu} x_e^{\gamma-1}}{c} \ll 1}, \tag{D.12}$$

which is (3.26). The conclusion is that $\mu \to \infty$ cannot satisfy the required condition for the emergence of the Airy scaling (3.5). However, this is possible at small $\hbar$, if $\gamma < 1$ on the complete Fermi surf, and if $\gamma > 1$ only for $x_e < \hbar^{1/(1-\gamma)}$.

Bibliography

[4] John Wishart. "The generalised product moment distribution in samples from a normal multivariate population". In: *Biometrika* (1928), pp. 32–52.

[5] Edoardo Amaldi, Oscar D'Agostino, Enrico Fermi, B Pontecorvo, Franco Rasetti, and Emilio Segrè. "Artificial radioactivity produced by neutron bombardment—II". In: *Proceedings of the Royal Society of London. Series A-Mathematical and Physical Sciences* 149.868 (1935), pp. 522–558.

[6] Niels Bohr. "Neutron capture and nuclear constitution". In: *Uspekhi Fizicheskikh Nauk* 16.4 (1936), pp. 425–435.

[7] Eugene P Wigner. "On the statistical distribution of the widths and spacings of nuclear resonance levels". In: *Mathematical Proceedings of the Cambridge Philosophical Society*. Vol. 47. 4. Cambridge University Press. 1951, pp. 790–798.

[8] Eugene Paul Wigner. *Statistical properties of real symmetric matrices with many dimensions*. Princeton University, 1957.

[9] Oriol Bohigas, Marie-Joya Giannoni, and Charles Schmit. "Characterization of chaotic quantum spectra and universality of level fluctuation laws". In: *Physical review letters* 52.1 (1984), p. 1.

[10] LP Gor'Kov and GM Eliashberg. "Minute metallic particles in an electromagnetic field". In: *Sov. Phys. JETP* 21.940 (1965).

[11] Philippe Di Francesco, Paul Ginsparg, and Jean Zinn-Justin. "2D gravity and random matrices". In: *Physics Reports* 254.1-2 (1995), pp. 1–133.

[12] Haim Sompolinsky, Andrea Crisanti, and Hans-Jurgen Sommers. "Chaos in random neural networks". In: *Physical review letters* 61.3 (1988), p. 259.

[13] Feng Luo, Jianxin Zhong, Yunfeng Yang, Richard H Scheuermann, and Jizhong Zhou. "Application of random matrix theory to biological networks". In: *Physics Letters A* 357.6 (2006), pp. 420–423.

[14] Ayumi Kikkawa. "Random matrix analysis for gene interaction networks in cancer cells". In: *Scientific reports* 8.1 (2018), pp. 1–12.

[15] Jean-Philippe Bouchaud and Marc Potters. "Financial applications of random matrix theory: a short review". In: *arXiv preprint arXiv:0910.1205* (2009).

[16] Wolfgang Pauli. "Über den Zusammenhang des Abschlusses der Elektronengruppen im Atom mit der Komplexstruktur der Spektren". In: *Zeitschrift für Physik* 31.1 (1925), pp. 765–783.

[17] David S Dean, Pierre Le Doussal, Satya N Majumdar, and Grégory Schehr. "Noninteracting fermions at finite temperature in a d-dimensional trap: Universal correlations". In: *Physical Review A* 94.6 (2016), p. 063622.

[18] Yvan Castin. "Basic theory tools for degenerate Fermi gases". In: *Ultracold Fermi gases*. IOS Press, 2007, pp. 289–349.

[19] David S Dean, Pierre Le Doussal, Satya N Majumdar, and Grégory Schehr. "Noninteracting fermions in a trap and random matrix theory". In: *Journal of Physics A: Mathematical and Theoretical* 52.14 (2019), p. 144006.

[20] John B Johnson. "Thermal agitation of electricity in conductors". In: *Nature* 119.2984 (1927), pp. 50–51.

[21] M Büttiker. "Scattering theory of thermal and excess noise in open conductors". In: *Physical review letters* 65.23 (1990), p. 2901.

[22] Th Martin and Rolf Landauer. "Wave-packet approach to noise in multichannel mesoscopic systems". In: *Physical Review B* 45.4 (1992), p. 1742.

[23] Anatoli Polkovnikov, Krishnendu Sengupta, Alessandro Silva, and Mukund Vengalattore. "Colloquium: Nonequilibrium dynamics of closed interacting quantum systems". In: *Reviews of Modern Physics* 83.3 (2011), p. 863.

[24] Tibor Antal, Zoltán Rácz, Attila Rákos, and Gunter M Schütz. "Transport in the XX chain at zero temperature: Emergence of flat magnetization profiles". In: *Physical Review E* 59.5 (1999), p. 4912.

[25] Aditi Mitra and Thierry Giamarchi. "Thermalization and dissipation in out-of-equilibrium quantum systems: A perturbative renormalization group approach". In: *Physical Review B* 85.7 (2012), p. 075117.

[26] Mario Collura, Márton Kormos, and Pasquale Calabrese. "Quantum quench in a harmonically trapped one-dimensional Bose gas". In: *Physical Review A* 97.3 (2018), p. 033609.

[27] Jean-Marie Stéphan. "Return probability after a quench from a domain wall initial state in the spin-1/2 XXZ chain". In: *Journal of Statistical Mechanics: Theory and Experiment* 2017.10 (2017), p. 103108.

[28] Kurt Schönhammer. "Full counting statistics for noninteracting fermions: Exact results and the Levitov-Lesovik formula". In: *Physical Review B* 75.20 (2007), p. 205329.

[29] Oleksandr Gamayun, Oleg Lychkovskiy, and Jean-Sébastien Caux. "Fredholm determinants, full counting statistics and Loschmidt echo for domain wall profiles in one-dimensional free fermionic chains". In: *SciPost Physics* 8.3 (2020), p. 036.

[30] O Gamayun, Yu Zhuravlev, and N Iorgov. "On Landauer–Büttiker formalism from a quantum quench". In: *Journal of Physics A: Mathematical and Theoretical* 56.20 (2023), p. 205203.

[31] Jacopo Viti, Jean-Marie Stéphan, Jérôme Dubail, and Masudul Haque. "Inhomogeneous quenches in a free fermionic chain: Exact results". In: *Europhysics Letters* 115.4 (2016), p. 40011.

[32] Alexandre Faribault, Pasquale Calabrese, and Jean-Sébastien Caux. "Quantum quenches from integrability: the fermionic pairing model". In: *Journal of Statistical Mechanics: Theory and Experiment* 2009.03 (2009), P03018.

[33] Laura Foini and Thierry Giamarchi. "Nonequilibrium dynamics of coupled Luttinger liquids". In: *Physical Review A* 91.2 (2015), p. 023627.

[34] Marcos Rigol, Vanja Dunjko, Vladimir Yurovsky, and Maxim Olshanii. "Relaxation in a completely integrable many-body quantum system: an ab initio study of the dynamics of the highly excited states of 1D lattice hard-core bosons". In: *Physical review letters* 98.5 (2007), p. 050405.

[35] Olalla A Castro-Alvaredo, Benjamin Doyon, and Takato Yoshimura. "Emergent hydrodynamics in integrable quantum systems out of equilibrium". In: *Physical Review X* 6.4 (2016), p. 041065.

[36] Bruno Bertini, Mario Collura, Jacopo De Nardis, and Maurizio Fagotti. "Transport in out-of-equilibrium x x z chains: Exact profiles of charges and currents". In: *Physical review letters* 117.20 (2016), p. 207201.

[37] Benjamin Doyon and Takato Yoshimura. "A note on generalized hydrodynamics: inhomogeneous fields and other concepts". In: *SciPost Physics* 2.2 (2017), p. 014.

[38] Isabelle Bouchoule, Benjamin Doyon, and Jerome Dubail. "The effect of atom losses on the distribution of rapidities in the one-dimensional Bose gas". In: *SciPost Physics* 9.4 (2020), p. 044.

[39] Alvise Bastianello, Vincenzo Alba, and Jean-Sébastien Caux. "Generalized hydrodynamics with space-time inhomogeneous interactions". In: *Physical Review Letters* 123.13 (2019), p. 130602.

[40] Viktor Eisler and Zoltán Rácz. "Full counting statistics in a propagating quantum front and random matrix spectra". In: *Physical review letters* 110.6 (2013), p. 060602.

[41] Tomasz Rolski. "A note on the history of the Poisson process". In: *Antiquitates Mathematicae* 13 (2019), pp. 3–17.

[42] Freeman J Dyson. "The threefold way. Algebraic structure of symmetry groups and ensembles in quantum mechanics". In: *Journal of Mathematical Physics* 3.6 (1962), pp. 1199–1215.

[43] Madan Lal Mehta. *Random matrices*. Elsevier, 2004.

[44] Peter J Forrester. *Log-gases and random matrices (LMS-34)*. Princeton university press, 2010.

[45] Karl Pearson. "LIII. On lines and planes of closest fit to systems of points in space". In: *The London, Edinburgh, and Dublin philosophical magazine and journal of science* 2.11 (1901), pp. 559–572.

[46] Yi-Kuo Yu and Yi-Cheng Zhang. "On the anti-Wishart distribution". In: *Physica A: Statistical Mechanics and its Applications* 312.1-2 (2002), pp. 1–22.

[47] Romuald A Janik and Maciej A Nowak. "Wishart and anti-Wishart random matrices". In: *Journal of Physics A: Mathematical and General* 36.12 (2003), p. 3629.

[48] Francesco Giacomo Tricomi. *Integral equations*. Vol. 5. Courier corporation, 1985.

[49] Vladimir A Marčenko and Leonid A Pastur. "Distribution of eigenvalues for some sets of random matrices". In: *Mathematics of the USSR-Sbornik* 1.4 (1967), p. 457.

[50] Terence Tao and Van Vu. "Random matrices: the universality phenomenon for Wigner ensembles". In: *Modern aspects of random matrix theory* 72 (2014), pp. 121–172.

[51] Greg W Anderson, Alice Guionnet, and Ofer Zeitouni. *An introduction to random matrices*. 118. Cambridge university press, 2010.

[52] Satya N Majumdar, Céline Nadal, Antonello Scardicchio, and Pierpaolo Vivo. "Index distribution of Gaussian random matrices". In: *Physical review letters* 103.22 (2009), p. 220603.

[53] Satya N Majumdar, Céline Nadal, Antonello Scardicchio, and Pierpaolo Vivo. "How many eigenvalues of a Gaussian random matrix are positive?" In: *Physical Review E* 83.4 (2011), p. 041105.

[54] Alexandre Krajenbrink and Pierre Le Doussal. "Linear statistics and pushed Coulomb gas at the edge of β-random matrices: Four paths to large deviations". In: *Europhysics Letters* 125.2 (2019), p. 20009.

[55] A. Borodin. "Determinantal point processes". In: *arXiv preprint arXiv:0911.1153* (2009).

[56] Morris Marden. *Geometry of polynomials*. 3. American Mathematical Soc., 1949.

[57] Gian-Carlo Wick. "The evaluation of the collision matrix". In: *Physical review* 80.2 (1950), p. 268.

[58] E Brézin and A Zee. "Universality of the correlations between eigenvalues of large random matrices". In: *Nuclear Physics B* 402.3 (1993), pp. 613–627.

[59] Peter J Forrester. "The spectrum edge of random matrix ensembles". In: *Nuclear Physics B* 402.3 (1993), pp. 709–728.

[60] Craig A Tracy and Harold Widom. "Level-spacing distributions and the Airy kernel". In: *Communications in Mathematical Physics* 159 (1994), pp. 151–174.

[61] Craig A Tracy and Harold Widom. "Level spacing distributions and the Bessel kernel". In: *Communications in mathematical physics* 161.2 (1994), pp. 289–309.

[62] Eugene P Wigner. "On the quantum correction for thermodynamic equilibrium". In: *Part I: Physical Chemistry. Part II: Solid State Physics* (1932), pp. 110–120.

[63] Jean-Marie Stéphan. "Free fermions at the edge of interacting systems". In: *SciPost Physics* 6.5 (2019), p. 057.

[64] David S Dean, Pierre Le Doussal, Satya N Majumdar, and Grégory Schehr. "Statistics of the maximal distance and momentum in a trapped Fermi gas at low temperature". In: *Journal of Statistical Mechanics: Theory and Experiment* 2017.6 (2017), p. 063301.

[65] Pierre Le Doussal, Satya N Majumdar, and Grégory Schehr. "Multicritical edge statistics for the momenta of fermions in nonharmonic traps". In: *Physical review letters* 121.3 (2018), p. 030603.

[66] Patrizia Vignolo and Anna Minguzzi. "Universal contact for a Tonks-Girardeau gas at finite temperature". In: *Physical review letters* 110.2 (2013), p. 020403.

[67] A Minguzzi, P Vignolo, and MP Tosi. "High-momentum tail in the Tonks gas under harmonic confinement". In: *Physics Letters A* 294.3-4 (2002), pp. 222–226.

[68] Pierre Devillard, A Benzahi, P Vignolo, and Mathias Albert. "Statistical properties of the momentum occupation numbers of the Tonks-Girardeau gas in a harmonic trap". In: *Physical Review A* 104.5 (2021), p. 053306.

[69] Klaus Hueck, Niclas Luick, Lennart Sobirey, Jonas Siegl, Thomas Lompe, and Henning Moritz. "Two-dimensional homogeneous Fermi gases". In: *Physical Review Letters* 120.6 (2018), p. 060402.

[70] Wolfgang Ketterle and Martin W Zwierlein. "Making, probing and understanding ultracold Fermi gases". In: *La Rivista del Nuovo Cimento* 31 (2008), pp. 247–422.

[71] Naftali R Smith, Pierre Le Doussal, Satya N Majumdar, and Grégory Schehr. "Counting statistics for noninteracting fermions in a rotating trap". In: *Physical Review A* 105.4 (2022), p. 043315.

[72] Naftali Smith, Pierre Le Doussal, Satya Majumdar, and Grégory Schehr. "Full counting statistics for interacting trapped fermions". In: *SciPost Physics* 11.6 (2021), p. 110.

[73] Pierre Devillard, Denis Chevallier, Patrizia Vignolo, and Mathias Albert. "Full counting statistics of the momentum occupation numbers of the Tonks-Girardeau gas". In: *Physical Review A* 101.6 (2020), p. 063604.

[74] Hiroki Moriya, Rikuo Nagao, and Tomohiro Sasamoto. "Exact large deviation function of spin current for the one dimensional XX spin chain with domain wall initial condition". In: *Journal of Statistical Mechanics: Theory and Experiment* 2019.6 (2019), p. 063105.

[75] Bernard Derrida, Benoît Douçot, and P-E Roche. "Current fluctuations in the one-dimensional symmetric exclusion process with open boundaries". In: *Journal of Statistical physics* 115 (2004), pp. 717–748.

[76] Joel G Broida and Stanley Gill Williamson. *A comprehensive introduction to linear algebra*. Vol. 4. Addison-Wesley Boston, MA, USA: 1989.

[77] Ivar Fredholm. "Sur une classe d'équations fonctionnelles". In: (1903).

[78] Mark Srednicki. "Entropy and area". In: *Physical Review Letters* 71.5 (1993), p. 666.

[79] Jens Eisert, Marcus Cramer, and Martin B Plenio. "Colloquium: Area laws for the entanglement entropy". In: *Reviews of modern physics* 82.1 (2010), p. 277.

[80] Martin B Plenio, Jens Eisert, J Dreissig, and Marcus Cramer. "Entropy, entanglement, and area: analytical results for harmonic lattice systems". In: *Physical review letters* 94.6 (2005), p. 060503.

[81] Guifre Vidal, José Ignacio Latorre, Enrique Rico, and Alexei Kitaev. "Entanglement in quantum critical phenomena". In: *Physical review letters* 90.22 (2003), p. 227902.

[82] Pasquale Calabrese, Mihail Mintchev, and Ettore Vicari. "Entanglement entropies in free-fermion gases for arbitrary dimension". In: *Europhysics Letters* 97.2 (2012), p. 20009.

[83] H Francis Song, Christian Flindt, Stephan Rachel, Israel Klich, and Karyn Le Hur. "Entanglement entropy from charge statistics: Exact relations for noninteracting many-body systems". In: *Physical Review B* 83.16 (2011), p. 161408.

[84] Israel Klich and Leonid Levitov. "Quantum noise as an entanglement meter". In: *Physical review letters* 102.10 (2009), p. 100502.

[85] Ovidiu Costin and Joel L Lebowitz. "Gaussian fluctuation in random matrices". In: *Physical Review Letters* 75.1 (1995), p. 69.

[86] Pasquale Calabrese, Pierre Le Doussal, and Satya N Majumdar. "Random matrices and entanglement entropy of trapped Fermi gases". In: *Physical Review A* 91.1 (2015), p. 012303.

[87] Estelle L Basor, Craig A Tracy, and Harold Widom. "Asymptotics of level-spacing distributions for random matrices". In: *Physical review letters* 69.1 (1992), p. 5.

[88] Craig A Tracy and Harold Widom. "Airy kernel and Painlevé II". In: *arXiv preprint solv-int/9901004* (1999).

[89] Satya N Majumdar and Grégory Schehr. "Top eigenvalue of a random matrix: large deviations and third order phase transition". In: *Journal of Statistical Mechanics: Theory and Experiment* 2014.1 (2014), P01012.

[90] Craig A Tracy and Harold Widom. "On orthogonal and symplectic matrix ensembles". In: *Communications in Mathematical Physics* 177 (1996), pp. 727–754.

[91] Pierpaolo Vivo, Satya N Majumdar, and Oriol Bohigas. "Large deviations of the maximum eigenvalue in Wishart random matrices". In: *Journal of Physics A: Mathematical and Theoretical* 40.16 (2007), p. 4317.

[92] Eytan Katzav and Isaac Pérez Castillo. "Large deviations of the smallest eigenvalue of the Wishart-Laguerre ensemble". In: *Physical Review E* 82.4 (2010), p. 040104.

[93] Bertrand Lacroix-A-Chez-Toine, Satya N Majumdar, and Grégory Schehr. "Rotating trapped fermions in two dimensions and the complex Ginibre ensemble: Exact results for the entanglement entropy and number variance". In: *Physical Review A* 99.2 (2019), p. 021602.

[94] Ioana Dumitriu and Alan Edelman. "Matrix models for beta ensembles". In: *Journal of Mathematical Physics* 43.11 (2002), pp. 5830–5847.

[95] Céline Nadal and Satya N Majumdar. "Nonintersecting Brownian interfaces and Wishart random matrices". In: *Physical Review E* 79.6 (2009), p. 061117.

[96] Pierpaolo Vivo, Satya N Majumdar, and Oriol Bohigas. "Large deviations of the maximum eigenvalue in Wishart random matrices". In: *Journal of Physics A: Mathematical and Theoretical* 40.16 (2007), p. 4317.

[97] Peter J Forrester and TD Hughes. "Complex Wishart matrices and conductance in mesoscopic systems: exact results". In: *Journal of Mathematical Physics* 35.12 (1994), pp. 6736–6747.

[98] Satya N Majumdar. In: *The Oxford handbook of random matrix theory.* Ed. by J. Baik G. Akemann and P. Di Francesco. Oxford University Press, 2010.

[99] Torsten Ehrhardt. "The asymptotics of a Bessel-kernel determinant which arises in Random Matrix Theory". In: *Advances in Mathematics* 225.6 (2010), pp. 3088–3133.

[100] Alan Edelman, Alice Guionnet, and S Péché. "Beyond universality in random matrix theory". In: (2016).

[101] Anthony Perret and Grégory Schehr. "Finite N corrections to the limiting distribution of the smallest eigenvalue of Wishart complex matrices". In: *Random Matrices: Theory and Applications* 5.01 (2016), p. 1650001.

[102] Gabriel Gouraud, Pierre Le Doussal, and Grégory Schehr. "Hole probability for noninteracting fermions in a d-dimensional trap: Supplemental material". In: *Europhysics Letters* 142.4 (2023), p. 41001.

[103] Salvatore Torquato, A Scardicchio, and Chase E Zachary. "Point processes in arbitrary dimension from fermionic gases, random matrix theory, and number theory". In: *Journal of Statistical Mechanics: Theory and Experiment* 2008.11 (2008), P11019.

[104] Antonello Scardicchio, Chase E Zachary, and Salvatore Torquato. "Statistical properties of determinantal point processes in high-dimensional Euclidean spaces". In: *Physical Review E* 79.4 (2009), p. 041108.

[105] Kurt Johansson. "Random matrices and determinantal processes". In: *arXiv preprint math-ph/0510038* (2005).

[106] David J Gross and Edward Witten. "Possible third-order phase transition in the large-N lattice gauge theory". In: *Physical Review D* 21.2 (1980), p. 446.

[107] Spenta R Wadia. "N= phase transition in a class of exactly soluble model lattice gauge theories". In: *Physics Letters B* 93.4 (1980), pp. 403–410.

[108] Kurt Johansson. "The longest increasing subsequence in a random permutation and a unitary random matrix model". In: *Mathematical Research Letters* 5.1 (1998), pp. 68–82.

[109] Folkmar Bornemann. "On the numerical evaluation of Fredholm determinants". In: *Mathematics of Computation* 79.270 (2010), pp. 871–915.

[110] Pasquale Calabrese and John Cardy. "Time dependence of correlation functions following a quantum quench". In: *Physical review letters* 96.13 (2006), p. 136801.

[111] Pasquale Calabrese and John Cardy. "Quantum quenches in extended systems". In: *Journal of Statistical Mechanics: Theory and Experiment* 2007.06 (2007), P06008.

[112] Pasquale Calabrese, Fabian HL Essler, and Maurizio Fagotti. "Quantum quench in the transverse-field Ising chain". In: *Physical review letters* 106.22 (2011), p. 227203.

[113] Aditi Mitra and Thierry Giamarchi. "Mode-coupling-induced dissipative and thermal effects at long times after a quantum quench". In: *Physical Review Letters* 107.15 (2011), p. 150602.

[114] Sin-itiro Tomonaga. "Remarks on Bloch's method of sound waves applied to many-fermion problems". In: *Progress of Theoretical Physics* 5.4 (1950), pp. 544–569.

[115] JM Luttinger. "An exactly soluble model of a many-fermion system". In: *Journal of mathematical physics* 4.9 (1963), pp. 1154–1162.

[116] Miguel A Cazalilla. "Effect of suddenly turning on interactions in the Luttinger model". In: *Physical review letters* 97.15 (2006), p. 156403.

[117] A Iucci and Miguel A Cazalilla. "Quantum quench dynamics of the Luttinger model". In: *Physical Review A* 80.6 (2009), p. 063619.

[118] Mario Collura, Pasquale Calabrese, and Fabian HL Essler. "Quantum quench within the gapless phase of the spin- 1 2 Heisenberg XXZ spin chain". In: *Physical Review B* 92.12 (2015), p. 125131.

[119] Laura Foini and Thierry Giamarchi. "Relaxation dynamics of two coherently coupled one-dimensional bosonic gases". In: *The European Physical Journal Special Topics* 226 (2017), pp. 2763–2774.

[120] Paola Ruggiero, Laura Foini, and Thierry Giamarchi. "Large-scale thermalization, prethermalization, and impact of temperature in the quench dynamics of two unequal Luttinger liquids". In: *Physical Review Research* 3.1 (2021), p. 013048.

[121] Paola Ruggiero, Pasquale Calabrese, Laura Foini, and Thierry Giamarchi. "Quenches in initially coupled Tomonaga-Luttinger Liquids: a conformal field theory approach". In: *SciPost Physics* 11.3 (2021), p. 055.

[122] Denis Bernard and Benjamin Doyon. "Energy flow in non-equilibrium conformal field theory". In: *Journal of Physics A: Mathematical and Theoretical* 45.36 (2012), p. 362001.

[123] Denis Bernard, B Doyon, and J Viti. "Non-equilibrium conformal field theories with impurities". In: *Journal of Physics A: Mathematical and Theoretical* 48.5 (2015), 05FT01.

[124] Luca Capizzi and Viktor Eisler. "Entanglement evolution after a global quench across a conformal defect". In: *SciPost Physics* 14.4 (2023), p. 070.

[125] Jean-Marie Stéphan and Jérôme Dubail. "Local quantum quenches in critical one-dimensional systems: entanglement, the Loschmidt echo, and light-cone effects". In: *Journal of Statistical Mechanics: Theory and Experiment* 2011.08 (2011), P08019.

[126] Toshiya Kinoshita, Trevor Wenger, and David S Weiss. "A quantum Newton's cradle". In: *Nature* 440.7086 (2006), pp. 900–903.

[127] Fabian HL Essler and Maurizio Fagotti. "Quench dynamics and relaxation in isolated integrable quantum spin chains". In: *Journal of Statistical Mechanics: Theory and Experiment* 2016.6 (2016), p. 064002.

[128] Vincenzo Alba and Pasquale Calabrese. "Entanglement and thermodynamics after a quantum quench in integrable systems". In: *Proceedings of the National Academy of Sciences* 114.30 (2017), pp. 7947–7951.

[129] Fabian HL Essler, Stefan Kehrein, Salvatore R Manmana, and NJ Robinson. "Quench dynamics in a model with tuneable integrability breaking". In: *Physical Review B* 89.16 (2014), p. 165104.

[130] Giuseppe Del Vecchio Del Vecchio, Andrea De Luca, and Alvise Bastianello. "Transport through interacting defects and lack of thermalisation". In: *SciPost Physics* 12.2 (2022), p. 060.

[131] Jean-Sébastien Caux and Robert M Konik. "Constructing the generalized Gibbs ensemble after a quantum quench". In: *Physical review letters* 109.17 (2012), p. 175301.

[132] Mario Collura, Spyros Sotiriadis, and Pasquale Calabrese. "Quench dynamics of a Tonks–Girardeau gas released from a harmonic trap". In: *Journal of Statistical Mechanics: Theory and Experiment* 2013.09 (2013), P09025.

[133] Manas Kulkarni, Gautam Mandal, and Takeshi Morita. "Quantum quench and thermalization of one-dimensional Fermi gas via phase-space hydrodynamics". In: *Physical Review A* 98.4 (2018), p. 043610.

[134] Mario Collura and Dragi Karevski. "Quantum quench from a thermal tensor state: Boundary effects and generalized Gibbs ensemble". In: *Physical Review B* 89.21 (2014), p. 214308.

[135] Viktor Eisler, Florian Maislinger, and Hans Gerd Evertz. "Universal front propagation in the quantum Ising chain with domain-wall initial states". In: *SciPost Physics* 1.2 (2016), p. 014.

[136] Gabriele Perfetto and Andrea Gambassi. "Ballistic front dynamics after joining two semi-infinite quantum Ising chains". In: *Physical Review E* 96.1 (2017), p. 012138.

[137] Márton Kormos. "Inhomogeneous quenches in the transverse field Ising chain: scaling and front dynamics". In: *SciPost Physics* 3.3 (2017), p. 020.

[138] Andrea De Luca, Jacopo Viti, Denis Bernard, and Benjamin Doyon. "Nonequilibrium thermal transport in the quantum Ising chain". In: *Physical Review B* 88.13 (2013), p. 134301.

[139] Spyros Sotiriadis. "Non-Equilibrium Steady State of the Lieb-Liniger model: exact treatment of the Tonks Girardeau limit". In: *arXiv preprint arXiv:2007.12683* (2020).

[140] Bruno Bertini and Maurizio Fagotti. "Determination of the nonequilibrium steady state emerging from a defect". In: *Physical Review Letters* 117.13 (2016), p. 130402.

[141] Bruno Bertini. "Approximate light cone effects in a nonrelativistic quantum field theory after a local quench". In: *Physical Review B* 95.7 (2017), p. 075153.

[142] Luca Capizzi, Stefano Scopa, Federico Rottoli, and Pasquale Calabrese. "Domain wall melting across a defect". In: *Europhysics Letters* 141.3 (2023), p. 31002.

[143] Marko Ljubotina, Spyros Sotiriadis, and Tomaž Prosen. "Non-equilibrium quantum transport in presence of a defect: the non-interacting case". In: *SciPost Physics* 6.1 (2019), p. 004.

[144] Fabian HL Essler. "A short introduction to Generalized Hydrodynamics". In: *Physica A: Statistical Mechanics and its Applications* (2022), p. 127572.

[145] Benjamin Doyon. "Lecture notes on generalised hydrodynamics". In: *SciPost Physics Lecture Notes* (2020), p. 018.

[146] Vincenzo Alba, Bruno Bertini, Maurizio Fagotti, Lorenzo Piroli, and Paola Ruggiero. "Generalized-hydrodynamic approach to inhomogeneous quenches: correlations, entanglement and quantum effects". In: *Journal of Statistical Mechanics: Theory and Experiment* 2021.11 (2021), p. 114004.

[147] Luca D'Alessio, Yariv Kafri, Anatoli Polkovnikov, and Marcos Rigol. "From quantum chaos and eigenstate thermalization to statistical mechanics and thermodynamics". In: *Advances in Physics* 65.3 (2016), pp. 239–362.

[148] H.J. Stockmann. In: (). URL: http://www.scholarpedia.org/article/Microwave_billiards_and_quantum_chaos.

[149] Nándor Simányi. *Ergodicity of Spheres in a Box*. Tech. rep. 1997.

[150] Victor Donnay and Carlangelo Liverani. "Potentials on the two-torus for which the Hamiltonian flow is ergodic". In: *Communications in mathematical physics* 135 (1991), pp. 267–302.

[151] John Earman and Miklós Rédei. "Why ergodic theory does not explain the success of equilibrium statistical mechanics". In: *The British Journal for the Philosophy of Science* 47.1 (1996), pp. 63–78.

[152] Josh M Deutsch. "Quantum statistical mechanics in a closed system". In: *Physical review a* 43.4 (1991), p. 2046.

[153] Mark Srednicki. "Chaos and quantum thermalization". In: *Physical review e* 50.2 (1994), p. 888.

[154] Mario Collura, Spyros Sotiriadis, and Pasquale Calabrese. "Equilibration of a Tonks-Girardeau gas following a trap release". In: *Physical Review Letters* 110.24 (2013), p. 245301.

[155] Balázs Pozsgay. "Algebraic construction of current operators in integrable spin chains". In: *Physical Review Letters* 125.7 (2020), p. 070602.

[156] Elliott H Lieb and Werner Liniger. "Exact analysis of an interacting Bose gas. I. The general solution and the ground state". In: *Physical Review* 130.4 (1963), p. 1605.

[157] Marvin Girardeau. "Relationship between systems of impenetrable bosons and fermions in one dimension". In: *Journal of Mathematical Physics* 1.6 (1960), pp. 516–523.

[158] Vladimir E Korepin, Nicholay M Bogoliubov, and Anatoli G Izergin. *Quantum inverse scattering method and correlation functions*. Vol. 3. Cambridge university press, 1997.

[159] Alvise Bastianello, Andrea De Luca, and Romain Vasseur. "Hydrodynamics of weak integrability breaking". In: *Journal of Statistical Mechanics: Theory and Experiment* 2021.11 (2021), p. 114003.

[160] J Friedel. "XIV. The distribution of electrons round impurities in monovalent metals". In: *The London, Edinburgh, and Dublin Philosophical Magazine and Journal of Science* 43.337 (1952), pp. 153–189.

[161] J Friedel. "Metallic alloys". In: *Il Nuovo Cimento (1955-1965)* 7.Suppl 2 (1958), pp. 287–311.

[162] John M Ziman. *Principles of the Theory of Solids*. Cambridge university press, 1972.

[163] Gabriele F Giuliani, Giovanni Vignale, and Trinanjan Datta. "RKKY range function of a one-dimensional noninteracting electron gas". In: *Physical Review B* 72.3 (2005), p. 033411.

[164] David Dean, Pierre Le Doussal, Satya Majumdar, and Gregory Schehr. "Impurities in systems of noninteracting trapped fermions". In: *SciPost Physics* 10.4 (2021), p. 082.

[165] Alessio Recati, Jean-Noël Fuchs, Claudia Sofia Peca, and Wilhelm Zwerger. "Casimir forces between defects in one-dimensional quantum liquids". In: *Physical Review A* 72.2 (2005), p. 023616.

[166] JN Fuchs, A Recati, and W Zwerger. "Oscillating Casimir force between impurities in one-dimensional Fermi liquids". In: *Physical Review A* 75.4 (2007), p. 043615.

[167] Francesco Massel, Adrian Kantian, Andrew J Daley, Thierry Giamarchi, and Päivi Törmä. "Dynamics of an impurity in a one-dimensional lattice". In: *New Journal of Physics* 15.4 (2013), p. 045018.

[168] David Stadler, Sebastian Krinner, Jakob Meineke, Jean-Philippe Brantut, and Tilman Esslinger. "Observing the drop of resistance in the flow of a superfluid Fermi gas". In: *Nature* 491.7426 (2012), pp. 736–739.

[169] Dominik Husmann, Shun Uchino, Sebastian Krinner, Martin Lebrat, Thierry Giamarchi, Tilman Esslinger, and Jean-Philippe Brantut. "Connecting strongly correlated superfluids by a quantum point contact". In: *Science* 350.6267 (2015), pp. 1498–1501.

[170] Benoît Douçot, Romain Danneau, Kang Yang, Jean-Guy Caputo, and Régis Mélin. "Berry phase in superconducting multiterminal quantum dots". In: *Physical Review B* 101.3 (2020), p. 035411.

[171] Andriani Keliri and Benoît Douçot. "Driven Andreev molecule". In: *Physical Review B* 107.9 (2023), p. 094505.

[172] Rolf Landauer. "Johnson-Nyquist noise derived from quantum mechanical transmission". In: *Physica D: Nonlinear Phenomena* 38.1-3 (1989), pp. 226–229.

[173] Markus Büttiker. "Scattering theory of current and intensity noise correlations in conductors and wave guides". In: *Physical Review B* 46.19 (1992), p. 12485.

[174] Ya M Blanter and Markus Büttiker. "Shot noise in mesoscopic conductors". In: *Physics reports* 336.1-2 (2000), pp. 1–166.

[175] Michael V Moskalets. *Scattering matrix approach to non-stationary quantum transport*. World Scientific, 2011.

[176] Harry Nyquist. "Thermal agitation of electric charge in conductors". In: *Physical review* 32.1 (1928), p. 110.

[177] John A Wheeler. "On the mathematical description of light nuclei by the method of resonating group structure". In: *Physical Review* 52.11 (1937), p. 1107.

[178] Leonid S Levitov and Gordey B Lesovik. "Charge distribution in quantum shot noise". In: *JETP LETTERS C/C OF PIS'MA V ZHURNAL EKSPERIMENTAL'NOI TEORETICHESKOI FIZIKI* 58 (1993), pp. 230–230.

[179] LS Levitov. "The Statistical Theory of Mesoscopic Noise: A short review". In: *Quantum Noise in Mesoscopic Physics* (2003), pp. 373–396.

[180] Israel Klich. "Full Counting Statistics: An elementary derivation of Levitov's formula". In: *arXiv preprint cond-mat/0209642* (2002).

[181] Eriko Kaminishi, Jun Sato, and Tetsuo Deguchi. "Recurrence time in the quantum dynamics of the 1D Bose gas". In: *Journal of the Physical Society of Japan* 84.6 (2015), p. 064002.

[182] Bertrand Lacroix-A-Chez-Toine, Pierre Le Doussal, Satya N Majumdar, and Grégory Schehr. "Non-interacting fermions in hard-edge potentials". In: *Journal of Statistical Mechanics: Theory and Experiment* 2018.12 (2018), p. 123103.

[183] Bertrand Lacroix-A-Chez-Toine, Pierre Le Doussal, Satya N Majumdar, and Grégory Schehr. "Statistics of fermions in a d-dimensional box near a hard wall". In: *Europhysics Letters* 120.1 (2017), p. 10006.

[184] Jerome Dubail, Jean-Marie Stéphan, Jacopo Viti, and Pasquale Calabrese. "Conformal field theory for inhomogeneous one-dimensional quantum systems: the example of non-interacting Fermi gases". In: *SciPost Physics* 2.1 (2017), p. 002.

[185] WN Mathews Jr. "Energy density and current in quantum theory". In: *American Journal of Physics* 42.3 (1974), pp. 214–219.

[186] Joseph H Eberly, NB Narozhny, and JJ Sanchez-Mondragon. "Periodic spontaneous collapse and revival in a simple quantum model". In: *Physical Review Letters* 44.20 (1980), p. 1323.

[187] David S Dean, Pierre Le Doussal, Satya N Majumdar, and Grégory Schehr. "Nonequilibrium dynamics of noninteracting fermions in a trap". In: *Europhysics Letters* 126.2 (2019), p. 20006.

[188] Gabriel Gouraud, Pierre Le Doussal, and Gregory Schehr. "Stationary time correlations for fermions after a quench in the presence of an impurity: Supplemental material". In: *Europhysics Letters* 142.4 (2023), p. 41001.

[189] Khosrow Chadan and Pierre C Sabatier. *Inverse problems in quantum scattering theory*. Springer Science & Business Media, 2012.

[190] Lorenzo Rossi, Fabrizio Dolcini, Fabio Cavaliere, Niccolò Traverso Ziani, Maura Sassetti, and Fausto Rossi. "Signature of generalized Gibbs ensemble deviation from equilibrium: negative absorption induced by a local quench". In: *Entropy* 23.2 (2021), p. 220.

[191] Pierre Le Doussal, Satya N Majumdar, and Gregory Schehr. "Periodic Airy process and equilibrium dynamics of edge fermions in a trap". In: *Annals of Physics* 383 (2017), pp. 312–345.

[192] John H Van Vleck. "The correspondence principle in the statistical interpretation of quantum mechanics". In: *Proceedings of the National Academy of Sciences* 14.2 (1928), pp. 178–188.

[193] Martin C Gutzwiller. "Phase-Integral Approximation in Momentum Space and the Bound States of an Atom". In: *Journal of mathematical Physics* 8.10 (1967), pp. 1979–2000.

[194] Thomas Dittrich, Carlos Viviescas, and Luis Sandoval. "Semiclassical propagator of the Wigner function". In: *Physical review letters* 96.7 (2006), p. 070403.

[195] David J Griffiths and Darrell F Schroeter. *Introduction to quantum mechanics*. Cambridge university press, 2018.

[196] Colin Rylands and Pasquale Calabrese. "Transport and entanglement across integrable impurities from Generalized Hydrodynamics". In: *arXiv preprint arXiv:2303.01779* (2023).

[197] Shachar Fraenkel and Moshe Goldstein. "Entanglement measures in a nonequilibrium steady state: exact results in one dimension". In: *SciPost Physics* 11.4 (2021), p. 085.

[198] Shachar Fraenkel and Moshe Goldstein. "Extensive long-range entanglement in a nonequilibrium steady state". In: *arXiv preprint arXiv:2205.12991* (2022).

[199] David S Dean, Pierre Le Doussal, Satya N Majumdar, and Grégory Schehr. "Wigner function of noninteracting trapped fermions". In: *Physical Review A* 97.6 (2018), p. 063614.

[200] Michael Victor Berry. "Semi-classical mechanics in phase space: a study of Wigner's function". In: *Philosophical Transactions of the Royal Society of London. Series A, Mathematical and Physical Sciences* 287.1343 (1977), pp. 237–271.

[201] Eldad Bettelheim and Paul B Wiegmann. "Universal Fermi distribution of semiclassical nonequilibrium Fermi states". In: *Physical Review B* 84.8 (2011), p. 085102.

[202] Vallee Olivier and Soares Manuel. *Airy functions and applications to physics*. World Scientific, 2010.

[203] Bernt Øksendal and Bernt Øksendal. *Stochastic differential equations*. Springer, 2003.

[204] Nancy Makri and William H Miller. "Exponential power series expansion for the quantum time evolution operator". In: *The Journal of chemical physics* 90.2 (1989), pp. 904–911.

[205] KV Bhagwat and SV Lawande. "A new derivation of the Feynman propagator for the inverse square potential". In: *Physics Letters A* 141.7 (1989), pp. 321–325.

[206] Lene I Lolle, CG Gray, JD Poll, and AG Basile. "Improved short-time propagator for repulsive inverse-power-law potentials". In: *Chemical physics letters* 177.1 (1991), pp. 64–72.

[207] Benjamin De Bruyne, David S Dean, Pierre Le Doussal, Satya N Majumdar, and Gregory Schehr. "Wigner function for noninteracting fermions in hard-wall potentials". In: *Physical Review A* 104.1 (2021), p. 013314.

[208] Rutger-Jan Lange. "Distribution theory for Schrödinger's integral equation". In: *Journal of Mathematical Physics* 56.12 (2015), p. 122105.

RÉSUMÉ

Cette thèse de doctorat porte sur l'étude de gaz de fermions sans interaction. En raison de leur nature, ces gaz permettent d'obtenir de nombreux résultats analytiques qui restent inaccessibles en présence d'interactions tout en rendant compte d'effets physiques non triviaux. Étant soumis au principe de Pauli, de nombreuses relations existent entre les fermions à l'équilibre et la théorie des matrices aléatoires. Dans cette thèse, nous examinons si ces liens sont préservés et comment ils se traduisent dans d'autres contextes.
Ainsi, nous étudions les propriétés statistiques de ces gaz dans un espace de dimension quelconque, ce qui est l'objet du chapitre un, ou lorsque ces gaz ne sont pas à l'équilibre, ce qui est l'objet des chapitres deux et trois.
Dans le chapitre deux, nous discutons de l'effet d'une impureté sur la dynamique hors équilibre, en particulier, nous observons l'émergence de corrélations non locales. Dans ce contexte, après avoir introduit la théorie hydrodynamique pour les systèmes intégrables, nous constatons que celle-ci ne permet pas d'expliquer les corrélations non-locales observées. Pour pallier à cela, nous envisageons une extension quantique de cette théorie.
Dans le chapitre trois, nous observons l'émergence de statistiques d'Airy au bord d'une vague de fermions dans le continu.
Au-delà des résultats obtenus lors du doctorat, ce manuscrit est l'occasion de présenter de nouvelles perspectives de recherche sur ces sujets interconnectés.

MOTS CLÉS

Dynamique hors équilibre, matrices aléatoires, hydrodynamique généralisée, fermions sans interaction, systèmes inhomogènes.

ABSTRACT

This thesis explores the study of noninteracting fermion gases. Due to their nature, these gases allow us to obtain many analytical results that remain inaccessible in the case of interacting systems, while accounting for many non-trivial physical effects. Being subject to the Pauli principle, many relations exist between fermions at equilibrium and random matrix theory. In this thesis, we examine if these relations are preserved and, if so, how they manifest in other contexts. Hence, we study the statistical properties of fermion gases in higher dimensions, which is the focus of chapter one, as well as their behaviour when driven out-of-equilibrium, explored in chapters two and three.
In the second chapter, we investigate the effect of an impurity on the out-of-equilibrium dynamics of fermions, particularly observing the emergence of non-local correlations. After introducing the hydrodynamic theory for integrable systems, it appears that this theory cannot predict the aforementioned non-local correlations. Therefore, we propose a quantum extension of the hydrodynamic theory.
In the third chapter, we observe the emergence of Airy statistics at the edge of a quantum propagating front for free fermions in the continuum.
Beyond the results presented in this thesis, this manuscript examines new perspectives on those interconnected fields of research.

KEYWORDS

Out-of-equilibrium dynamics, random matrix theory, generalised hydrodynamics, noninteracting fermions, inhomogeneous systems.